ELECTROCHEMICAL CHARACTERISATION OF CONDUCTING POLYMER LAYERS AND THEIR USE AS GAS SENSORS.

by

Timothy Paul McCormac

A Thesis Presented to
Dublin City University
for the award of PhD.

Prepared under the supervision of Dr. John Cassidy, Chemistry Department, Dublin Institute of Technology, Kevin Street and under the direction of Dr. Johannes G. Vos, School of Chemical Sciences, Dublin City University.

August 1994.

DECLARATION

I hereby certify that this material, which I now submit for assessment on the programme of study leading to the award of Doctor of Philosophy is entirely my own work and has not been taken from the work of others save and to the extent that such work has been cited and acknowledged within the text of my work.

Signed: Timothy M Cormac **ID No.:** 91700779

Timothy Paul McCormac

Date: _____

ELECTROCHEMICAL CHARACTERISATION OF CONDUCTING POLYMER LAYERS AND THEIR USE AS GAS SENSORS.

Timothy Paul McCormac.

ABSTRACT.
The main aim of this work was to develop an SO_2 sensor based upon a conducting polymer. The methodology and properties of a conducting polymer sensor along with the electrochemical characterisation of various polypyrrole layers is described.
It was found that polypyrrole layers containing Copper (ll) Phthalocyanine - 3,4',4'', 4'''-tetrasulphonate anions (PPTSP), as the dopant, upon electrochemical switching exhibit cation movement in and out of the polymer matrix. A concentration, pH, temperature and scan rate study was performed on the process of cation movement. Also anions, such as ClO_4^-, dodecylbenzenesulphonate (DBS) were employed as the dopants within the polypyrrole matrix. In this work it is described that the low level of non-faradaic current, characteristic of PPDBS layers, was due to the presence of the DBS anion in solution rather than the polymer morphology.
Differential Pulse Voltammetry is applied to various polypyrrole layers and sigmoidal differential current outputs were obtained. A model is proposed for this behaviour which includes a set of resistances in parallel. Potential Step experiments were also performed on the polypyrrole layers. A transmission line model is proposed to explain the behaviour of the polymer film.
For several electroconducting polymers spectroelectrochemical studies were carried out. The absorption spectra are quantitatively analysed using the Nernst equation by a 'Monomer Unit Model. The reaction between pyrrole and tetracyanoethylene (TCNE) was studied electrochemically and spectroscopically. It was found that TCNE forms a charge transfer complex with pyrrole, and it is present within the PPTCNE layer as the dopant anion. The influence of solvent composition upon the ferricyanide/ferrocyanide system was investigated electrochemically. It was found that in organic solvents ferrocyanide is a strong reducing agent.
Polypyrrole layers were deposited across interdigital array electrodes and their responses to various organic vapours and 5% SO_2 were investigated. The use of Prussian Blue films as possible overlayers upon the polypyrrole layers is described. Also solid state voltammetry was performed upon Prussian Blue films, and when these mixed valent films were exposed to certain saturated vapours in nitrogen, good reversible responses were obtained. Also the interaction of organic vapours and polypyrrole films, deposited upon ITO electrodes, was investigated by UV/vis spectroscopy.

TABLE OF CONTENTS

APPENDIX ONE

Fortran Simulation Programme
for Differential Pulse Voltammetry
of Conducting Polymer Layers. (i) - (iv)

Acknowledgements

Firstly I would like to thank my two supervisors, Dr J.G.Vos and Dr J.F.Cassidy for their help. I am grateful to John for his guidance and encouragement over the past three years.

I would like to thank Mr E.Rothery and Dr N.R.Russell for the use of facilities within the Chemistry Department, Kevin Street, College of Technology. Also I would like to thank the technical staff of the Chemistry Department in Kevin Street for all their assistance over the past number of years.

I am grateful to Dr R.Foster of Kevin Street for the screen printed carbon ink electrodes and Dr D.Cameron for the sputtered gold interdigital array electrodes.

I would like to thank Dr J.F. Cassidy for the Fortran simulation program in Appendix 1, and Mr S.McCormac, Department of Electrical Engineering, Kevin Street, for the modified circuit employed for the gas sensing experiments.

I am grateful to Ms. M.Brady in Kevin Street for her professionalism and patience in the typing of this thesis.

Finally I would like to thank my family, friends and the chemistry post graduate students within Kevin Street for all their encouragement and support over the past number of years.

CHAPTER 1

INTRODUCTION

It is accepted that most polymer systems are insulating in character, as can be readily seen from the many applications they serve, for example the coating of electrical wires with insulating polymers to prevent shorting.

However over the past 20 years a novel class of polymers have received widespread attention. This new group of polymers has the ability to conduct electric current.

By the late 1970's there was excitement over the possibility of developing new materials with electronic and optical properties of metals and semiconductors. These conductive polymers are characterised by electronic conductivities ranging from 10^{-6} Siemens per cm up to 10^{5} Siemens per cm, a conductivity comparable in magnitude to that of iron.

One of the major discoveries that launched the field of conducting polymers, was the high conductivity of polysulphurnitride $(SN)_x$, an inorganic explosive polymer, which was found to become superconducting at 0.3K. It was also one of the first polymeric materials to exhibit metallic properties.

However it was polyacetylene, which consists of coupled chains of carbon - hydrogen units arranged in a one dimensional lattice, that initiated interest in the field of conducting polymers.

It was in 1974 that a silvery film of polyacetylene was accidently prepared by Hideki Shirakawa at the Tokyo Institute of Technology, by means of a Ziegler-Natta type catalyst. However the film was found to be insulating in character. In 1977, Shirakawa in Japan, MacDiarmid of the University of Pennsylvania and Heeger of the University of California prepared polyacetylene films with conductivities of the order of 10^3 Siemens per centimetre. Throughout the range of conducting polymers, Polyacetylene has been found to have the highest conductivity [1].

The initial chemically prepared conducting polymers were found to be insoluble, not processible with poor mechanical properties.

Three other conducting polymers which can be electrochemically prepared have been studied extensively since the early 1980's, these are polypyrrole, polythiophene and polyaniline. Researchers at IBM in San José found in 1979 that polypyrrole, previously known as an intractable black powder, could be obtained as a film by electrochemically oxidising pyrrole in acetonitrile. Later polythiophene in 1982, was prepared by anodic oxidation of thiophene by Tourillon and Garnier at Laboratorie de Materiaux Molecularies in Thiais, France and the IBM Group.

Recently great progress has been made in the field of conducting polymers, with a better understanding of the molecular features which are required to achieve and control the electronic properties of the polymer. Several soluble conducting polymers have been developed, being either soluble in water or organic solvents [2].

It is possible to switch these conducting polymers from oxidised to reduced states. All conducting polymers contain extended π-conjugated systems. It has been described that due to this alteration of bonds along the polymeric chain that this gives rise to the formation of a superorbital [3]. When the polymer is in the conductive state, it is the passage of positive charges (holes) or electrons which are injected into the superorbital that gives rise to electronic conduction.

This injection of charge leads to the polymer backbone being either positively or negatively charged, and to maintain charge neutrality, ionic species from solution pass into the polymer matrix. These ionic species are electrostatically held within the polymeric system.

The transformation of a polymer to its conducting state by either chemical oxidation or reduction is often called doping of the polymer, this can be compared to a certain extent of the doping of a semiconductor. Hence there has been an analogy drawn between conducting polymers and semiconductor systems.

Both oxidative and reductive doping are possible, but it is oxidative doping which has been explored more extensively, as the polymers formed by reductive doping have been proven to be unstable in air [4].

Oxidative doping results in electrons being removed from the extended π system of the polymer, resulting in a net positive charge being carried by the organic backbone. Thus oxidative doping is also known as p-doping. For reasons of charge neutrality an anion, known as the counterion or dopant, passes into the polymer system.

The charge on the polymer chain is thought to be mobile, moving along the conjugation of the π backbone of the polymer. It is possible to undope a polymer upon reduction, this gives rise to the counterion passing out of the polymer matrix and simultaneously electrons being injected into the polymer backbone. Upon reduction the polymer becomes undoped and less conductive. Therefore it is possible for a polymer to be switched electrochemically between the conducting and insulating forms.

It is this switching capability of a conducting polymer that is utilised in the various applications of these polymers such as ion gates.

Due to the increasing environmental concern in the past few years a need for new sensors for measuring both physical and chemical parameters has been created. Sensors for a wide range of gases have received much attention, with the monitoring of pollutants, flammable gases and stack gases such as SO_2 and CO_2 being the most important. Several methods for gas detection have been reported. Mass sensitive systems based on incorporating piezoelectric crystals

[5,6] and surface acoustic wave (SAW) devices [7] were first employed as detectors for hydrocarbons in gas chromatography [8].

The development of the Clark oxygen sensor led to the importance of electrochemical detection methods, such as, voltammetry and amperometry. All of the aforementioned methods have been extensively studied in relation to gas sensing. The development of semiconducting polymeric organic materials has shown promise for the measurement of a wide range of toxic gases at room temperature [9].

The conducting polymers have a wide range of applications such as rechargeable batteries, electrochromic devices and within the field of sensor technology. One of the most promising applications of conducting polymers is rechargeable batteries. This area has been pioneered by MacDiarmid, Heeger and co-workers [10]. The advantages in using the polymers as active electrodes are that they are light and flexible and they have the ability to reversibly accept and donate electrical charge. One of the first commercial applications of conducting polymers has been in the high cycle 3 volt battery of Bridgestone Seiko [11] based on Li^+.

The use of conducting polymers as the sensing element within chemical sensors has been explored by Bartlett [12-14]. It is usually the change in conductivity [6] of the polymer upon exposure to certain gases that is monitored. Little work has been done in exploring the interaction between the conductive polymers and organic vapours. However recently [15] Blackwood and Josowicz have examined the mechanisms of the interactions between polypyrrole and

polyphenylene films and various organic vapours by means of uv/visible spectroscopy and by the Kelvin probe technique.

Polypyrrole films electrochemically deposited over interdigital arrays has shown responses to nitrogen dioxide and hydrogen sulphide [9]. The use of conducting polymers within the field of gas sensing has been investigated, but many problems still exist. There is a continuing requirement for specific and sensitive gas sensors that are both durable and their response stable.

Conducting polymers have also been utilised for the production of biosensors. Iwakura et al [16] demonstrated the operation of a biosensor, which was based upon polypyrrole, that measured glucose concentration. One of the most novel and promising applications of conducting polymers is their use in field effect transistor devices. These electronic devices have been developed by Janata et al [17] for gas sensor applications.

As can be seen the field of conducting polymers is both an exciting and growing research field. They have a wide range of applications, which only now are becoming commercially available. As time passed the field has grown substantially. Several review articles [1] along with textbooks [18] are now available on the subject of conducting polymers.

REFERENCES

1. M.G. Kanatziclis, 1990, December 3, Chemical and Engineering News.
2. K. Taha-Bouamri, J.J. Aaron, S. Aeiyach and P.C. Lacaze, J. Chem. Soc., Chem. Commun., (1994), 777-779.
3. G. Bidan, Sensors and Actuators, B6, (1992), 45-56.
4. M.A.Druy, M.F.Rubner and S.P.Walsh, J.Electrochem.Soc.Ext.Abs., 84,(1984) 617.
5. J.M. Slater, E.J. Watt, Analyst, (1991), 116, 1125.
6. J.M. Slater, E.J. Watt, N.J. Freeman, I.P. May, D.J. Weir, Analyst, (1992), 117, 1265.
7. M.S. Niewenhuizen, A.J. Nederlof, A.W. Barendsz, Anal. Chem., (1988), 60, 230-235.
8. W.H. King Jr., Anal. Chem., (1964), 36, 1735.
9. J.J. Miasik, A. Hooper and B.C. Tofield, J. Chem. Soc. Faraday Trans.1, (1986), 82, 1117-1126.
10. P. J. Nigrey, A.G. MacDiarmid and A.J. Heeger, J. Chem. Soc., Chem. Commun, (1979), 594.
11. T. Nakajima and T. Kawagoe, Synthetic Metals, (1989), 28, C629.
12. P. N. Bartlett, P.B.M. Archer and S.K. Ling-Chung, Sensors and Actuators, (1989), 20, 126-139.
13. P.N. Bartlett and S.K. Ling-Chung, Sensors and Actuators, (1989), 20, 287- 292.
14. P.N. Bartlett and S.K. Ling-Chung, Sensors and Actuators, (1989), 19, 141- 150.

15. D. Blackwood and M. Josowicz, J. Phys. Chem., (1991), 95, 493-502.

16. C. Iwakura, Y. Kajiya and H. Yoneyama. J. Chem. Soc., Chem. Commun., 15, (1988), 1019.

17. M. Josowicz, J. Janata, K. Ashley and S. Pons, Anal. Chem.,(1987), 59, 253-258.

18. T.A. Skotheim, Handbook of Conducting Polymers, M. Dekker, New York, (1986).

CHAPTER 2

ELECTROCHEMICAL CHARACTERISATION OF CONDUCTING POLYMER LAYERS

2.1 INTRODUCTION

Over the past thirty years, modified electrodes have received widespread attention. An important property of all electrode materials is that they have the ability to transfer charge. Recently many electrodes have been modified with polymers (containing redox species) where the electron moves by transfer between discrete centres. For example $[Fe(CN)_6]^{4-}$, $[IrCl_6]^{2-}$ in quaternised PVP. Conducting polymers such as polypyrrole, polyaniline and polythiophene have also been used.

One of the most extensively studied of these is polypyrrole. This conducting polymer was first prepared as a powder [1,2] in 1916, by the action of hydrogen peroxide on the pyrrole monomer. However it was not until 1968 [3] that it was reported by Dall Olio that the electrochemical oxidation of pyrrole in aqueous sulphuric acid gave rise to a conducting polymer film on a platinum electrode. However the film was found to be brittle with a conductivity of 8 Siemens per

cm at room temperature. Little interest was shown in these results, and it was not until 1979 when Diaz et al [4-6] showed that in acetonitrile containing about 1% H_2O stable polypyrrole films were formed by the anodic oxidation of pyrrole. The films obtained showed metal like conductivity. This sparked off a great deal of research within this field. The preparation of these polymers by galvonostatic or potentiostatic methods has been carried out [4,6].

In 1982 Street et al [7] were unsuccessful in trying to grow polypyrrole films electrochemically under anhydrous and oxygen free conditions in the absence of electrolyte. However Street et al found that in the presence of silver salts as the electrolyte, pyrrole polymers could be grown.

The electrochemical oxidation of pyrrole is irreversible following a complex mechanism in both aqueous [8] and non aqueous solvents. In aqueous media the onset of the pyrrole oxidation commences around 0.65V vs. SCE. The curves have multiple peaks with peak potentials lying between 0.8V and 1.1V vs. SCE. For acetonitrile solutions peak potentials appear between 1.0 and 1.3V vs. SCE. It is important that the potential sweep upon formation of the polymer, does not go beyond the peak potentials, as this can lead to an irreversible loss of activity.

It is still unclear by which mechanism the polymer film was formed. It was reported previously [9] that oxidation of the dopant anion might be the first step in the polymerization process. This mechanism was proved to be unacceptable as the potential at which most common dopant anions (BF_4^-, ClO_4^-, NO_3^-, SO_4^{2-}) are oxidized are more positive than the potential at which the polypyrrole films are formed.

Figure 2.1(a) shows the proposed mechanism for the electrochemical formation of polypyrrole [10]. The first step involves the creation of a cation radical by the oxidation of pyrrole [10]. Diaz et al [11, 12] pointed to a radical-radical coupling step (Step (a) in Scheme) rather than a radical-monomer mechanism (Step (b) in Scheme) as proposed by Inoue and Yamase [10]. Nucleation has been shown to explain the formation and growth of the polypyrrole layer onto the electrode surface. The theory of nucleation has been applied to the cathodic deposition of metals [13]. Cyclic voltammetry and Potential step experiments have been used [12, 8] to characterise the nucleation mechanism in the formation of pyrrole.

As mentioned previously upon oxidation of the pyrrole monomer to form a polycation, an anion passes into the polymer matrix for reasons of charge neutrality. This removal of electrons from the polymer backbone leads to two types of defects, namely polarons and bipolarons. These defects shall be discussed in detail in Chapter 3, where the behaviour of various polypyrrole layers (upon electrochemical switching) are investigated by visible spectroscopy. The doping process of a polymer can be carried out chemically or electrochemically. The original oxidative dopants, that is, dopants that remove an electron from the polymer matrix, included strong and weak agents such as AsF_5 and I_2 [14]. The identities of the anionic counterions is not straight forward. By Mössbauer spectroscopy SbF_6^-, SbF_5 an SbF_3 have been identified in polyacetylene doped by SbF_5 [15]. Also for polyacetylene doped by $FeCl_3$ [16], $FeCl_4^-$ and $FeCl_2$ have been identified within the polymer.

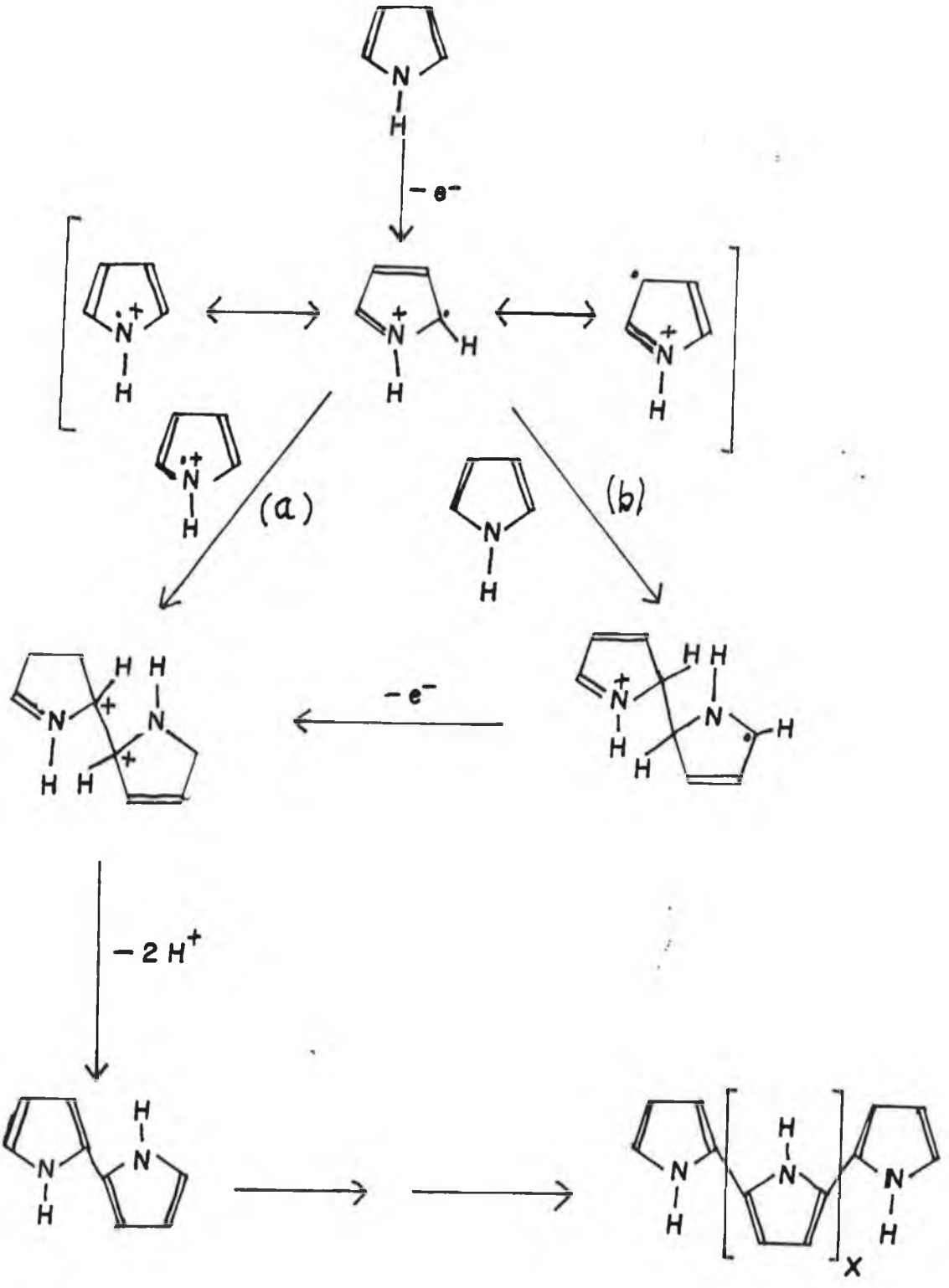

Figure 2.1. Proposed Mechanism for the oxidative polymerisation of pyrrole. Route (a) represents the radical-radical coupling step and (b) represents the radical-monomer coupling route.

The identities of the counterions from reductive doping, that is, where electrons are donated into the polymer matrix, are easier to identify. An example of a donor doping reagent is sodium napthalide dissolved in tetrahydrofuran [17]. The polymer is reduced by the napthalide radical anion and the sodium cation is the counterion.

However, has already been mentioned previously, reductive doping leads to films that are unstable in air. The conductivity of these conjugated organic polymers in their pure undoped state is comparable to that of electronic insulators. Systems such as poly (p-phenylene) and poly (p-phenylene sulphide) have conductivities in the undoped state of $< 10^{-12} S\ cm^{-1}$ [14,18,19]. The doping process of the conjugated polymers, leads to higher conductivities, by increasing the carrier concentration. Doping leads to defects present within the polymer matrix, as already mentioned. It is the passage of these defects along and between chains that lead to increased conductivity. It is important that the defect, namely a positive charge, can overcome the coulombic binding energy to the dopant anion so that movement along the chain can be accomplished.

The properties of electrical conductivities and carrier type and transport will be discussed in more detail in Chapters 3 and 4.

The electrochemical switching of the polymer between oxidised and reduced states can be investigated by cyclic voltammetry. The apparent formal potential of the polymer is found to be dependent upon the dopant anion present in the matrix. Electrochemically deposited polypyrrole layers in the presence of background electrolyte with small anions exhibit inclusion and expulsion of

anions on oxidation and reduction respectively. However, if larger anions are used as dopants, such as poly (4-styrene sulphonate) [20,21], polyvinylsulphonate [22], copper tetrasulphonated phthalocyanine [23,24], cobalt carboxy phenylporphyrin complexes [25], ferrocyanide [26-29], or large surfactants such as dodecylsulphonates [30-32], it was found that when the layers are oxidised and reduced, the movement of cations primarily maintains electroneutrality within the layers. Because metal-containing porphyrins and phthalocyanines exhibit electrocatalytic behaviour [33-35], their immobilisation into conducting layers and subsequent stability is of interest.

In this Chapter the electrochemical behaviour of two polypyrrole layers doped with bulky anions, namely dodecylbenzenesulphonate (DBS) and Copper(II) tetrasulphonated phthalocyanine (CuTSP) anions is described. Electrochemical characterization of these two layers is undertaken, by means of cyclic voltammetry. For the polypyrrole tetrasulphonated phthalocyanine layer, the process of cation inclusion and expulsion, upon electrochemical switching is investigated. A cation concentration, pH, scan rate and temperature study are undertaken upon this layer. For the polypyrrole dodecylbenzenesulphonate layer, the nature of the charge carrying ions and the presence of the so called 'double layer charging current' is investigated.

2.2 THEORY OF CYCLIC VOLTAMMETRY

Cyclic voltammetry is a potential sweep technique which has been applied to an increasing range of systems. It is possible to determine specific kinetic parameters for a particular mechanism by means of cyclic voltammetry. However, this technique and other sweep techniques have proved most useful in mechanistic investigations. Cyclic voltammetry is the technique of choice when studying the formation of cations/anions in a new system.

Cyclic voltammetry is an extension of linear sweep voltammetry. The latter involves sweeping the potential, at a known rate ν, between two potential limits, then stopping the sweep. The potential limits that can be applied depends on the electrodes employed, the solvent and the background electrolyte.

The potential time profiles used in cyclic voltammetry is shown in Figure 2.2(a). In this case the waveform is the same as in linear sweep voltammetry, however on reaching E_2 the sweep is reversed. When the initial potential, E_1, is reached again, the sweep can be terminated, reversed or continued on to another potential E_3. In cyclic voltammetry the resultant current is monitored as a function of the applied potential.

A variety of sweep rates are used in cyclic voltammetry experiments, ranging from a few millivolts per second up to a few hundred volts per second. However rates of several thousand Vs^{-1} have been employed, but this introduces

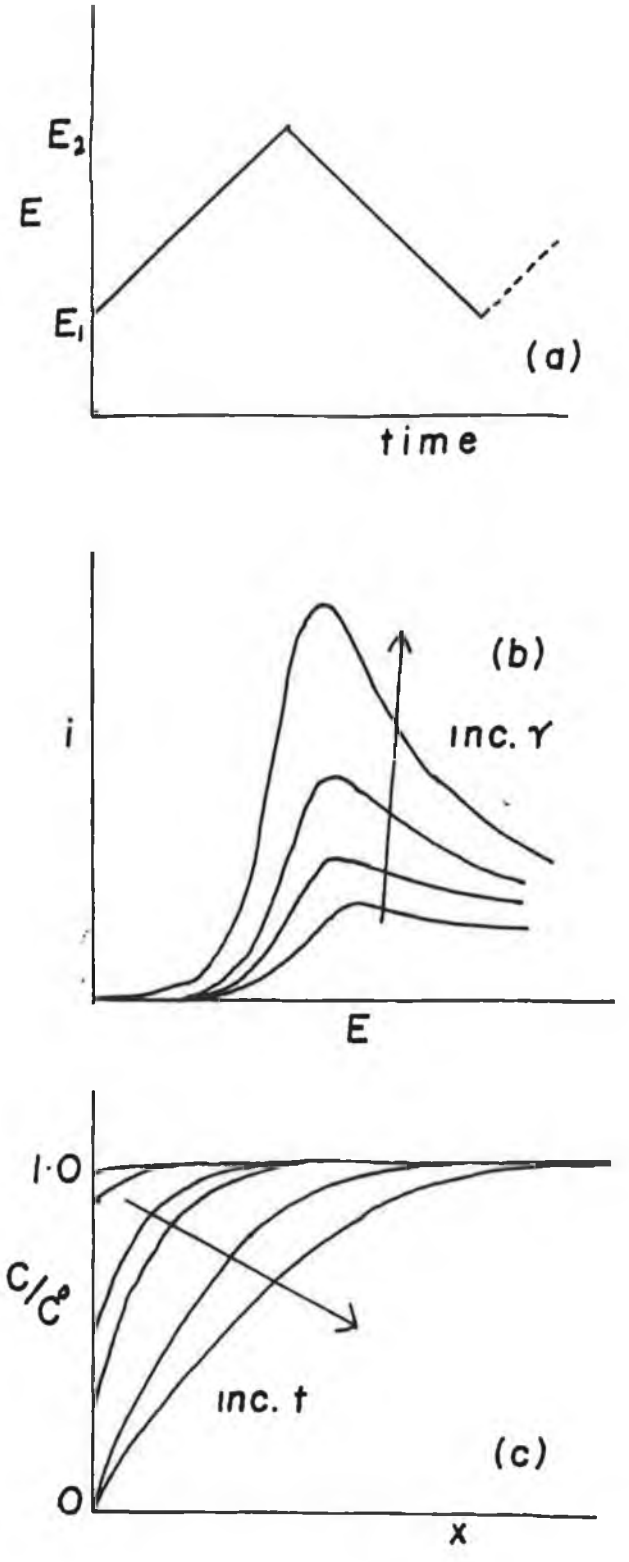

Figure 2.2 (a) Potential Time profiles used for cyclic voltammetry.

Figure 2.2 (b) A Series of linear sweep voltammograms for the reaction $O + ne^- \rightarrow R$, at several potential scan rates.

Figure 2.2 (c) Shows the concentration profiles for the species O during a sweep experiment.

the problem of double layer charging current and iR drop. For this reason microelectrodes are used for such large scan rates [36].

To see what form the voltammograms take, it is convenient to consider the case of a reversible reaction of the type described by the reduction.

$$O + ne^- \rightarrow R \qquad E_F \qquad \ldots\ldots\ldots \qquad (2.1)$$

The formal potential E_F is defined as the potential of the cell when the ratio $\frac{[O]}{[R]}$ is equal to 1, where [O] and [R] represent the concentrations of the species O and R respectively.

Figure 2.2(b) shows a series of voltammograms for the reaction described by equation (2.1) at different potential sweep rates. To explain the shapes of these voltammograms, the concentration profiles of O as a function of potential must be considered. It is assumed that the formal potential of the couple lies between the limits E_1 and E_2.

For a reversible reaction the ratio of $\frac{[O]}{[R]}$ is given by the Nernst equation, at the electrode surface. Figure 2.2(c) shows the concentration profiles for the species O during a sweep experiment. Initially the working electrode is held at a potential where no faradaic current flows, that is no reduction occurs. Let this potential be E_2. As the potential is made more negative, the surface

concentrations of both species must change as the Nernst equation is obeyed. Hence the region close to the electrode known as the Nernst diffusion layer. As the potential is being swept further negative the diffusion layer begins to develop out in solution. At high sweep rates the diffusion layer does not have time to relax out into solution. As a result of this the concentration profiles are not linear as can be seen from Figure 2.2(c).

Diffusion of species O from bulk solution begins but at the same time the electrode potential is changing and thus the surface concentration of O is decreased until it reaches zero.

The concentration gradient at the surface, for any given potential, is greater than for the steady state case, therefore the currents magnitude is greater. However once the concentration of O reaches zero, the concentration gradient decreases and hence the current decreases. These processes give rise to a peaked response, as seen in Figure 2.3.

In cyclic voltammetry, the i-E response during the reverse scan is also recorded. On the reverse sweep when the potential approaches E_F, the species R at the electrode is reoxidised, due to the fact that the surface concentrations must change so as Nernstian behaviour is obeyed, and a reverse current is obtained. The current on the reverse sweep will also exhibit a peaked response, using similar arguments as above. There are several diagnostic tests that can be applied to a system to see if Nernstian equilibrium is maintained.

For a reversible system the peak separation ΔE_P (mV) is close to $^{58}/_{n}$ mV at

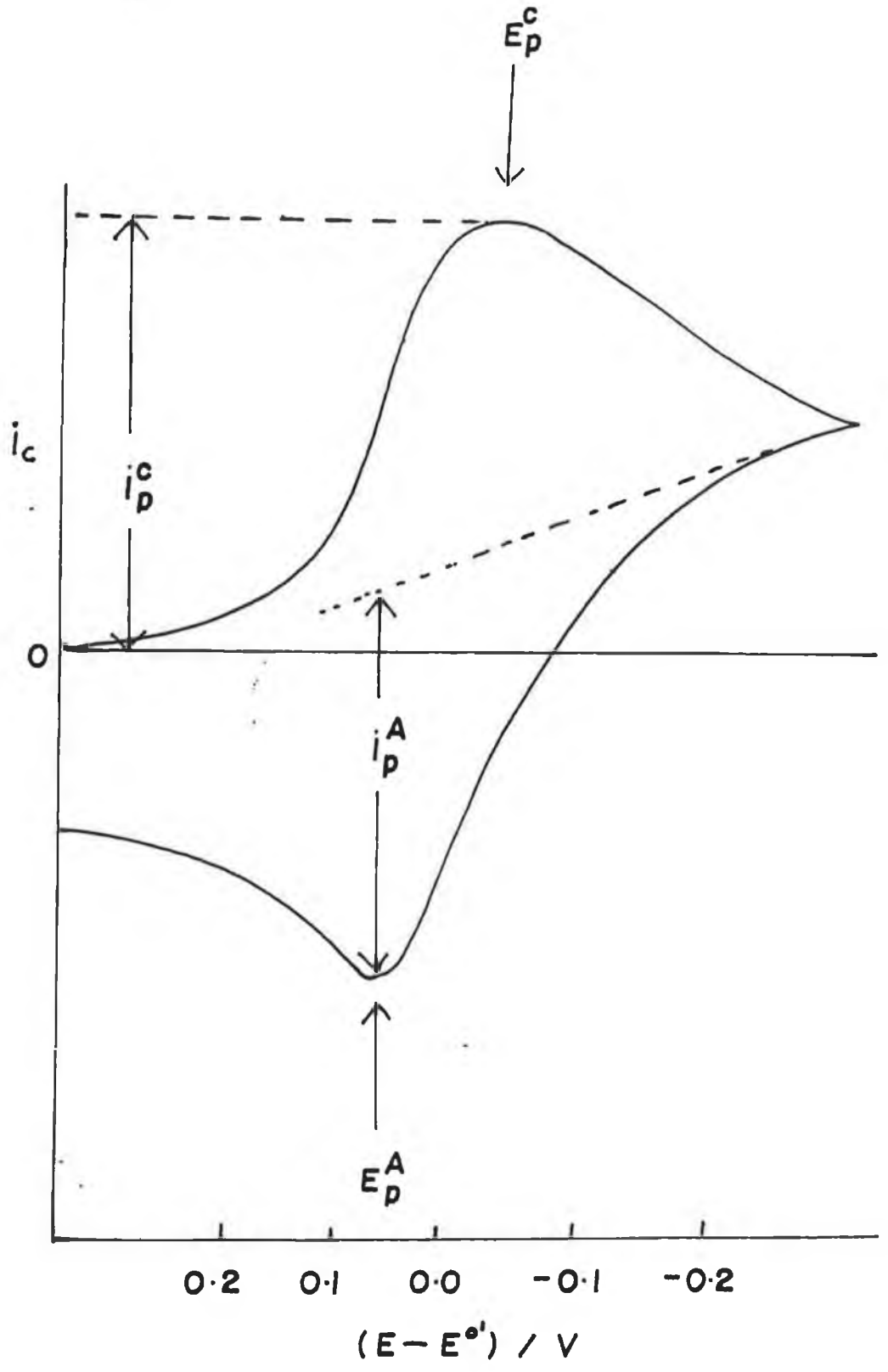

Figure 2.3 Cyclic Voltammogram for a reversible process $O + ne^- \rightarrow R$. Initially only O present in solution.

25°C, where n is the number of electrons transferred. A characteristic for a reversible reaction, is that the peak potentials do not shift in value with changing scan rate, but upon decreasing the scan rate, the peak current will decrease.

Two characteristic parameters for a cyclic voltammogram are the peak potential and peak current. Randles and Sevcik have developed an equation that relates the peak current to the scan rate for a reduction species, at 298K [37].

$$i_p = 2.69 \times 10^5 \, n^{3/2} \, A \, \sqrt{D_O} \, \sqrt{\nu} \, C_O \quad \ldots\ldots\ldots \quad (2.2)$$

Where

i_p	=	**amps**
n	=	**no. of electrons transferred**
A	=	**electrode area (cm^2)**
D_O	=	**diffusion coefficient for species O (cm^2s^{-1})**
v	=	**scan rate (V/s)**
C_O	=	**concentration of electroactive species O ($mol\ cm^{-3}$)**

The cathodic peak current can be measured directly from the zero-current axis, however the anodic peak current cannot be measured from the baseline. The direct graphical determination of i_p^a is seen in Figure 2.3.
Nicholson developed a direct determination of the anodic peak current [38].

$$\frac{i_{pa}}{i_{pc}} = \frac{(i_{pa})_o}{i_{pc}} + \frac{0.485\,(isp)_o}{i_{pc}} + 0.086 \quad \ldots\ldots\ldots \quad (2.3)$$

Where

i_{pa}	=	**anodic peak current**
i_{pc}	=	**cathodic peak current**
$(i_{pa})_o$	=	**uncorrected anodic peak current**
$(i_{sp})_o$	=	**uncorrected current at the switching potential**

These parameters are illustrated in the cyclic voltammogram in Figure 2.3.

For a reversible system, the rate of electron transfer is greater than the rate of mass transport, so that Nernstian equilibrium is always maintained at the electrode surface. For an irreversible system, the electron transfer is the rate determining step and Nernstian equilibrium is not maintained. In a totally irreversible system, a reverse peak may be absent due to the product undergoing a further chemical reaction. The peak current is related to the scan rate by [39,40].

$$i_p = (2.99 \times 10^5)\, n\, (x n_a)^{1/2}\, A\, C\, D^{1/2}\, \nu^{1/2} \quad \ldots\ldots \quad (2.4)$$

Where

x	=	**transfer coefficient**
n	=	**number of electrons involved in the overall step**
n_a	=	**number of electrons involved in the rate determining step**

The absence of a reverse peak is not a definite mark of a irreversible system, several other diagnostic tests can be applied. For a reversible case it was seen

that the peak potential does not vary with scan rate, whereas for an irreversible system Ep is a function of scan rate. It shifts in a negative direction by $30/xn_a$ mV for each decade increase in ν at 25°C [39].

It is possible for a process that is reversible at low scan rates to become irreversible at higher scan rates. This is due to the fact that at low sweep rates electron transfer is able to maintain Nernstian equilibrium, however at higher sweep rates the rate of mass transport increases and becomes greater than that of electron transfer. When a system changes from a reversible to an irreversible one, it passes through a region known as quasi-reversible.

For a quasi-reversible system, the peak to peak separation is greater than $59/_n$ mV and it increases with increasing scan rate, also the ratio of the anodic to cathodic peak current should be 1, if $x_a = x_c = 0.5$.

Cyclic voltammetry is not the ideal technique for the estimation of kinetic parameters such as heterogeneous rate constants, k^θ.
However it is possible to obtain k^θ values from peak to peak separation values. Curves have been obtained [38], where $n\Delta E_p$ is a function of the variable ψ, which is defined by

$$\psi = \frac{(RT)^{1/2}\ k^\theta}{(nFD\pi\nu)^{1/2}} \qquad \text{.....} \qquad (2.5)$$

It is possible from these working curves, from a knowledge of the peak to peak separation, to obtain values of k^θ for the system under study [41].

2.3. EXPERIMENTAL

All chemicals employed were reagent grade. Pyrrole was distilled and stored under nitrogen in the dark. Electrochemical experiments were performed in a single compartment three electrode cell. A saturated calomel electrode was used as the reference electrode. A carbon rod was used as the auxiliary and a platinum disk (d = 3mm) as the working electrode. The working electrode was polished, prior to layer formation, with 0.3μm alumina. All solutions employed in electrochemical experiments were degassed with oxygen free nitrogen for approximately 10 minutes.

A ramp generator (H.B. Thompson 16 bit) a potentiostat (Edt ECP 100) and an electronic integrator (Sycopel DP301S) linked to a J.J. LLoyd PL3 X-Y recorder were used for cyclic voltammetry. All voltammetric experiments were carried out at room temperature.

2.3.1 POLYMER LAYER FORMATION

A fresh solution of 0.1M pyrrole and 1.3 x 10^{-3}M Cu(ll) TSP was degassed with oxygen free nitrogen for approximately 10 minutes. The potential of the platinum disk working electrode was held at 0.9V until 25mC of charge had been passed.

The layer was removed and rinsed with deionized water. The electrode was then immediately transferred to a fresh degassed solution of background electrolyte for the cation concentration studies.

Polypyrrole chloride layer was formed from a solution of 0.1M pyrrole and 0.1M NaCl by holding the potential of the working platinum disk electrode at 0.8V until 25mC of charge had been deposited.

Polypyrrole dodecylbenzenesulphonate and polypyrrole perchlorate were formed from solutions of 0.1M pyrrole and 0.1M dopant anion by scanning continuously between 0V and 0.8V until 20mC of charge had passed.

2.4 RESULTS AND DISCUSSION

The doping and undoping of a conducting polymer can be achieved by electrochemically switching the polymer between an oxidised state and a reduced state.

Using cyclic voltammetry the characteristic switching between insulator and conductor for a polypyrrole chloride layer can be seen.

Figure 2.4 shows the cyclic voltammogram (CV) of a PPCl layer in an aqueous solution of NaCl (0.1M). When the polymer is reduced, the anion is expelled from the layer into solution, this is seen by the presence of a reduction peak in the CV.

Conversely when the layer is reoxidised the anion passes back into the layer, this accounts for the presence of an oxidation peak. This process of anions moving in and out of the layer can be depicted by the reaction mechanism,

$$nX^-_{soln} + nPy^0 \rightarrow n(Py^+X^-) + ne^- \quad \ldots\ldots\ldots \quad (2.6)$$

$$n(Py^+X^-) + ne^- \rightarrow nPy^0 + nX^-_{soln} \quad \ldots\ldots\ldots \quad (2.7)$$

Scheme (2.6) and (2.7) show oxidation and reduction of the polymer respectively. This passage of anions into the layer occurs both to maintain charge neutrality within the polymer matrix and also for double layer charging of the conducting strands within the polymer. The presence of this capacitive or

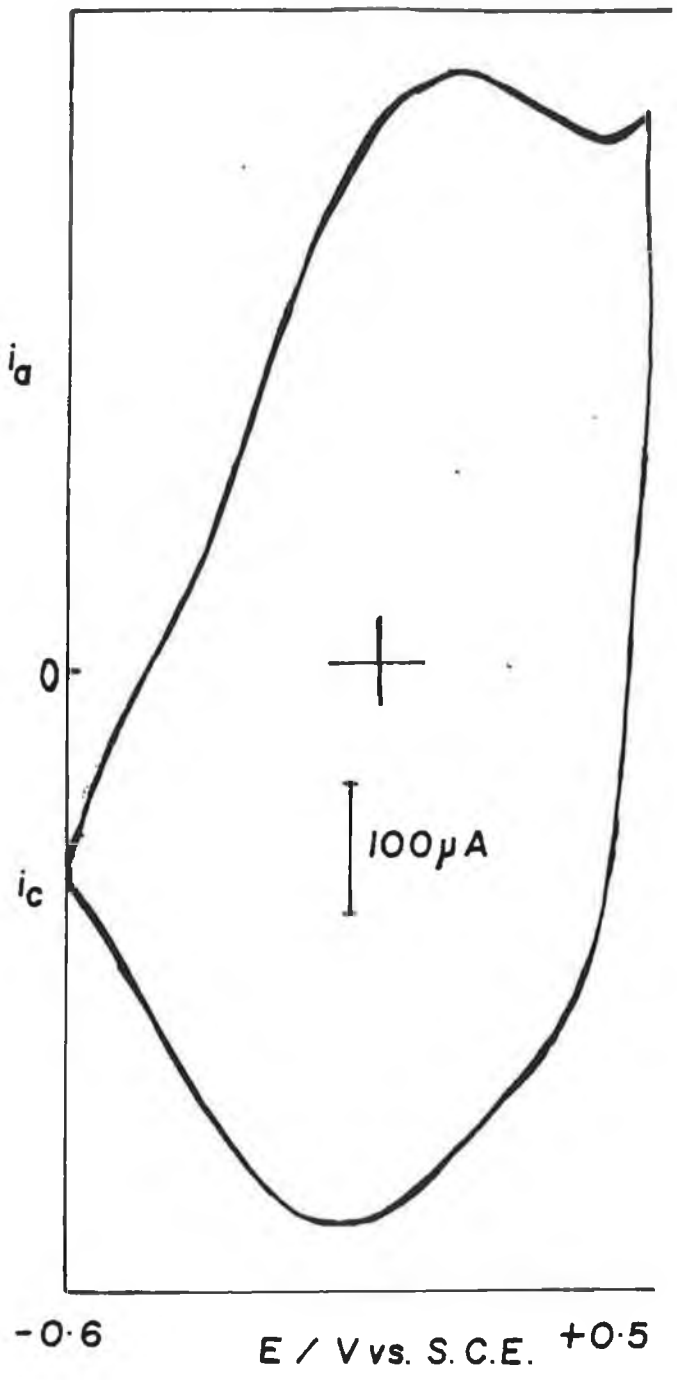

Figure 2.4 Cyclic voltammogram of a PPCl layer in a degassed aqueous solution of 0.1M NaCl. The layer being previously deposited by holding the potential at 0.8V in 0.1M pyrrole and 0.1M NaCl. Scan Rate = 100mV/s.

non-faradaic current is characteristic of all conducting polymers and is observed as an apparent double layer charging component of the voltammogram, as seen in Figure 2.4. This component of the current will be discussed in more detail in Chapter Three.

Metal tetrasulphonated phthalocyanines (TSP) were chosen as an option for the dopant anion in the formation of a polypyrrole layer, since phthalocyanines were found to exhibit catalytic properties [42,43]. Copper(II) TSP was employed, which was found to possess no electrochemistry in the potential range under study. The formation of polypyrrole layers in Cl^- electrolyte are usually carried out in solutions of reasonably high concentration; 0.1 mol dm^{-3} or greater, as already mentioned for the polypyrrole chloride layer. It was found that even with low concentrations (1.3×10^{-3} mol dm^{-3}) of Copper(II) phthalocyanine - $3,4^{I}$, 4^{II}, 4^{III}, - tetrasulphonate (TSP), that stable polypyrrole layers could be formed.

Figure 2.5(a) shows the C.V. of a PPTSP layer subsequently run in a degassed aqueous solution of NaCl (0.1M). It can be seen that the formal potential of the polymer occurs at a much more negative potential (E_f = -0.41V, in 0.1M NaCl) compared to polypyrrole chloride (E_f = +0.04V, in 0.1M NaCl).
It was found that there was no release of the TSP anion into the electrolyte on sweeping the potential continuously. This led to the conclusion that cation insertion was a possible explanation for the results obtained. This theory has previously been reported for a polypyrrole cobalt TSP layer [44]. According to this process when the polymer is reduced to PP^{o} the TSP anion instead of passing into bulk solution remains within the layer and a cation, from the

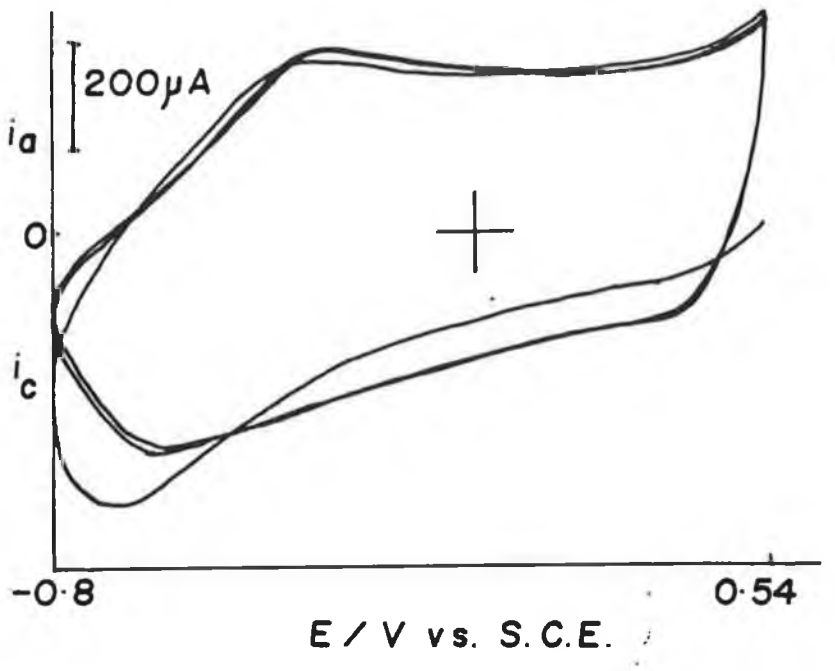

Figure 2.5 (a) Cyclic voltammogram of a PPTSP layer in a degassed aqueous solution of NaCl (0.1M). The layer being previously deposited by holding the potential at 0.9V in 0.1M pyrrole and 1.3 x 10^{-3} M Cu(II) TSP.
Scan Rate = 100mV/s.

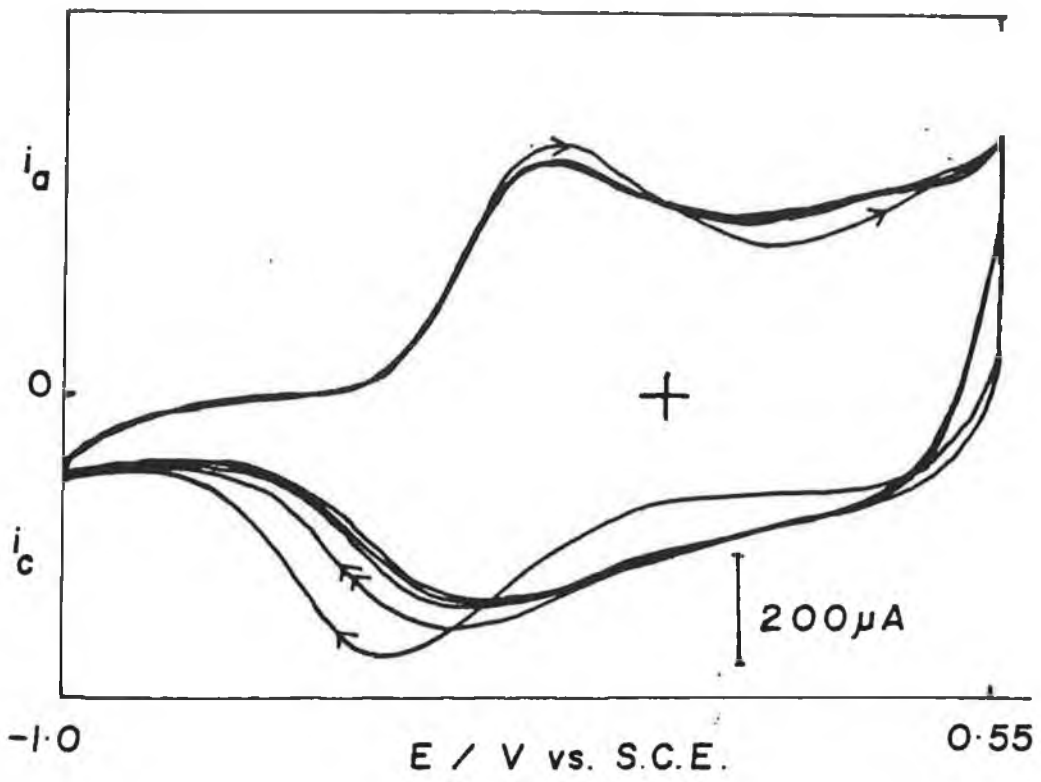

Figure 2.5 (b) Cyclic voltammogram of a polypyrrole layer, previously formed as described in Figure 2.5 (a), in a degassed aqueous solution of 0.1M CsCl.
Scan Rate = 100mV/s.

supporting electrolyte, is inserted into the layer for reasons of charge neutrality. This process of cation inclusion and expulsion has already been introduced.

The reaction mechanisms can be depicted by (2.8) and (2.9).

$$nNa^{+}_{soln} + ne^{-} + (PP^{+})n(TSP)^{n-} \rightarrow PP^{o}\, n(TSP)^{n-}\, (Na^{+})^{n} \quad \ldots. (2.8)$$

$$PP^{o}\, n(TSP)^{n-}\, (Na^{+})^{n} \rightarrow nNa^{+}_{soln} + ne^{-} + (PP^{+})n\, (TSP)^{n-} \quad \ldots. (2.9)$$

Figure 2.5(b) shows the CV of the PPTSP layer in a degassed aqueous solution of CsCl(0.1M). It is not perfect thin layer behaviour since $Ep_a - Ep_c = O$, indicating a possible resistance effect or that the diffusion layer remains within the layer. It can be seen that the formal potential of the polymer has shifted to a more positive value (E_p = -0.235V) as compared to the PPTSP layer run in NaCl(0.1M). It can also be seen that there is a difference in the shape of the CV during the first few scans and for the final scan. This effect has been seen elsewhere [29].

2.4.1 CATION CONCENTRATION STUDY

The cation concentration study was performed by oxidising and reducing the layer according to Scheme 2.3 and 2.4 respectively. The effect of changing the concentration of background electrolyte on the voltammetric behaviour of the polymer is shown in Figure 2.6 for a range of cations (Li^{+}, Na^{+}, K^{+}, Cs^{+}). The resulting cyclic voltammograms may be compared to those in previous work where polypyrrole incorporating $[Fe(CN)_6]^{4-}$ as an anion was cycled under similar conditions of differing electrolytes [29]. The principal difference

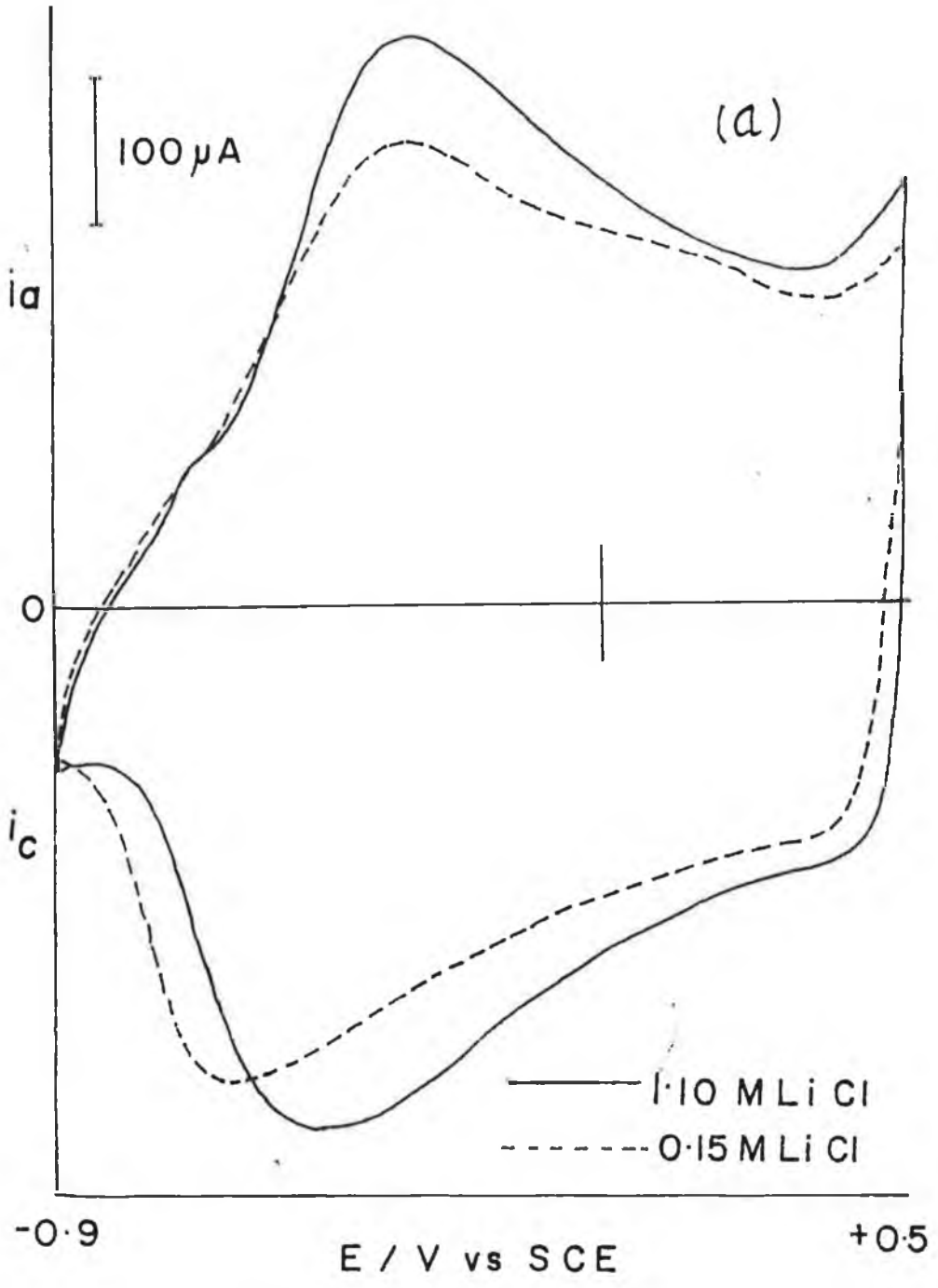

Figure 2.6 Cyclic voltammogram of a PPTSP layer, formed from an aqueous solution of pyrrole (0.1M) and 1.3 x 10^{-3}M Cu(II) TSP, cycled in a degassed aqueous solution of

(a) 0.15M LiCl (--) and 1.10M LiCl (-)

(b) 0.15M NaCl (--) and 1.10M NaCl (-)

(c) 0.15M KCl (--) and 1.10M KCl (-)

(d) 0.15M CsCl (--) and 1.10M CsCl (-)

Scan Rate = 100mV/s.

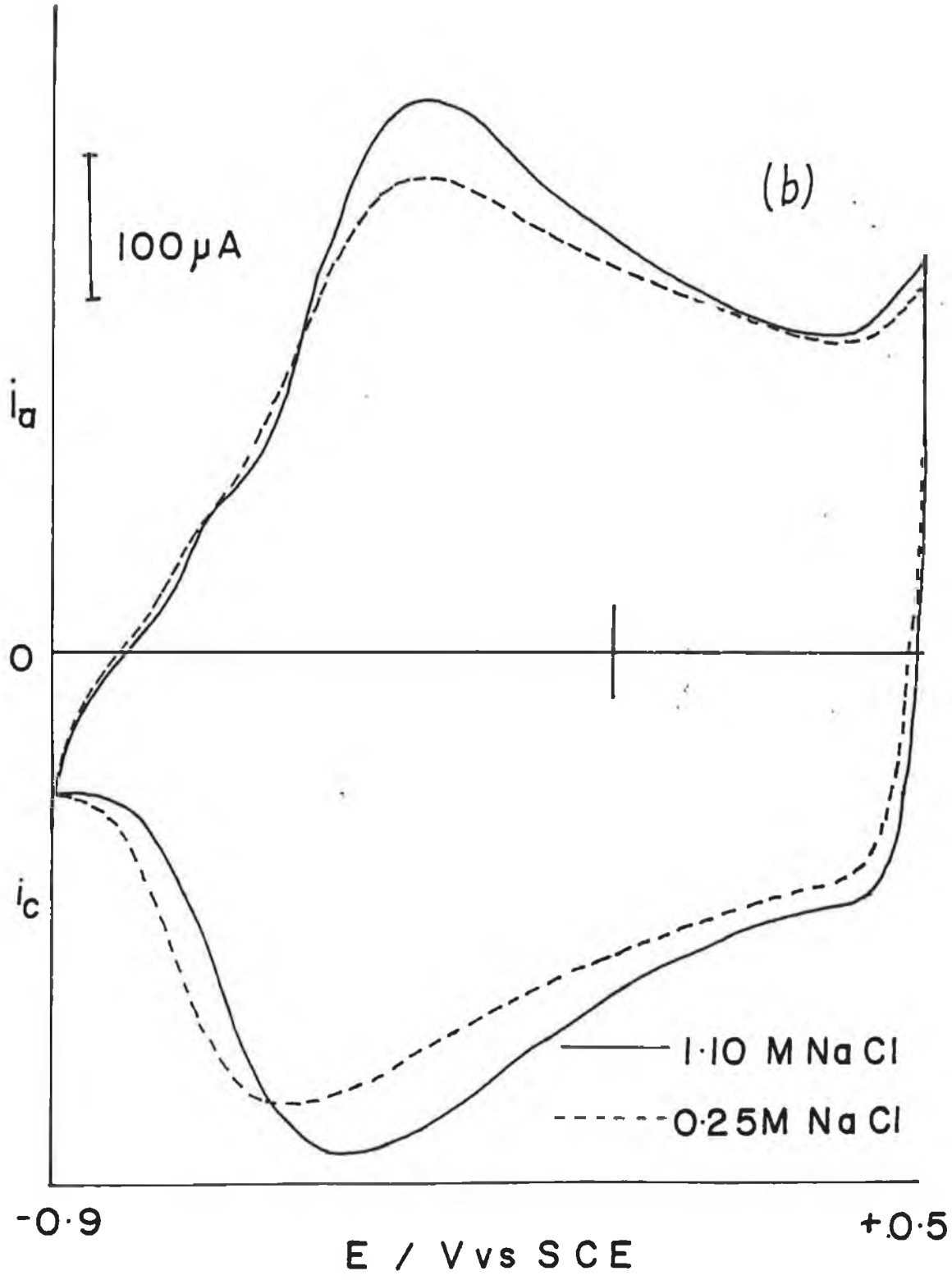
100 μA
(b)
i_a
0
i_c
1·10 M Na Cl
0·25M Na Cl
-0·9
+0·5
E / V vs S C E

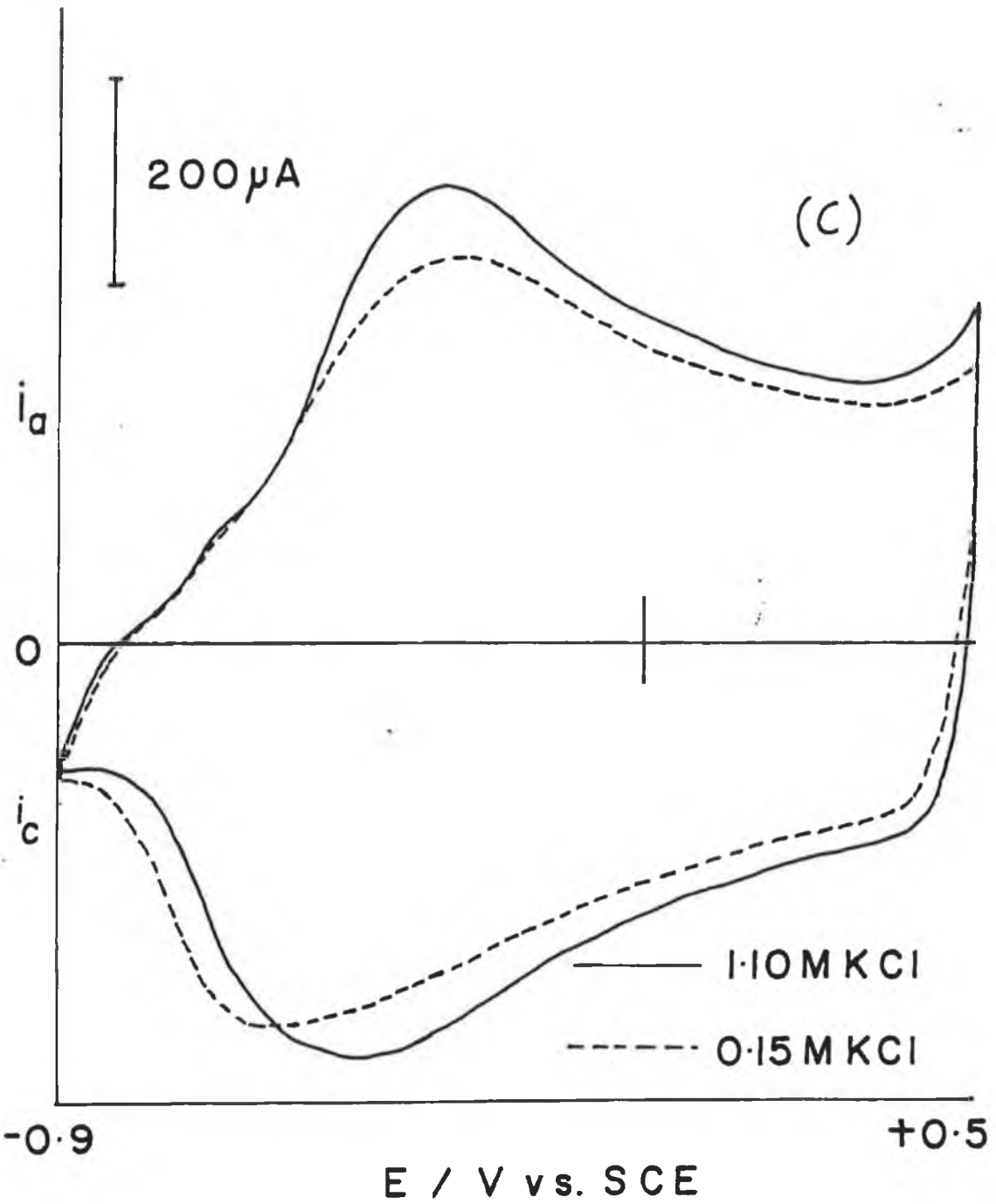
200μA
(C)
i_a
0
i_c
1·10 M KCl
0·15 M KCl
-0·9
+0·5
E / V vs. SCE

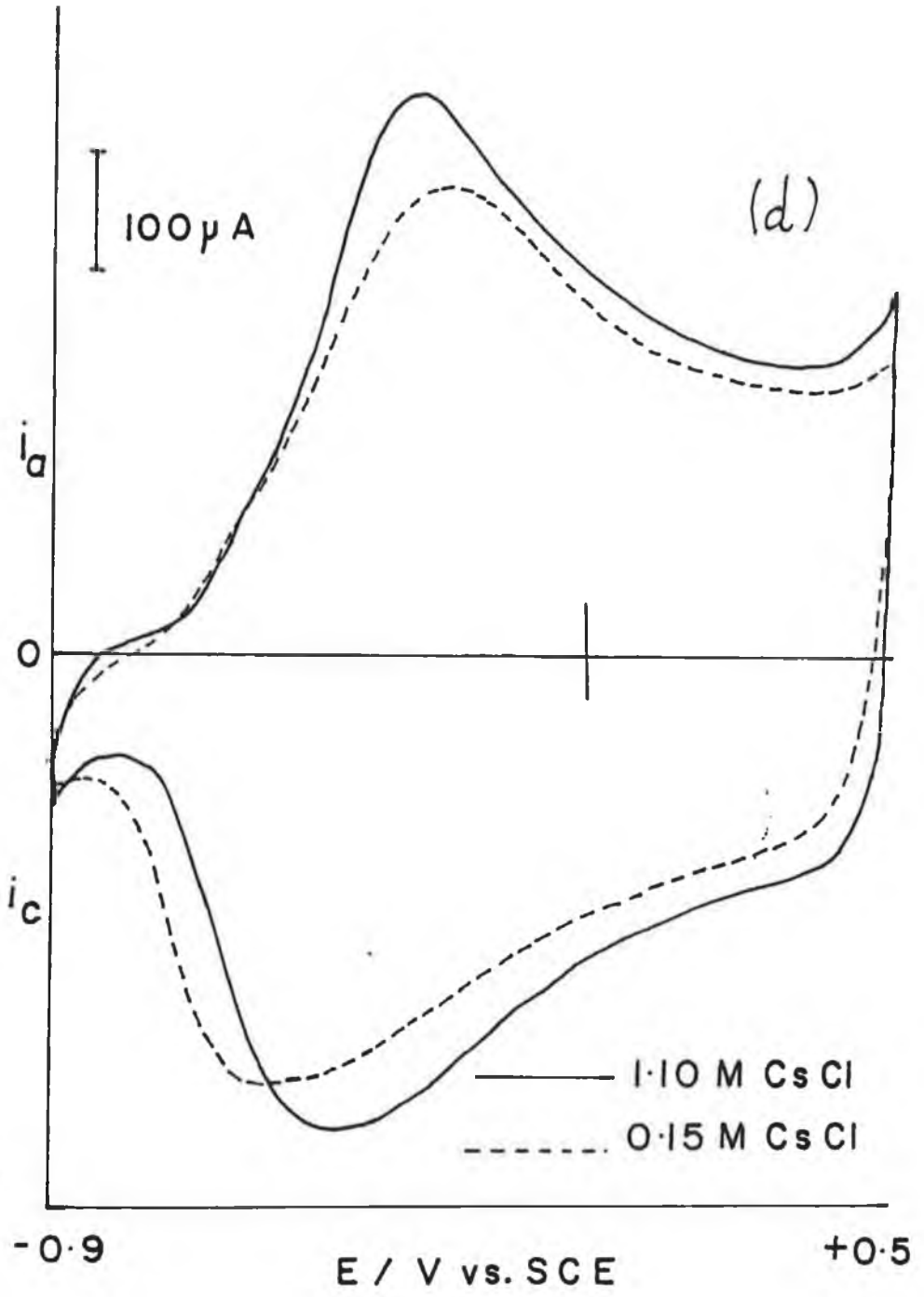
100 μ A
(d)
i_a
0
i_c
1·10 M Cs Cl
0·15 M Cs Cl
-0·9
E / V vs. SCE
+0·5

between the PPFCN layers and the PPTSP layers is that the PPFCN layers were cycled in a potential region where the polypyrrole was always in an oxidised form. The $[Fe(CN)_6]^{4-}$ electrochemistry was under study. In the case of the PPTSP layers however, it is the layer itself which is undergoing oxidation and reduction rather than a probe molecule within the layer. In the case of the PPFCN layers, a 'breaking-in' step was required, between the formation of the PPFCN layer and achieving a 'steady state' continuous cyclic voltammogram. In the case of the PPTSP, this breaking in step was not required. A general similarity between the use of a probe molecule (PPFCN) and looking at the layer electrochemistry itself is that the reduction peak shifts more than the oxidation peak with increasing electrolyte concentration. Looking at Figure 2.6 the cathodic peak shifts while the position of the anodic peak does not change greatly with electrolyte concentration. The reason for the small shift in the anodic peak may be due to a combination of decrease in peak separation and shift of peaks to more positive potentials with increasing electrolyte concentration.

It is also seen that there is no great difference in voltammetric behaviour from one cation to the next, (Figure 2.6(a)-(d)) indicating that the layer is porous enough for alkali cations. It can also be seen from Figure 2.6 that the current more positive of the peaks, the so called 'double layer charging current' is quite constant and does not vary much in magnitude with electrolyte concentration.

It is this cation movement in and out of the layer which is under study. Several electroactive probes have previously been incorporated into polypyrrole layers for permeability studies [29,45]. Redox couples have also been incorporated in Nafion coatings on electrodes transfer [46,47].

Replicate analysis was carried out to see if Nernstian behaviour was followed, as for $[Os(bpy)_3]^{2+}$ in Nafion [48]. The peak potentials of the polymer as a function of $\log[C_b^+]$, where C_b^+ is the cation concentration in bulk solution, are plotted for the anodic (Figure 2.7(a)) and cathodic (Figure 2.7(b)) peaks for different cations. A linear plot was obtained between $[C_b^+] = 0.15M$ and 1.10M for both peak potentials for all four cations studied. Within this concentration range the CV's are reasonably symmetrical, however at low cation concentrations there is a divergence away from linearity, with associated asymmetry in the CV's shape. This effect has previously been reported for a polypyrrole layer containing $[Fe(CN)_6]^{4-}$ [29].

Table 2.1 lists the slopes of the peak potentials versus $\log[C_b^+]$ for the four alkali metal cations, along with the polymer's apparent formal potential. The dominant shift in the cathodic peak over the anodic peak is reflected in the slope values. It can be seen that upon cation insertion no trend exists as a function of ionic or hydrated cation size, contrary to previously reported [29].

It can be seen that the formal potential, $(E_p^a + E_p^c)/ 2$ obeys equation 2.8 since the slope of E_f vs $\log[C_b^+]$ is close to 59mV, see Table 2.1.

However there is a trend between the nature of the cation and the E_f values calculated as being halfway between the forward and reverse peaks. The slope associated with E_f varies least for Cs^+ (greatest ionic radius) and most for Li^+ (least ionic radius) for PPTSP. This follows the same trend as was observed for the electrochemistry of $[Fe(CN)_6]^{4-}$ within polypyrrole as a function of electrolyte nature. Plots for E_f are seen in Figure 2.7(c).

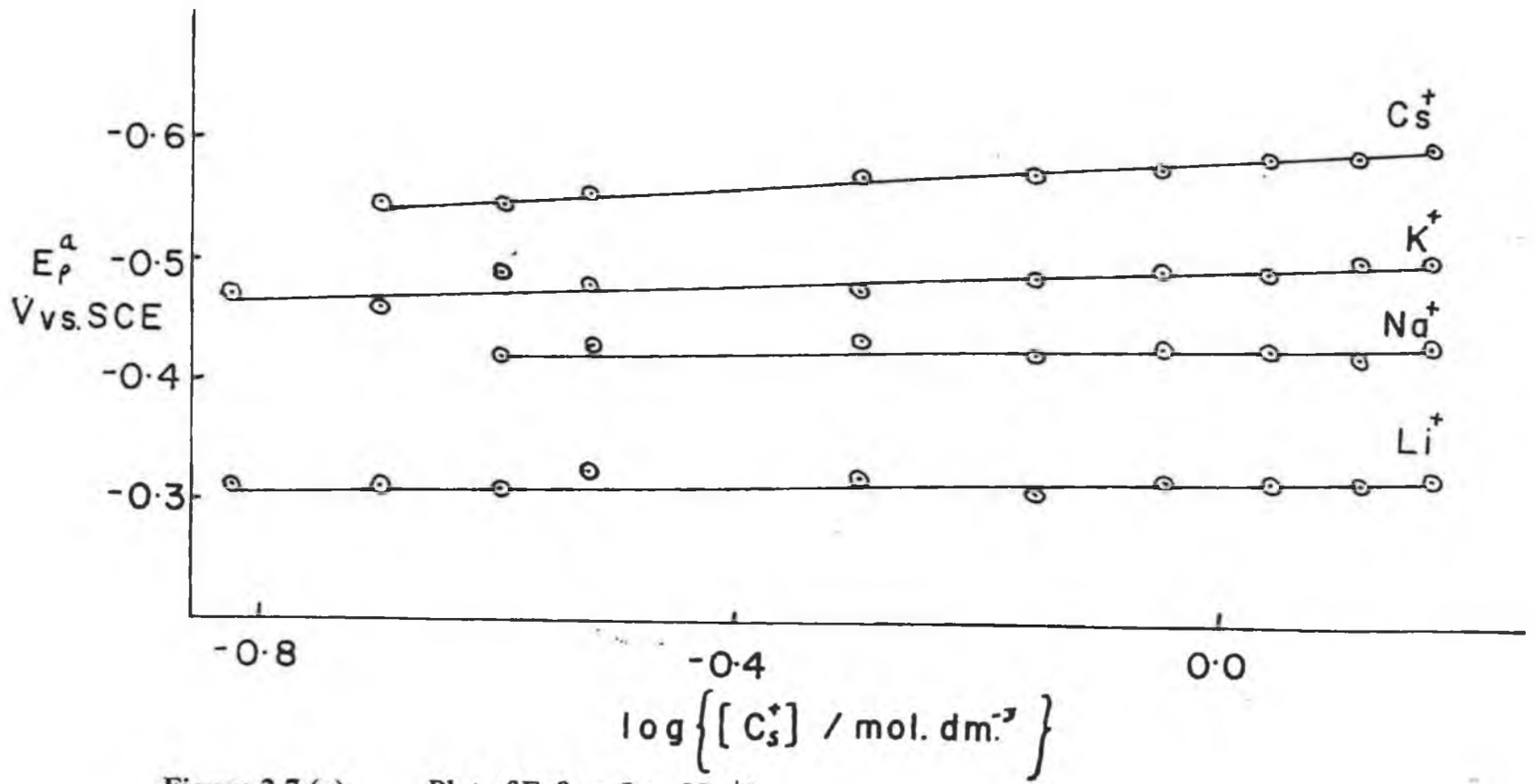

Figure 2.7 (a) Plot of E_p^a vs. Log $[C_b^+]$.
Each line has been displaced by 100mV for clarity.
Li^+ (+0mV) ; Na^+ (+100mV); K^+ (+200mV) ;
Cs^+ (+300mV).

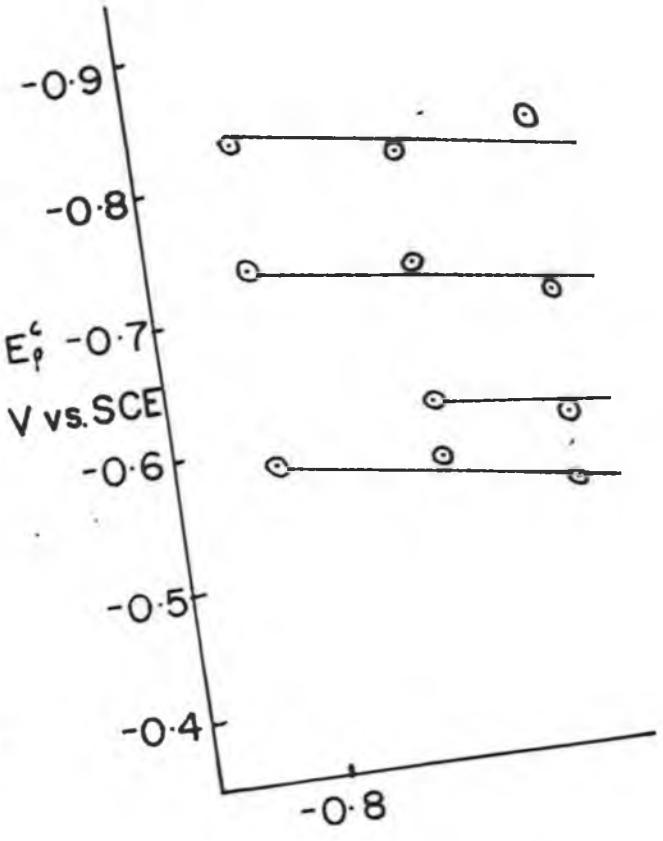

Figure 2.7 (b)

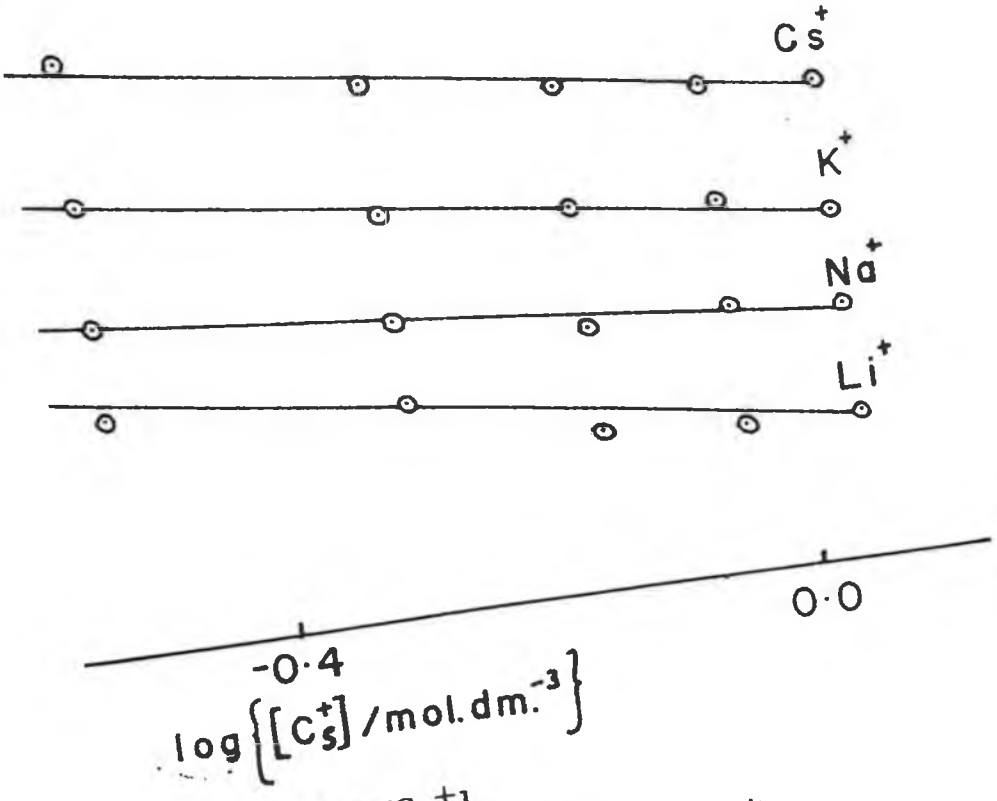

Plot of E_p^c vs. Log $[C_b^+]$.
Each line has been displaced by 100mV for clarity.
Li^+ (+0mV) ; Na^+ (+100mV) ; K^+ (+200mv) ;
Cs^+ (+300mv).

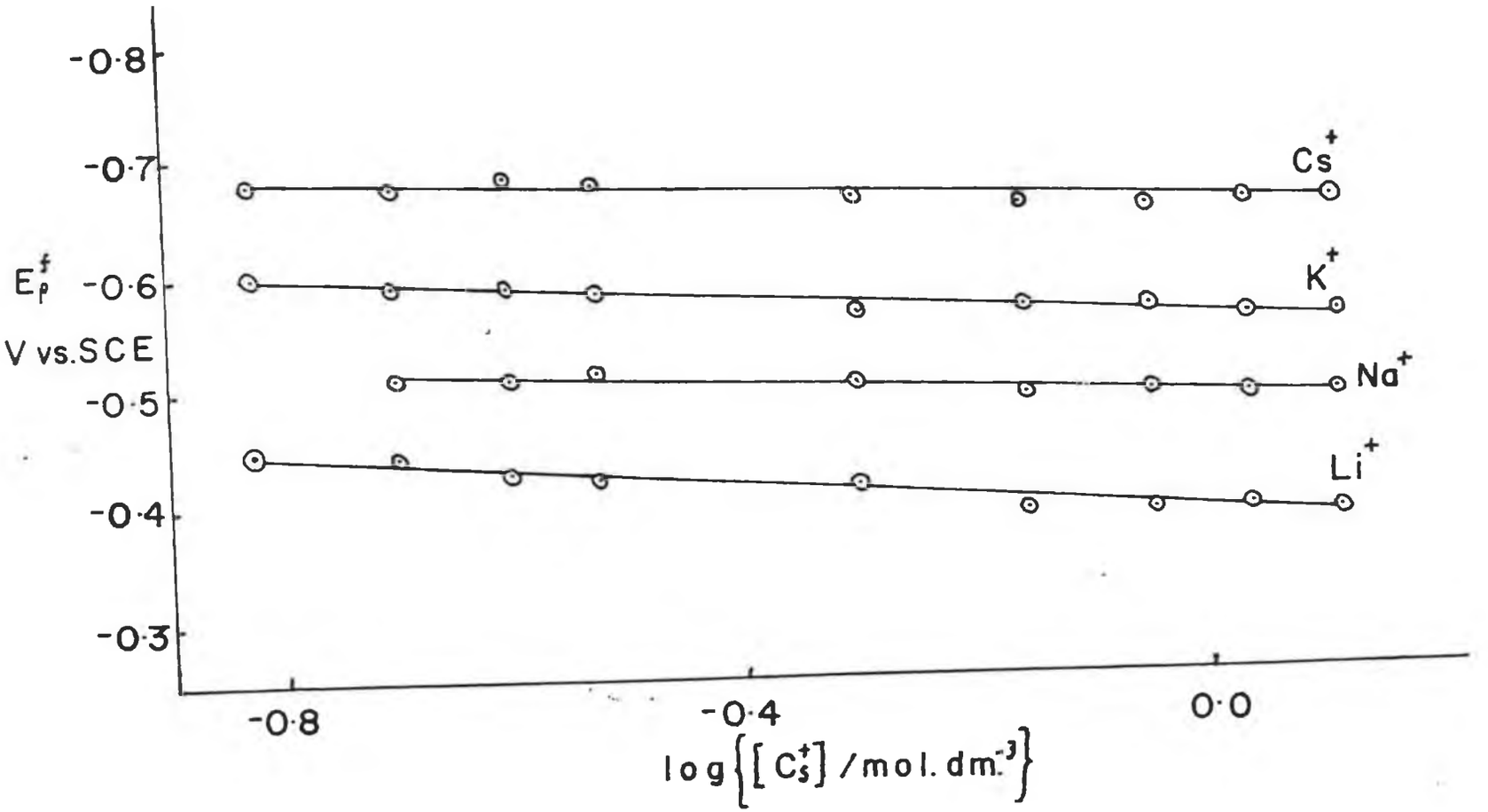

Figure 2.7 (c) Plot of E_p^f vs. Log $[C_b^+]$.
Each line has been displaced by 100mV for clarity.
Li^+ (+0mV) ; Na^+ (+100mV) ; K^+ (+200mv) ;
Cs^+ (+300mv).

			PPTSP			PPFCN		
Cation	ionic radius /nm	hydrated radius/nm	E_{pa} mV/decade	E_{pc} mV/decade	E_f mV/decade	E_{pa} mV/decade	E_{pc} mV/decade	E_f mV/decade
Li^+	0.086	0.340	-5± 7	158±18	77±10	98±9	134±2	117±11
Na^+	0.112	0.276	-5±13	123±17	49±8	76±16	120±2	97±11
K^+	0.144	0.232	-23±17	153±22	53±8	45±1i	85±2	56±1
Cs^+	0.184	0.228	-65±15	153±24	35±9	46±11	75±4	51±10

Table 2.1. Slopes of the peak potentials versus log $[C_b^+]$ for the four alkali metal cations, along with the apparent formal potential of the polymer. Values for PPFCN are from reference [29].

Overall it can be seen that the layer electrochemistry is not as simple as that of a redox species containing non-conducting layer and that it is not as easy to interpret as a conducting layer with a probe molecule such as $[Fe(CN)_6]^{4-}$. It is questionable for example whether E_f should be determined as halfway between the forward and reverse peaks since one shifts more than the other.

It has been previously reported that continuous cycling of the polymer between conducting and insulating forms causes changes in the polymer morphology, with the polymer becoming porous [49]. Also it has been reported that porosity of polymer films formed in aqueous solution is greater than layers formed in acetonitrile [50].

To elucidate the porosity of the PPTSP layer, a 25mC layer was formed in the usual manner, placed in an aqueous solution of NaCl (0.1M) and cycled between 0.5V and -0.9V. The layer was removed in the neutral state, washed and placed in an aqueous solution of tetrabutylammonium hydrogensulphate (0.1M). The polymer was then cycled between -0.9V and +0.5V continuously, the resulting CV is seen in Figure 2.8(a). It can be seen that an anodic peak is observed on the first scan, indicating the ejection of a Na cation, and then upon reduction of the polymer no definite cathodic peak is observed. Upon continuous cycling, the current both faradaic and non-faradaic, decrease dramatically, leading to the steady state scan depicted as a dashed curve in Figure 2.8(b). This evidence implies that the TBA^+ cation is unable to enter the polymer upon reduction. This result was interesting as the ionic size of TBA (5.12Å) is similar to the hydrated diameter of Na^+ (5.52Å), which is seen to enter and exit the polymer

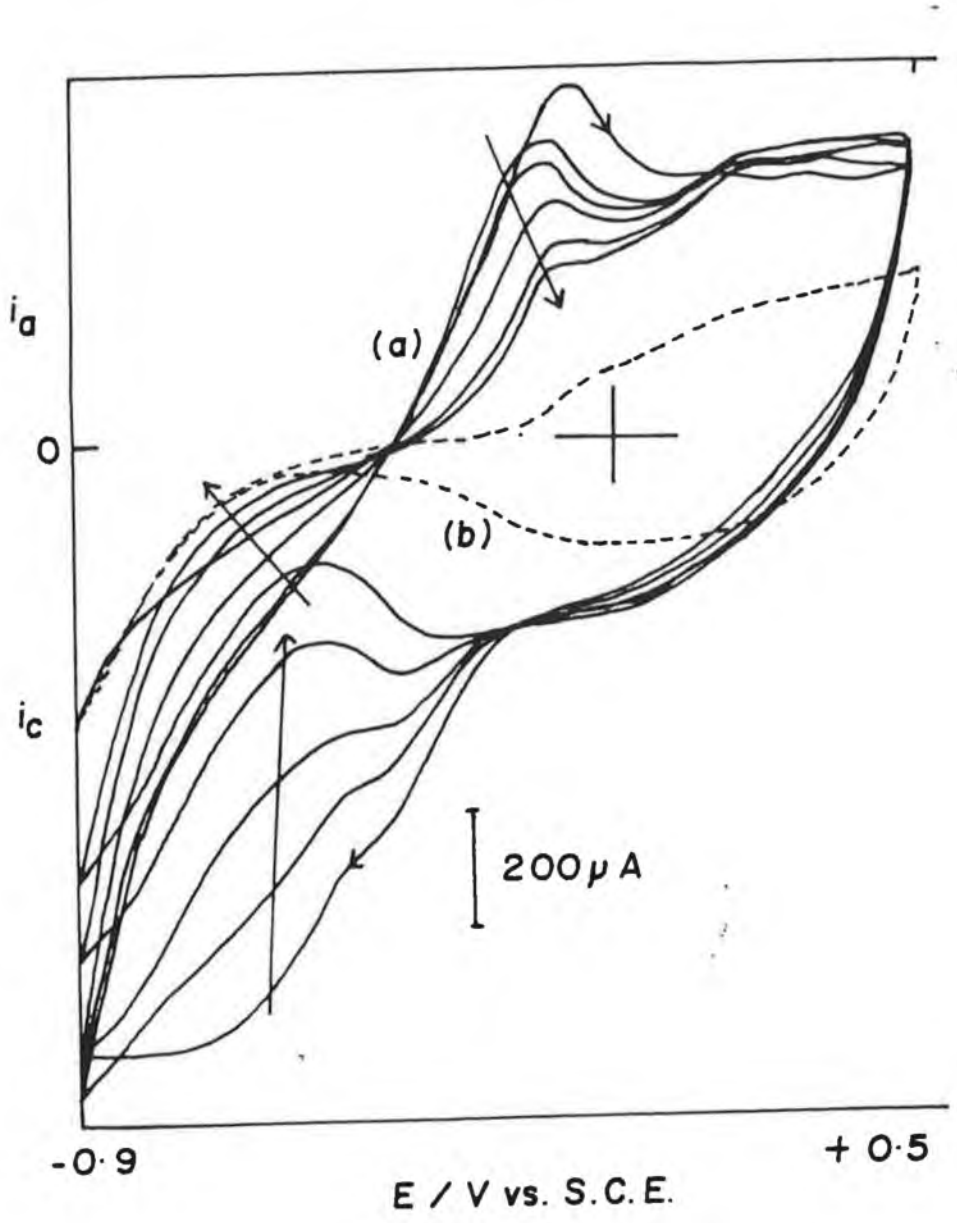

Figure 2.8 (a) Cyclic voltammogram of a PPTSP broken in 0.1M NaCl, washed and transferred to 0.1M tetrabutylammonium hydrogensulphate. The layer being previously formed as described in Figure 2.6. The steady state response obtained is indicated by the dashed curve, (b).
Scan Rate = 100mV/s.

readily, as described earlier. This implies that the ions enter into the layer in a partially dehydrated state. A similar situation has been reported previously [51].

The charge used to deposit each layer is 25 mC and it was found that the amount of charge under both the oxidation and reduction half of each cyclic voltammogram in Figure 2.6 is $11 \pm 0.9\%$ of that used to deposit the layer irrespective of what cation was employed. From these results it is seen that the PPTSP layer is better behaved than for example a polypyrrole dodecylbenzene sulphonate layer, where reoxidation was reported to be difficult and the CV is not very symmetric. It also implies that the layer is not completely oxidised or reduced.

There is only a slight trend in the values of the formal potentials for the different cations, these are shown in Table (2.2).

TABLE 2.2. Formal potentials of PPTSP layers as a function of cation electrolyte nature, $[C_b^+] = 1.0M$.

Cation	E^0 (mV)
Li^+	-381 ± 4
Na^+	-380 ± 3
K^+	-358 ± 5
Cs^+	-349 ± 5

These results can be used by considering the redox reaction of two polymer layers, $PP^{o}TSPP^{-}Li^{+}$ and $PP^{o}TSPP^{-}Cs^{+}$,

$$e^{-} + Cs^{+} + (PP^{+})(TSPP)^{-} \rightarrow (PP^{o})(TSPP)^{-}Cs^{+} \quad \ldots\ldots\ (2.10)$$

$$e^{-} + Li^{+} + (PP^{+})(TSPP)^{-} \rightarrow (PP^{o})(TSPP)^{-}Li^{+} \quad \ldots\ldots\ (2.11)$$

Both Scheme (2.10) and (2.11) represent an equilibrium between the oxidised and reduced polymer involving two different cations. The Nernst equation can be applied to the two layers to give

$$E = E^{o}_{PPCs} + \frac{RT}{nF} \ln\left\{\frac{[Cs^{+}]\,[PP^{+}TSP^{-}]}{[PP^{o}TSP^{-}Cs^{+}]}\right\} \quad \ldots\ldots\ (2.12)$$

$$E = E^{o}_{PPLi} + \frac{RT}{nF} \ln\left\{\frac{[Li^{+}]\,[PP^{+}TSP^{-}]}{[PP^{o}TSP^{-}Li^{+}]}\right\} \quad \ldots\ldots\ (2.13)$$

By equating equations (2.12) and (2.13) and substituting in values for the formal potentials of both polymer layers, equation (2.14) is obtained.

$$32 \times 10^{-3}\ V = \frac{RT}{nF} \ln\left\{\frac{[Li^{+}]\ [PP^{o}TSP^{-}Cs^{+}]}{[Cs^{+}]\,[PP^{o}TSP^{-}Li^{+}]}\right\} \quad \ldots\ldots\ (2.14)$$

By using the equation for Gibbs Free Energy, a final expression is obtained

$$K = \exp\left[\frac{-nF\ (32 \times 10^{-3}V)}{RT}\right] \quad \ldots\ldots\ (2.15)$$

Where K is the equilibrium constant for the following reaction equilibrium

$$PP^{0}TSP^{-}Li^{+} + Cs^{+} \Leftrightarrow Li^{+} + PP^{0}TSP^{-}Cs^{+} \quad \ldots\ldots\ldots \quad (2.16)$$

It was found that K was less than 1, therefore the equilibrium lies to the left. This implies that the reduced form of the polymer with a Li^{+} cation, present within the polymer matrix, is slightly more stable than if a Cs^{+} cation as inserted.

For the above schemes to be true, it is assumed that the system is in thermodynamic equilibrium, where $\frac{E_{Pa} + E_{Pc}}{2}$ is the formal potential, E^{o1}, of the polymer.

However due to the fact that the cathodic peak is electrolyte concentration dependent more so than the anodic peak hints that the system may not be in thermodynamic equilibrium. To investigate this, a scan rate study was undertaken on various PPTSP layers.

2.4.2 SCAN RATE STUDY OF A PPTSP LAYER

Previously electrochemical parameters such as rate constants and capacitances of polypyrrole films were studied [50]. The electrochemical behaviour of the PPTSP layers, prepared in aqueous medium are considered here. For this purpose several layers of PPTSP, of different thicknesses, were prepared. Scan rate dependencies of the cyclic voltammograms of several PPTSP layers, of four different thicknesses (5mC, 10mC, 15mC, 25mC) are shown in Figure 2.9.

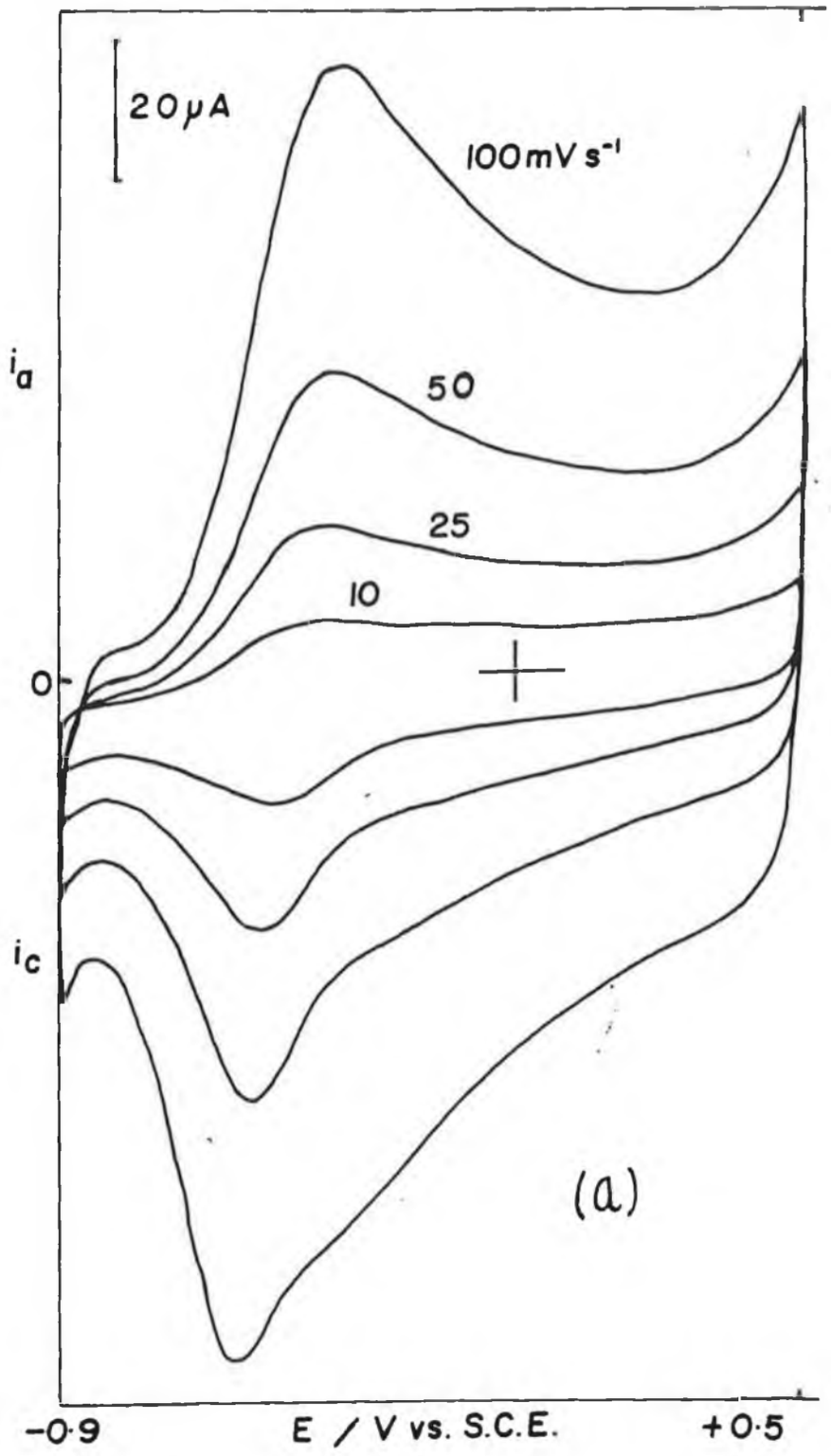

Figure 2.9 Scan Rate dependencies of cyclic voltammograms in aqueous 0.3M KCl for PPTSP layers prepared as described in Figure 2.6, with (a) 5mC
(b) 10mC
(c) 15mC
(d) 25mC

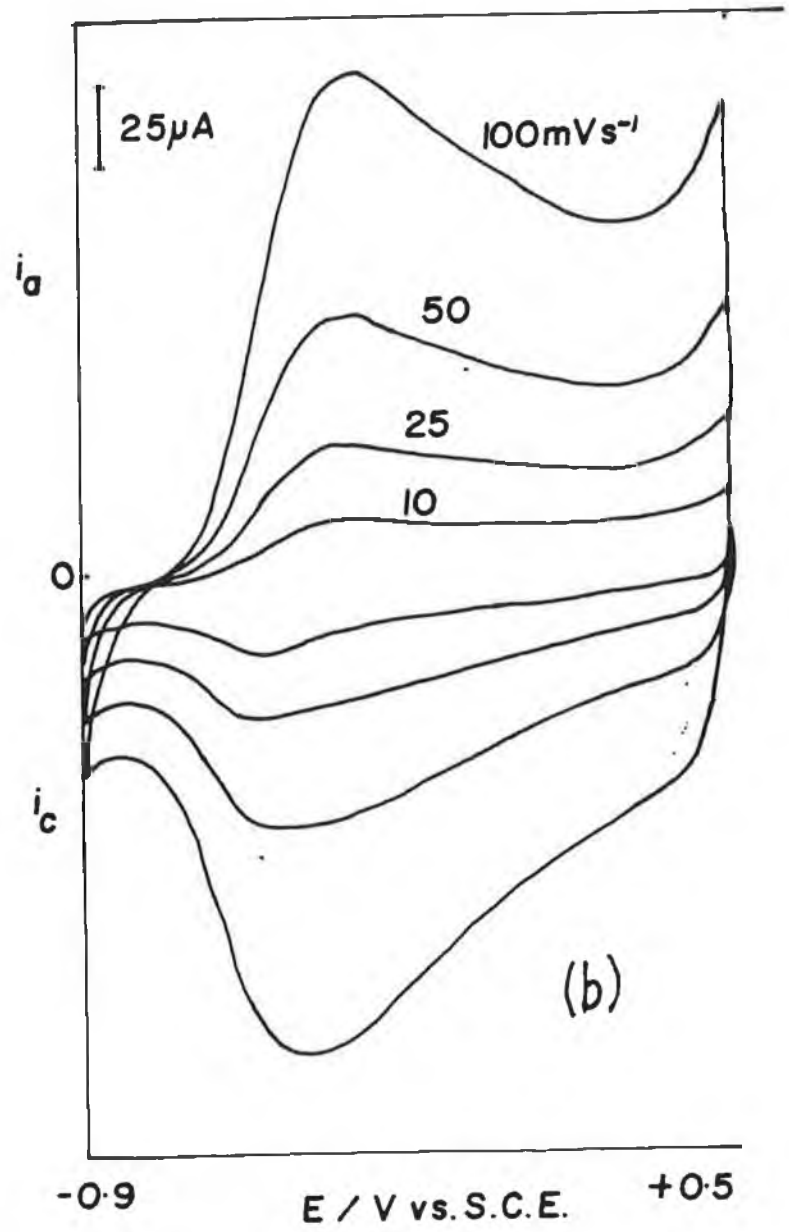
25μA
100mVs⁻¹
50
25
10
i_a
0
i_c
(b)
-0·9
E / V vs. S.C.E.
+0·5

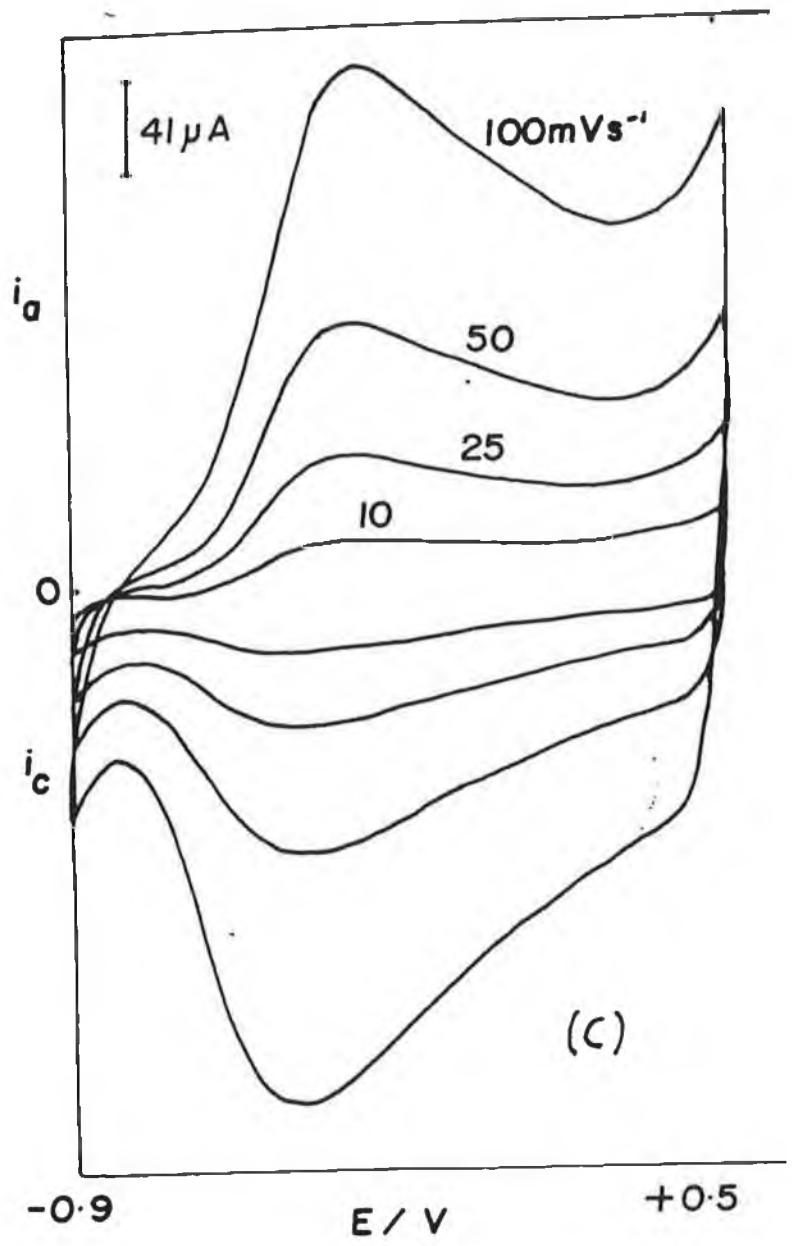
41 μA
100mVs⁻¹
50
25
10
i_a
0
i_c
(C)
-0·9
E / V
+0·5

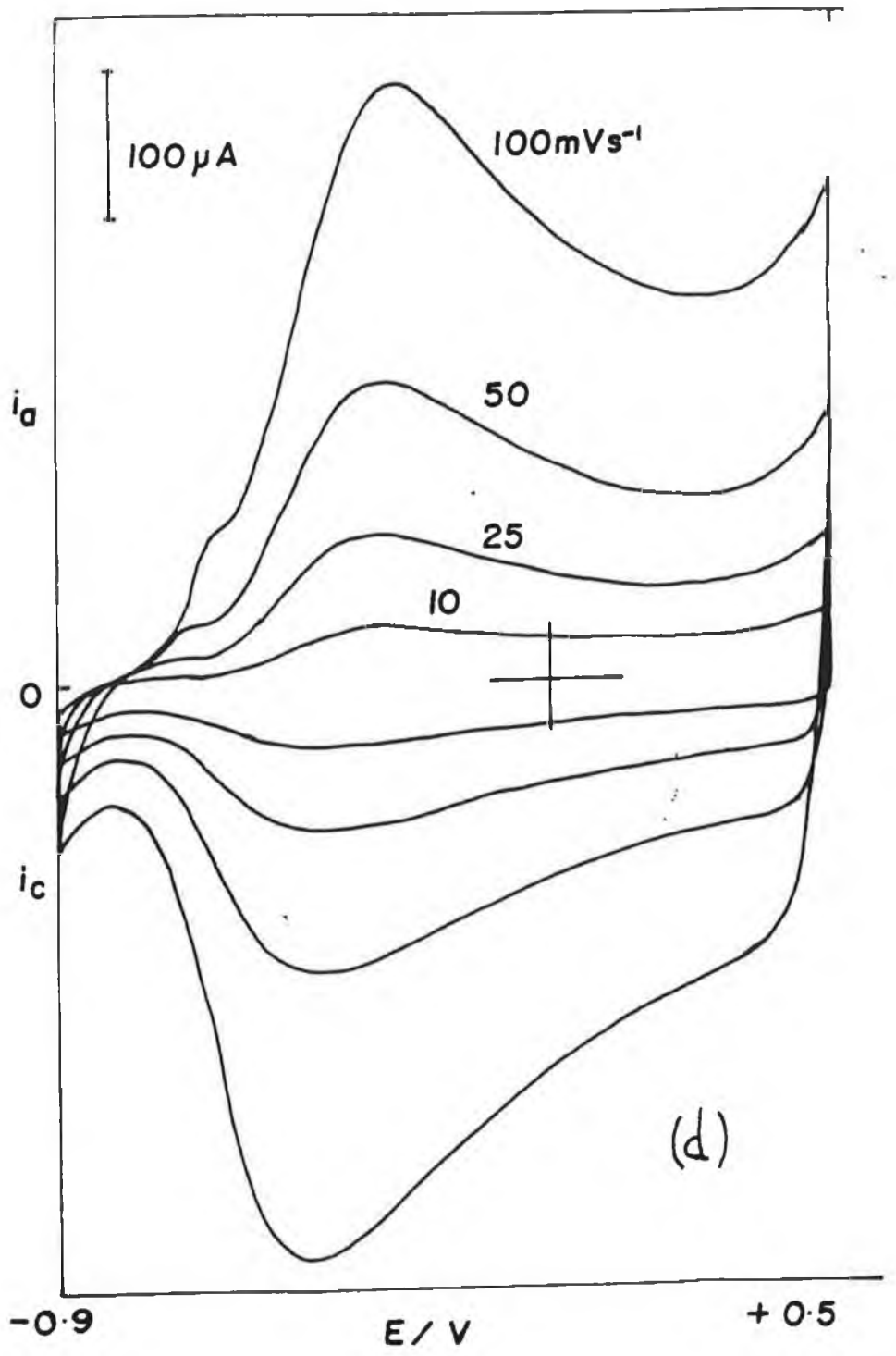
100 μA
100mVs⁻¹
50
25
10
i_a
0
i_c
(d)
-0·9
E / V
+ 0·5

These CV's were recorded in an aqueous solution of KCl (0.3M). It was found that peak currents are proportional to the scan rates for all 4 layers.

This is illustrated in Figure 2.10 where the log of anodic peak current is plotted as a function of log of scan rate for all four films. The slopes of the plots vary from 1.270 to 1.032 for the 5 mC and 25 mC layers respectively, these values agree with figures reported previously [50]. The value of these slopes indicated that the peak current was directly proportional to the scan rate. This indicating true thin layer behaviour rather than bulk solution behaviour [52].

It has previously been reported [50] that the cyclic voltammetric currents beyond 0.5V, after the faradaic component of the current has decayed, consists mainly of capacitive components. From the cyclic voltammograms in Figure 2.9, currents were measured at 0.5V, and they showed a linear dependance on scan rates as shown in Figure 2.11, according to the equation

$$i_c = C.A. \frac{dV}{dt} \quad \ldots\ldots\ldots \quad (2.17)$$

Where C is the capacitance, A the electrode area and $^{dv}/_{dt}$ represents the voltage scan rate.

Two assumptions are made so that this equation may be applied, these are that the capacitance is not a function of scanning voltage and that the electrode area is constant. The slopes of the lines shown in Figure 2.11 can yield capacitances of the polypyrrole films prepared in aqueous solution. The capacitance values

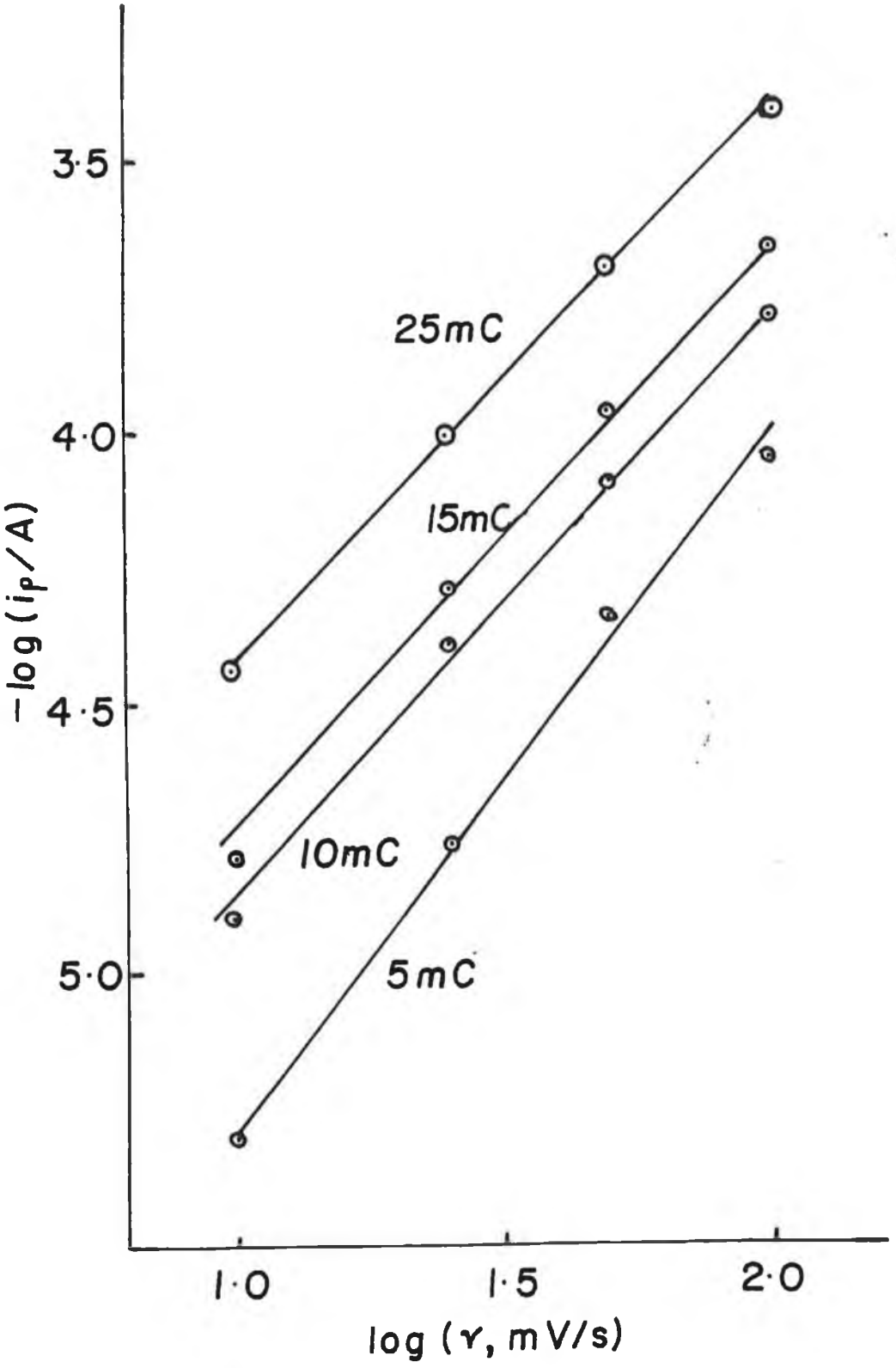

Figure 2.10 Plot of log of anodic peak current (i_p^a) versus the log of scan rate (υ), for the 4 PPTSP layers, 5mc, 10mC, 15mC and 25mC.

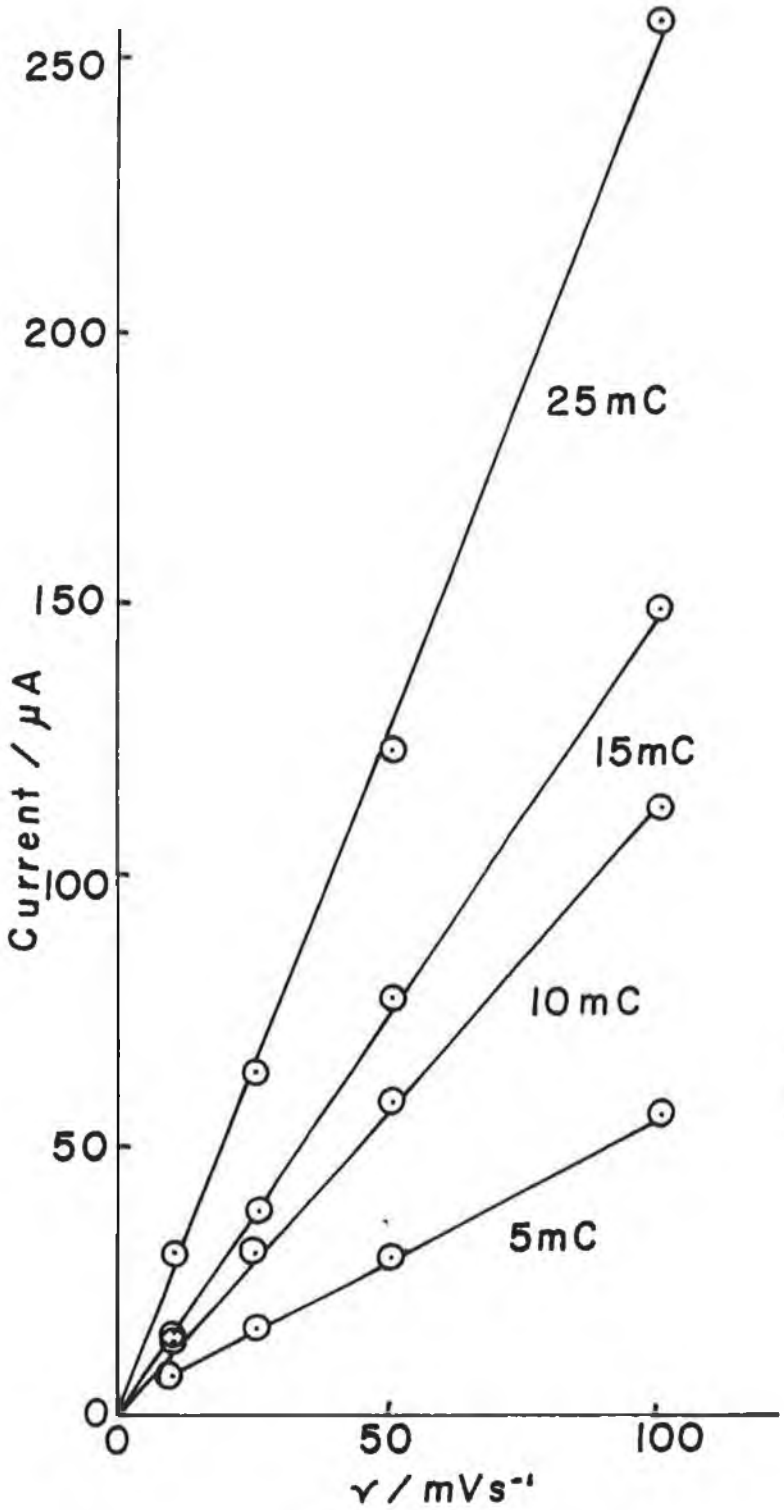

Figure 2.11 Plots of capacitance current vs. scan rate (υ), for the 5mC, 10mC, 15mC and 25mC PPTSP layers.

obtained from Figure 2.12 translate into 350 F/cm^3, (See Graph Figure 2.12) which agree with values previously reported [50].

Figure 2.12 shows the capacitance of the polymer films plotted as a function of layer thickness. It can be seen that thinner films have a lower capacitance value than thicker films, a similar situation being reported previously [50]. These values of capacitance for thick and thin films have possibly a relation to the porosity and morphology of the layers.

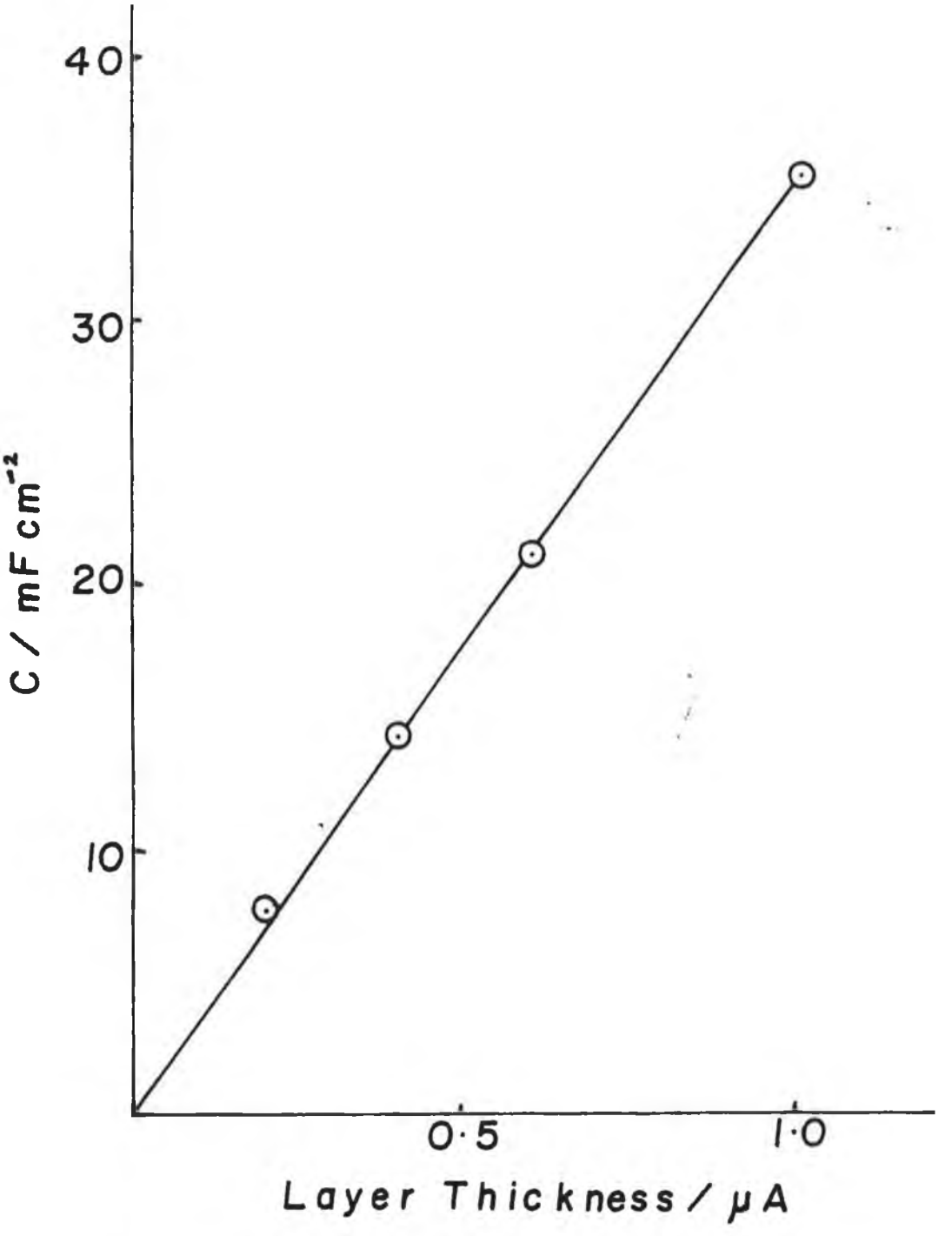

Figure 2.12 Plot of layer capacitance (C) vs. layer thickness, for PPTSP layers.

2.4.3 pH STUDY

A pH study was carried out on a 25mC PPTSP layer, deposited on a glassy carbon electrode, by the addition of 0.1M HCl to a solution of 0.15M KCl.

Figure 2.13 shows the cyclic voltammograms at various pH values. Both the anodic and cathodic peaks are seen to shift upon the addition of H^+ ions into solution.

It can be seen that a fast equilibration, on continuous scanning, is observed for pH = 4.04, where the first and sixth scans are shown. However for pH = 2.20, there is a slow equilibration observed. This could be explained by the fact that a competition between two processes occurs. That is where the protons are entering the layer for reasons of charge neutrality or for protonation of the four sulphonate groups present on the phthalocyanine anion. The pH values where this slow equilibration is observed could correspond to the pK_a values of the sulphonate groups. A similar situation was reported previously [29], where the effect of pH on a polypyrrole layer containing $[Fe(CN)_6]^{4-}$ was studied.

Therefore at low pH's (pH < 1.5) the sulphonate groups are neutralised and that the ion movement within the layer was due to Cl^- movement rather than cation movement for charge neutrality. This process may be observed in that the formal potential for the layer shifts dramatically from -0.35V above pH 2.5 to +0.10V below a pH of 2.5.

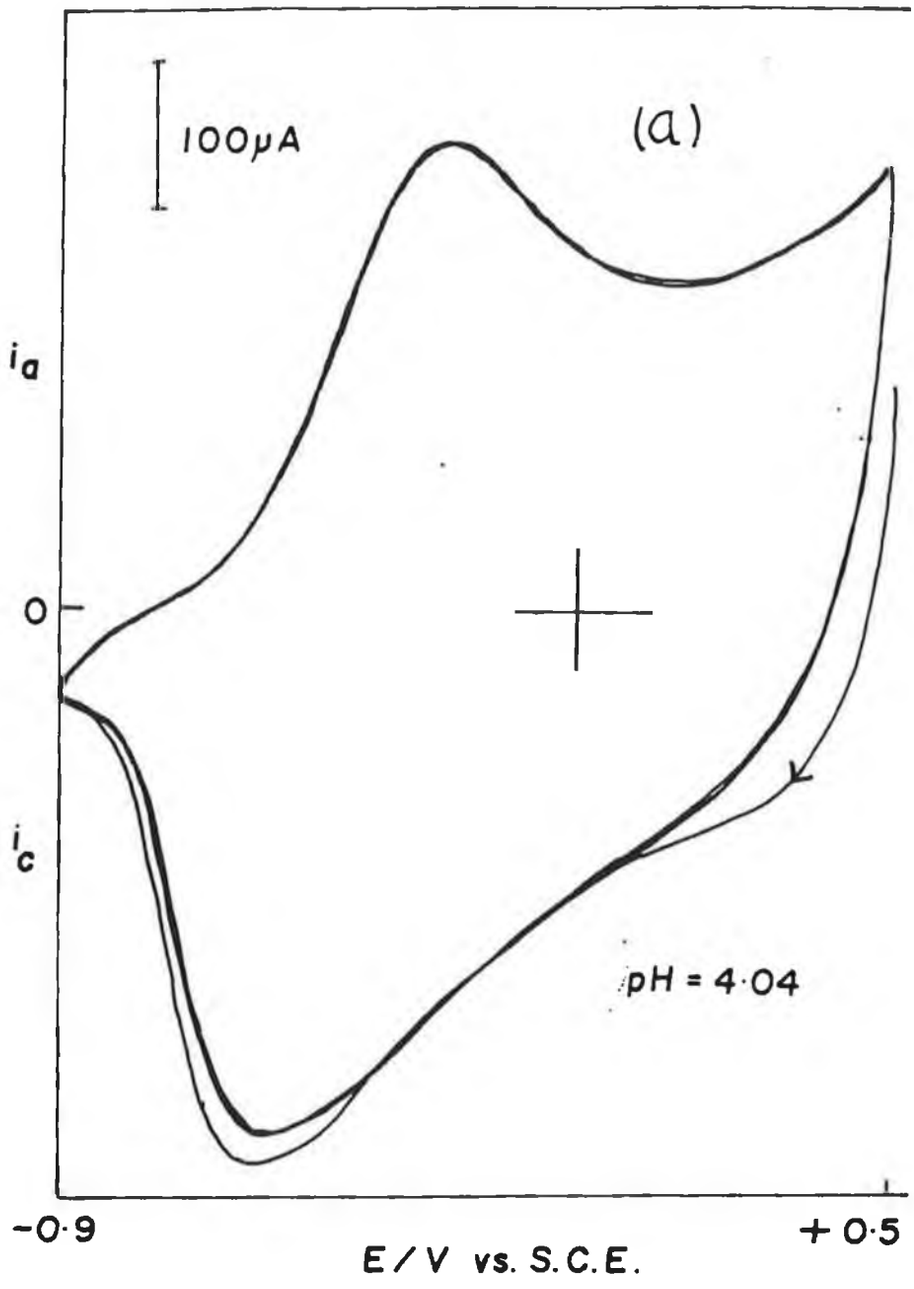

Figure 2.13 Cyclic voltammograms of a PPTSP layer, grown on a glassy carbon electrode as described in Figure 2.6, in 0.15M KCl at various pH's by the addition of 0.1M HCl.
Scan Rate = 100mv/s.

(a) pH = 4.04
(b) pH = 2.20
(c) pH = 1.50

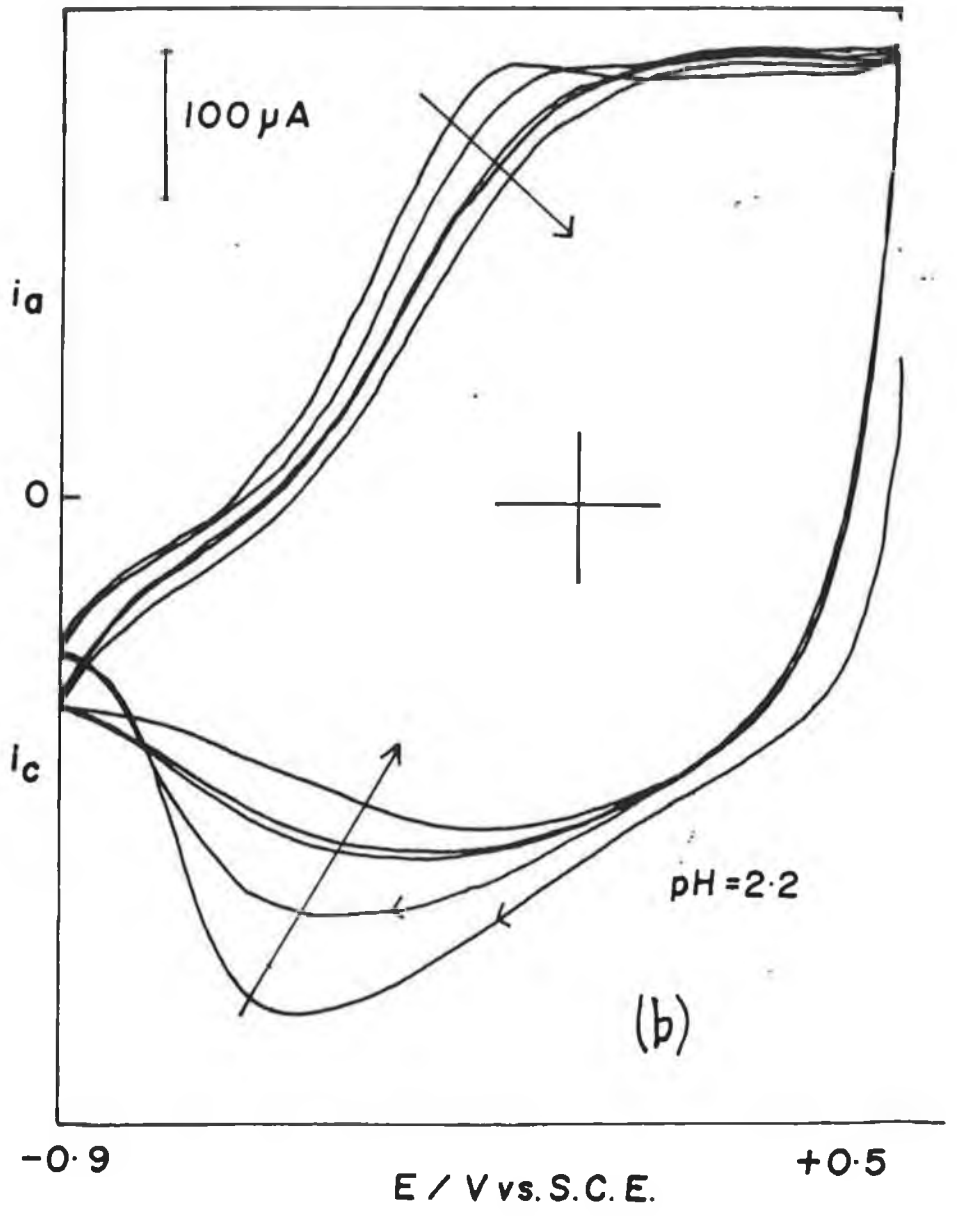
100 μA
i_a
0
i_c
pH = 2·2
(b)
−0·9
+0·5
E / V vs. S.C.E.

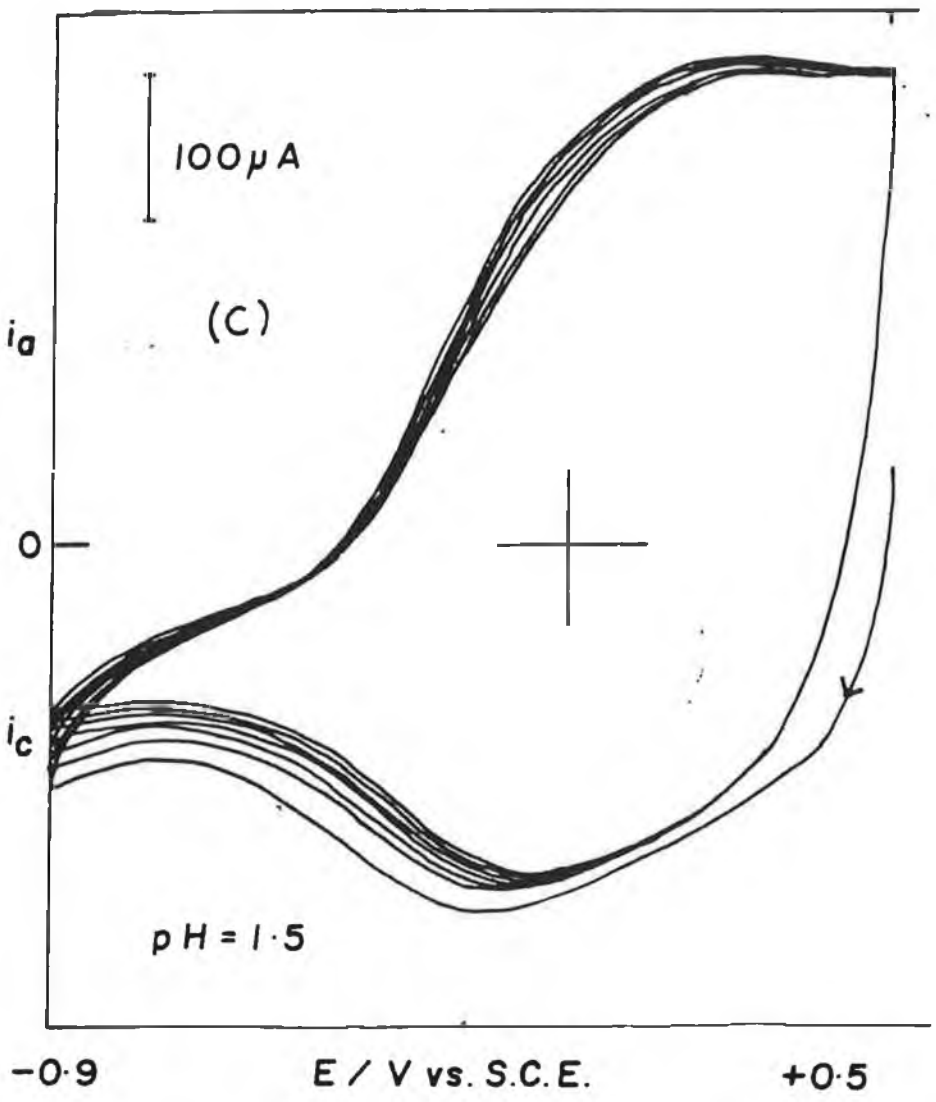
100μA
(C)
i_a
0
i_c
pH = 1·5
−0·9
E / V vs. S.C.E.
+0·5

Figure 2.14 shows the effect of pH on the Ep_a (a), Ep^f (b), Ep^c(c) of the polymer. The dramatic shift in the peak positions with change in pH of electrolyte solution is illustrated. It is seen that up to a pH value of 3, all three plots have a constant slope. Below pH 3 there is a dramatic shift in peak potentials and formal potential of the polymer this is illustrated by a change in slope for all three plots. Once the sulphonate groups of the phthalocyanine anion have been protonated, with Cl^- passing in and out of the polymer matrix, then there is a subsequent change in slope for all three plots.

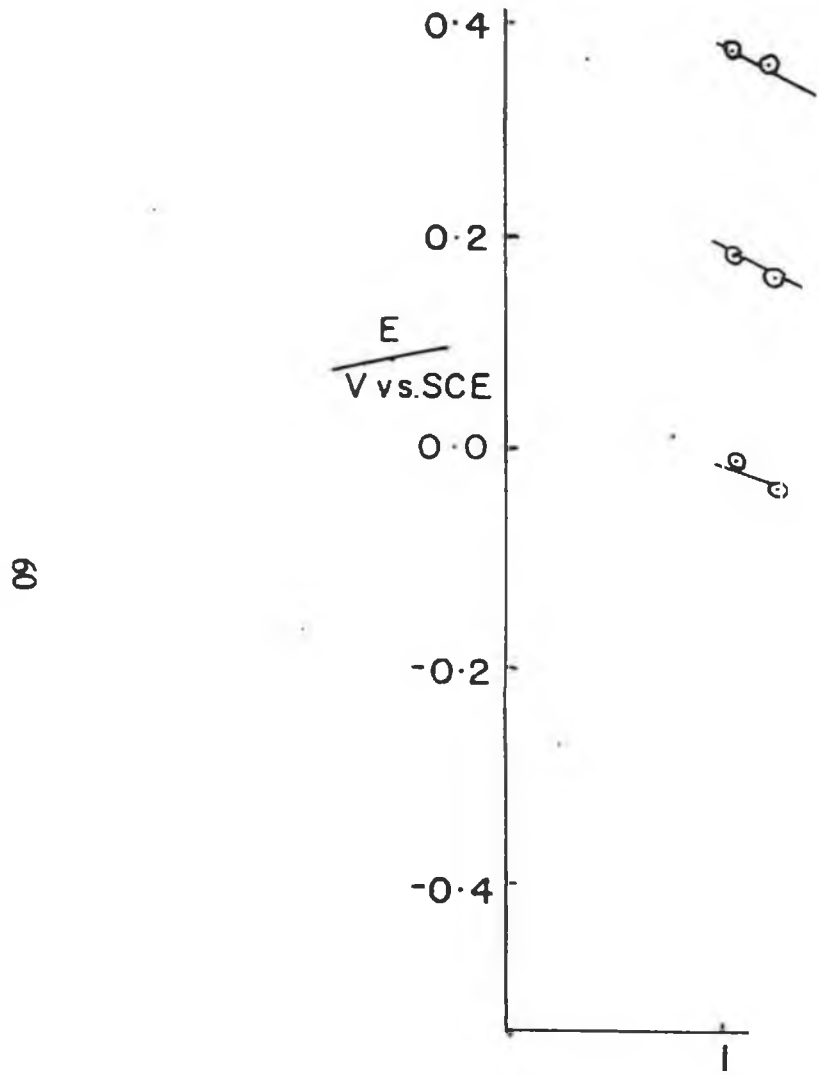

Figure 2.14

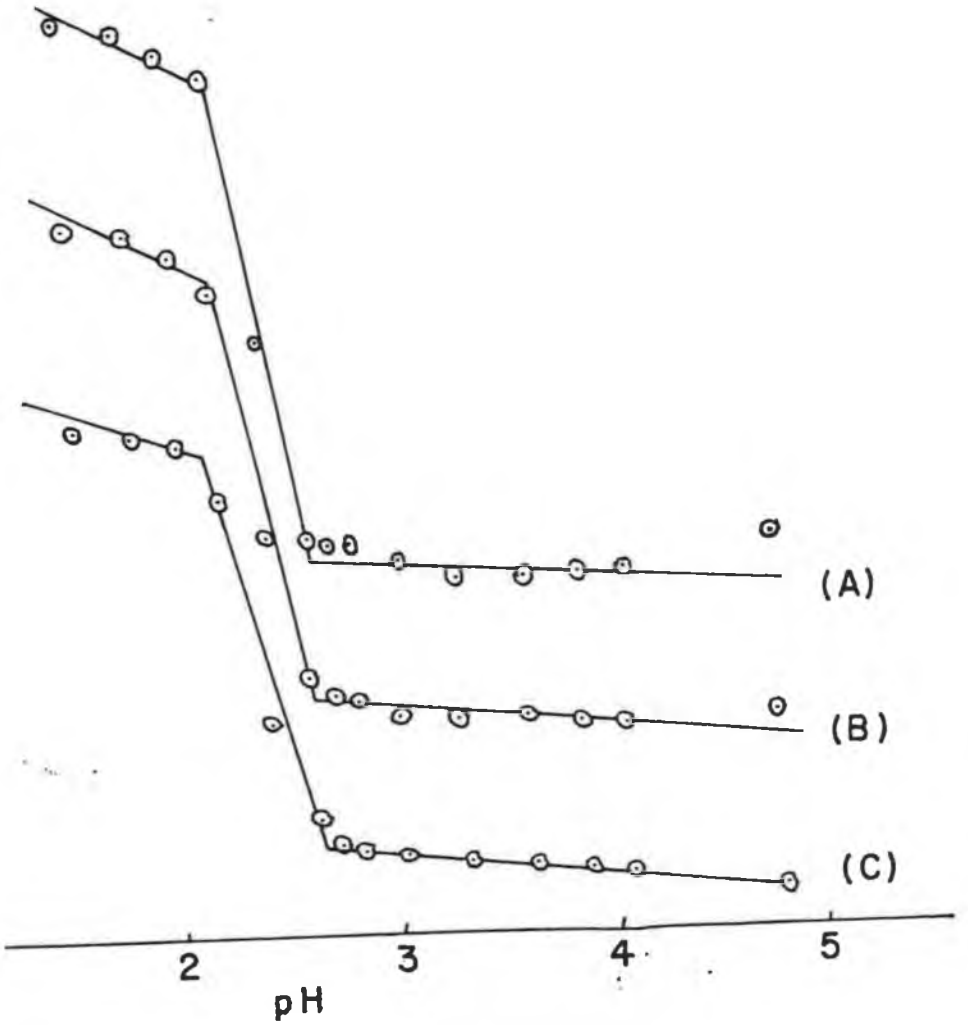

Plot of (a) E_p^a, (b) E_p^f and (c) E_p^c for the PPTSP layer as a function of solution pH.

2.4.4. CONCLUSION

It was observed that a polypyrrole Cu(ll) tetrasulphonated phthalocyanine layer exhibited cation insertion and expulsion upon electrochemical switching of the polymer between conducting and insulating forms.

The effect of cation nature and concentration on the cyclic voltammetric behaviour of the PPTSP layer was examined. The peak potentials of the polymer were examined and the effect of cation concentration, pH and temperature upon these potentials was noted.

It was found that there is no relationship between the ease of insertion and expulsion of the alkali metals and their ionic hydrated radius. H^+ was seen to act differently, acting as a charge neutralising species and protonating the sulphonate groups present on the phthalocyanine anion. Values of layer capacitance were also calculated for various layer thicknesses, with an increase in layer capacitance with layer thickness.

2.4.5 CYCLIC VOLTAMMETRY OF POLYPYRROLE DODECYLBENZENESULPHONATE LAYERS

Figure 2.15 shows the cyclic voltammetry of a polypyrrole perchlorate layer ($PPClO_4$), prepared as described earlier, and cycled in an aqueous solution of 0.1 mol dm^{-3} $LiClO_4$. The characteristic 'double layer charging - like' behaviour, which is common to most conducting polymers, can be seen clearly

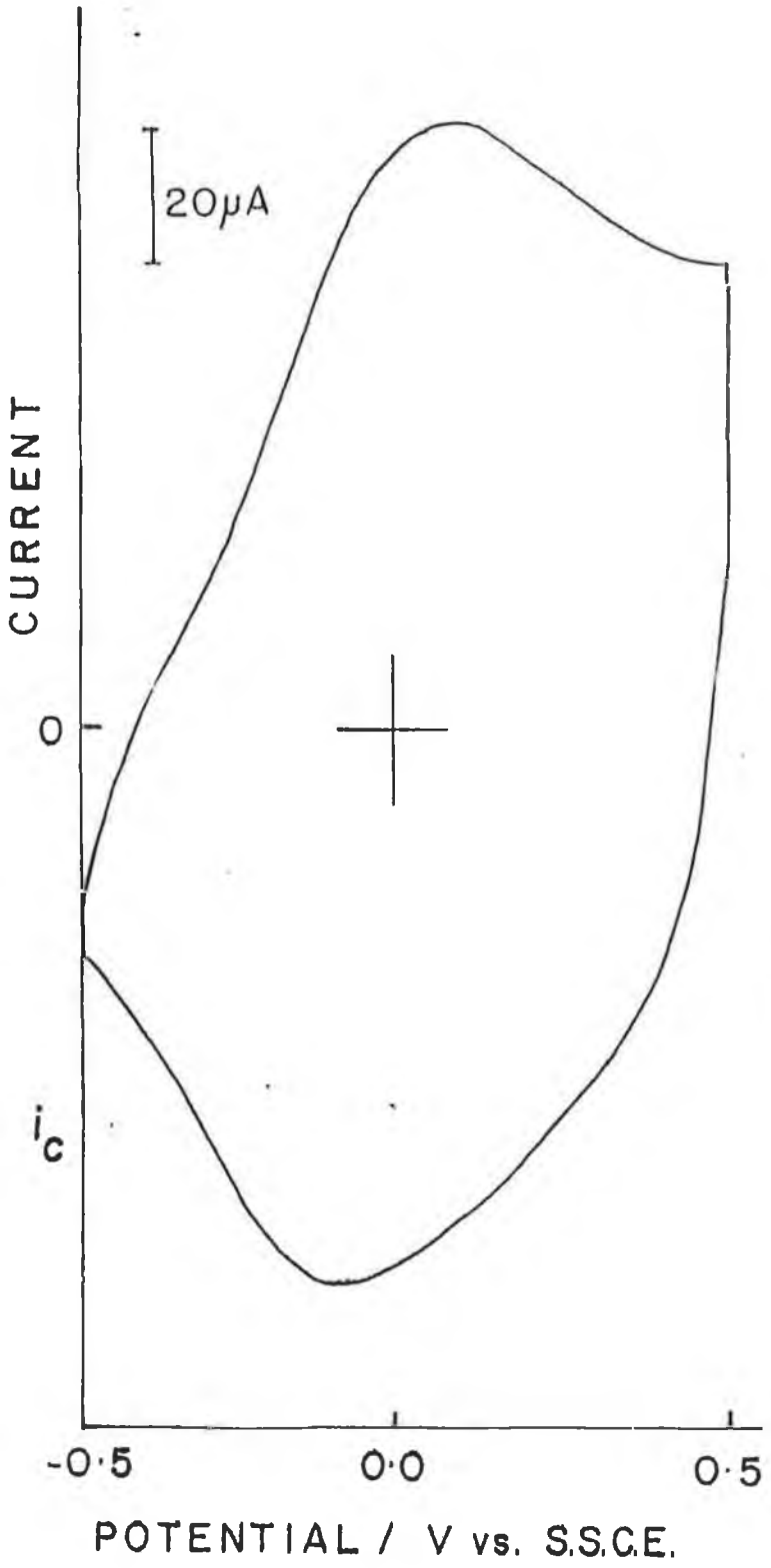

Figure 2.15 Cyclic voltammetry of a layer formed in 0.1 mol dm^{-3} $LiClO_4$/0.1 mol dm^{-3} pyrrole by scanning continuously between 0 an 0.8V until 20 mC of charge had passed. The layer was then transferred to 0.1 mol dm^{-3} $LiClO_4$.
Scan Rate = 50 mV/s, and the Pt electrode area is 0.0707 cm^2.

and the current magnitude at the switching potential has previously been used to determine the capacitance of the layer [53].

The broad nature of the voltammetry indicates that the system does not merely consist of a simple surface confined redox species [46]. Models for the behaviour include that of a series of oligomers, each of which has a characteristic formal potential leading to a broad voltammetry [54]. It has also been proposed that the broad voltammetry has been due to electrostatic repulsions between oxidised site of the polymer [55,56]. Such a capacitance like behaviour has been seen for polypyrrole, previously formed in solutions of pyrrole and tetrabutylammonium perchlorate, and run in electrolytes such as NaCl, $NaNO_3$, and has been absent in solutions of Na_2CO_3 and Na_2SO_4 [57].

Figure 2.16 shows a polypyrrole dodecylbenzenesulphonate layer (PPDBS) cycled in aqueous 0.1M $NaClO_4$. The voltammograms in Figure 2.15 and 2.16 represent the final steady state voltammetry of the layer in the particular electrolyte. It may take 20-30 scans to reach a situation where a steady state voltammetry is seen. Previously it has been reported that continued cycling causes a greater than equilibrium concentration of electrolyte in the pores for the film [49], which may account for the 'breaking-in' process. The small degree of double layer charging, seen at the switching potential in Figure 2.16, has been attributed to the ordering of the layer during its formation in the surfactant solution [58,59,32]. It can be seen that the predominant ionic movement is that of cations since the peak shifts in a positive direction with increasing electrolyte concentration; this is in common with previous experimental results [60,61]. If the potential is scanned over a potential region more positive than -0.2V, there is

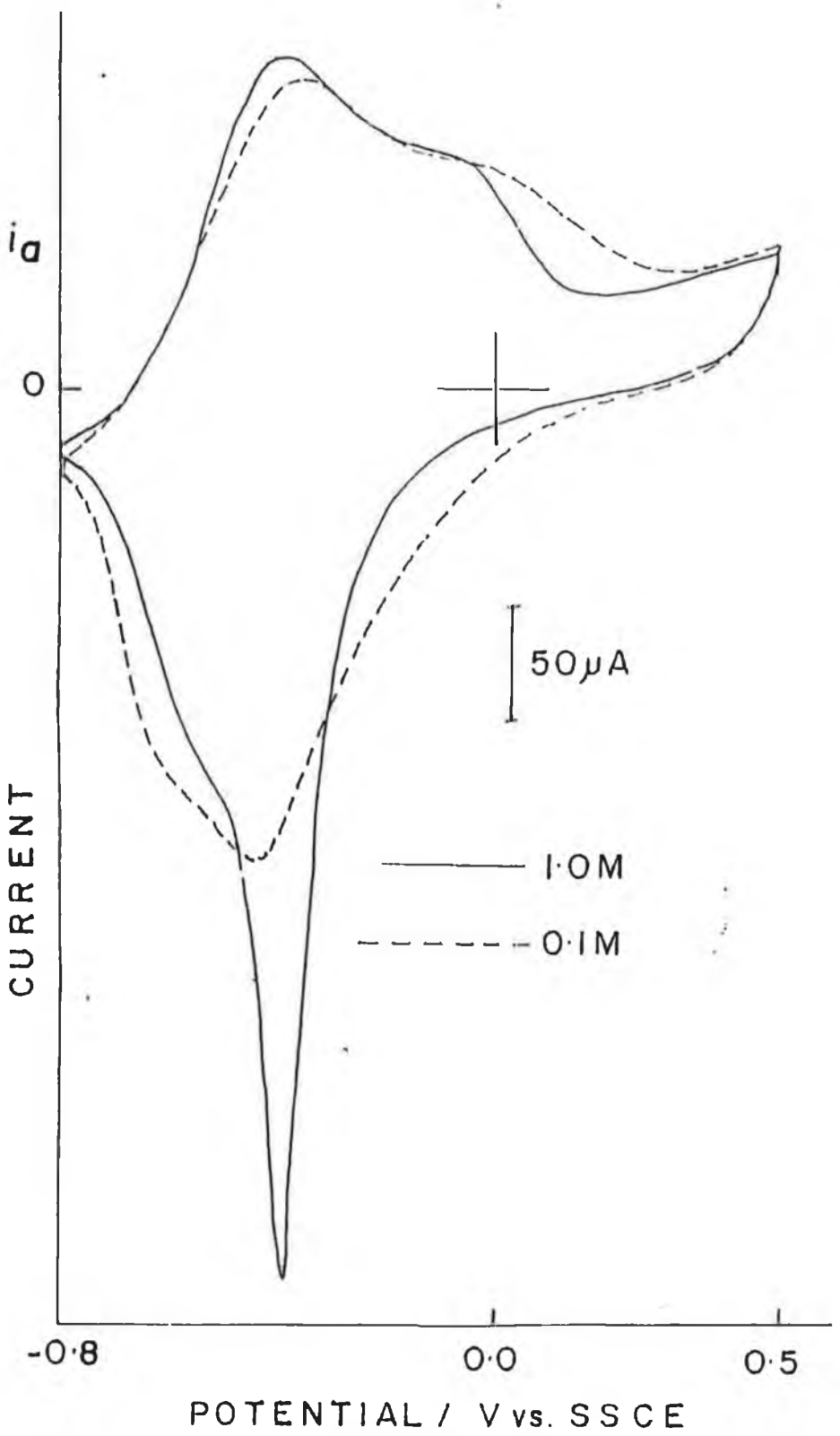

Figure 2.16 Cyclic voltammetry of a layer formed in 0.1 mol dm^{-3} NaDBS/0.1 mol dm^{-3} pyrrole by scanning continuously between 0 and 0.78V until 20 mC of charge had passed. The layer was then transferred to $NaClO_4$ solutions where the concentrations are shown in the figure.
Scan Rate = 50 mV/s, and the Pt electrode area is 0.0707 cm^2.

very little capacitive-like current which has been reported to be due to the morphology of the layer [62,47].
Most CV studies of polypyrrole layers formed from a solution of a large anions, were run in solutions with smaller anions where cation incorporation was evident (Figure 2.16).

Figure 2.17 shows the voltammetry of a $PPClO_4$ cycled in DBS solutions.
It can be seen that there is a definite change in the electrochemical characteristics of the film when a layer is formed in $NaClO_4$ and transferred to a surfactant solution. There appears a sharp peak at -0.7V, similar to but more negative than that in Figure 2.16. It can be seen from Figure 2.17, that despite the size of DBS, it can replace some ClO_4^- in the layer.
Once DBS has entered into the layer, it is cation movement that defines the ionic mobility as can be seen when the background electrolyte concentration is increased the peak moves in a positive direction. The DBS irreversibly enters into the layer, since when this electrode was subsequently placed in 0.1M $NaClO_4$, the DBS did not fully exchange out on cycling. Since the morphology of the layer is determined by the conditions of its formation, the double layer charging characteristics of Figure 2.15 is a function of the electrolyte since it has been suppressed in DBS solution.

It can be seen however that the current magnitude is much less in Figure 2.17 than in the first two figures indicating that there is only partial exchange of ClO_4^- with DBS. It has been shown elsewhere [6] by probe beam deflection that Cl^- ions partially replace dodecylsulphate from a polypyrrole layer anions is possible in polypyrrole layers. That is in contrast to previous reports of solely

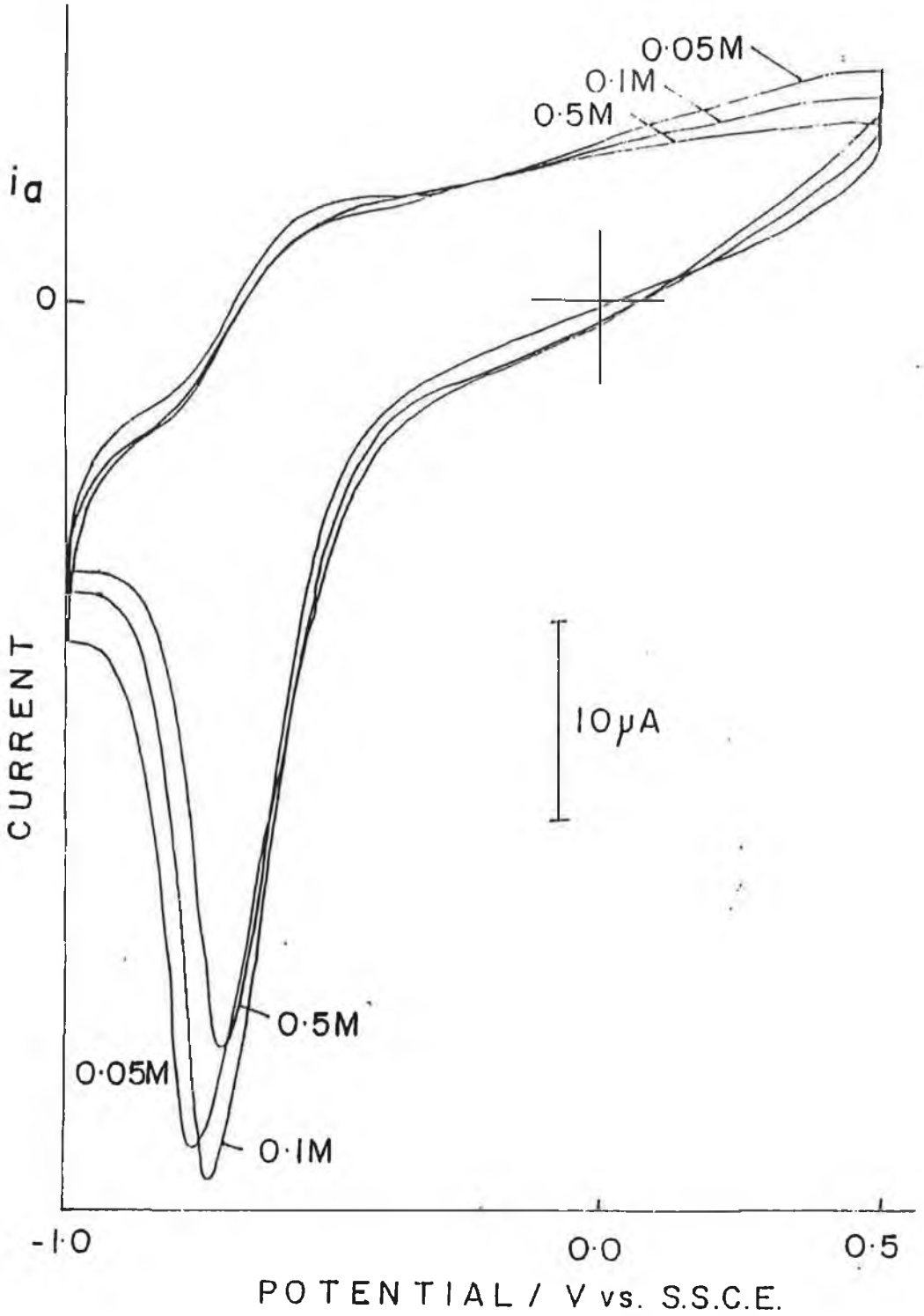

Figure 2.17 Cyclic voltammetry of a layer formed in 0.1 mol dm^{-3} $NaClO_4$/0.1 mol dm^{-3} pyrrole by scanning continuously between 0 and 0.8V until 20 mC of charge had passed. The layer was then transferred to NaDBS solutions and the concentrations are shown in the figure.
Scan Rate = 50 mV/s, and the Pt electrode area is 0.0707 cm^2.

cation movement for dodecylsulphate [61,64,65,22,23] and dodecylbenzenesulphonate [66].

Figure 2.18 shows a layer formed in a solution of 0.1 mol dm^{-3} NaDBS and 0.1 mol dm^{-3} pyrrole and transferred to a solution of 0.1 mol dm^{-3} $LiClO_4$. In the ClO_4^- solution it can be seen that a peak at negative potentials is characteristic of the movement of cations. However it can also be seen that there is a peak due to the movement of ClO_4^- close to 0.0V, which is not as dominant in $NaClO_4$ (See Figure 2.16). This may be because of the greater hydrated radius of Li^+ which makes its incorporation more difficult. For polypyrrole layers formed with $[Fe(CN)_6]^{4-}$ as anions [29], Li^+ was the most difficult cation of the alkalis to be incorporated, which is also the case for polypyrrole formed in the presence of cupric hexacyanoferrate [67].

It should be noted that the concentration of the surfactant (0.1M), is above the critical micelle concentration (1.2 x 10^{-3} mol dm^{-3} [68]). It was found that a layer formed in a 1 x 10^{-3} mol dm^{-3}DBS/0.1 mol dm^{-3} pyrrole, which takes a greater number of scans to form, exhibits identical behaviour to that in Figure 2.18 showing that the layer morphology is not affected by the DBS concentration in the solution in which the polypyrrole is formed.

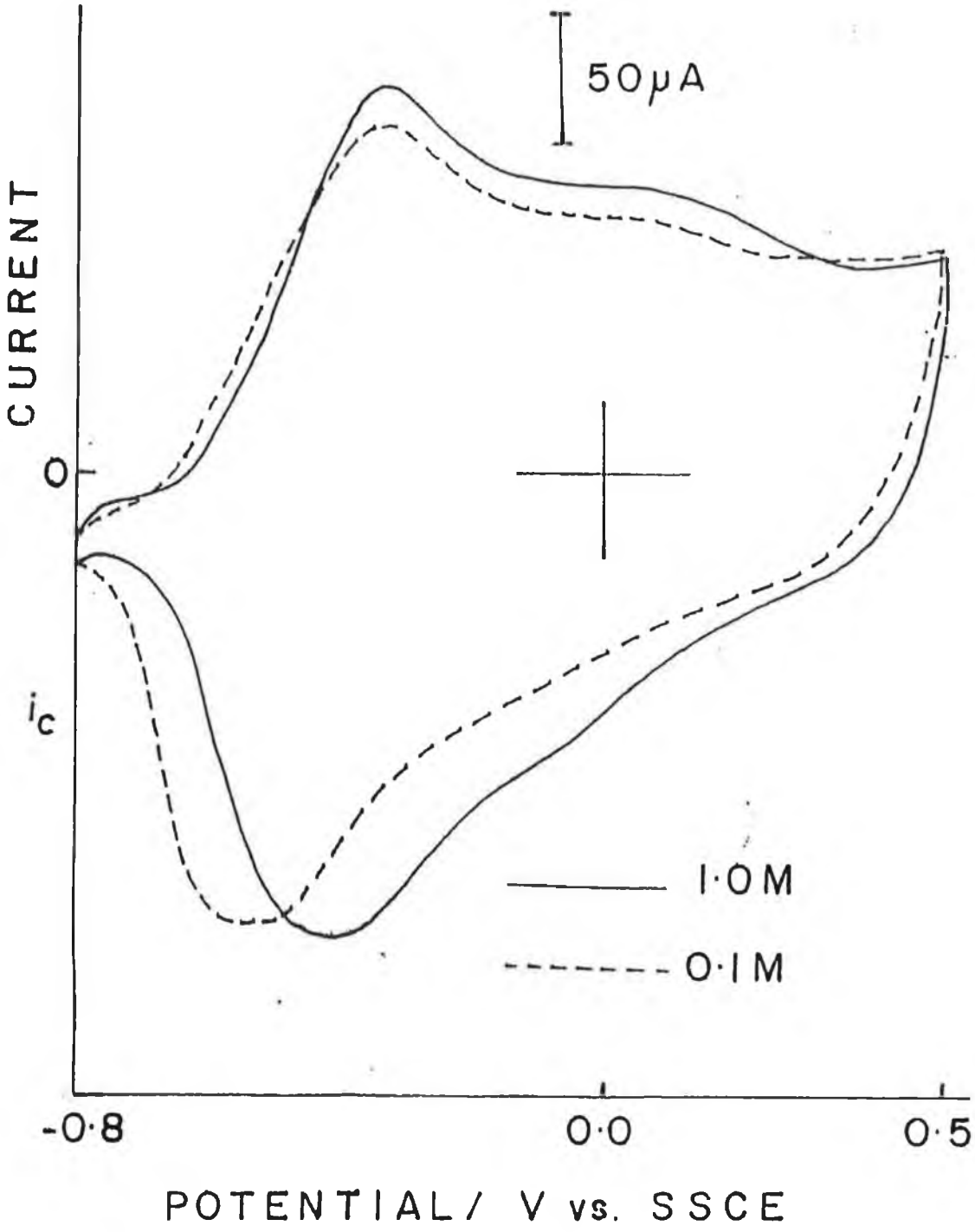

Figure 2.18 Cyclic voltammetry of a layer formed in 0.1 mol dm^{-3} NaDBS/0.1 mol dm^{-3} pyrrole by scanning continuously between 0 and 0.8V until 20 mC of charge had passed. The layer was then transferred to $LiClO_4$; the concentrations are shown in the figure.
Scan Rate = 50mV/s, and the Pt electrode area is 0.0707 cm^2.

2.4.6 CONCLUSION

It can be seen that the DBS irreversibly enters into polypyrrole layers and that electrochemistry is dominated by cation movement. So much so that when a $PPClO_4$ layer is placed in a DBS solution, the DBS extracts itself into the layer and the electrochemistry on cycling is dominated by cation movement.

That the layer electrochemistry is not due to the morphology of the layer can be seen since when a layer formed in ClO_4^- (cauliflower like morphology, viewed by SEM [12]) is placed in DBS, its electrochemistry is similar to that formed in DBS (which has a flatter morphology viewed by SEM). Therefore the electrochemistry and notably the small double layer charging current is due to the presence of a large anion in solution rather than the polymer morphology as has previously been implied.

2.5 REFERENCES

1. A. Angeli, Gazz. Chim. Ital. 1916, 46, II 279.
2. A.Angeli, L. Allessandri, Gazz. Chim. Ital. 1916, 46, II 283.
3. A. Dall Olio, Y. Dascola, V. Varacca, V. Bocchi, C.R. Hebd. Sceances, Acad. Sci. Ser. C., 267 (1969), 433.
4. A.F. Diaz, K.K. Kanazawa, G.P. Gardini. J. Chem. Soc., Chem. Commun., (1979), 635.
5. K.K. Kanazawa, A.F. Diaz, R.H. Geiss, W.D. Gill, J.F. Kwak, J.A. Logan and J.F. Rabolt. J. Chem. Soc., Chem. Commun, (1979), 854.
6. K.K. Kanazawa, A.F. Diaz, W.D. Gill, P.M. Grant, G.B. Street, G.P. Gardini, J.K. Kwak, Synth. Met., (1979/80), 1, 329.
7. G.B. Street, T.C. Clarke, M. Krounbi, K. Kanazawa, V. Lee, P. Pfluger, J.C. Scott, G. Weiser, Mol. Cryst. Liq-Cryst, (1982), 83, 253.
8. S. Asarapiriyanont, G.K. Chandler, G.A. Gunawardena, D. Pletcher, J. Electroanal. Chem. Interfacial Electrochem., (1984), 177, 229.
9. J. Prejza, I. Lundsträm, T. Skotheim, J. Electrochem. Soc., (1982), 129, 1685.
10. T. Inoue, T. Yamase, Bull. Chem. Soc. Jpn. 56, (1983), 985.
11. A. Diaz, Chem. Scr., (1981), 17, 145.
12. E.M. Genies, G. Bidon, A.F. Diaz, J. Electroanal. Chem. Interfacial Electrochem., (1983), 149, 101.
13. 'A First Course in Electrode Processes', Derek Fletcher, Pg. 37-44.
14. J.F. Rabolt, T.C. Clarke, K.K. Kananzawa, J.R. Reynolds, G.B. Street. J. Chem. Soc. Chem Commun., 347 (1980).

15. F. Godler, B. Perscheid, G. Kaindl, K. Menke, S. Roth. J. Phys. Part C.3 44, 233 (1983).

16. H. Sakai, Y. Maeda, T. Kobayashi, H. Shirakawa. Bull. Chem. Soc. Japan 56, 1616 (1983).

17. A.G. MacDiarmuid, A.J. Heeger. Synth. Met. 1, 101 (1980).

18. D.M. Ivory, G.G. Miller, J.M. Sowa, L.W. Shacklette, R.R. Chance, R.H. Baughmain. J. Chem. Phys. 71, 1506 (1979).

19. R.R. Chance, L.W. Shacklette, G.G. Miller, D.M. Ivory, J.M. Sowa, R.L. Elsenbaumer, R.H. Baughman. J. Chem. Soc. Chem. Commun. 348 (1980).

20. C.K. Baker, Y-.J. Qiu and J.R. Reynolds, J. Phys. Chem., 95, 4446, (1991).

21. K. Naoi, M.M. Lien and W. H. Smyrl, J. Electroanal. Chem., 272, 273, (1989).

22. K. Naoi, M.M. Lien and W.H. Smyrl, J. Electrochem. Soc., 138, 440 (1991).

23. C.S. Choi an H. Tachikawa, J. Am. Chem. Soc., 112, 1757, (1990).

24. T.A. Skotheim, M.V..Rosenthal and C.A. Linkous, J. Chem. Soc. Chem. Comm., 612, (1985).

25. F. Bedioui and J. Davynck, J. Chem. Soc. Faraday Trans., 88, 1567, (1992).

26. Q.X. Zhou, C.J. Kolaskie and L.L. Miller, J. Electroanal. Chem., 223, 283, (1987).

27. G. Lian and S. Dong, J. Electroanal. Chem., 260, 127, (1989).

28. J. Tietje-Girault, J.M. Anderson, I. MacInnes, M. Schroder, G. Tennant and H.H. Girault, J. Chem. Soc. Chem. Comm., 1095, (1987).

29. W. Breen, J.F. Cassidy and M.E.G. Lyons, J. Electroanal. Chem., 297, 445, (1991).

30. L.F. Warren and D.P. Anderson, J. Electrochemical Soc., 134, 101, (1987).

31. R. Noufi, D. Tench and L. F. Warren, J. Electrochem. Soc. 128, 2596, (1981).

32. M.E.G. Lyons, W. Breen and J.F. Cassidy, J. Chem. Soc., Faraday Trans. 87, 115, (1991).

33. X. Qui, R.P. Baldwin, H. Li and T.F. Guarr, Electroanalysis, 3, 119, (1991).

34. A. Elzing, A. van der Putten, W. Vischer and E. Barendrecht, J. Electroanal. Chem., 233, 99 and 113, (1987).

35. S. Dong and T. Kuwana, Electroanalysis, 3, 485, (1991).

36. J.F. Cassidy and M.B. Foley, Chemistry in Britain, September (1993), Pg. 1-6.

37. A.J. Bard and L.R. Faulkner, 'Electrochemical Methods, Principles and Applications', New York, John Wiley, (1980), Pg. 218.

38. R.S. Nicholson, Anal. Chem., 37 (1965), 1351.

39. R.S. Nicholson, I. Shain, Anal. Chem., 36 (1964), 706.

40. Y.P. Gokhshtein, Dokl. Akad. Nauk. SSR, 126 (1959), 598.

41. J. Cassidy, W. Breen, A. McGee, T. McCormac, M.E.G. Lyons., J. Electroanal. Chem., 333 (1992), 313-318.

42. A. Elzing, A. Van. Der Putten, W. Visscher, E. Barendrecht, J. Electroanal. Chem. (1987), 233, 99-112.

43. A. Elzing, A. Van Der Putten, W. Visscher, E. Barendrecht, J. Electroanal. Chem., (1987), 233, 113-123.

44. T.A. Skotheim, M.V. Rosenthal, C.A. Linkous, J. Chem. Soc., Chem. Commun, (1985), 612.

45. H. Mao, P.G. Pickup, J. Electroanal. Chem., (1989), 265, 127.

46. J. Redepenning, F.C. Anson, J. Phys. Chem. (1987), 91, 4549.

47. R. Naegeli, J. Redepenning, F.C. Anson, J. Phys. Chem., (1986), 90, 6227.

48. H.S. White, J. Leddy, A.J. Bard, J. Am. Chem. Soc., 104 (1982), 4811.

49. G.L. Duffit, P.G. Pickup, J.Chem. Soc. Faraday Trans. (1992), 88 (10), 1417.

50. J.M. Ko, H.W. Rhee, S.M. Park, C.Y. Kim, J. Electrochem. Soc. (1990), 137, No. 3, 905-909.

51. F. Girard, S. Ye, G. Laperriere, D. Belanger, J. Electroanal. Chem., (1992), 334, 35-55.

52. Electrochemical Methods Fundamentals and Applications, A.J. Bard, L.R. Faulkner, Pg. 409-413.

53. S. Panero, P. Prosperi, S. Passerini, B. Scrosati, D.P. Permutter, J. Electrochem. Soc., 136, 3729, (1989).

54. J. Heinze, M. Strozbach, J. Mortensen, Ber. Bunsenges, Physikal, Chemie, 91, 960, (1987).

55. M.E.G. Lyons, H.G. Fay, T. McCabe, J. Corish, J.G. Vos and A.J. Kelly, J. Chem. Soc. Faraday Trans, 86, 2905, (1990).

56. M.E.G. Lyons, H.G. Fay and T. McCabe, Key Eng. Materials, 72/74, 381 (1992).

56. R. John and G.G. Wallace, J. Electroanal. Chem., 354, 145 (1993).

57. L.F. Warren and D.P. Anderson, J. Electrochem. Soc. 134, 101 (1987).

58. L.F. Warren, J.A. Walker, D. P. Anderson, C.G. Rhodes and L.J. Buckley, J. Electrochem. Soc., 136, 2286, (1989).

59. M.E.G. Lyons, W. Breen and J.F. Cassidy, J. Chem. Soc. Faraday Trans. 87, 115, (1991).

60. M.E.G. Lyons, C.H. Lyons, C. Fitzgerald and T. Bannon, Analyst, 118, 361 (1993).

61. C. Zhong and K. Doblhofer, Electrochim. Acta, 35, 1971 (1990).

62. D. Blackwood, M. Josowicz, J. Phys. Chem., (1991), 95, 493-502.

63. V.M. Schmidt, C. Barbero and R. Kotz, 352 (1993), 301.

64. C. Zhong, K. Doblhofer and G. Weinberg, J. Chem. Soc. Faraday Discuss. 88 (1989), 307.

65. M.A. de Padi, S. Panero, P. Prospero and B. Scrasati, E.A. 35, (1990), 1145.

66. M.A. de Padi, S.C.D. Peres, S. Panero and B. Scrasati, E.A. 37 (1992), 1173.

67. Y. Li, W. Zhang and S. Dong, Electroanalysis, 5, 431, (1993).

68. R.J. Hunter, 'Zeta Potential in Colloid Science, Principles and Applications', Academic Press, London, (1981).

CHAPTER 3

DIFFERENTIAL PULSE VOLTAMMETRY OF CONDUCTING POLYMER LAYERS

3.1 INTRODUCTION

It has already been discussed in the preceeding chapters that conducting polymers can be switched between doped and undoped states. This switching process involves both electron and ion transport within the polymer film. Therefore conducting polymers can be said to possess both electronic and ionic conduction. Curtin et al [1] found that polypyrrole may also act as a solid state anion conductor along with electrical conductivity. They performed anion exchange experiments on electrochemically prepared thin films of polypyrrole perchlorate, and found that the anions are not tightly bound to the polymer matrix.

Shimadzu and coworkers [2,3] reported that ion transport in polypyrrole can be controlled by the use of polymeric anions. The ion transport properties of polypyrrole/polyanion composites will be different from polypyrrole films doped with small anions, as upon electrochemical switching the polymer films doped with the large anions involve cation transport through the polymer matrix.

Many of the applications of conducting polymers arise from their reversible switching between doped and undoped states. Therefore a knowledge of the redox kinetics and the associated mass/charge transport processes is essential. The kinetics of the redox switching of conducting polymers has been investigated by ac impedance [4-6], chronocoulometry [7-9], cyclic voltammetry [10,11] and chronoamperometry [12].

It is generally agreed that when the polymer is in a conducting state the rates of oxidation and reduction are limited by counterion motion within the film. In a.c. experiments this motion is measured as an ionic resistance. In cyclic voltammetric and potential step experiments, counterion motion has been treated as diffusion.

Pickup and Osteryoung [9] showed that potential step data from polypyrrole are better characterised by using a migration model. However, Schlenoff and Chien [13] concluded that migration effects in potential step experiments are unimportant. Paulse and Pickup [14] have found that following a potential step, the major mode of counterion transport through the polypyrrole film is by migration. They also show that uncompensated solution resistance causes errors in film ionic resistance measured by chronoamperometry and chronocoulometry.

There is disagreement among researchers in regard to whether ion movement within the layer is due to diffusion or migration for the movement of charge balancing ions. This leads to different kinetic models being applied to the polymer films behaviour. Certain groups [14,15] believe that the polymer film behaves like a porous electrode, where ion movement is due to migration and is

driven by a potential gradient. Others [16] have used the model proposed for redox polymers [17] and metal oxide electrodes [18] to explain their impedance data. In this treatment, the counterion movement is assumed to be a diffusion process.

Ren and Pickup [19] investigated the ionic conductivities of two types of polypyrrole layers, namely polypyrrole poly(styrenesulphonate) (PPPSS) and polypyrrole perchlorate ($PPClO_4^-$). The latter involves the movement of anions and the former, cation movement upon electrochemical switching.

The ionic conductivity of the PPPSS was found to be significantly higher than that of $PPClO_4^-$ at all potentials, indicating that cations in the former are more mobile than the ClO_4^- in $PPClO_4^-$.

To fully understand the behaviour of conducting polymer electrodes in electrolyte solutions; an understanding of the nature of the charge transport processes that occur at the polymer/solution interface is required. Impedance studies [20] have been performed to try to fully understand the polymer structure. The modelling of ionic and electronic conduction through membranes like conducting polymers has received much attention. The use of transmission lines as circuit elements has been advocated by Rubinstein [21] and Buck [22]. The classical transmission line has a distributed capacitance which connects a resistive line to a wire of zero resistance. This is appropriate when talking about two charge carriers, one more mobile than the other. The more mobile being the wire of zero resistance and the resistive line describes the less mobile carrier.

Albery et al [23] developed a novel transmission line in which a distributed capacitance is placed between two resistive elements. These resistive elements represent the transport of electrons, R_E, and counterions, R_I, within the polymer. They used this transmission line to model impedance data for polypyrrole.

Albery et al [24] claim to have observed a case where the ionic and electronic resistances are comparable. Recently, Ren and Pickup [43] tested Albery's transmission line model for conditions ranging from where the ionic and electronic resistances are unequal ($R_E >> R_I$ and $R_I >> R_E$). They found that the model works well for when the resistances are very unequal, however when the resistances are equal anomalous results were obtained. Fletcher [25] recently proposed an electrical model circuit that can reproduce the small amplitude impedance behaviour of conducting polymer electrodes in electrolyte solution. The model is that of a porous electrode containing a large number of identical non-interconnected pores. The model circuit of a single pore is characterised by three impedances, one characteristic of the pore interior, one for the solid part of the polymer and the third being of the polymer solution interphase. It has been reported previously that electrochemical cycling of polypyrrole causes a non-equilibrium build up of electrolyte in the polymer [26]. Therefore these films exhibit a higher ionic conductivity than uncycled films. Recently [27] the ionic conductivity of polypyrrole films formed in water and acetonitrile upon cycling was monitored by impedance spectroscopy. It was found that water solvates the polymer and greatly increases the mobility of its counterions, but solvation by acetonitrile is not effective in promoting counterion mobility.

A conducting polymer has also been characterised as a particular example of a redox polymer [27]. Thus it has characteristics similar to those of complex-containing Nafion films [28,29], in that the formal potential of the system varies with external electrolyte concentration [30,31]. Furthermore the capacitive like behaviour has been said to be due to a range of formal potentials associated with different oligomer lengths [32].

The capacitance effect observed in the cyclic voltammograms of conducting polymers has been analyzed by ac impedance mesurements, [6]. Shallowly trapped ions were found to be responsible for the capacitance effect, with deeply trapped ions giving rise to a noncapacitive current and being responsible for the broadening of the reduction peak.

In an effort to probe the polymer system, a differential pulse waveform, which is popular in analysis for reducing the effects of capacitance [33,34] was applied to the layers. The naive expectation that this waveform would remove the capacitance effects and yield only faradaic current was not realised. The response was determined by the resistance of the system characteristic upon the change in resistance of the polymer layer upon switching. Wallace et al [31,35] observed a sigmoidal change in resistance upon electrochemical switching of the polymer.

3.2. THEORY

3.2.1. THEORY OF POTENTIAL STEP EXPERIMENTS

Potential Step Techniques in electrochemistry involve changing the potential of the working electrode rapidly from one potential value, E1, to another E2. E1 is usually chosen to be a potential where no current flows. A current time response (chronoamperometry) or a charge-time response (chronocoulometry) can be recorded. Most potential step techniques are carried out where diffusion is the only from of mass transport present.

Let us consider the electrode reaction:

$$O + ne^- \rightarrow R \quad ..... \quad E^{01} \qquad 3.1$$

where only the species O is initially present in solution.

The potential time profile applied to the working electrode is illustrated in Figure 3.1. The potential of the working electrode can be stepped into 3 separate regions. These regions are where the current is diffusion controlled, under mixed control and where the current is purely kinetically controlled. The current-time transient produced for the reaction (3.1), when the current is

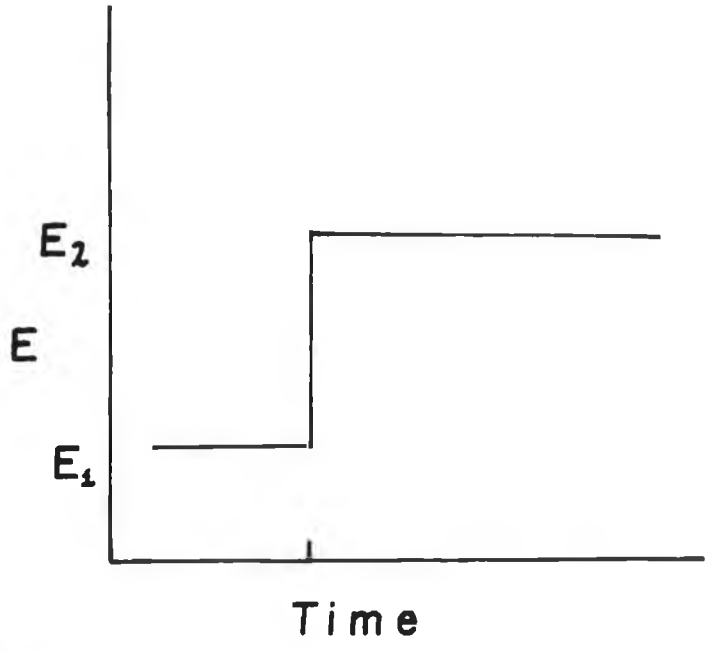

Figure 3.1 The potential - time profile for a single potential step chronoamperometric experiment.

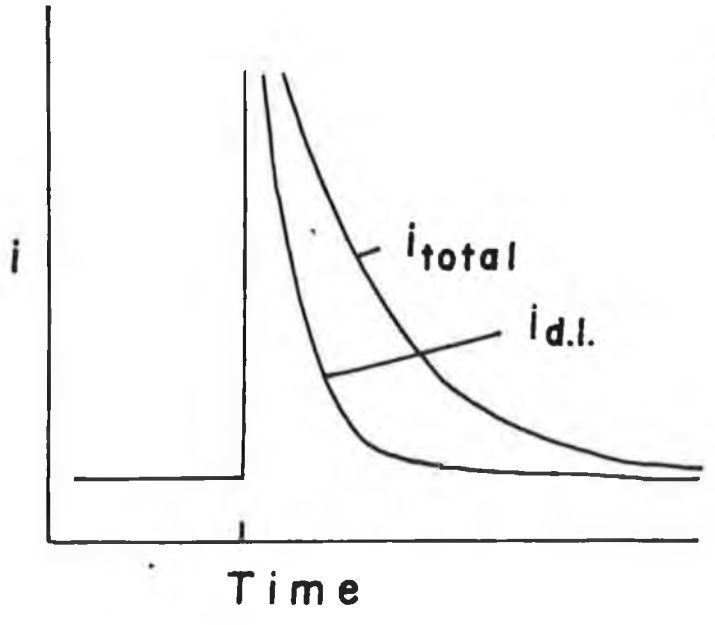

Figure 3.2 Current time transient for a potential step experiment. The total current and the double layer charging current components are shown.

diffusion controlled is illustrated in Figure 3.2. It can be seen from Figure 3.2 that there are two components to the current, one being the associated faradaic current and also the double layer charging current. This is one problem associated with potential step techniques, the presence of the double layer current. This current usually takes in the order of a few hundred microseconds to decay. Time to decay can depend on electrolyte concentration.

The response to a potential step for reaction (3.1), into a diffusion controlled region can be explained by considering the growth of the diffusion layer out into solution. If the potential of the working electrode is stepped to a large negative overpotential, rapid reduction of species O at the electrode surface will occur. Effectively the surface concentration of O decreases from bulk solution value to zero. At short times the concentration of O will only have changed from its initial bulk solution value, at points close to the electrode surface, and hence the concentration profile will be steep. As time increases, diffusion occurs, causing the concentration profiles to relax further out into solution.

The response will be a transient where the current density falls with time, as seen in Figure 3.2.

The resulting Faradaic current is governed for linear one dimensional diffusion by the equation [33]

$$i = \frac{nFA\, D^{1/2}\, C^*}{(\pi t)^{1/2}} \qquad \text{.....} \qquad 3.2$$

where n is the number of electrons transferred, D is the diffusion coefficient and C* is the bulk concentration of the reactant. This equation has been used to determine if an electrode reaction is diffusion controlled within the applied potential range and values of the diffusion coefficient for species may be determined once the electrochemical area A is known.

If the potential is stepped into a region of mixed control, kinetic parameters, such as rate constants, can be determined [33].

3.2.2 THEORY OF DIFFERENTIAL PULSE VOLTAMMETRY

Pulse Voltammetric Techniques were developed to increase sensitivity in analytical applications. There are a number of pulse voltammetric techniques, including normal pulse voltammetry and differential pulse voltammetry. The potential-time waveform applied to the working electrode for a differential pulse voltammetric experiment is shown in Figure 3.3(a).

The applied waveform shown in Figure 3.3(a) consists of a ramp base potential, upon which pulses of constant amplitude are applied.

The pulse height ΔE is usually between 10 and 100mV, and is maintained at a constant magnitude. Also two current measurements are taken, one being at a time τ_1, immediately before the pulse, and the second being at a time τ_2, late in the pulse. For the particular instrument employed, (EDT potentiostat, ECP 100), the time difference between the two samples was of the order of 55

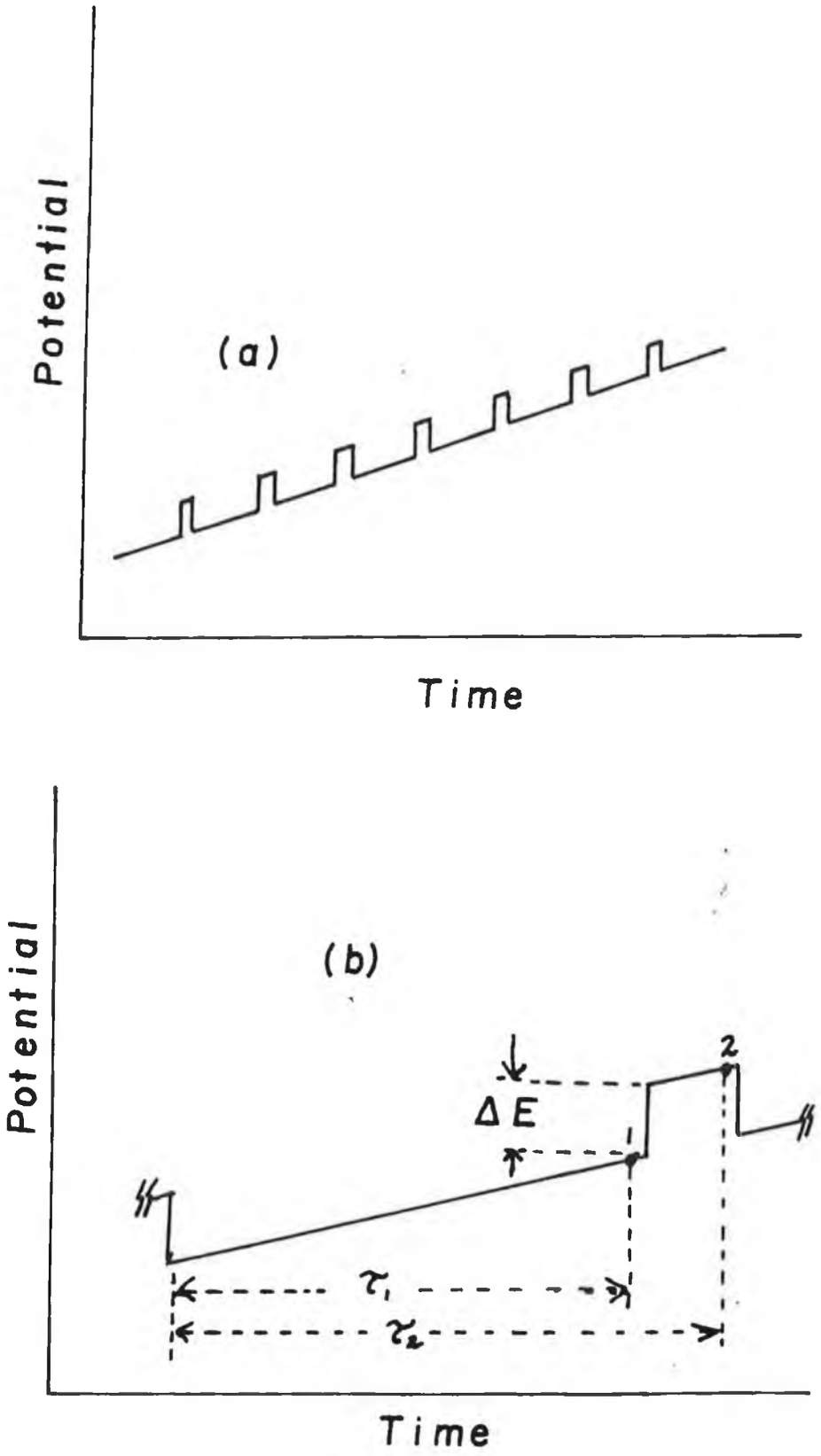

Figure 3.3 (a) The potential time profile applied to the working electrode for a differential pulse voltammetric experiment.

(b) Current sampling technique of differential pulse voltammetric experiment.

milliseconds. It is also the difference between the currents sampled at τ_1 and τ_2 which is output as a function of the base potential.

For Polarography, Differential Pulse Polarograms are peak shaped and the limit of detection for amalgam forming metals is about one order of magnitude lower than that for normal pulse voltammetry i.e., 10^{-9} mol dm^{-3} [33].

When using a dropping mercury electrode, the applied pulses are synchronised with the drop time. The pulse is applied late in the life of the drop, and as the potential is returned to the base potential the drop is knocked off.

The current sampling technique of differential pulse voltammetry is illustrated in Figure 3.3(b). For differential pulse polarography the height of the peaked waveform is given by the equation [33].

$$\delta i_{max} = \frac{nFAC_0^* D_0^{1/2}}{\pi^{1/2} (\tau_2 - \tau_1)^{1/2}} \frac{(1-\sigma)}{(1+\sigma)} \quad \ldots\ldots \quad 3.3$$

where $$\sigma = \exp\left[\frac{nF}{RT}\frac{\Delta E}{2}\right]$$

and ΔE is the pulse amplitude.

For large pulse amplitudes, the term $\frac{1-\sigma}{1+\sigma}$ approaches unity.

However under usual conditions the quotient term never equals unity, thereby

δi_{max} never reaches its possible maximum value.

One of the major advantages of differential pulse voltammetry over other conventional electroanalytical techniques is the absence of the double layer charging current. This is primarily due to the sampling delay ($\tau_2 - \tau_1$) of the current. It is believed that within the time delay, the non-faradaic component of the current will have decayed to zero. However for differential pulse polarography the charging current is reduced but never decays to zero due to the area of the mercury drop changing with time, thereby requiring a new double layer.

The differential charging current for a DME is given by the equation [33]

$$\delta\iota_C = -0.00567 C_\iota \Delta E m^{2/3} \tau_2^{-1/3} \quad \ldots\ldots \quad 3.4$$

where m is the rate of mercury flow from the dropping mercury electrode capillary which implies that as ΔE decreases the contribution of double layer charging current decreases.

3.3 EXPERIMENTAL

All chemicals employed were reagent grade. Pyrrole was distilled and stored in the dark under a nitrogen atmosphere. Electrochemical experiments were carried out in a three electrode one compartment cell. A platinum disk surrounded by teflon, diameter = 3mm, was used as a working electrode. A saturated calomel electrode was used as a reference electrode. For cyclic voltammetry experiments, a H.B. Thompson waveform generator (Model DRG

16) was used and a EDT potentiostat (ECP 100) and an integrator (Sycopel DP3015) were linked to a JJ Lloyd XY Recorder (PL3). For differential pulse experiments the drop time was 1 second and the pulse width was 55ms.

The polypyrrole tetrasulphonated phythalocyanine layers were prepared electrochemically by holding the platinum electrode potential at 0.9 Volts (vs SCE) in an degassed aqueous solution of pyrrole (0.1M) and Cu(ll) tetrasulphonated phthalocyanine obtained as a sodium salt from Aldrich, (1×10^{-3}M). Layer thicknesses were changed by varying the amount of charge deposited, ranging from 5mC to 25mC.

The polypyrrole chloride layers were prepared electrochemically by holding the potential of the working electrode at 0.8 volts vs SCE in a degassed aqueous solution of pyrrole (0.1M) and NaCl (0.1M).

The polypyrrole containing $[Fe(CN)_6]^{4-}$ was also prepared electrochemically. The potential of the working electrode was held at 0.8V vs SCE for 1 minute in a degassed aqueous solution of $[Fe(CN)_6]^{4-}$ (0.1M) and pyrrole (0.1M). The layer was removed and rinsed with deionised water. It was then transferred to an aqueous solution of the chosen electrolyte and cycled between -0.2V and +0.5V until a steady state continuous cyclic voltammogram was obtained. This was necessary since a 'breaking-in' process occurs.

The Ru^{2+} modified electrodes were prepared by first polishing the platinum electrode with alumina (0.3μm) and coating the electrode with a solution of the polymer in methanol and allowing it to cure.

3.4 RESULTS AND DISCUSSION

3.4.1 DIFFERENTIAL PULSE VOLTAMMETRY OF POLYMER LAYERS

The cyclic voltammetric behaviour of the polypyrrole tetrasulphonated phthalocyanine layer (PPTSP) has already been mentioned in the preceeding chapter. Due to the structure of most conductive polymers, there is a large non faradaic component of the current in the cyclic voltammogram. This is illustrated in Figure 3.4, which shows the cyclic voltammogram (CV) of a PPTPS layer in a solution of NaCl (0.1M).

It is the presence of this non faradaic current component that makes measurement of the faradaic current, associated with oxidation and reduction, difficult to measure. The main aim for the application of differential pulse voltammetry (DPV) to the conducting polymer coated electrode was to differentiate between these two components. This technique has not previously been applied to conductive polymer layers and has previously been used to remove capacitive currents in polarographic experiments [33].

This technique was applied to a 25mC PPTSP layer, formed as previously described. The layer was washed and cycled in a degassed aqueous solution of NaCl (0.05M) until a steady state cyclic voltammogram was obtained. The layer was then transferred to a fresh degassed aqueous solution of NaCl (0.05M). DPV was carried out on the layer by scanning the potential between 0.5V and -0.9V, with the application of pulses of constant amplitude chosen between 10mV and 50mV. Figure 3.5 shows the current resulting from the application of

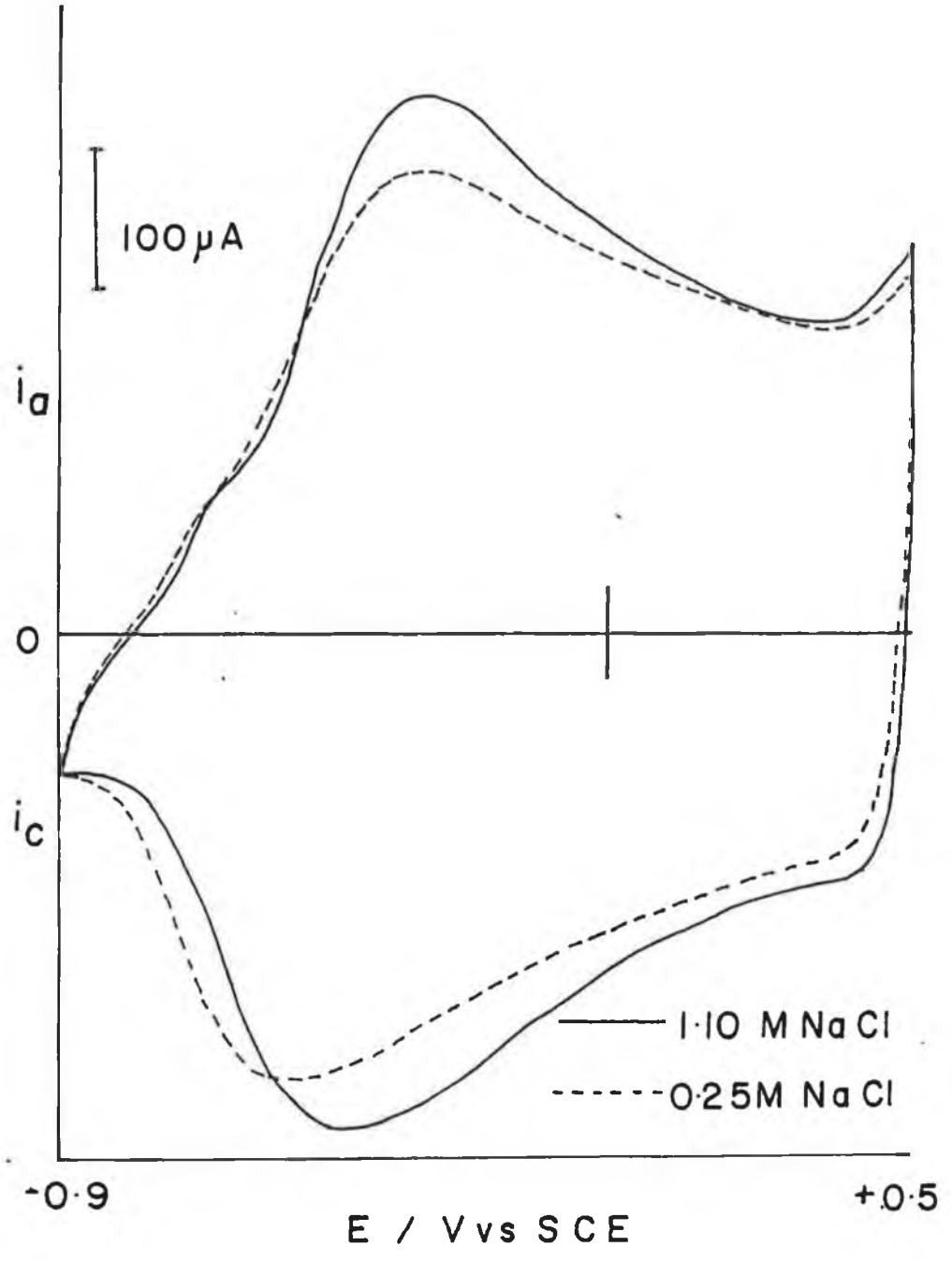

Figure 3.4 Cyclic voltammogram of a PPTSP layer in NaCl electrolyte. The layer being previously deposited by holding the potential at 0.9V in 0.1M pyrrole and 1 x 10^{-3}M Cu(II) TSP. Scan Rate = 100mV/s.

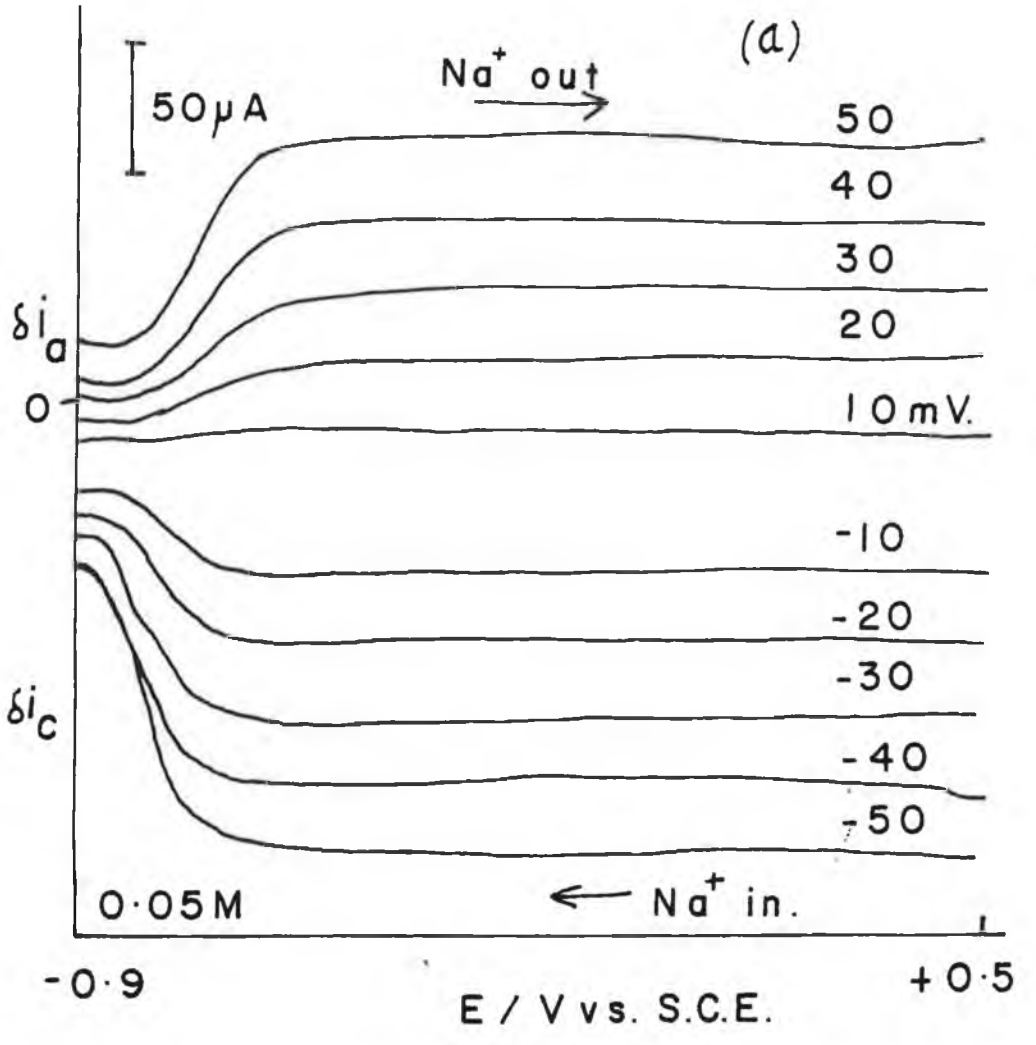

Figure 3.5 Differential Pulse voltammograms of PPTSP layers, formed as described in Figure 3.4, in 0.05M NaCl solutions.
Scan Rate = 10mV/s. RC time constant = 0.1.
(a) 25mC (b) 20mC (c) 15mC (d) 10mC.

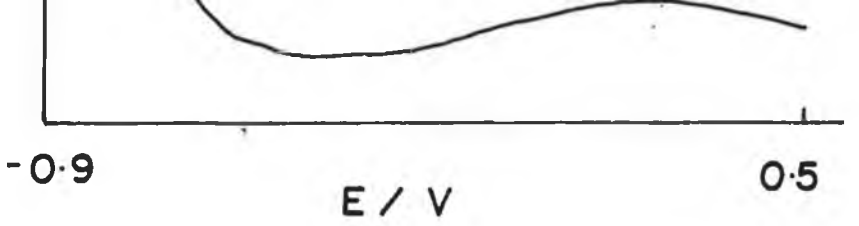
-0·9
E / V
0·5

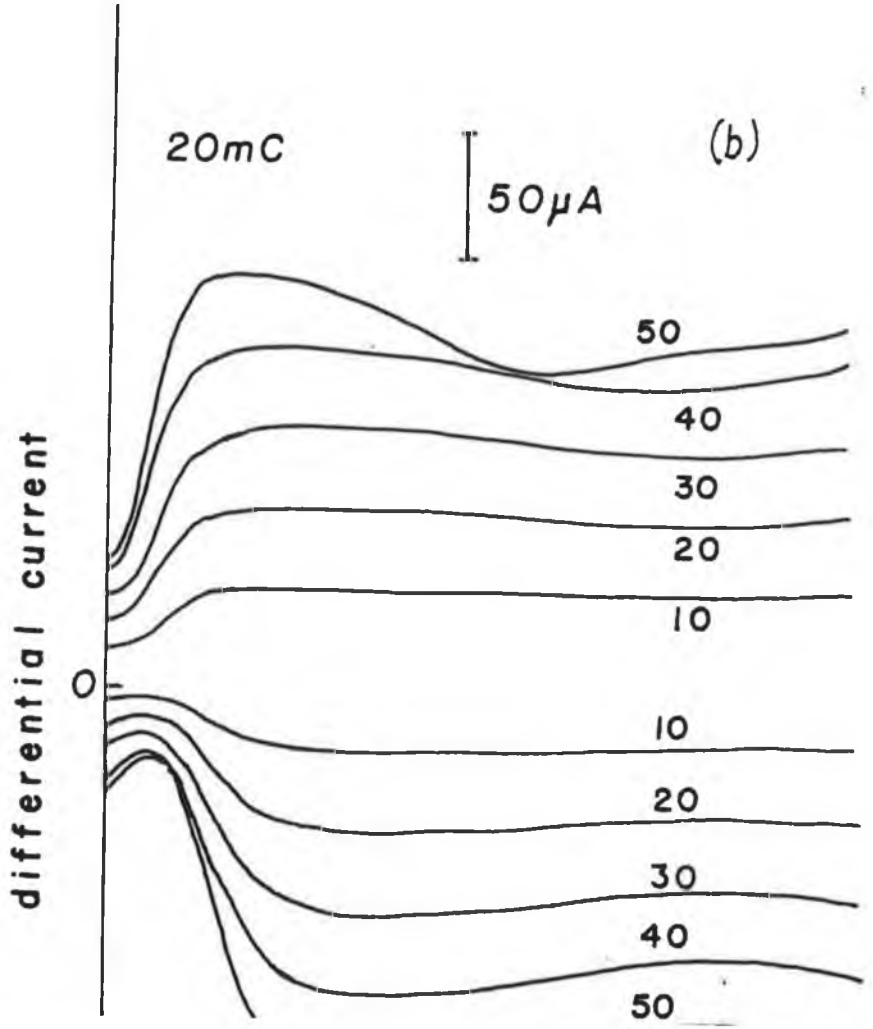
20mC
50μA
(b)
50
40
30
20
10
0
10
20
30
40
50
differential current

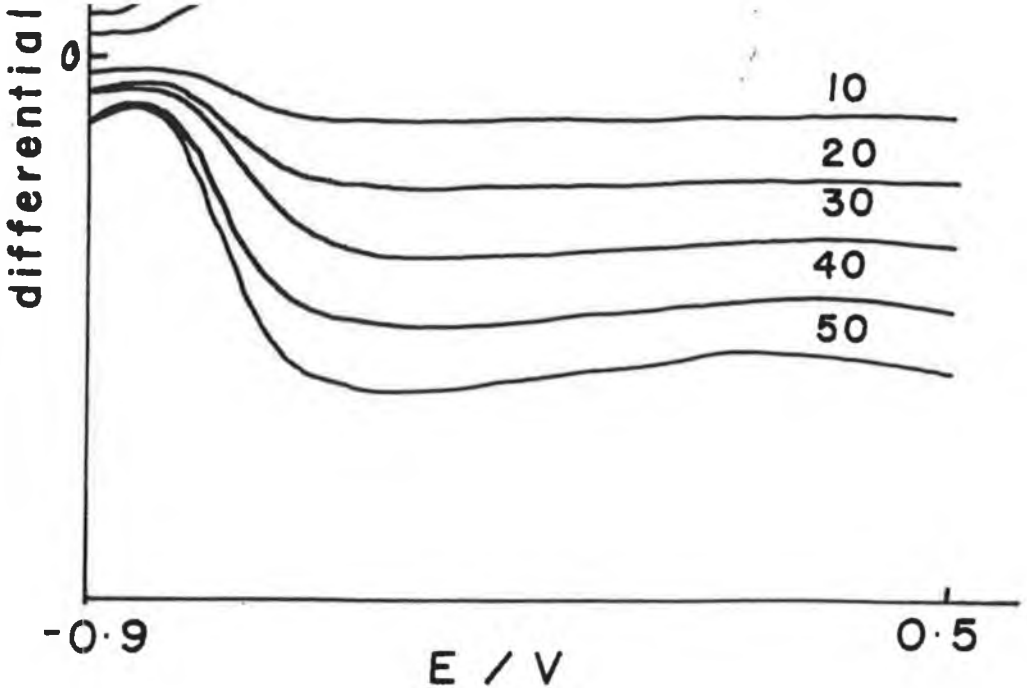
differential
0
10
20
30
40
50
-0·9
0·5
E / V

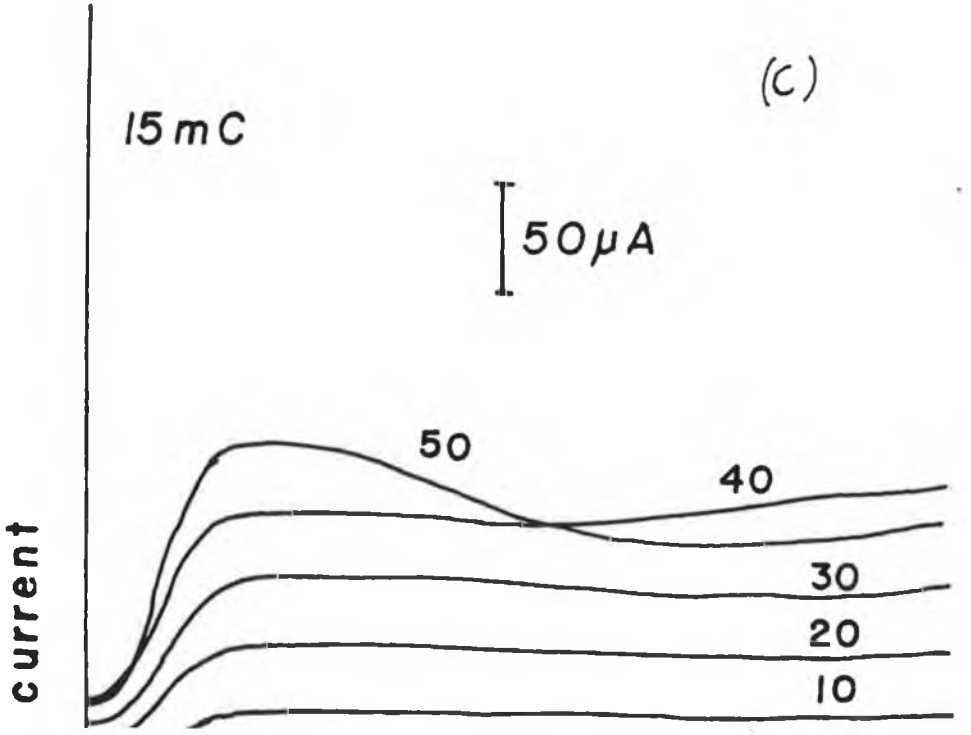
(C)
15 mC
50μA
50
40
30
20
10
current

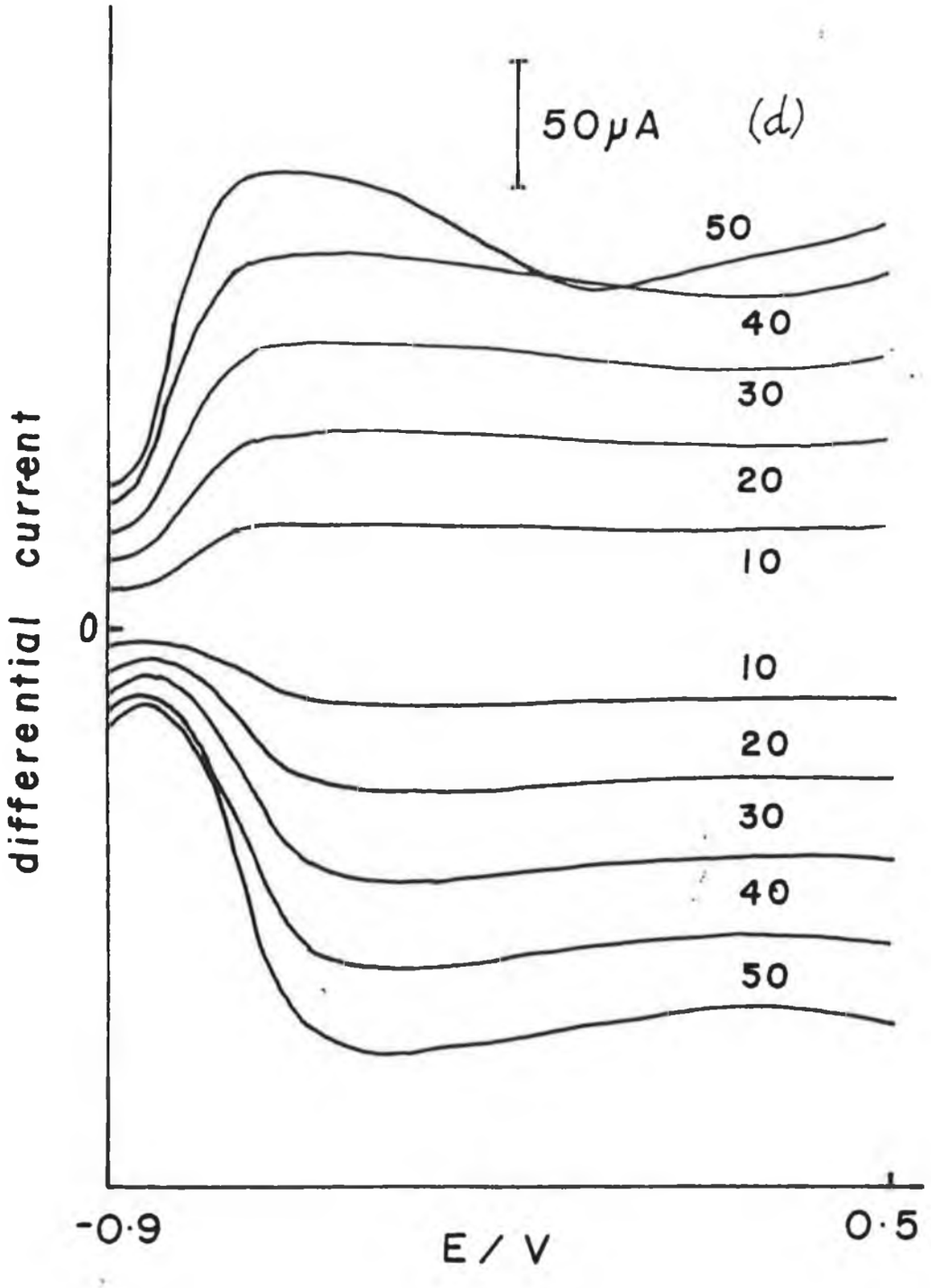
50μA
(d)
50
40
30
20
10
0
10
20
30
40
50
differential current
-0·9
E / V
0·5

a differential pulse waveform to a PPTSP layer for both positive and negative going scans for a range of layer thicknesses. It can be seen that no definite cathodic or anodic peak was obtained. The response reaches a plateau characteristic of resistive behaviour. If a DPV potential waveform is applied to a resistor the differential current obtained is constant. It was found that the limiting differential current magnitude varied linearly with pulse amplitude, for both the oxidised and reduced froms of the layer. Figure 3.6 shows the plots, for the PPTSP layer, of the limiting differential current magnitude against pulse amplitude.

Resistances of $357 \pm 11\Omega$ and $1176 \pm 176\Omega$ were estimated for the oxidised and reduced layers respectively.

To investigate if the limiting currents were dependent upon external electrolyte concentration, a differential pulse voltammetric waveform was applied to a platinum electrode modified with a known ionically conducting layer poly (4-vinylpyridine) (PVP) bound ruthenium bis (2,2'-bipyridyl) (bpy) complex [37], $[Ru(bpy)_2(PVP)_5Cl]Cl$.

Cyclic voltammetry was performed on the layer in an aqueous solution of 0.2M $NaClO_4$. The resulting cyclic voltammogram is shown in Figure 3.7. It can be seen that thin layer voltammetry is not observed, but rather bulk solution behaviour is seen for the modified electrode. Oxidation and reduction of the layer correspond to the $1e^-$ oxidation of Ru(ll) to Ru(lll). The cyclic voltammogram also exhibits an assymmetric shape with a peak to peak separation of 200 mV.

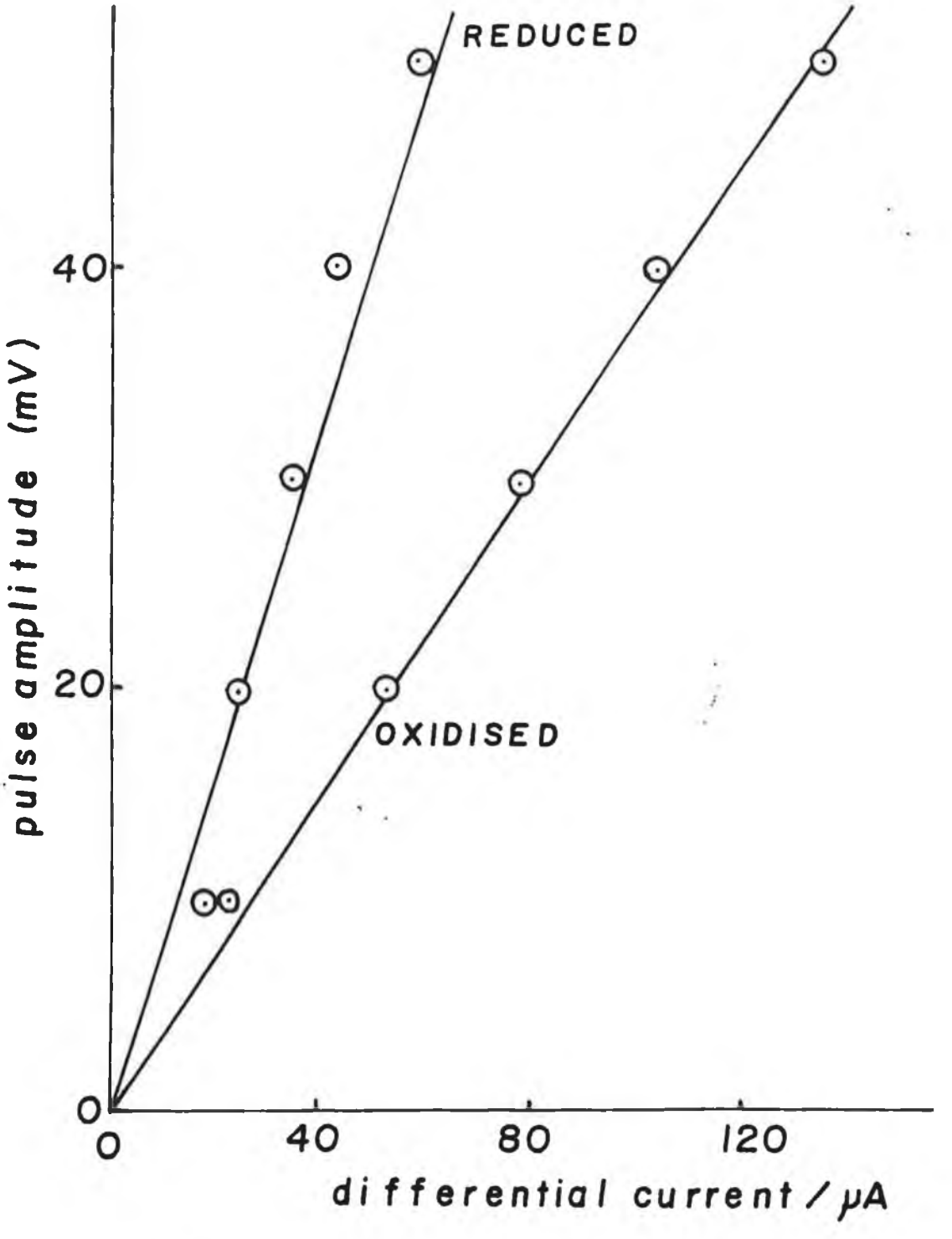

Figure 3.6 Plot of the limiting differential current magnitude against pulse amplitude for both the oxidised and reduced forms of the PPTSP layer.

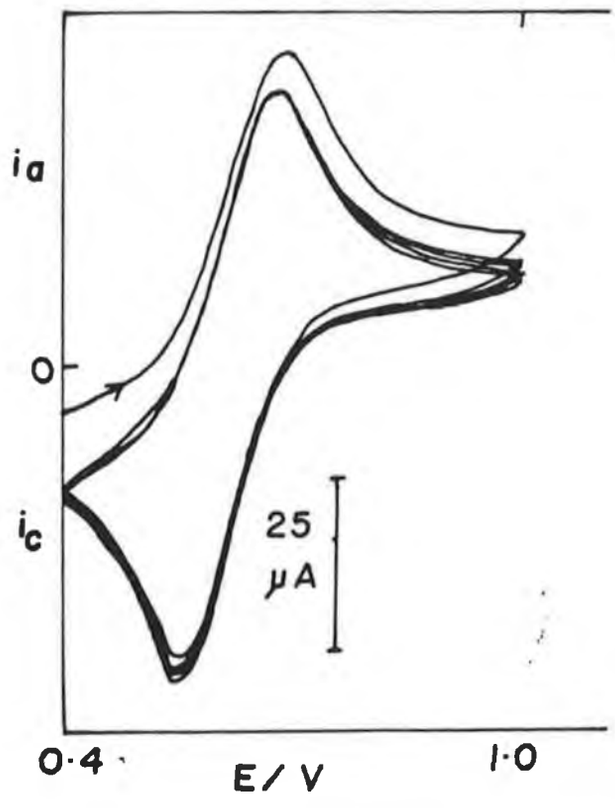

Figure 3.7 Cyclic voltammogram of a Ru^{2+} layer in an aqueous solution of 0.2M $NaClO_4$.
Scan Rate = 50mV/s.

A Ru^{2+} polymer layer was formed on a platinum electrode, as previously described. The layer was then cycled in an aqueous solution of $LiClO_4$ (1.0M) until a steady cyclic voltammogram was obtained.

The layer after cycling was then stepped to a positive potential where the oxidation of the Ru^{2+} to Ru^{3+} was diffusion controlled. The decay in current was then recorded and a plot of current versus $1/\sqrt{t}$ was plotted as seen in Figure 3.8.

It can be seen that a linear plot is obtained, indicating that the current is diffusion controlled. However when the time is equal to 6 seconds or more, deviation away linearity is observed, with the current decaying to zero. This was expected, as it indicates that the depletion layer has extended out to the boundaries of the layer. Therefore the concentration of the reduced species approaches zero, thus the current decays to zero.

Figure 3.9 shows the peaked differential current output obtained for the $[Ru(bpy)_2(PVP)_5Cl]Cl$ layer upon the application of a DPV waveform. It can be seen that two well defined peaks are observed with a more symmetric shape being observed (ΔEp = 80mV). No limiting current plateau is observed therefore leading to the conclusion that the current plateau observed in Figure 3.5 is characteristic of the conducting polymer and not due to resistance associated with the external electrolyte concentration.

The effect of layer thickness on the differential current response was examined. PPTSP polymer layers were deposited with 20mC, 15mC and 10mC of charge.

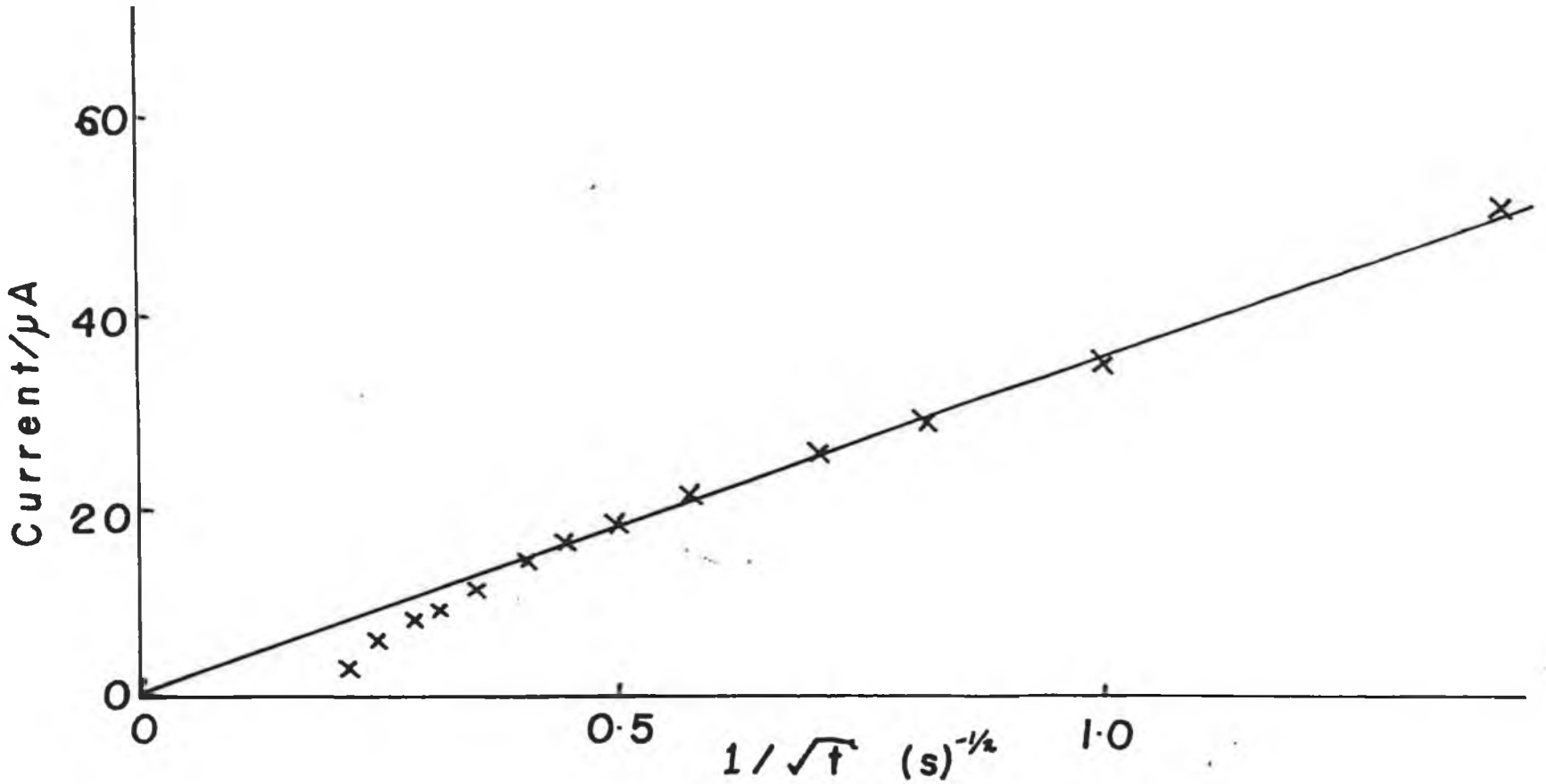

Figure 3.8 Plot of decay current obtained for the Ru^{2+} layer after a potential step, versus $t^{-½}$.

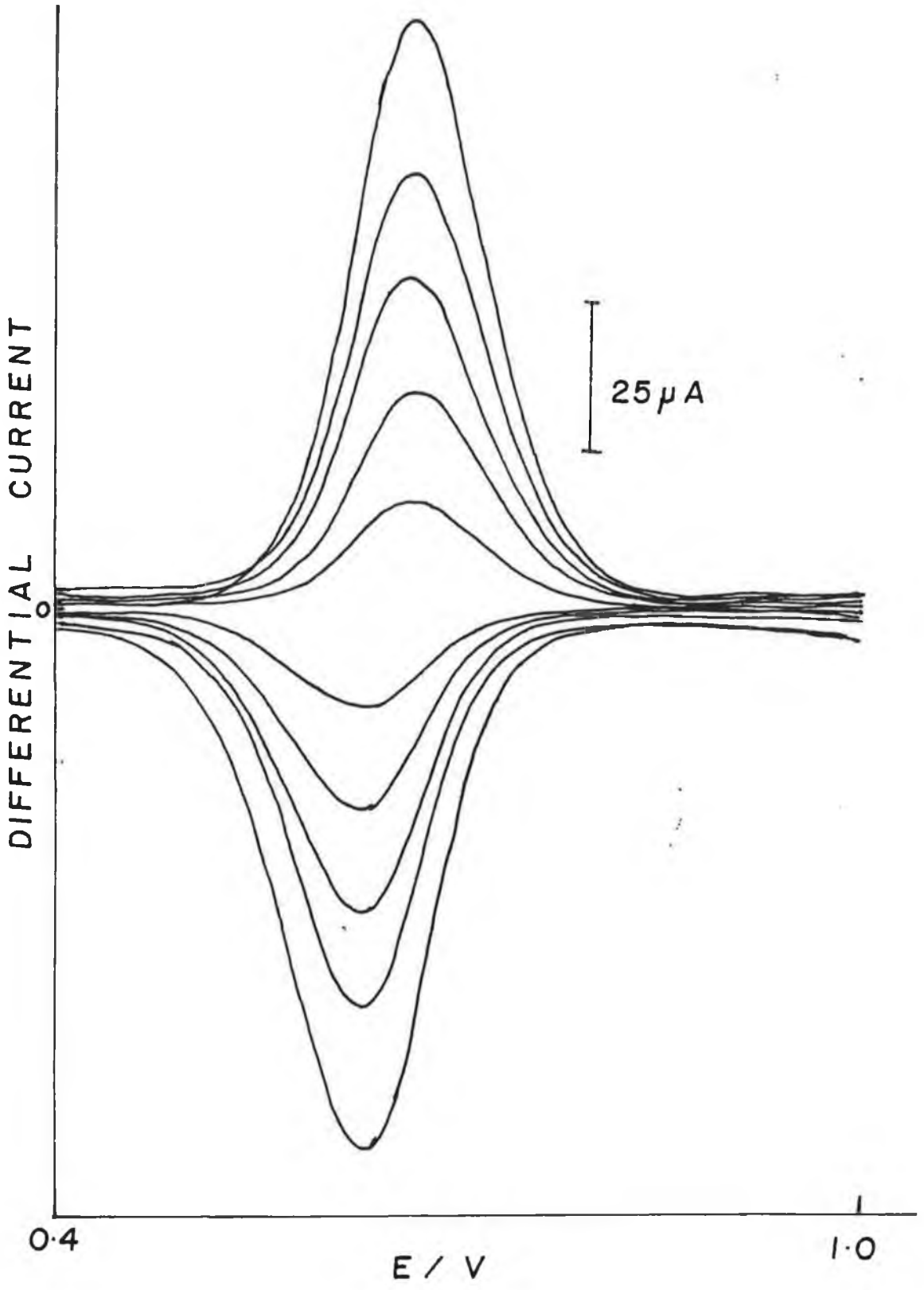

Figure 3.9 Differential pulse voltammogram of a Ru^{2+} layer in a 0.2M $NaClO_4$. Scan Rate = 10mV/s. RC time constant = 0.1.

Figure 3.5(b) to (d) show the resulting differential pulse voltammograms for the various polymer layers. It can be seen that identical behaviour is observed , with a sigmoidal current response, for all layers. This may possibly indicate that the dominent resistance being observed is that of an interface between the surface of the polymer layer and the solution. Alternatively it may indicate that under these conditions the diffusion layer does not extend to the polymer solution interface.

DPV was also carried out on a polypyrrole chloride layer (PPCl).
A 25 mC layer was prepared electrochemically, from an aqueous solution of pyrrole (0.1M) and NaCl (0.1M) by holding the potential at 0.8 volts (SCE). The layer was washed and cycled in a solution of NaCl (0.05M). When a steady state cyclic voltammogram was obtained the layer was transferred to a fresh solution of NaCl (0.05M) and DPV was performed.

Figure 3.10 shows the resulting voltammogram obtained. Again, as with the PPTSP layer no definite cathodic or anodic peak were obtained.

The PPCl showed less of a simple resistive behaviour than the PPTSP layer, though a limiting current plateau is still observed.

The effect of background electrolyte concentration, on the differential current outputs for the PPTSP layer was examined. A new layer was formed, cycled in an aqueous solution of NaCl (3.0M) until a steady state cyclic voltammogram was obtained. The layer was then transferred to a fresh solution of NaCl (3.0M) and DPV was applied to the layer. Figure 3.11 shows the DPV obtained for this

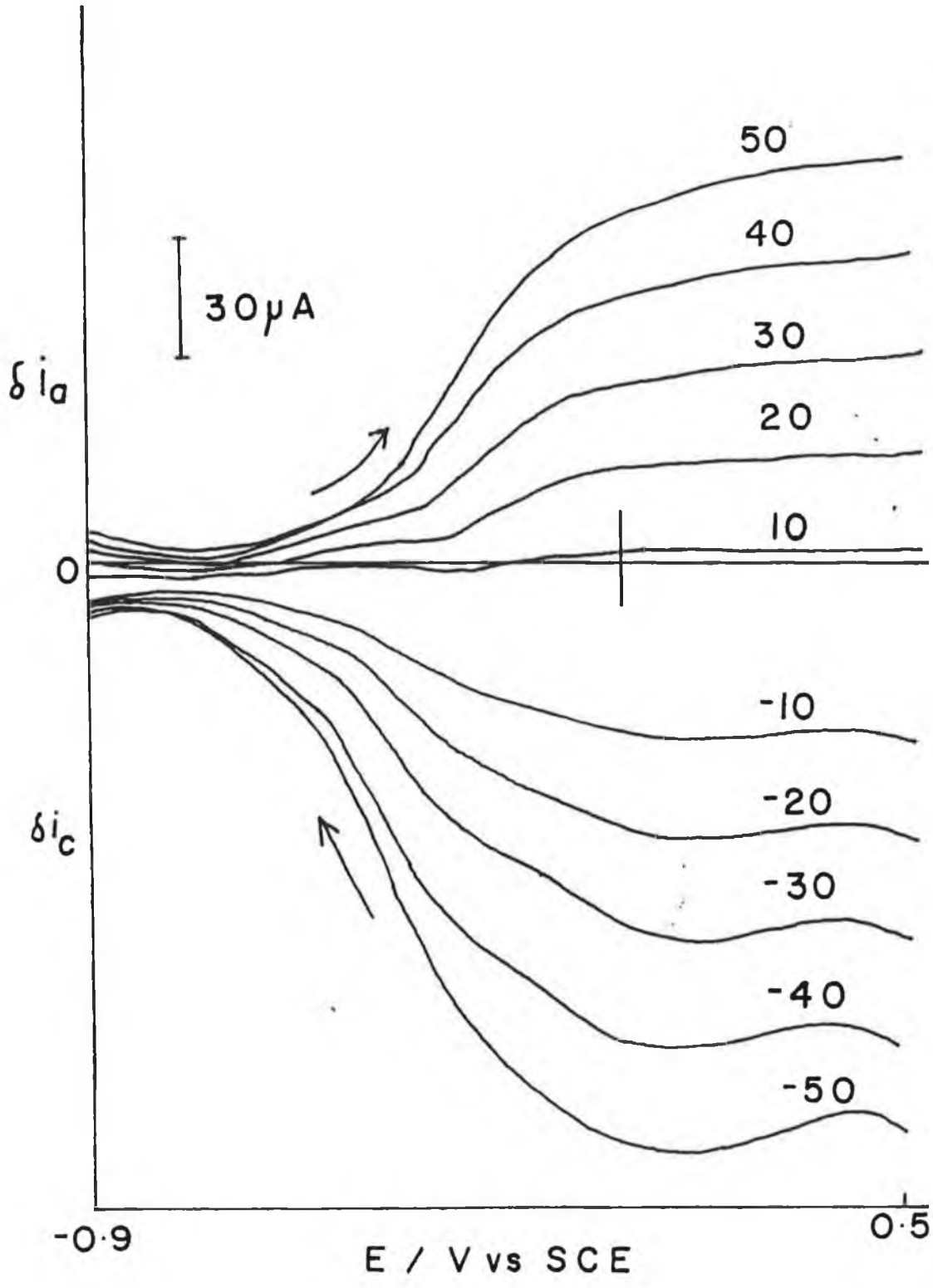

Figure 3.10 Differential pulse voltammogram of a PPCl layer in an aqueous 0.05M NaCl solution. The layer previously being formed by holding the potential of the working electrode at 0.8V in a degassed aqueous solution of 0.1M pyrrole and 0.1M NaCl.
Scan Rate = 10mV/s. RC time constant = 0.1.

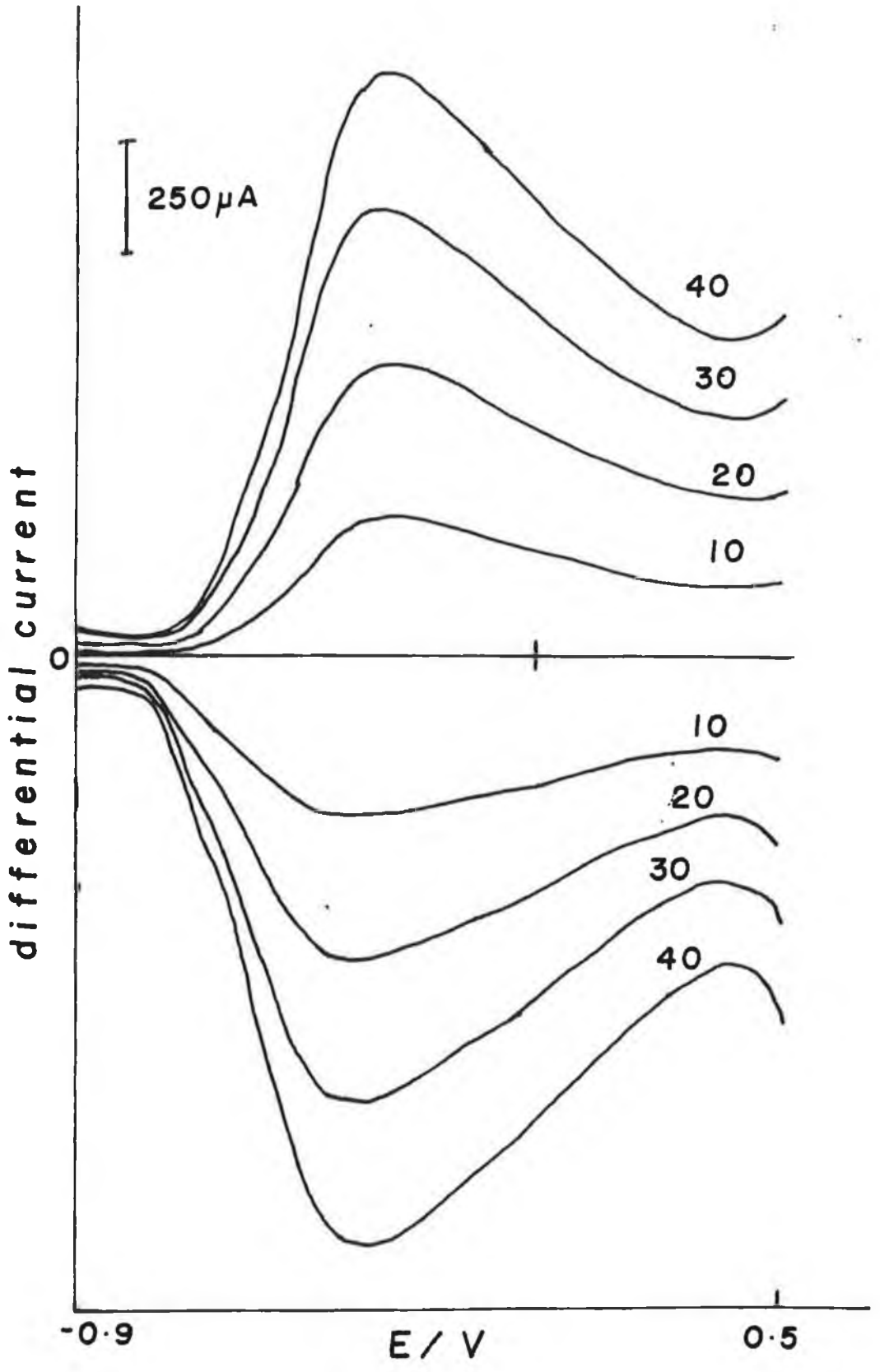

Figure 3.11 Differential pulse voltammogram of a PPTSP layer, formed as described in Figure 3.4, in a 3.0M NaCl solution.
Scan Rate = 10mV/s. RC time constant = 0.1.

PPTSP layer. It can be seen that a more definite cathodic and anodic peaks are obtained, with no current plateau being obseved.

These results imply that the resistive behaviour of the layer is dependent upon the electrolyte concentration. A similar situation was previously reported for a polypyrrole layer [36], where the film resistance was found to be dependent on the solution electrolyte concentration.

Due to these results obtained, a study of the change in film resistance with electrolyte concentration was performed. A 25mC PPTSP was formed in the usual manner, washed, and run in an aqueous solution of KCl (0.3M) until a steady state cyclic voltammogram was obtained. The layer was transferred to a fresh solution of KCl (0.3M). The potential was scanned continuously between +0.5V and -0.9V with the application of a pulse of amplitude 40mV. The concentration of the supporting electrolyte was varied from 0.3M to 0.075M, and a change in film resistance was noted.
Figure 3.12 shows the DPV obtained. Table 3.1, below summarises the results obtained.

TABLE 3.1 Apparent film resistance versus electrolyte concentration.

ELECTROLYTE CONCENTRATION MOLES/l	FILM RESISTANCE OHMS
0.214	84.6±1.7
0.188	93.7±1.9
0.150	107.2±2.1

0.120	129.5±2.6
0.100	146.5±2.9
0.075	294.1±5.9

This increase in film resistance with decreasing electrolyte concentration has been previously found for a polypyrrole layer [36], using a series of current pulses. These results can be explained in terms of the ionic conduction of the polymer film. It is possible that excess electrolyte is incorporated into the polymer phase within the pores. It has been reported [36], that in terms of ionic conduction, polypyrrole doped with a certain anion could be viewed as two parallel resistors. A resistor, R_1, associated with the movement of charge balancing species and a resistor, R_2, associated with the movement of excess electrolyte within the film. The total resistance, R_T, of the layer is a combination of both. By the application of an equation which relates the total film conductivity (L_T) to concentration of electrolyte C_E, [36].

$$L_T = L_1 + 2KC_E (U_{+f} + U_{-f}) \frac{FA}{d} \quad \ldots\ldots 3.5$$

A value for the ionic conductivity (L_1) of the polymer due to the movement of charge balancing ions can be calculated.

In the above equation, K is the partition coefficient for the electrolyte between the solution and the polymer phases, U_{+f} and U_{-f} are the mobilities of K^+ and Cl^- ions respectively in the film, A is the polymer area and d is the film thickness.

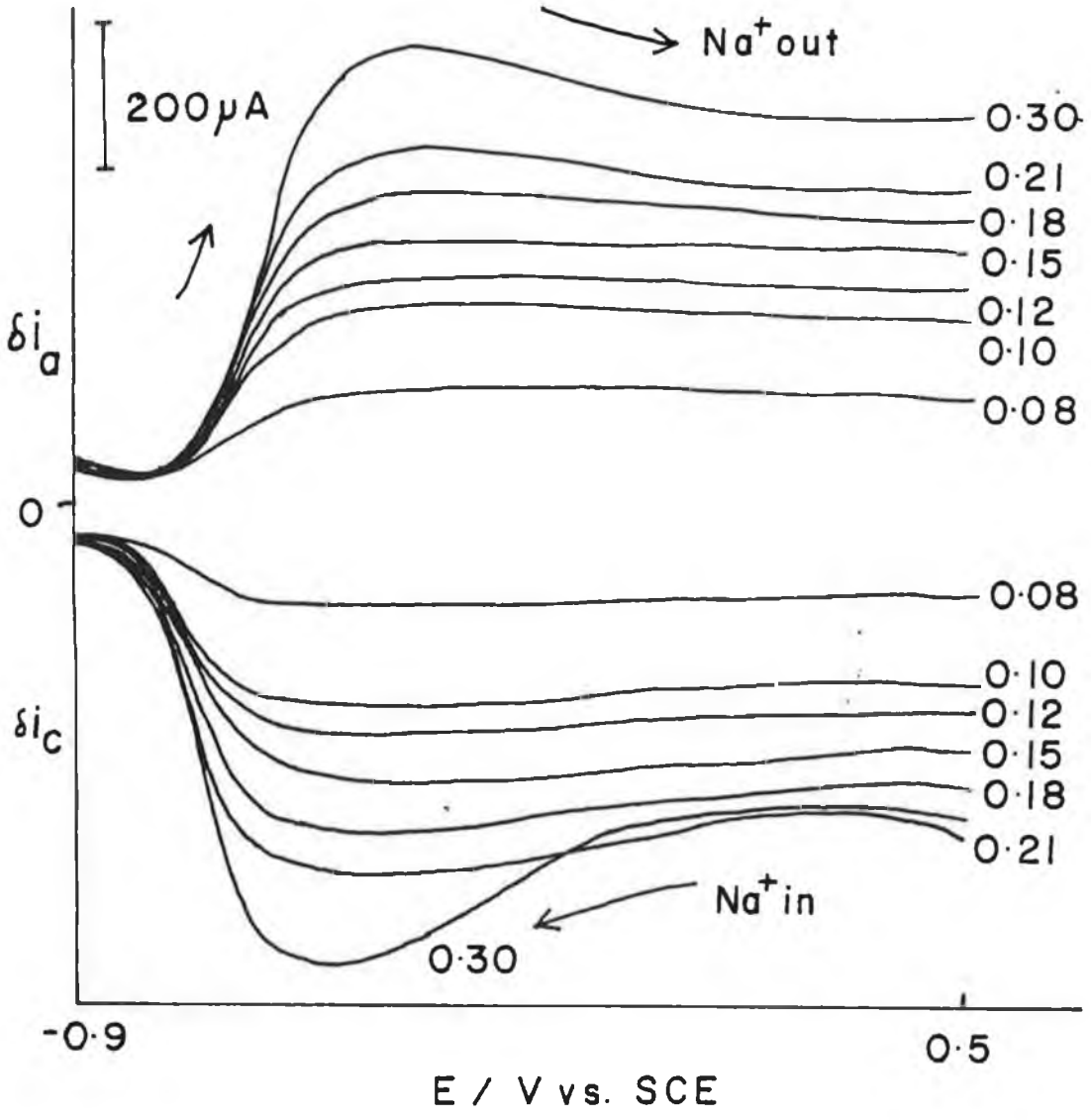

Figure 3.12 Differential pulse voltammograms of a PPTSPP layer, formed as described in Figure 3.4, at various background electrolyte concentrations.
Scan Rate = 10mV/s. Pulse amplitude = 40mV. RC time constant = 0.1.

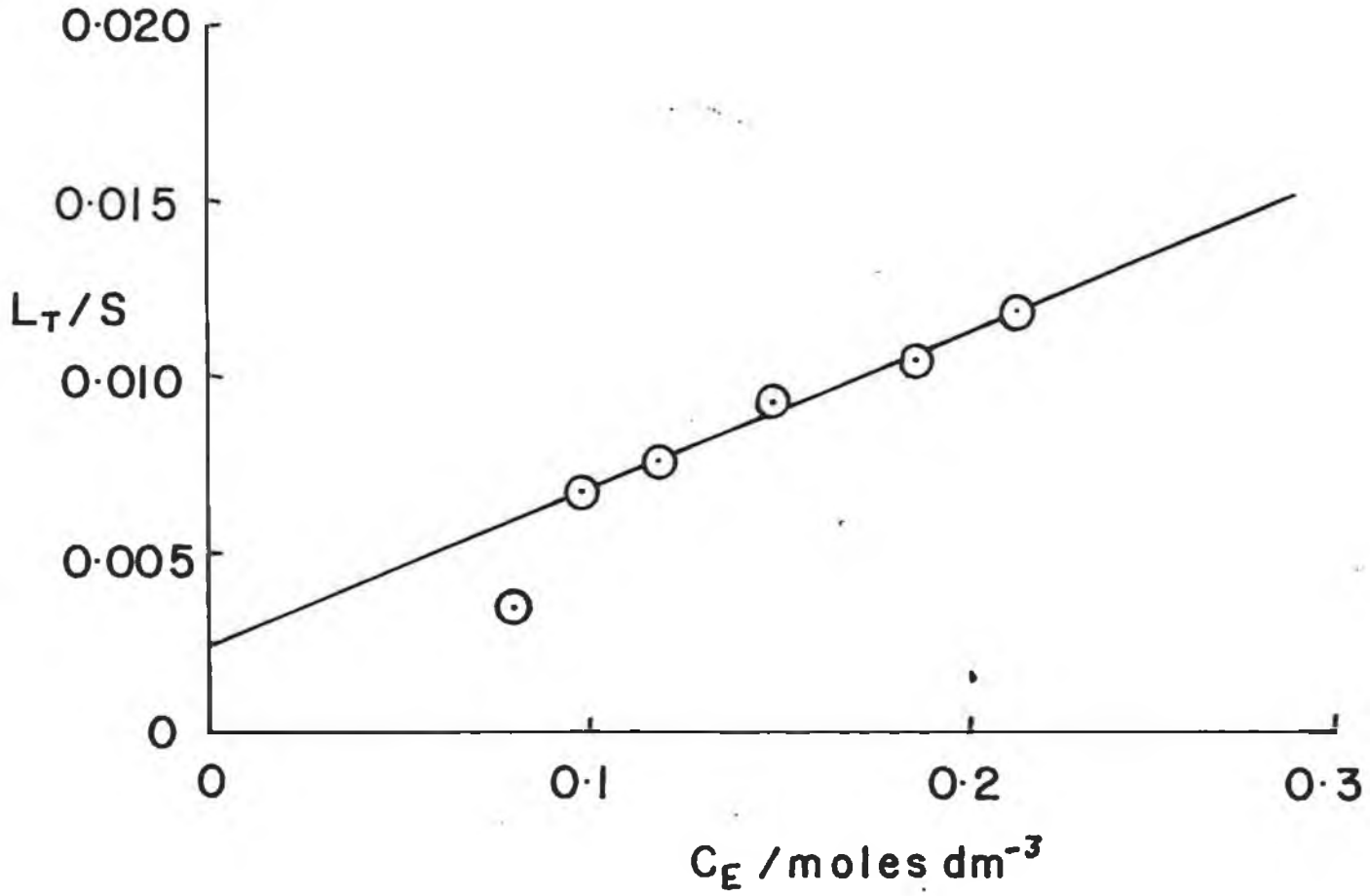

Figure 3.13 Plot of film conductivity, L_T, as a function of electrolyte concentration, C_E.

A plot of apparent film conductivity, L_T, as a function of the electrolyte concentration, C_E, is shown in Figure 3.13, for the 25mC layer. It can be seen that a linear plot was obtained, with a downward curvature observed at low electrolyte concentration (0.075M). A similar situation has been reported previously for a polypyrrole layer [36]. A value for L_1 can be obtained by extrapolation of the L_T versus C_E curve to C_E = O. A value or $2.4 \pm 0.2 \times 10^{-3}$ siemens was obtained, this corresponding to a resistance value of $422 \pm 34\Omega$, for the 25mC PPTSP layer. It was also noted that above electrolyte concentration of 0.1M, the majority of ionic conduction is accomplished by excess electrolyte from Figure 3.13.

To explain the sigmoidal current responses obtained for the conductive polymers, a model is proposed in the next section which attempts to simulate the differentiated current vs applied voltage output.

3.4.2 THEORY OF PROPOSED MODEL

The model assumes a redox species A confined within a layer of thickness d. This is similar to the $[Ru(bpy)_2\ Cl(PVP)_5]Cl$ layers; typical of a surface confined species [37,38]. Cyclic voltammetry was applied to the system and the following two diffusion equations were solved where A is the oxidised form and B is the reduced form of the couple

$$\frac{\partial C_A}{\partial t} = D \frac{\partial^2 C_A}{\partial x^2} \qquad \text{..... 3.6}$$

$$\frac{\partial C_B}{\partial t} = D \frac{\partial^2 C_B}{\partial x^2} \qquad \text{..... 3.7}$$

The concentration profiles and the currents were calculated using orthogonal collocation [39,40]. The peak current was found to equal the following at low scan rate [33].

$$i_p = \frac{n^2F^2\ C\ V\upsilon A}{4RT} \qquad \text{.....3.8}$$

and a value of 0.4463 was obtained for the Nicholson and Shain function $\sqrt{\pi}\chi(at)$ at faster scan rates [41].

Next a pulse waveform was applied on top of the linear potential sweep. The current was sampled just before the potential pulse was applied and again just before the end of the pulse duration. The peak current difference was found to be equal to that of the equation from the literature for peak current magnitude for a range of pulse amplitudes

$$\delta i_p = \frac{nFA\sqrt{DC}}{\sqrt{\pi(\tau-\tau')}} \frac{(1-\sigma)}{(1+\sigma)} \qquad \text{..... 3.9}$$

Where $\sigma = \exp\left[\frac{nF\Delta E}{2RT}\right]$

τ' is the time when the current is sampled just before the application of the pulse and τ is the time where the current is sampled well after the pulse is applied, when the double layer charging current has fallen to zero.

Using the total current from this program on effective resistance R_F, characteristic of this faradaic current, was obtained as $R_F = E_{APPLIED}^*/i$ where i is the faradaic current. $E_{APPLIED}^*$ is the potential felt by the polymer. R_F was then placed in the circuit as shown in Figure 3.14. The resistance in parallel represent the polymer matrix with R_S being characteristic of the resistance of the bulk electrolyte solution. The resistance R_I is a constant background resistance characteristic of the reduced state of the polymer and is independent of applied potential. Furthermore the resistance R_E^* is due to the movement of electrolyte within the polymer and is dependent on potential. This model is of similar nature to that of Cai and Martin [36], which has a resistance due to excess electrolyte and a resistance due to charge balancing ions in parallel.

In Figure 3.14, R_S is the solution resistance and so for a certain applied potential, $E_{APPLIED}$, the potential felt by the layer is $E_{APPLIED}^*$ determined by a voltage divider. An assumption of this model is that the ionic resistance R_E^* is dependent on the applied potential, since when the layer is oxidised, the greatest resistance is due to electrolyte within the pores. It has been found in the literature that the concentration of electrolyte in the pores of the polymer has been as high as 3 mol dm^{-3} [14]. The electrolyte concentration has been experimentally determined to be greater than equilibrium, on continuous cycling [42].

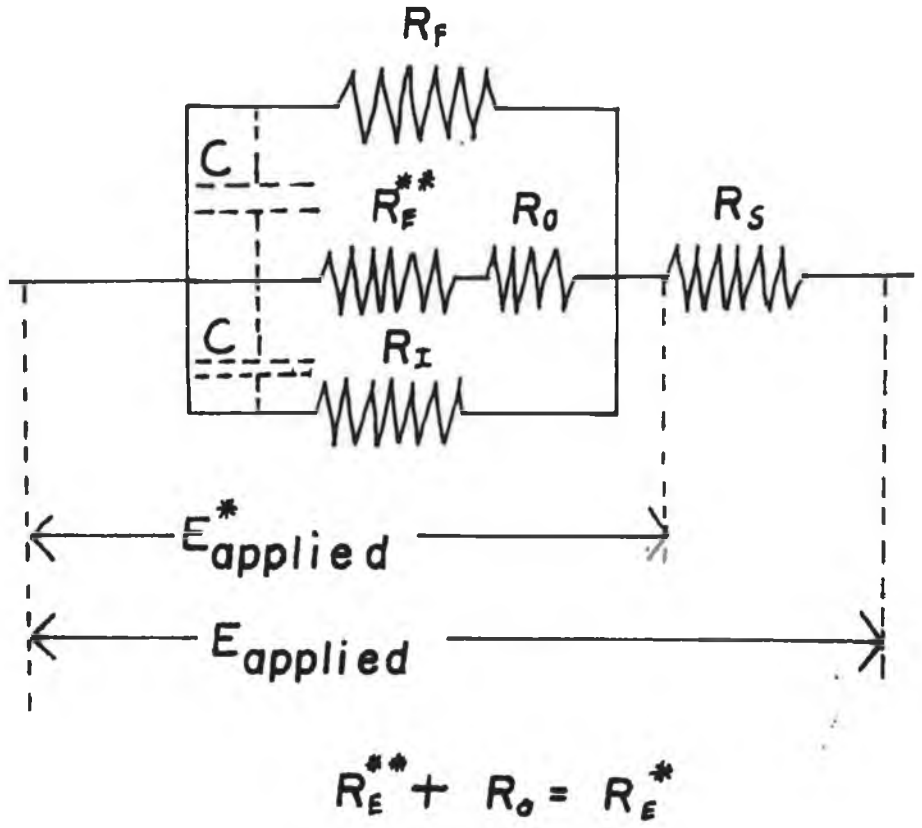

Figure 3.14 Proposed circuit for modelling of polymer structure.

However the ionic conductivity has also been seen to vary anomalously. It has been found to decrease with increased potential for poly-[1-methyl-3-(pyrrol-1 ylmethyl] pyridium perchlorate [43].

To find the total current associated with the circuit, the equation

$$E = E^{o1} + \frac{RT}{nF} \ln \left\{ \frac{(f_L - f)}{(f)} \right\} \quad \ldots\ldots 3.10$$

is manipulated. Equation 3.10 represents the current potential curve for a reversible electrode reaction using a steady state technique such as polarography or RDE.

f_L is taken to be the limiting differential current plateau obtained for the differential pulse voltammograms, where in this case

$$f_L = \frac{nF}{RT} \frac{\Delta E}{RE} \quad \ldots\ldots 3.11$$

ΔE is the pulse amplitude and R_B is the resistance characteristic of the oxidised state of the polymer.

By rearrangement of equation 3.10 the units of f_L are Ω^{-1} since they are taken, technically to be the difference in current divided by the pulse amplitude i.e., $^{A}/_{V} = {}^{1}/_{R}$ with integration , equation 3.12 is obtained

$$i = f_L \int \frac{1}{1 + e\left\{\frac{nF(E-E^{o1})}{RT}\right\}} dE \quad \ldots\ldots 3.12$$

Solving this integral, the final equation is obtained where i is the total current response which would yield a sigmoidal differential output should a differential pulse waveform be applied to it.

$$i = \frac{RT}{nF} f_L \ln\left\{\frac{(x)}{(x+1)}\right\} \quad \text{..... 3.13}$$

where $$x = \exp\left\{\frac{[nF(E^{1o}-E_{APPLIED}^{*})]}{RT}\right\} \quad \text{.....3.14}$$

where f_L can be calculated by equation 3.11 with R_B being an input to the fortran program (Appendix 1).

The first step in the program involves the calculation of f_L, then the total current is obtained with values of R_E^* being calculated from the equation

$$R_E^* = \frac{E_{APPLIED}^*}{i} + R_O = R_E^{**} + R_O \text{..... 3.15}$$

An assumption of the model is that the capacitance present in the system is invisible because of the differential waveform. If the resistance R_E^* and R_I are large, for example in a redox species containing polymer $[Ru(bpy)_2Cl(PVP)_5]Cl$, then the response is primarily faradaic for the differential current output.

If R_F and R_I are large compared to R_E^*, then a sigmoidal response is seen for the differential output as the electronic conductivity of the layer gradually increases from a low value characteristic of a conducting layer. The assumptions of the model is that the capacitance is not seen, and also that the layer is homogeneous in nature, which is hardly seen experimentally [25,44,6].

3.4.3 SIMULATION OF DPV FOR THE POLYMER MODEL

The data for simulation of the Faradaic current were obtained from a number of sources. Layer thicknesses were taken to be 10^{-4} cm. This value is typical of polymer layers deposited with 20mC of charge onto electrodes of area $0.07cm^2$ [22]. Diffusion coefficients of 10^{-8} - 10^{-7} cm^2 s^{-1} were employed [31] and resistance values were from the literature [43,45]. In the calculation, the resistor R_O, is present to prevent R_E^* from decaying to zero. R_O is taken as being equal to R_S in these calculations.

A sigmoidal behaviour for R_E^* is not expected since this would give rise to a peak in the differential current output.

Figure 3.15 shows the behaviour of R_E^* according to equation 3.15. This decay in R_E^* with potential is responsible for the sigmoidal behaviour in the differential current output. It can be seen that the resistance does not decay to zero, due to the presence of the constant background resistor, R_O. R_E^{**} is obtained through an input resistance R_B (equation 3.13,3.14).

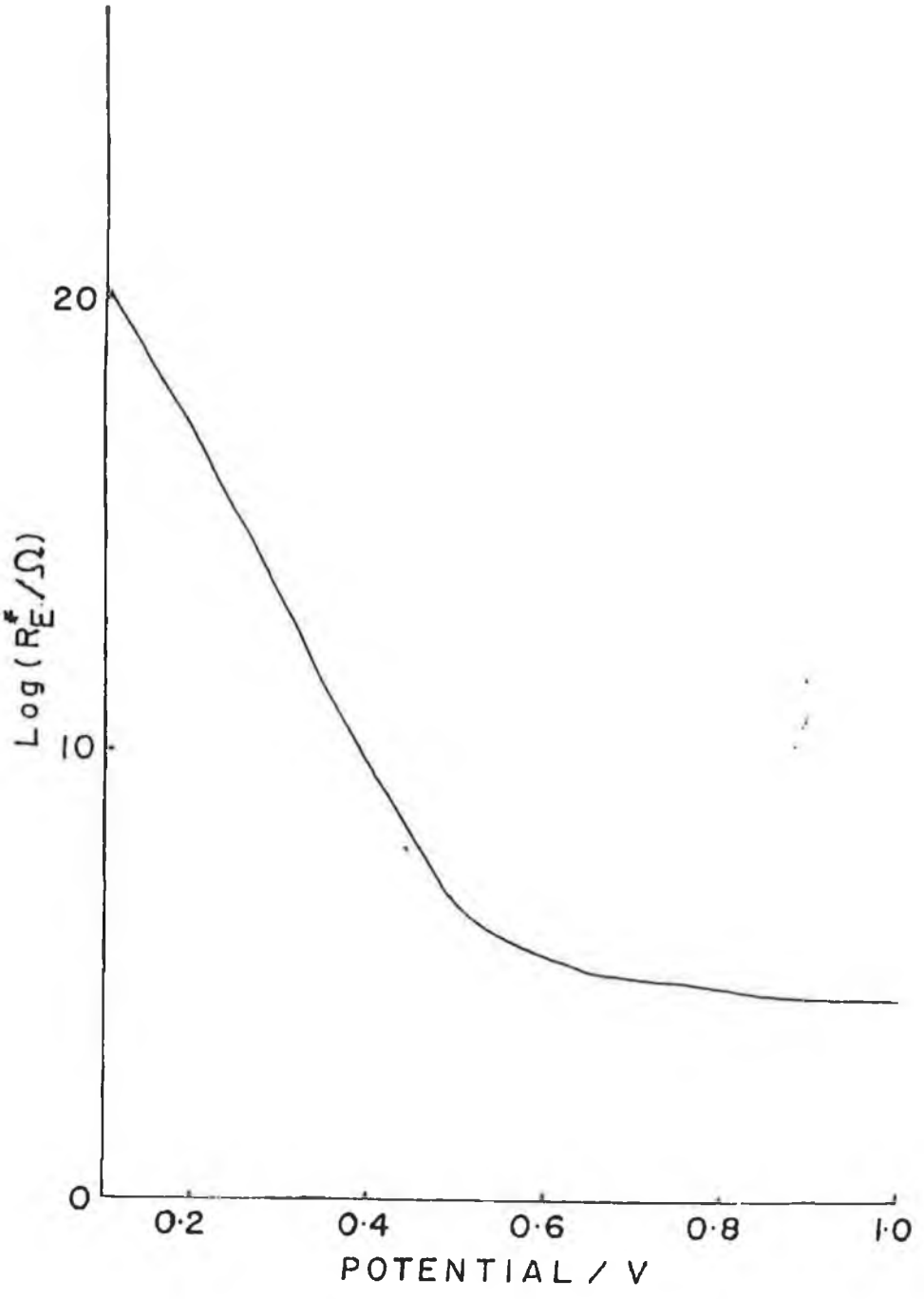

Figure 3.15 Plot of resistance, R_E^*, as a function of applied potential, E. This behaviour being responsible for the sigmoidal differential current outputs.

Two primary cases must be considered, these being the differential current outputs when the resistances are small in magnitude and when the resistors are large.

The values of the resistances of the oxidised and reduced layers, obtained from the experimental DPV sigmoidal current outputs, were of the order of 350Ω and 1000Ω respectively.

These values of resistance were used for the simulation, to investigate whether from the model a sigmoidal current output could be obtained. The resulting simulated current response obtained is illustrated in Figure 3.16.

It can be seen clearly that a peaked response is obtained with the anodic peak potential occurring at the formal potential, $E^{o1} = 0.500V$. This behaviour is characteristic of thin layer behaviour. It was seen that upon increasing the resistances of R_B and R_I beyond these values, thin layer behaviour is observed. This thin layer behaviour is discussed later with a scan rate study and layer thickness study being performed for high values of R_B and R_I.

The values of R_B and R_I were varied in magnitude. It can be seen, in Figure 3.16, that by decreasing the magnitude of the resistor R_B to 100Ω and R_I to 1000Ω still gives rise to a peaked response, but with a less pronounced thin layer behaviour. However the peak potential is still equal to the formal potential. It can also be seen that when R_B is kept constant at 100Ω and R_I decreased, the currents magnitude only increased but identical behaviour is

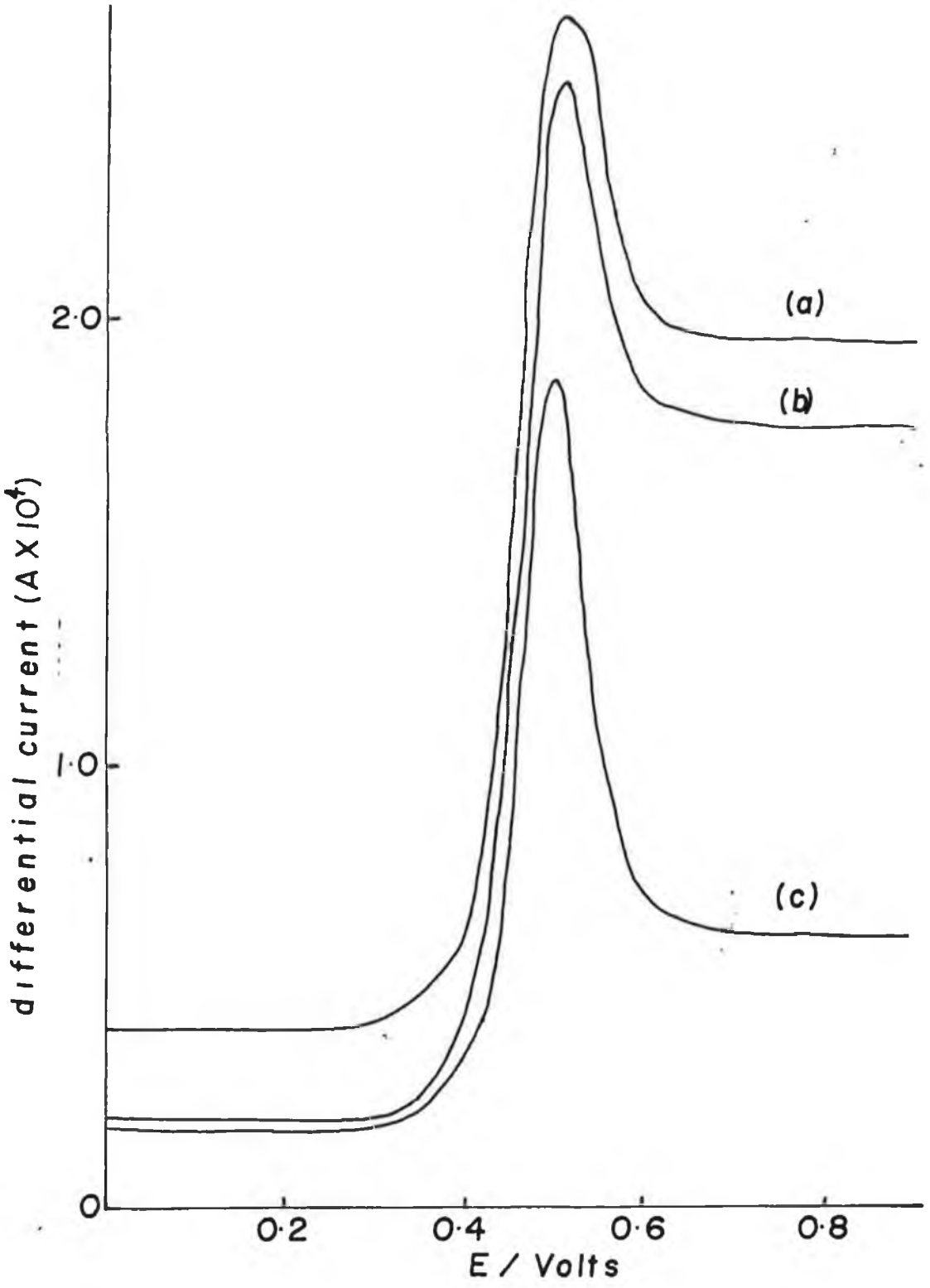

Figure 3.16 Simulated DPP output where E_{start} - 0.0V, E_{final} = 1.0V, E^{ol} = 0.5V, pulse amplitude (PA) = 20mV, concentration = 0.1 mol dm^{-3}, scan rate = $2mVS^{-1}$, D = 10^{-9} cm^2S^{-1}, layer thickness = 1μm, drop time = 1 sec, pulse width = 55mS.

(a) $R_B = 100\Omega$, $R_S = 1.0\Omega$, $R_I = 500\Omega$

(b) $R_B = 100\Omega$, $R_S = 1.0\Omega$, $R_I = 1000\Omega$

(c) $R_B = 350\Omega$, $R_S = 1.0\Omega$, $R_I = 1100\Omega$

observed. Note that in Figure 3.16 that there is a constant response after the peak.

Figure 3.17 shows where the resistors R_B and R_I are varied to lower values. Thin layer behaviour is not observed, due to the presence of a limiting current beyond 0.6 volts, with a shift in the peak potential from the formal potential ($E^{o1} = 0.500V$) to 0.520V. However these curves do not agree in full with the experimental curves which have a peak. As mentioned above, experimentally there is a capacitance present.

Again the values of the resistors R_B and R_I are decreased in magnitude. Figure 3.18 shows the response of the model to a DPV waveform when R_B is 25Ω and R_I is varied. It is seen that no definite peak is observed, with the current reaching a maximum value when the potential is at 0.60V, therefore indicating that thin layer voltammetry is not observed. Also the current, for both the oxidised and reduced forms of the layer is a limiting plateau, in agreement with the experimental curves.

It was observed in the experimental curve, (Figure 3.5) that the limiting current plateau observed for the oxidised and reduced states of the polymer increased in magnitude when the pulse amplitude was increased from 10mV to 50mV. When the pulse magnitude was 50mV, a sigmoidal current response was also recorded.

Figure 3.19 shows the effect of the pulse amplitude on the simulated response, where the values of R_B, R_I and R_S are $4 \times 10^{-5}\Omega$, $5 \times 10^{-3}\Omega$, and $1 \times 10^{-5}\Omega$ respectively. There is a similarity in the response between the experimental

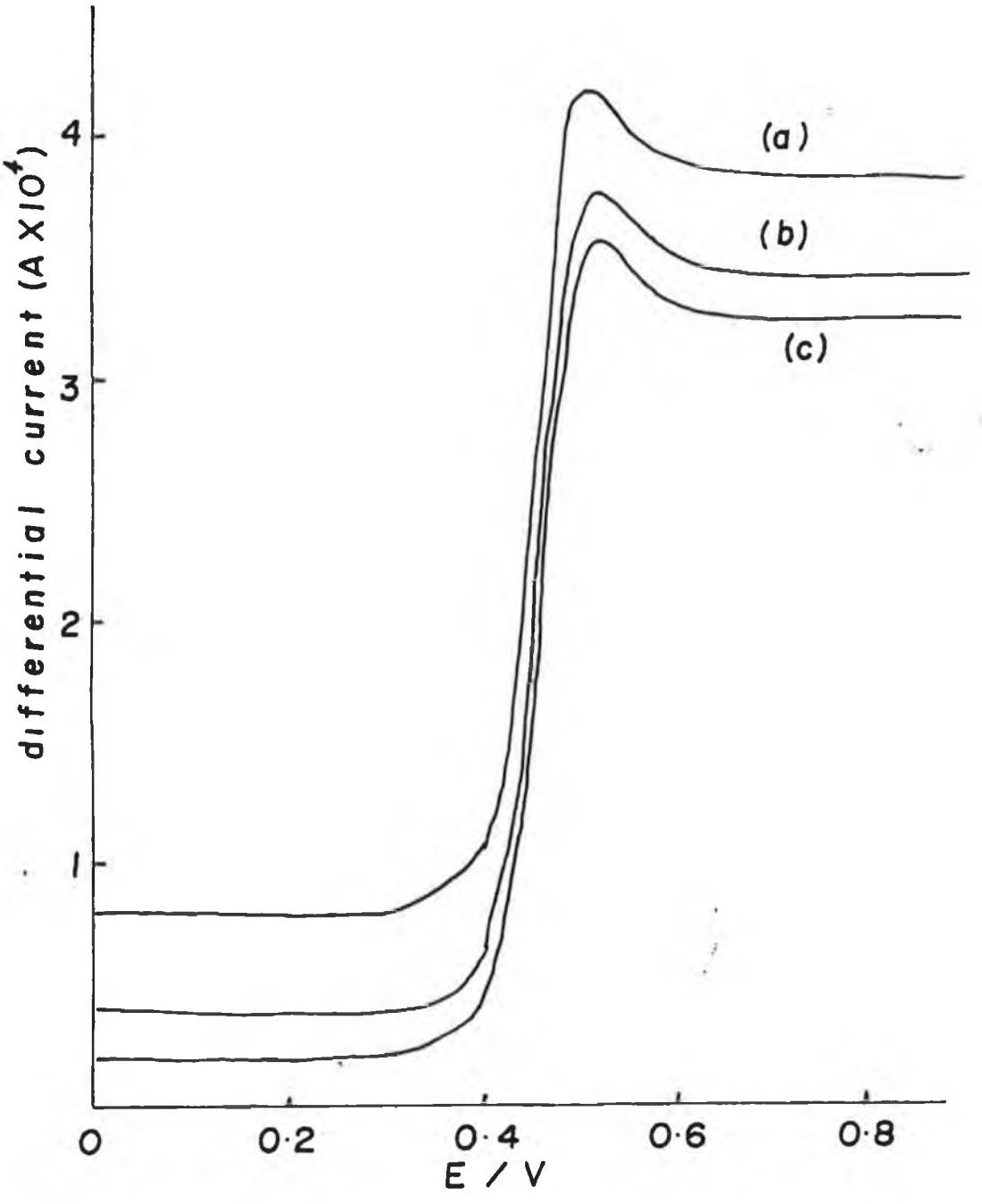

Figure 3.17 Simulated DPP output curves for the same conditions as in Figure 3.16.
(a) $R_B = 50\Omega$, $R_S = 1.0\Omega$, $R_I = 250\Omega$
(b) $R_B = 50\Omega$, $R_S = 1.0\Omega$, $R_I = 500\Omega$
(c) $R_B = 50\Omega$, $R_S = 1.0\Omega$, $R_I = 1000\Omega$

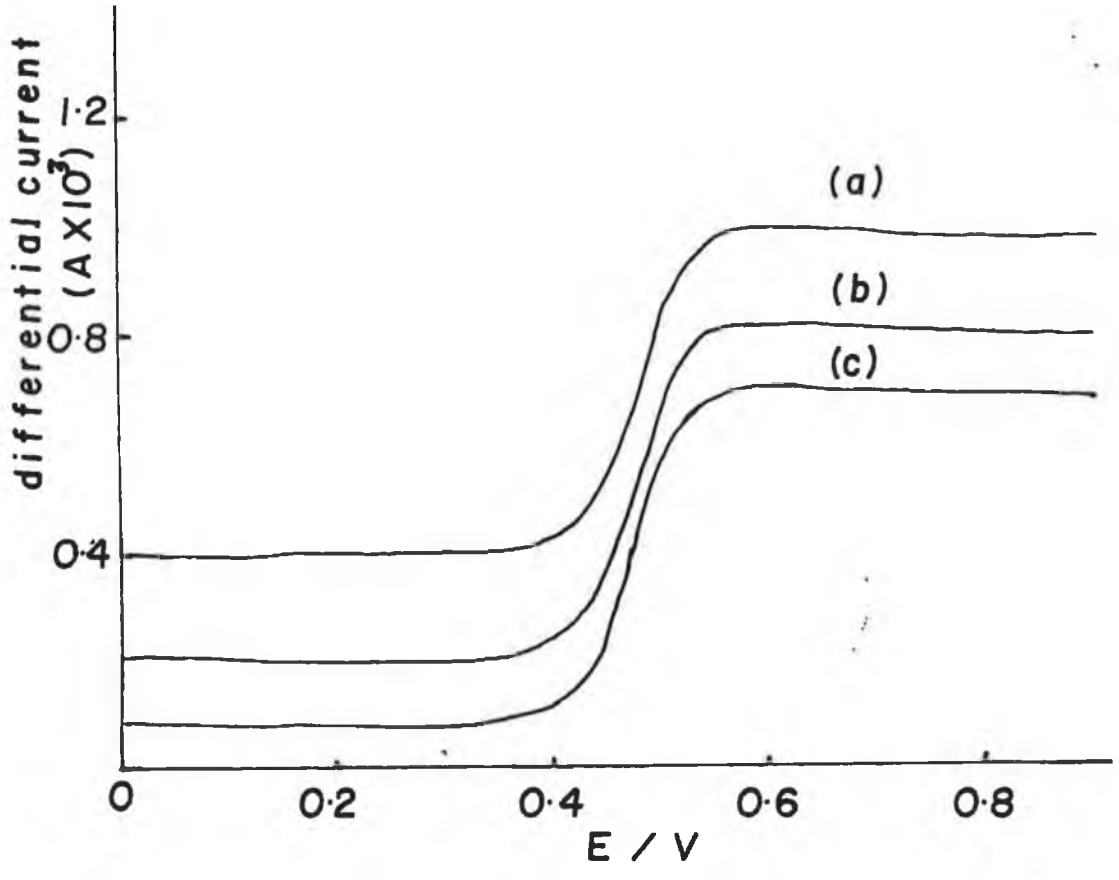

Figure 3.18 Simulated DPP output curves for the same conditions as in Figure 3.16.
(a) $R_B = 25\Omega$, $R_S = 1.0\Omega$, $R_I = 50\Omega$
(b) $R_B = 25\Omega$, $R_S = 1.0\Omega$, $R_I = 100\Omega$
(c) $R_B = 25\Omega$, $R_S = 1.0\Omega$, $R_I = 250\Omega$

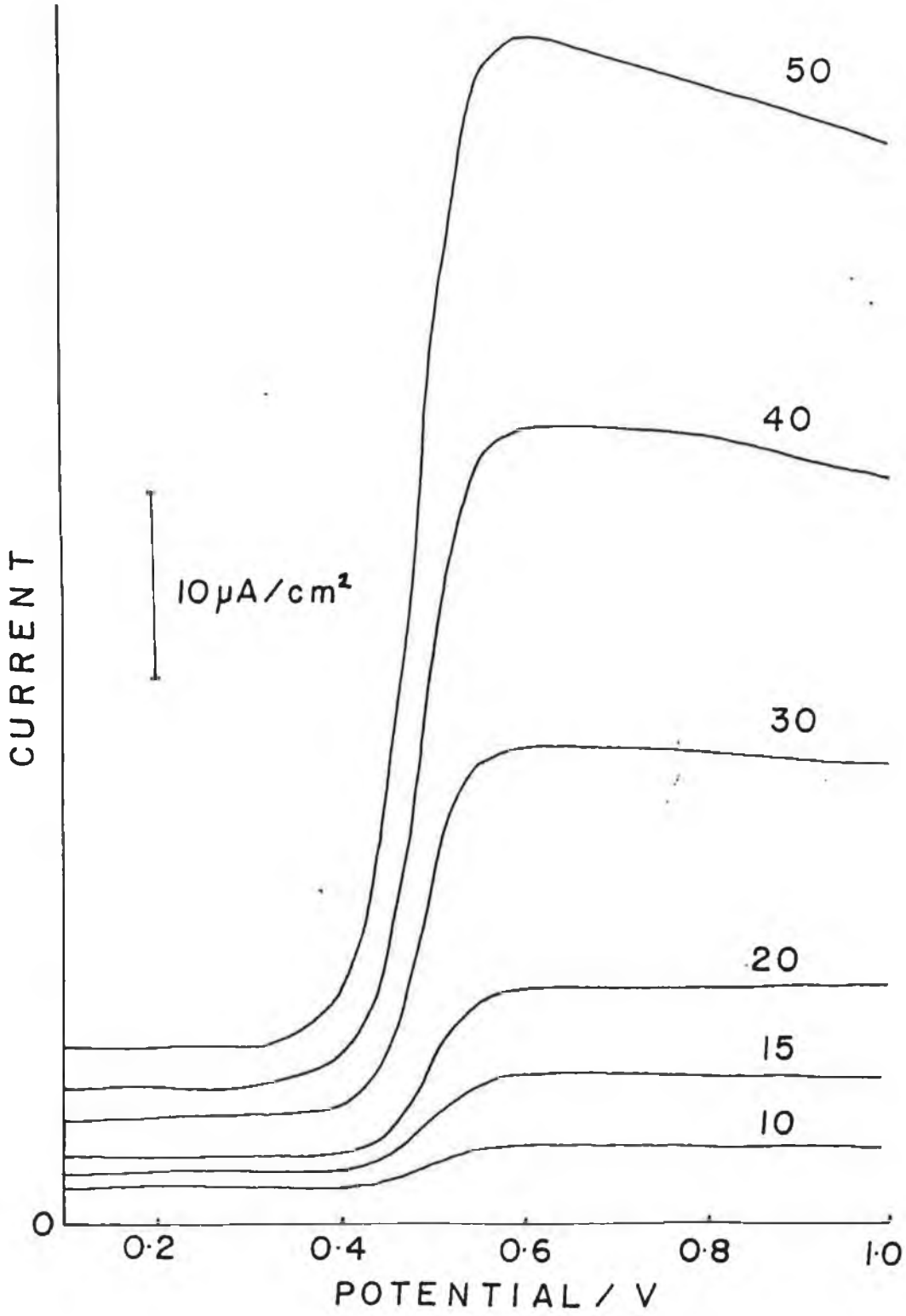

Figure 3.19 Simulated DPV output curves as a function of pulse amplitude for the same conditions as Figure 3.16 except with $R_B = 4 \times 10^{-5}\Omega$, $R_S = 1 \times 10^{-5}\Omega$ and $R_I = 5 \times 10^{-3}\Omega$.

response in Figure 3.5 and the theoretical response in Figure 3.19 showing that resistance dominates the response. This is curious in that there is a capacitive contribution to the experimental plots which is neglected in the simulation.

It has already been mentioned that a range of layer thicknesses were investigated. It was observed that for all layers, a sigmoidal current response was obtained upon the application of DPV, experimentally. This may indicate that the diffusion layer does not reach the polymer/solution interface.

The effect of layer thickness upon the simulated response under the conditions similar to Figure 3.19 was investigated. The layer thicknesses investigated were 0.1μm and 1.0μm it was noted that sigmoidal current responses were obtained with the magnitude of the limiting current, in the oxidised state of the polymer, being independent of layer thickness. This was in agreement with the experimental curves in Figure 3.5.

Figure 3.20 shows the differential current output using the model for the circuit as a function of solution resistance R_S. It can be seen that since the resistances are so small that the current is dominated by the resistance in the layer. R_F is relatively large and so the current flows through the smaller resistances in parallel. It can also be seen that the half wave potential changes as R_S increases because of the drop in $E_{applied}$* on account of the voltage divider.

Figure 3.21 shows the simulated curve where the input value of R_B was varied. When the resistance is increased the faradaic peak begins to make an appearance. By comparing Figures 3.12 and 3.21, the polymer resistance R_B

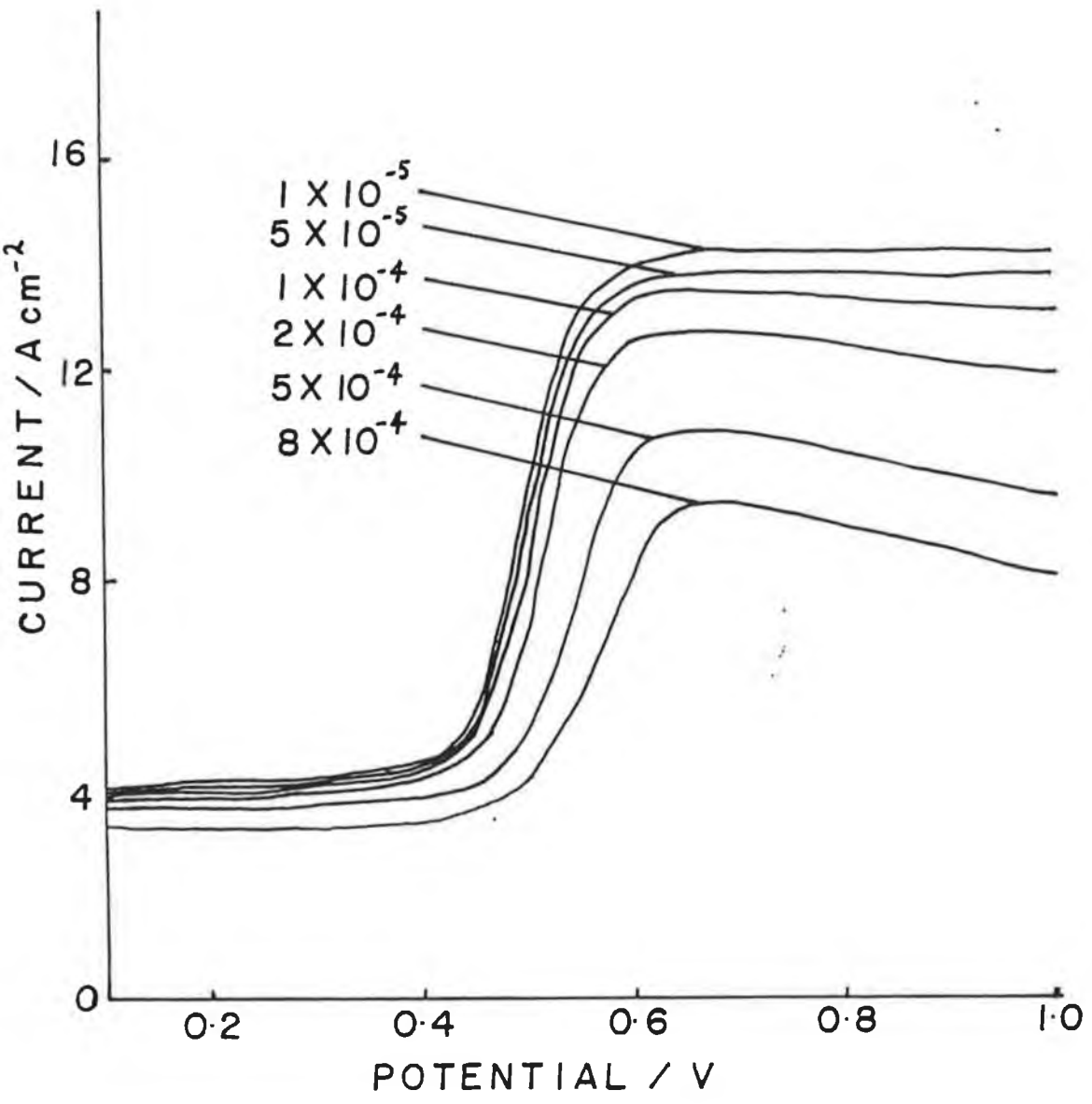

Figure 3.20 Simulated DPV output curves as a function of solution resistance for the same conditions as in Figure 3.16 except with $R_B = 4 \times 10^{-5}\Omega$, $R_I = 5 \times 10^{-3}\Omega$.

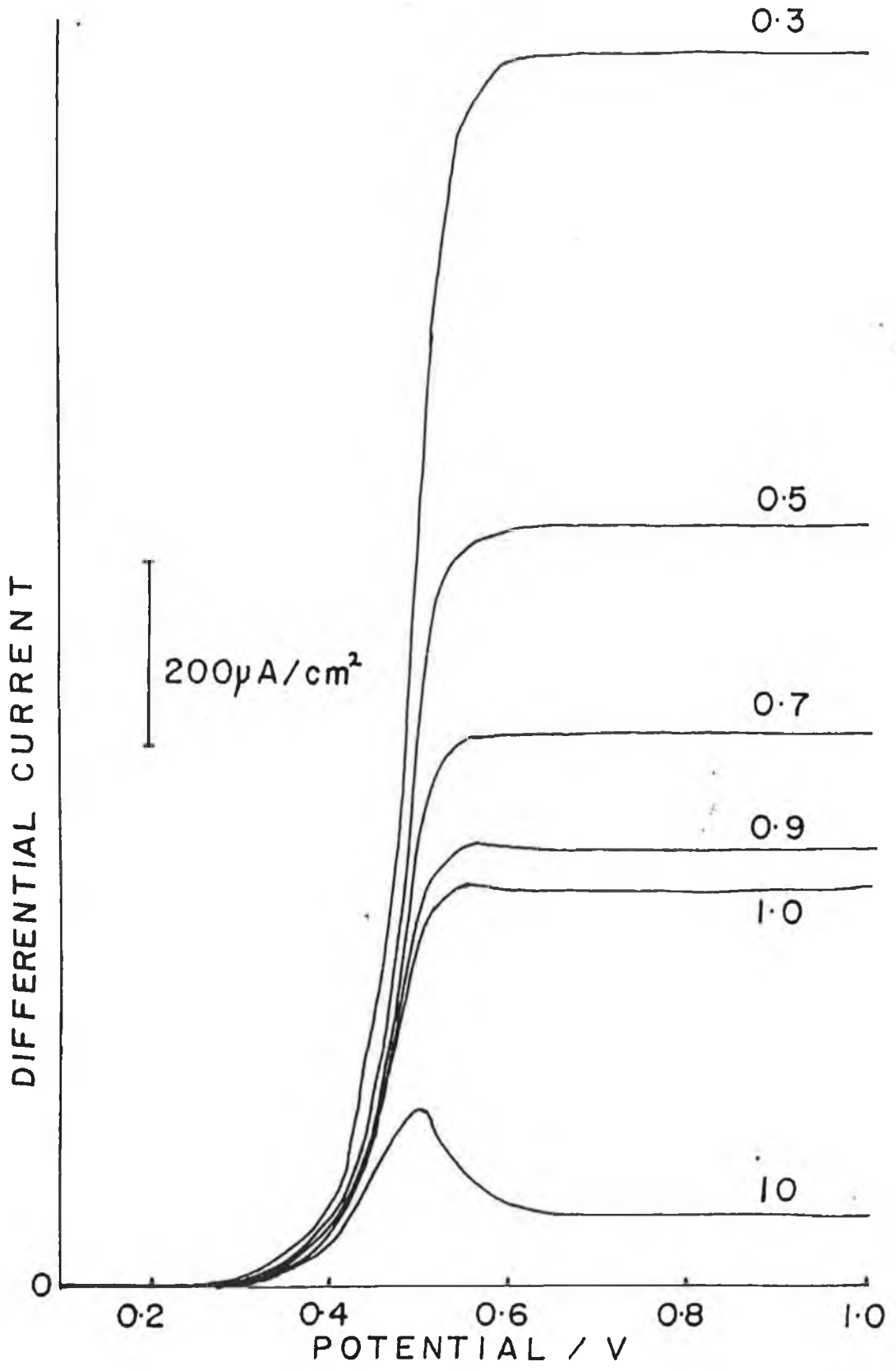

Figure 3.21 Simulated current output curves when a DPV waveform is applied to a layer with different values of R_B, where $R_S = 1 \times 10^{-1}\Omega$, $R_I = 500\Omega$ and other conditions as in Figure 3.16.

has the same effect as the background electrolyte concentration. R_B may be due to the presence of charge balancing ions required to change the state of the layer from oxidised to reduced and therefore depends on electrolyte concentration.

The behaviour of the model, when the resistances are of the order 10^3 ohms, is characteristic of thin layer behaviour. Figure 3.22 shows the thin layer behaviour of the polymer model when the value of the resistors R_B, R_S and R_I are $0.1 \times 10^5\Omega$, 1.0Ω and $5.0 \times 10^5\Omega$ respectively.
It is essentially a plot of the total faradaic current versus the applied potential. The formal potential is equal to 0.5V, and it can be seen that the peak potential is at this value. Also the current decays away to zero on both sides of the formal potential. These two observations are characteristic of thin layer behaviour, showing that the depletion layer will extend out to the edge of layer, upon oxidation thereby the current decays to zero indicating all the electroactive species within the layer is being oxidised.

A scan rate study was performed with the values of the resistances being kept constant at the values stated in Figure 3.22. It can be seen that the current does decay with a decrease in scan rate. It is expected that the peak width at half height should be equal to $^{90}/_{n}$ mV [33] independent of scan rate. The value of n is taken to be equal to 1. When the scan rate is 20 mV sec^{-1} the peak width at half height is equal to 110mV, and when the scan rate is decreased to 5 $mVsec^{-1}$ the peak width at half height is 90 mV.

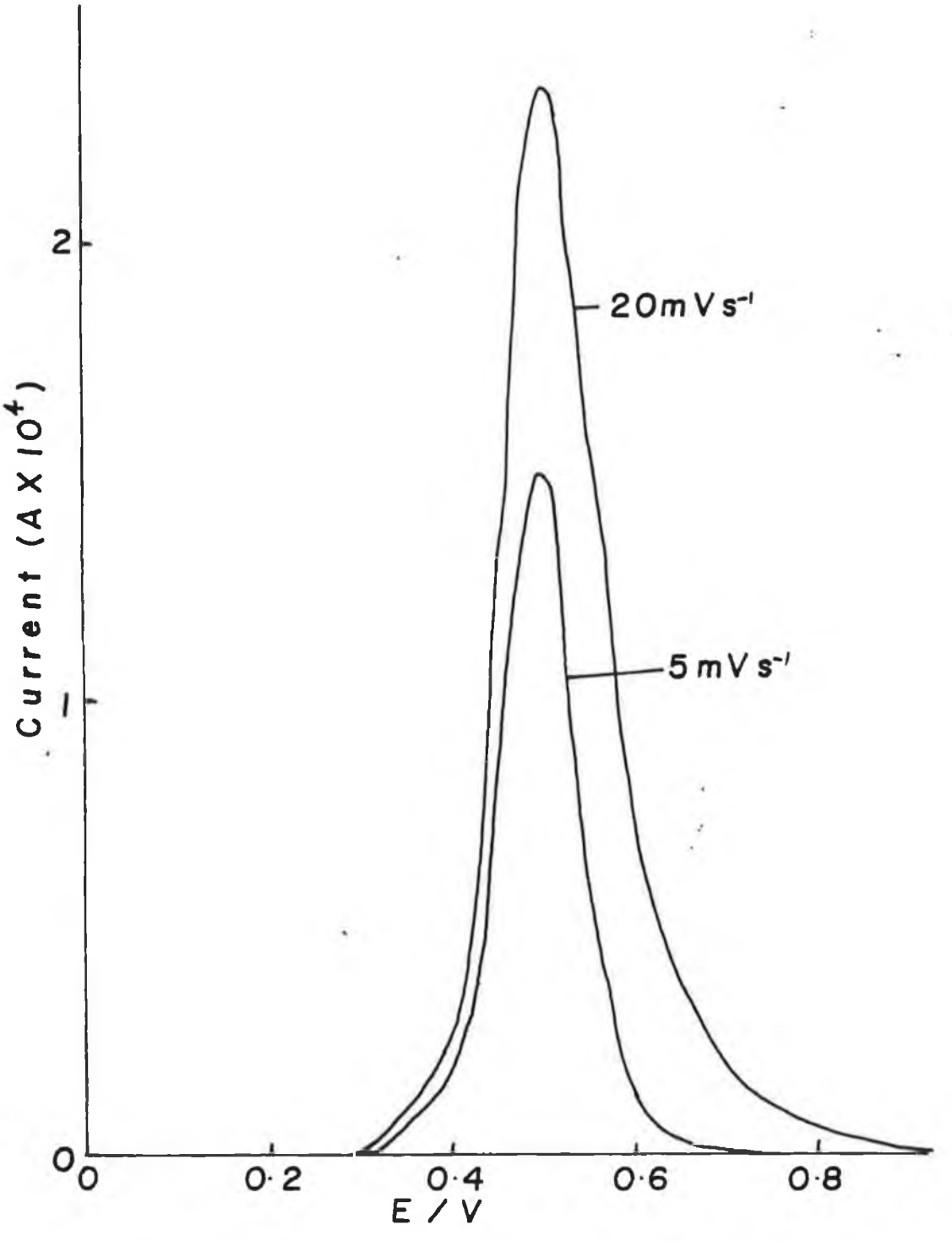

Figure 3.22 Simulated DPV output curves for the total faradaic current versus the applied potential, as a function of scan rate. Same conditions as in Figure 3.16 except with R_B = 01 x $10^5\Omega$, R_S = 1.0Ω and R_I = 5 x $10^5\Omega$.

Also the differential current was recorded when the values of the resistances were high. It can be seen in Figure 3.23, that a peaked response is obtained. This response in the differential current can be seen not to be a pure derivative of the faradaic current, observed in Figure 3.22.

A scan rate study was also performed for the differential current output. It can be seen that there is only a slight decrease in the current observed. This is in keeping with equation 3.9 which does not predict a scan rate dependence for i_p.

It was noted that to increase the solution resistance led to problems concerning the voltage divider. If R_S was high (100Ω), or larger than R_B or R_I then the layer would not feel the applied potential.

This model differs from others in that the resistance decays rather than following a sigmoidal fall as has been seen previously [31,35]. If a sigmoidal decay in resistance had been employed, then the predicted differential current output would have been peaked. The model is tentative and includes no capacitances. There is qualitative agreement between the experimental curves (Figures 3.5 and 3.12) and the simulated curves (Figures 3.19 and 3.20) respectively, showing that capacitance may interfere with the current magnitude but not the shape. The reason for the sigmoidal differential current output is due to resistance, a fact which is not obvious from the cyclic voltammetry. Using DPV, it is possible to estimate the apparent resistance of the reduced and oxidised forms of the layer. Using a model with pure resistances, resistance behaviour such as in Figure 3.15 is required to predict experimental behaviour.

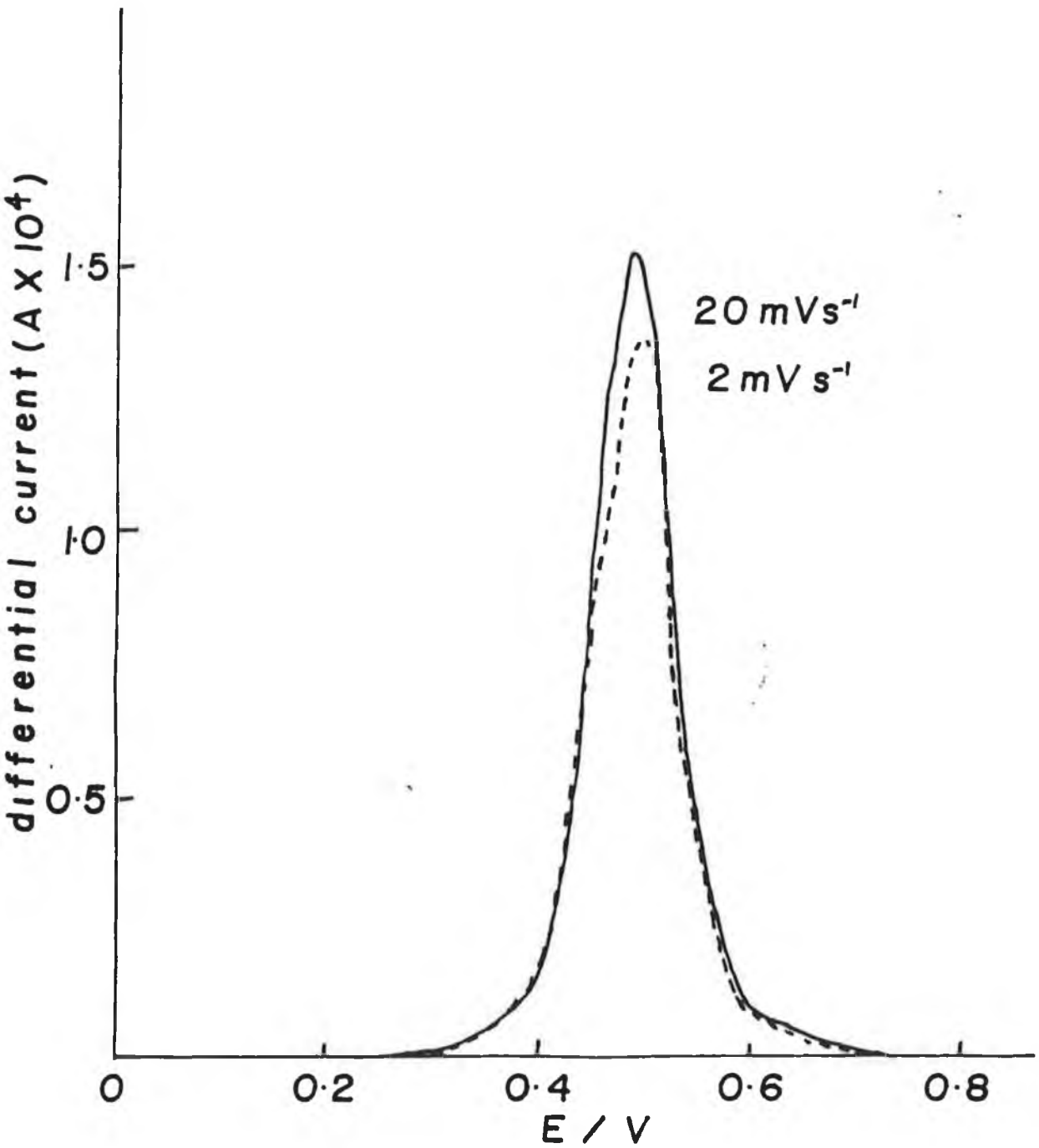

Figure 3.23 Simulated DPV output curves for the differential current versus the applied potential, as a function of scan rate. Same conditions as in Figure 3.22

Experimentally much longer sampling times are required to match experimental and theoretical curves.

3.4.4 POTENTIAL STEP OF A PPTSP LAYER

A PPTSP layer was formed on a platinum electrode as described previously. The layer was washed and placed in an aqueous solution of NaCl (0.1M), and cycled until a steady state cyclic voltammogram was obtained. The layer was then transferred to a fresh solution of NaCl (0.1M) and potential step experiments were carried out.

The layer was kept at a voltage (0.300 volts) where it was in the conducting state. The faradaic current was allowed to decay, it does not decay to zero but to a constant value, and then the potential was stepped to 0.350V and the decay of the current was recorded.

The current decays but never reaches zero, as would be expected according to the Cottrell equation. Instead the current reaches a steady state value, taking 3 minutes to do so.

The experiment was repeated several times with varying the potential step applied from 10mV to 52mV. The potential steps were chosen so as to match the pulses applied, in the DPV experiments, in magnitude. It was seen that for all the potential steps, constant currents were obtained decreasing in magnitude with decreasing potential steps.

This behaviour of the layer is summarised in table 3.2

TABLE 3.2. Ultimate constant current resulting from potential step experiments in the oxidised form of the polymer.

Potential Step mV	Limiting Current μA
10	0.360±0.007
16	0.400±0.008
33	0.500±0.010
42	0.560±0.011
52	0.600±0.012

If the limiting current is plotted against potential step, a linear plot is obtained indicating resistive behaviour of the layer.

Figure 3.24 shows this plot. A value of 64kΩ was obtained for the resistance of the layer. This value does not agree with the value of 1000Ω obtained for the oxidised state of the layer, obtained by DPV. The reason is possibly due to the different timescales of the experiments and that capacitance was ignored in the DPV study. For the DPV experiments, the current is sampled before and after the application of the pulse. The time delay is sampling is of the order of 55 milliseconds, whereas the limiting currents measured for the potential step experiments were taken 200 seconds after the pulse being applied.
Therefore this could account for the small currents observed in the potential step experiments and hence the large resistance value obtained.

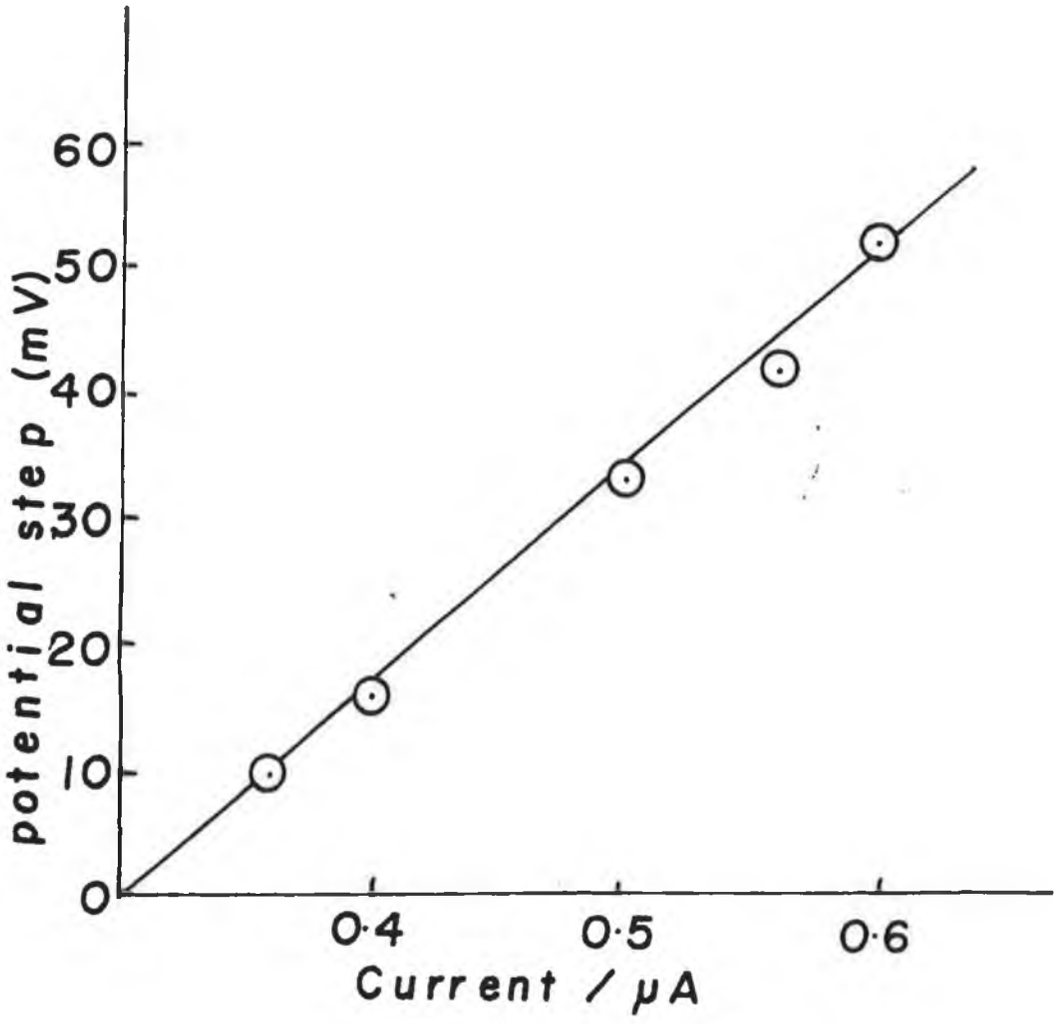

Figure 3.24 Plot of limiting current against potential step for the PPTSP layer.

3.4.5 DIFFERENTIAL PULSE VOLTAMMETRY OF A POLYPYRROLE LAYER CONTAINING $[Fe(CN)_6]^{4-}$

Recently an electrochemical study of the cation permeability into polypyrrole containing $[Fe(CN)_6]^{4-}$,PPFCN, was investigated [46]. The layer was formed on a platinum electrode as described previously. The layer was then broken in, in an aqueous solution of NaCl (3.0M), by cycling the layer between -0.2V and +0.5V until a steady cyclic voltammogram was obtained. The resulting cyclic voltammogram is shown in Figure 3.25. The electrochemistry of the $[Fe(CN)_6]^{4-}$ / $[Fe(CN_6)]^{3-}$ is seen on top of a capacitive background of the polymer.

Ideal thin layer behaviour is not observed due possibly to the presence of the double layer charging current, associated with the polypyrrole. This situation has been reported previously [46].

The PPFCN layer was then rinsed and transferred to a fresh solution of NaCl (3.0M) and differential pulse voltammetry was applied to the layer. The resulting DPV is seen in Figure 3.26. The electrochemistry of the ferro-ferricyanide species, within the layer is only barely observed. It is noted that again perfect thin layer behaviour is not observed with a peak to peak separation of 90mV when the pulse amplitude was 50mV and the RC time constant equal to 1.0. However when the RC time constant is increased to 10, thin layer behaviour is observed with zero peak to peak separation.

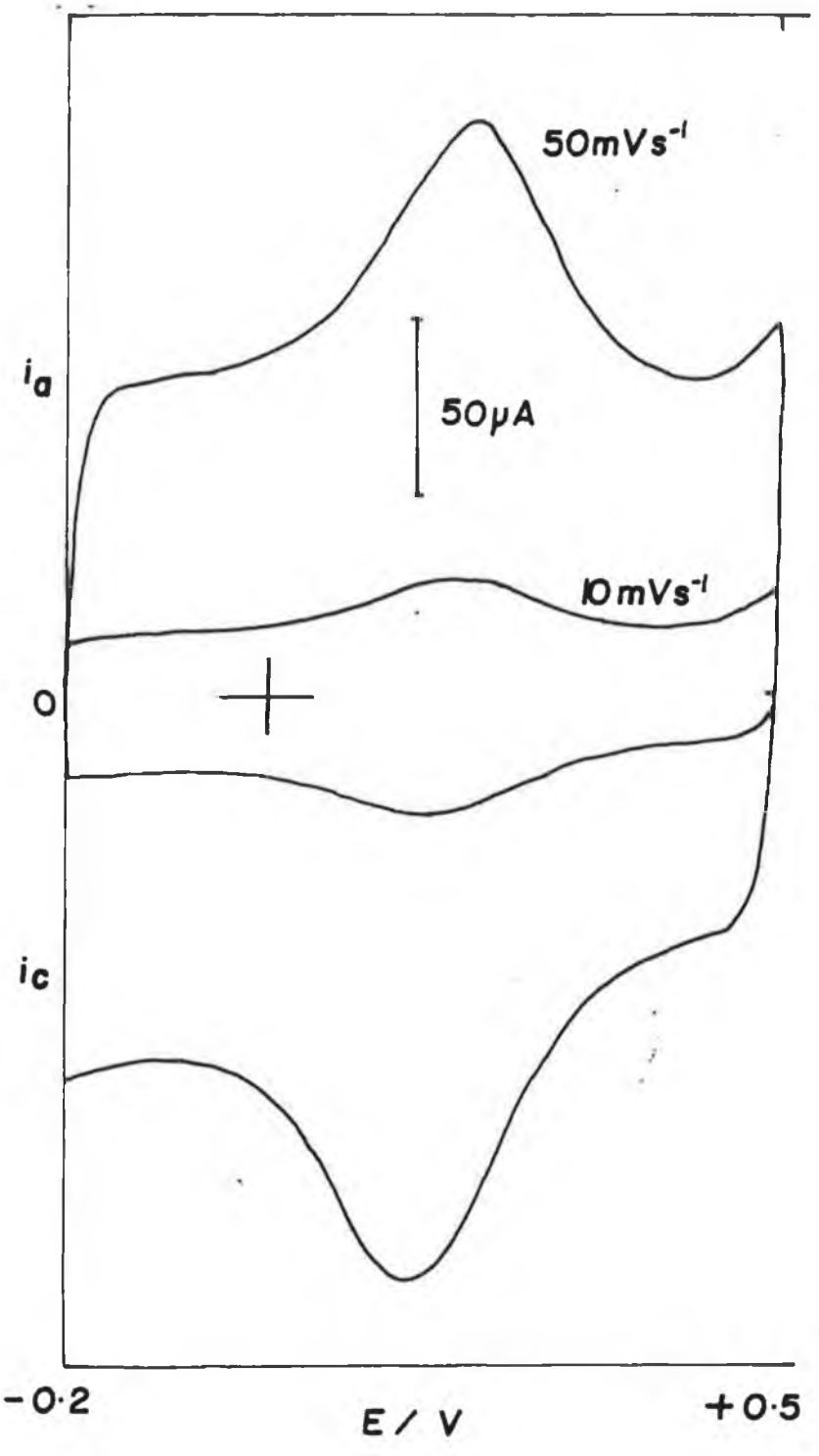

Figure 3.25 Cyclic voltammogram of a PPFCN layer in 3.0M NaCl. The layer was previously formed by holding the potential at 0.8V in 0.1M pyrrole and 0.1M $[Fe(CN)_6]^{4-}$, and broken in, in an aqueous solution of 3.0M NaCl.

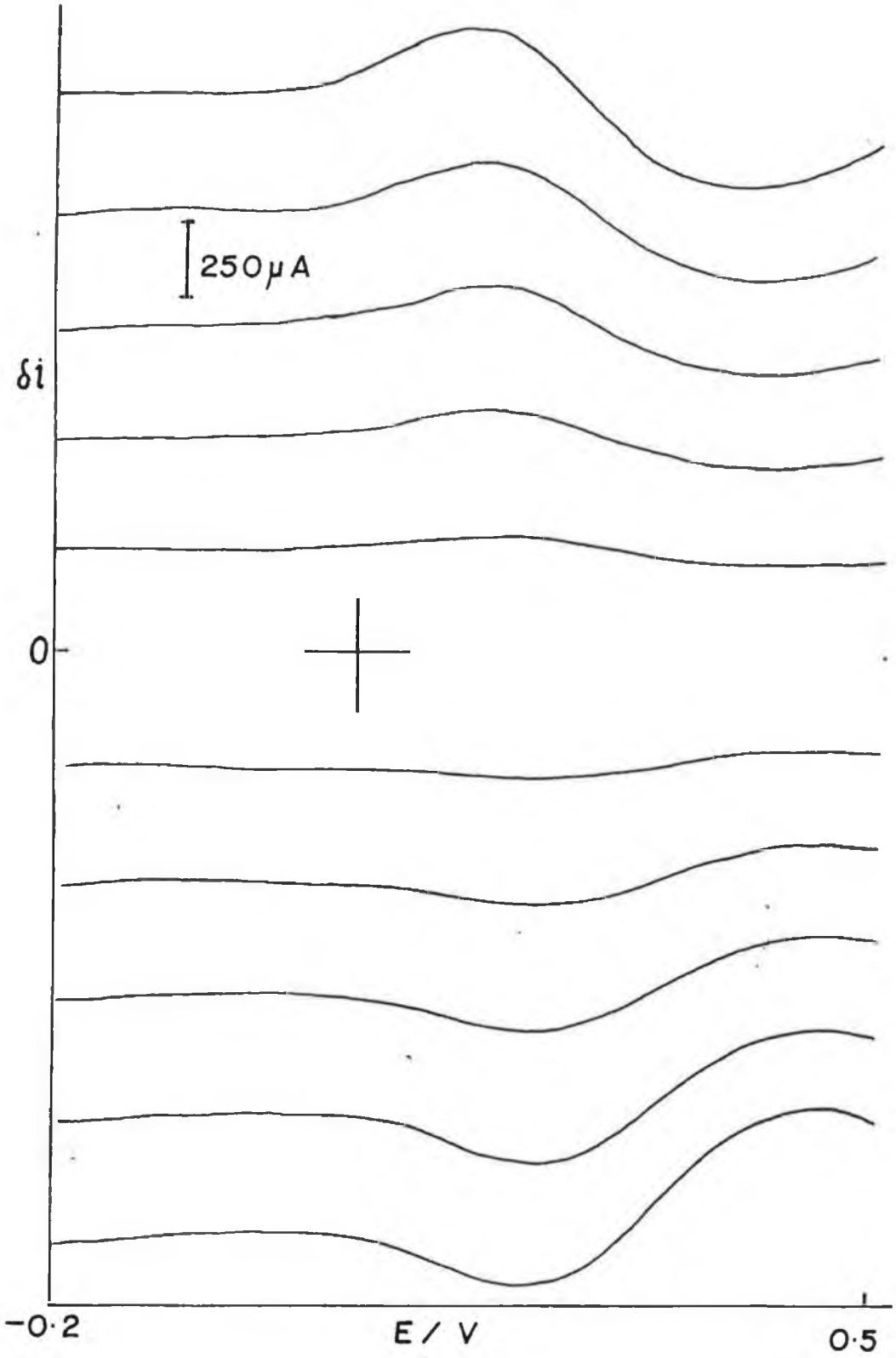

Figure 3.26 Differential pulse voltammogram of the PPFCN layer, in Figure 3.25, in 3.0M NaCl.
Scan Rate = 10mV/s. RC time constant = 0.1.

It is interesting that the DPV profile has very little evidence of the faradaic couple. This implies that the layer is seen primarily as a resistance and capacitance network, rather than the naive expectation that the double layer charging current is removed. A model for this network is described below.

3.4.6 TRANSMISSION LINE CIRCUIT FOR POLYMER MODELLING

It was seen in Section 3.4.4 that when a potential step of magnitude between 10mV and 50mV was applied to a polypyrrole layer in the conductive state, that the current decayed to a limiting value. The value of this limiting current increased with potential, and it took 3 minutes to reach this value.
To help explain this behaviour, transmission line theory can be employed. Here the polymer is considered as a non-inductive leakage free cable where the resistance is treated as the controlling term in the series impedance.

This is illustrated in Figure 3.27, where r and C are the resistance and capacitance per unit length, respectively.

The equation governing this system is similar to the diffusion equation

$$\frac{\partial V}{\partial t} = \frac{1}{rC}\frac{\partial^2 V}{\partial x^2} \qquad \text{..... 3.16}$$

Should a potential step, V_0, be applied then the solution to equation 3.16 is, [47],

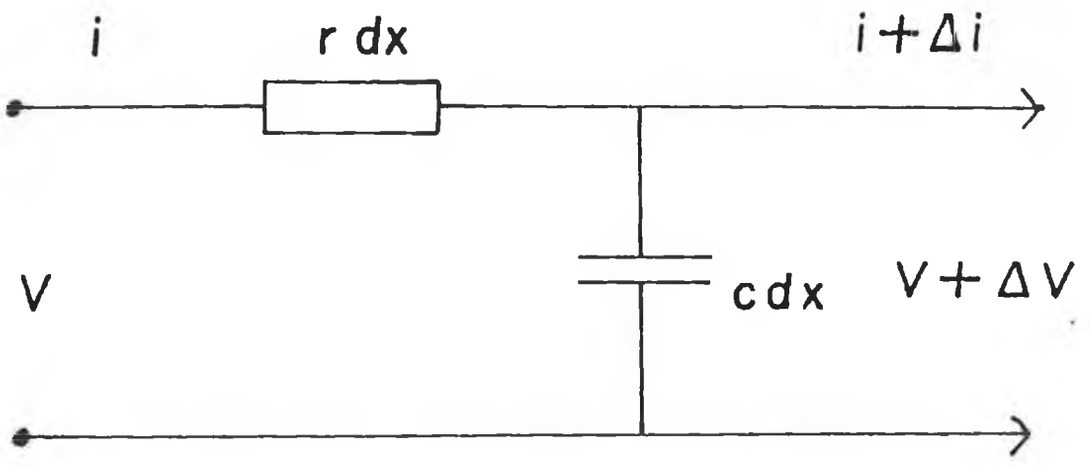

Figure 3.27 Transmission line circuit to model polymer.

$$V = V_0 \left[1 - \operatorname{erf}\left\{\frac{(x\sqrt{rC})}{(2\ t)}\right\}\right] \qquad \ldots\ldots 3.17$$

where $\operatorname{erf} w = {}^{2}/_{\pi} \int e^{-y2}\, dy$

the resulting current is given by

$$i = \frac{-1}{r}\frac{dV}{dx} \qquad \ldots\ldots 3.18$$

Differentiating equation 3.17, [48] we get

$$i = \frac{-1}{r}\frac{d}{dx}\left[V_0\left(1-\operatorname{erf}\left\{\frac{x\sqrt{rC}}{2\ t}\right\}\right)\right] \qquad \ldots\ldots 3.19$$

By simplifying the above equation, equation 3.20 is obtained

$$= V_0 \sqrt{rC}\, \frac{1}{r\ \sqrt{\pi}\ \sqrt{t}}\, \frac{1}{e^{Z}} \qquad \ldots\ldots 3.20$$

where $Z = \dfrac{x^2 rC}{4t}$

By expanding, and for large values of t, this leads to

$$i \cong \frac{Vo\sqrt{rC}}{r\sqrt{\pi}\sqrt{t}} \qquad \text{..... 3.21}$$

It can be seen that the current decays as a function of $1/\sqrt{t}$ and the slope equals

$$\frac{V_o\sqrt{C}}{\sqrt{r}\sqrt{\pi}},$$

therefore the slope should increase with applied potential.

A fresh PPTSP layer was formed on a platinum electrode as described previously. The layer was cycled in NaCl (0.1M), then potential step experiments were performed, as described in Section 3.4.4.

The potential steps ranged from 12mV to 49mV, the resulting experimental current decays are illustrated in Figure 3.28. The application of equation 3.21 to the experimental current decay curves yield linear plots at each potential step. These plots are shown in Figure 3.29.

Table 3.3 summarises the results obtained for the slopes from Figure 3.29, for each potential step.

TABLE 3.3. Slope of decay curves as a function of applied potential

POTENTIAL STEP (mV)	$Vo\sqrt{C}/(\sqrt{\pi}\sqrt{r})$ x 10^{-9} A $S^{1/2}$
12.0	9.0±1.0
26.0	30.0±1.4
34.0	45.0±5.0
49.0	54.0±3.8

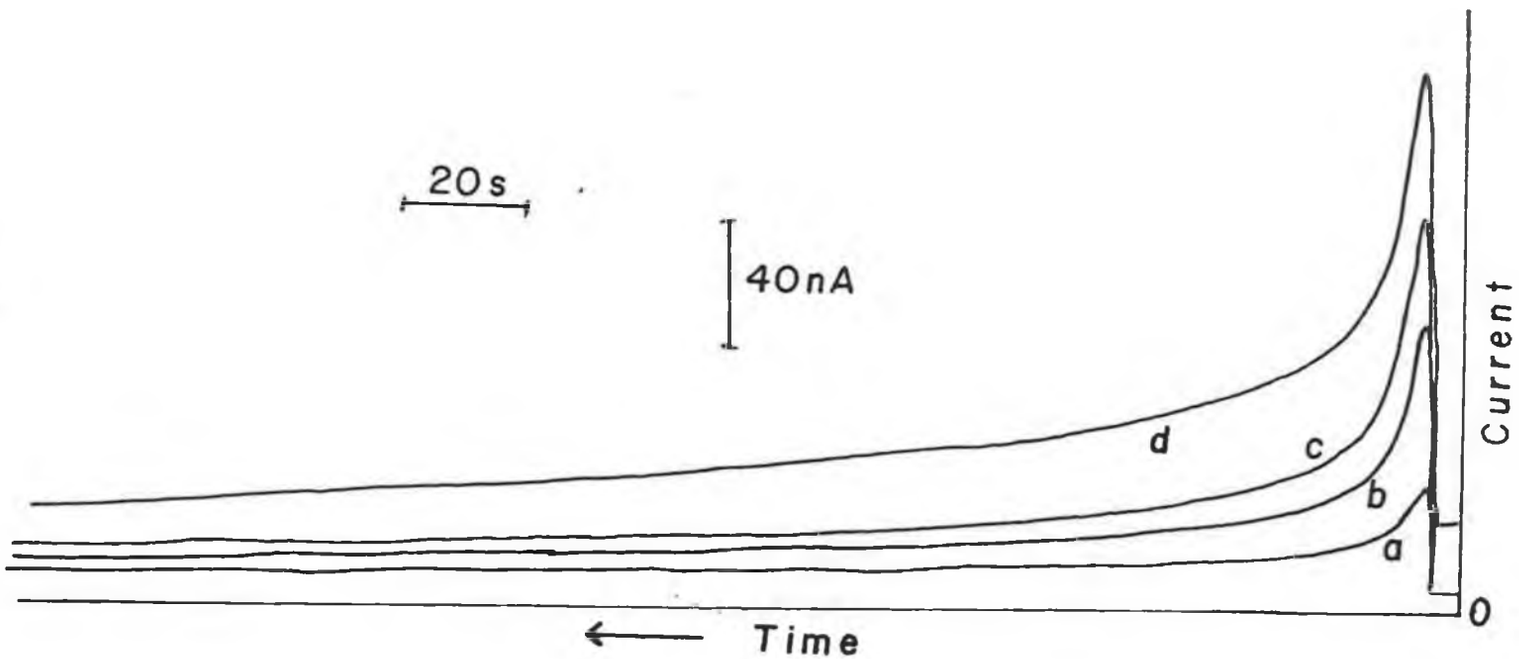

Figure 3.28 Experimental current decay curves obtained for a PPTSP layer, previously formed as described in Figure 3.4, for potential step experiments
(a) 12.0mV (b) 26.0mV (c) 34.0mV (d) 49.0mv.

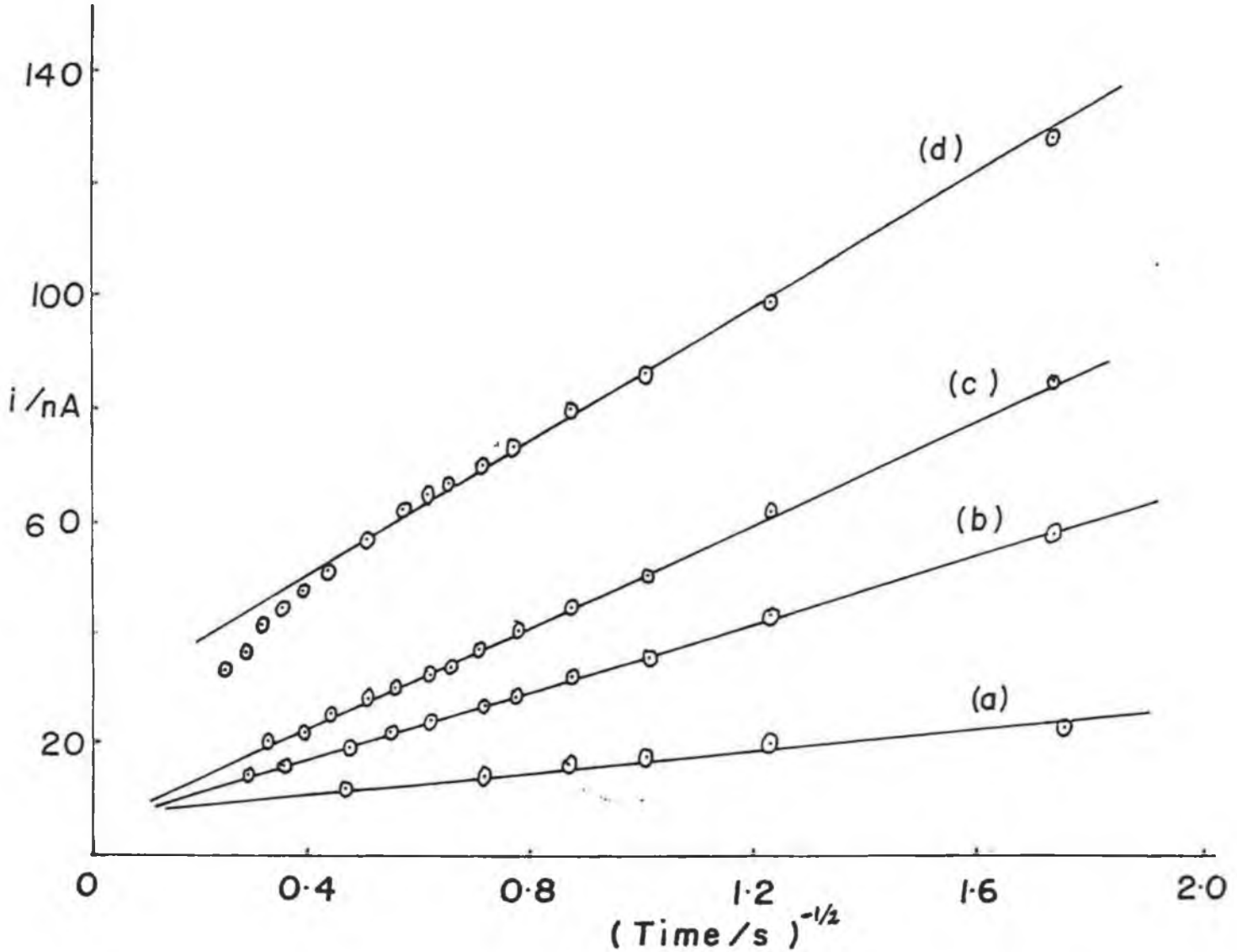

Figure 3.29 Plots of the decay current as a function of $1/\sqrt{t}$, for the PPTSP layer described in Figure 3.28.

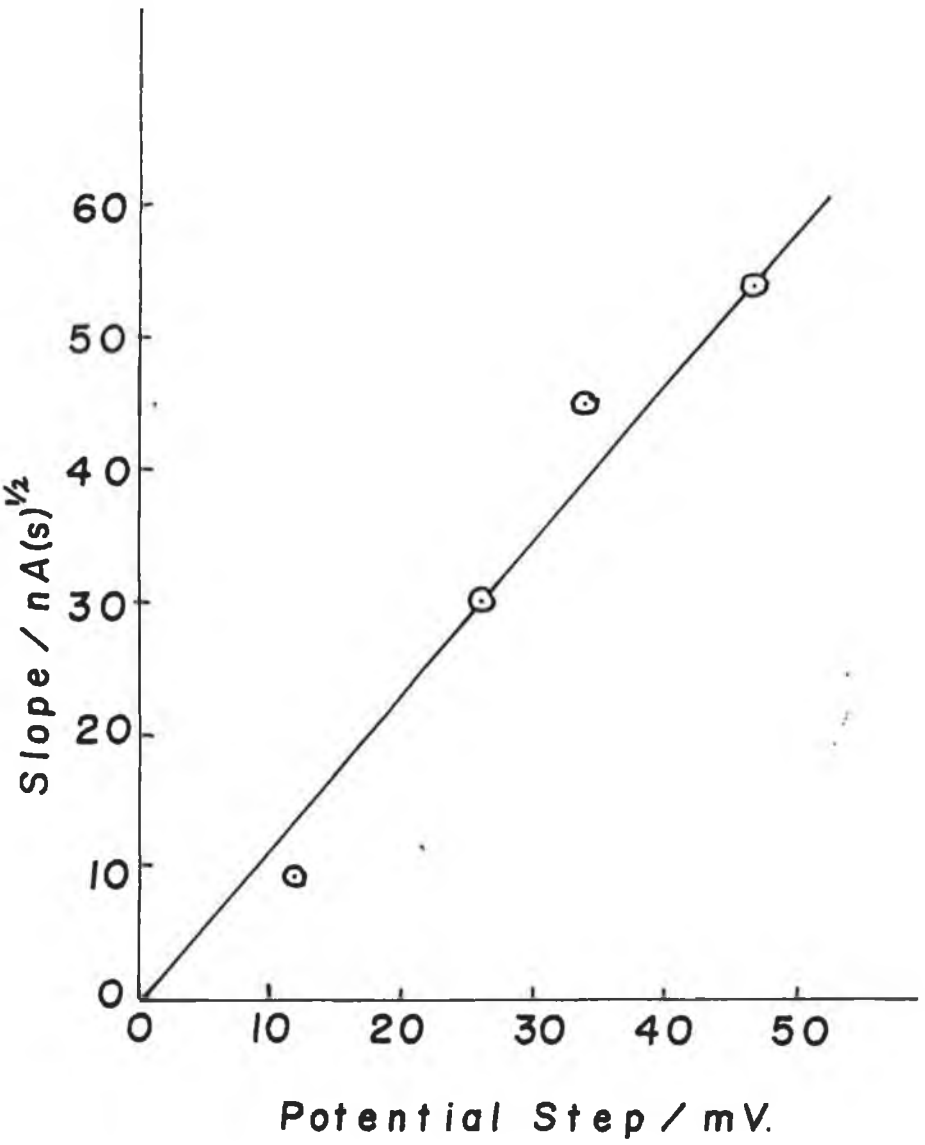

Figure 3.30 Plots of the slopes of Figure 3.29 plots as a function of potential step magnitude.

Figure 3.30 shows that the value of these slopes in the above table are linear with the magnitude of the potential step. This illustrates that these series of potential steps are not diffusion controlled in terms of concentration since for a series of potential steps of different magnitudes, the slope should be the same.

It is difficult to separate current associated with the oxidation of the polymer and current associated with the above circuit since any diffusion coefficients estimated from Cottrell plots may be incorrect.

3.5 CONCLUSION.

Differential Pulse Voltammetry was applied to conductive polypyrrole layers, with sigmoidal current responses being obtained. A model was proposed to help explain this behaviour of the polymer film. The model was composed of resistive elements, with a Fortran programme being used to simulate the DPV responses of the polymer film. Under certain conditions, it was found that the sigmoidal current outputs could be generated by assuming certain values for the resistive elements. A severe approximation was that the capacitive contributions were ignored. However a similarity in the shape of differential current output curves obtained experimentally and those simulated, using the simple model, was observed.

Potential Step Experiments were also undertaken upon the polymer films, from the limiting current plateaus obtained a transmission line model for the polymer is proposed.

The difference between the two models is that the capacitances associated with the polymer system are included within the transmission line model. The data obtained from the Potential Step Experiments was observed to fit the non inductive transmission line model.

3.6. REFERENCES

1. L.S. Curtin, G.C. Komolin, W.J. Pietro, J.Phys.Chem. (1988), 92, 12-13.
2. T,Iyoda, A. Ohtani, T. Shimidzu, K. Honda, Chem.Lett. (1986) 697-690.
3. T. Shimidzu, A. Otani, T. Iyoda, K. Honda. J.Electroanal.Chem., (1987), 224, 123-125.
4. R.A Bull, F.-R.F. Fran, A.J.Bard, J. Electrochem Soc., (1987), 129, 1009- 1115.
5. S.H.Clarum, J.H.Marshal, J. Electrochem. Soc., (1987), 134, 142-147.
6. J.Tanguy, N.Mermilliod, M.Hoclet, J. Electrochem. Soc. (1987), 134, 795-802.
7. E.M.Genies, G Bidan, A.F. Diaz, J. Electroanal.Chem. (1983), 149, 101- 113.
8. E.M.Genies, J.M. Pernaut, Synth. Metals. (1984/85), 10, 117-129.
9. P.G.Pickup, R.A.Osteryoung, J. Electroanal.Chem. (1985), 195, 271-288.
10. T.Osaka, K.Naoi, H.Sakai, S. Ogano, J. Electrochem.Soc. (1987), 134, 285-289.
11. T. Shimidzu, A. Ohtani, T. Iyoda, K. Honda. J. Electroanal. Chem. (1987), 218, 107-118.
12. P. Marque, J. Roncali, F. Garnier, J. Electroanal. Chem. (1987), 218, 107-118.
13. J.B.Schlenoff, J.C.W.Chien, J. Amer.Chem.Soc. (1987), 109, 6269-6274.

14. C.D. Paulse, P.G. Pickup, J.Phys.Chem. (1988), 92, 7002-7006.

15. A.M. Waller, R.G. Compton, J.Chem.Soc. Faraday Trans 1, 85, 977, (1989).

16. R.M. Penner, C.R. Martin, J.Phys.Chem. 93, 984, (1989).

17. C. Gabrielli, O. Haas, H. Takenouti, J.Appl.Electro.Chem. 17, 82 (1987).

18. C. Ho, I.D. Raistrick, R.A. Huggins, J.Electrochem.Soc., 127, 343, (1980).

19. X. Ren, P.G. Pickup, J.Phys.Chem., (1993), 97, 5356-5362.

20. J.Tanguy, M.Slama, M.Hoclet, J.L.Baudouin, Synth.Met., 28,(1989),C145.

21. I. Rubinstein, E. Sabatini, J. Rishpen, J.Electrochem.Soc, 134, (1987), 3078.

22. R.P. Buck, J.Electroanal.Chem. 210, (1986).

23. W.J. Albery, C.M. Elliott, A.R. Mount, J.Electroanal.Chem., 288, (1990), 15.

24. W.J. Albert, Z. Chen, B.R. Horrocks, A.R. Mount, P.J. Wilson, D. Bloor, A.T. Monkman, C.M. Elliot. Faraday Discuss. Chem. Soc., (1989), 88, 247.

25. S. Fletcher, J. Electroanal. Chem. 337,(1992),127-145.

26. G.L. Duffit, P.G. Pickup, J. Phys. Chem., (1991), 95, 9634.

27. K. Doblhofer, J. Electroanal. Chem., 331, (1992), 1015.

28. R. Naegli, J. Redepenning and F.C. Anson, J. Phys. Chem., 90, (1986), 6227.

29. J. Redepenning and F.C. Anson, J. Phys. Chem., 91 (1987), 4549.

30. M.E.G. Lyons, C.H. Lyons, C. Fitzgerald and T. Bannon, Analyst, 118, (1993), 361.

31. J. Heinze, M. Storzbach, J. Mortensen, Ber. Bunsenges, Physikal Chemie, 91, (1987), 960.

32. R. John, C.G. Wallace, J. Electroanal. Chem., 354, (1993), 145.

33. A.J. Bard, L.R. Faulkner, 'Electrochemical Methods', Wiley, New York, (1980).

34. J. Wang, 'Stripping Analysis; Principles, Instrumentation and Applications' VCH Publications, Deerfield Beach, (1984).

35. R. John, A. Talarie and G.G. Wallace, J. Electroanal. Chem., 319, (1991), 365.

36. Z. Cai and C.R. Martin, J. Electroanal. Chem., 300, (1991), 35.

37. J. F. Cassidy and J.G. Vos, J. Electroanal. Chem., 218, (1987), 341.

38. J. F. Cassidy and J.G. Vos, J. Electroanal. Chem., 235, (1987), 41.

39. S. Pons in 'Electroanalytical Chemistry' Ed. A.J. Bard, M. Dekker, New York, 13, (1984), 115.

40. J. Cassidy, S. Pons, A.S. Hinman and B. Speiser, Can J. Chem., 62, (1984), 716.

41. R.S. Nicholson and I. Shain, Anal. Chem., 36, (1964), 706.

42. G.L. Duffit and P.G. Pickup, J. Chem. Soc. Faraday Trans., 88, (1992), 1417.

43. X. Ren and P.G. Pickup, J. Chem. Soc. Faraday. Trans., 89, (1993), 321.

44. S. Fletcher, J. Chem. Soc. Faraday. Trans 89, (1993), 311.

45. X. Ren and P.G. Pickup, J. Electrochem. Soc., 139, (1992), 2097.

46. W. Breen, J.F. Cassidy, M.E.G. Lyons, J. Electroanal. Chem., 297, (1991), 445.

47. Techniques of Circuit Analysis, G.W.Carter and A.Richardson, Cambridge Univ. Press, (1972).

48. Modern Electrochemistry, J.O.M.Bocris and A.K.N.Reddy, Plenum/Rosetta Press, New York, 3rd Edition (1977).

CHAPTER 4

SPECTROSCOPIC INVESTIGATION OF CONDUCTING POLYMER LAYERS

4.1 INTRODUCTION

It has already been mentioned in previous chapters that doping of π conjugated polymers results in a highly conducting state of the polymer. At low doping levels the conductivity of the polymer increases considerably and additional absorption bands are observed within the optical gap of the undoped polymer. However above a critical doping concentration the properties of the polymer become essentially metallic-like in character.

This discovery of relatively high conductivities in doped organic polymers [1] was surprising due to organic systems having large band gaps.

This implied that simple band theory could not be used to explain the electrical conductivity of conductive polymers. The high conductivities of polymers in the dry state have led to the development of theories from a quantum mechanical stance [2-6].

The electrical conductivity of doped polyconjugated polymers are explained in terms of the presence of defects along the one dimensional polymer chain [7].

Depending on the type of polymer these defects are termed polarons, bipolarons and solitons.

Conducting polymers can be broadly divided into two types, those with a degenerate ground state with solitons as the defect, and those with non-degenerate ground states with the passage of polarons and bipolarons being responsible for the conductive nature of the polymer.

These defects (bipolarons, polarons) are band gap energy states created when electrons are removed from the top of the valence band of the conjugated polymer. A polaron is a radical cation that is only partially delocalized over several monomeric units, causing them to deform structurally. The energy level associated with this polaron is a destabilized bonding orbital, and it has a spin of ½.

At high doping levels, defects known as bipolarons are thought to form in certain polymers [8]. These are created when an electron is removed from the already oxidised polymer segment containing the polaron. However an electron can be removed from another part of the polymer chain, giving rise to another independent polaron.

Bipolarons are theoretically expected to be favoured over polarons [7]. However it was found in polypyrrole [9,10] that high concentrations of polarons exist, using electron spin resonance among other techniques.

Zotti and Schiavon [11] used an optical spectroelectrochemical method to determine the polaron concentration in doped polypyrrole and polyaniline. They

confirmed that polarons are stable intermediate species in these systems with the maximum polaron concentration attained at 50% oxidation of reversible charge, are 80% and 90% for polypyrrole and polyaniline respectively.

Bipolarons are spinless defects which extend over about four pyrrole rings in polypyrrole.

Figure 4.1(i) and 4.1(ii) show a representation of a polaron and a bipolaron species within the one dimensional polymer lattice of polypyrrole.

For polyacetylene, spinless charged solitons are thought to be the mobile species responsible for conduction at low doping concentration [12,13].

Trans $(CH)_X$ exhibits a double degenerate structured ground state, these are two resonance forms differing physically in the phase of the bond length alternation. In polyacetylene the bipolaron dissociates into two independent cations, namely the spinless solitons. The proposed soliton has been described [14] as a link in the electron-lattice system: a bond alternation domain link connecting the two degenerate ground state phases of polyacetylene.

Above a certain critical dopant concentration doped trans-polyacetylene is metallic in character as has been verified by the observation of a high Pauli susceptibility [15,16]. The nature of the metallic state of highly doped conjugated systems is one of the unresolved problems within the field of conducting polymers. Several models have been applied to help explain the metallic properties of trans-polyacetylene at high doping levels.

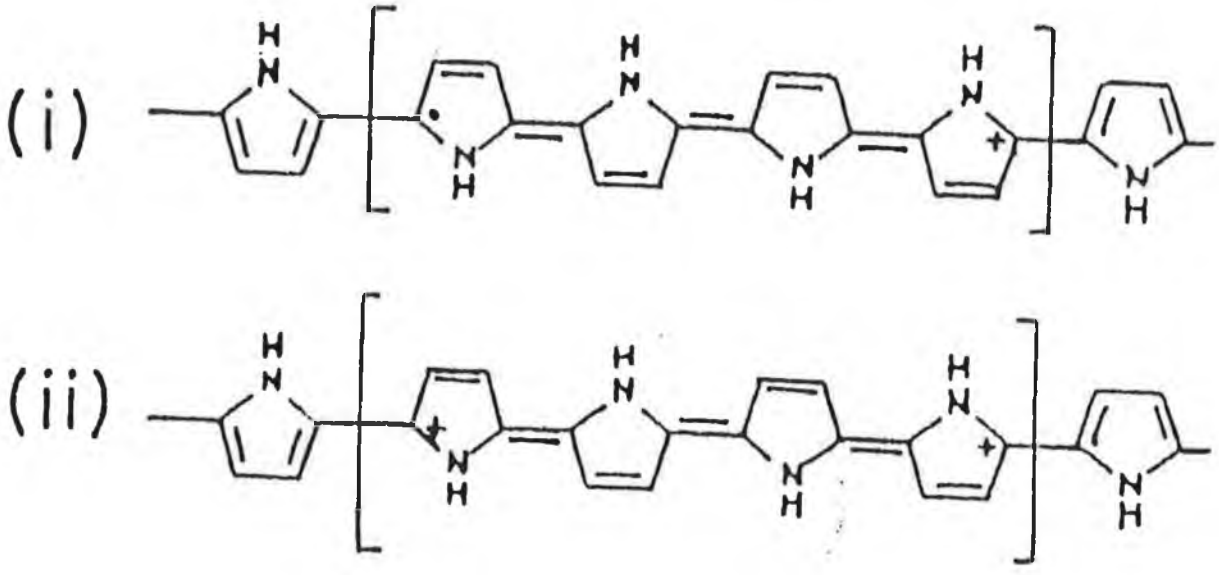

Figure 4.1 Schematic diagram of
(i) a polaron defect on polypyrrole
(ii) a bipolaron defect on polypyrrole

Mele and Rice [17] have included a potential field due to that of the dopant counterions in their calculation of the density of states for the trans-$(CH)_X$ at different doping levels. In the model Mele and Rice use a soliton lattice with the solitons pinned to the counterions. It is observed that disorder in the impurity potential and three dimensional inter-chain couplings are responsible for the experimentally observed semiconductor - metal transition of trans- $(CH)_X$ at high doping levels.

Harigaya and Terai [18] used a similar model to that of Mele and Rice. They found that the energy gap vanishes around a dopant concentration of 12%.

However other workers [19,20] have found that for more ordered and homogeneously doped samples of polyacetylene the transition into the metallic state is sharper as a function of doping level. It seems clear that disorder does not drive the polymer into a metallic state.

Several other models have been employed to try and explain the metallic behaviour of trans-$(CH)_X$ above certain doping levels.

Kivelson and Heeger [21] proposed that at a certain doping level, there was a crossover from a soliton lattice to a polaron lattice, with one electronic band corresponding to the polaron defects being half filled and contributing to the metallic properties of the polymer.

Conwell and co-workers [22,23] took into account the influence of counterions at the chain ends. They found that if the counterions at the end groups are not present then the electronic states localised to the ends become destabilized.

Dinter [24] proposes that a new type of superlattice exists for trans-$(CH)_X$ which is responsible for the metallic properties of the polymer.

Several attempts [25,26] have been made to try and explain the metallic behaviour of the polymer at high doping levels, taking into account the presence of counterions and electron-electron interactions [27]. It was found [28] that the potential field of the ion has a strong affect on the position of the soliton or polaron levels.

It is clear that even though a high concentration of solitons gives rise to quite a broad midgap band, the gap around the Fermi energy is still too large to explain the metallic properties [29]. Coulombic interactions between the defects and dopants is important in trying to establish the reason for the metallic behaviour of conducting polymers.

In amorphous semiconductors, carrier transport is by a hopping mechanism to which the carrier transport of conductive polymers may be compared. Pickup et al [30] found that for lightly doped samples of polyacetylene that a model of anisotropic variable range hopping is consistent with their data. Also for heavily doped polyacetylene, in addition to hopping, temperature independent tunnelling between large conducting domains has to be assumed.

Tunnelling is a quantum-mechanical effect which has been applied in the charge transport across PN junctions through depletion layers [31].

It is described as occurring when an electron confined by a potential barrier, higher than its energy, can still pass through the barrier if the barrier is narrow enough. These processes of hopping and tunnelling have been used to describe the non-intrinsic transport mechanisms within doped polyacetylene samples [30]. The intrinsic conductivity of a sample is the conductivity within a conjugated strand, and the non-intrinsic being the charge transport from strand to strand and from fibre to fibre.

It should be noted that in semiconductors there are two main types of scattering, lattice and impurity, that can perturb the movement of the charge carriers. Electron-phonon coupling has been given as a reason why most organic systems have low conductivities [32]. Phonons are thermally caused, lattice pressure waves that also have particulate properties. They are created when atoms within the crystal lattice vibrate around their proper place due to thermal energy. Upon collision between current carriers and phonons, the carrier is scattered and thus loses the kinetic energy. The carrier is again accelerated by the external field but then it can undergo further collision.

Impurity scattering is caused by the presence of charged impurity atoms within the matrix. Due to their charge they exert a force on the free carrier causing it to change direction.

It is concluded [30] that conceptually there is a continuous transition from tunnelling between domains to variable range hopping between individual sites

within the polymer matrix. A conjugated segment of a polymer chain can be regarded as a small conductive domain or as a fairly extended localized state.

Within this chapter, Nernst plots are constructed from absorption data collected during the reduction of the polypyrrole layers. The data are analyzed according to a monomer unit model [33] and values for the formal potentials and number of electrons transferred are calculated. The bandgap of the neutral polypyrrole is calculated, by a method used previously by Blackwood et al [34] to calculate the bandgap of polypyrrole and poly p-phenylene polymers. Also the concentration profiles of bipolarons, polarons and neutral pyrrole monomers are calculated.

The reaction between pyrrole and the strong π-acid tetracyano-ethylene is characterised by spectroscopic and electrochemical techniques. It has been shown before that tetracyanoethylene forms electron donor-acceptor complexes (EDA) with several aromatic donors [35-38]. These complexes have been characterised by Isaacs [36].

Finally a $[Fe(CN)_6]^{3-}$ complex is prepared, that is soluble in aprotic solvents, and the electrochemistry of this compound is reported in various solvent mixtures. The shift observed [39] in the ferri- and ferrocyanide electrochemistry upon addition of water and methanol is discussed.

4.2 U.V. ANALYSIS OF POLYPYRROLE LAYER

4.2.1 EXPERIMENTAL

All chemicals employed were reagent grade. Pyrrole was distilled and stored under nitrogen in the dark. Electrochemical experiments were performed in a single compartment three electrode cell. A carbon rod was used as the auxiliary and an indium tin oxide electrode as the working electrode, for layer formation. A saturated calomel electrode was used as the reference electrode. The working electrode was washed several times with distilled water and acetone, prior to layer formation. All solutions employed in electrochemical experiments were degassed with oxygen free nitrogen for approximately 10 minutes.

A ramp generator (H.B. Thompson 16 bit) a potentiostat (Edt ECP 100) and an electronic integrator (Sycopel DP301S) were used. All experiments were carried out at room temperature.

A fresh solution of 0.1M pyrrole and 0.1M sodium dodecylbenzenesulphonate was prepared. Polymerization was carried out potentiostatically, with the potential of the ITO working electrode set at 1.0V, using a potentiostat (Edt ECP 100 model). Once a PPDBS layer was formed, the film on the ITO was thoroughly rinsed with distilled water. Fresh electrolyte solution, 0.1M NaCl, was introduced into the cell for spectrochemical experiments. A simple one compartment thin layer glass cell was employed. The working electrode was the ITO electrode with the deposited polymer film. Aluminium foil served as the

auxiliary with a Ag/AgCl reference electrode. The working and the auxiliary electrodes were separated by a piece of plastic.

A series of in situ absorption spectra of polymer films were measured on a double beam UV-visible spectrometer (Shimadzu Model UV-160 resolution $\pm$ 4nm). A reference cell was employed; this was a glass cell, with an ITO electrode and fresh electrolyte solution. After the polymer films were deposited and rinsed, the potential of the working electrode, coated with the polymer film, was set to the rest potential of 0.4V. The cell was switched on and the current allowed to decay to a steady value. The potential was then scanned in a negative direction at a scan rate of 0.1 mV/s. The absorbance of the polymer film at a series of wavelengths was recorded at every 0.020 volt interval. The experiment was terminated once the polymer film had been fully reduced.

The experiment was repeated for a polypyrrole perchlorate layer. The polymer film was formed on the ITO electrode from an aqueous solution of pyrrole (0.1M) and $NaClO_4$ (0.1M). Polymerization was again carried out potentiostatically by holding the potential of the working electrode.

4.2.2 THEORY OF THE MONOMER UNIT MODEL

As previously stated, the spectroelectrochemical behaviour of Polypyrrole films can be analyzed by application of the Nernst equation. Recently [33] however, a 'monomer unit model' was used to analyze the polymers spectral behaviour. This model is similar to the application of the Nernst equation [40-43], however three main assumptions are made so as the monomer unit model may be applied.

The three assumptions are as follows:

(1) the overlapping in the absorption spectra of neutral, polaron and bipolaron species is ignored,

(2) only three chemical species, neutral monomers, slightly oxidised monomers (polarons) and fully oxidised monomers (bipolarons) are said to exist in the polymer film at a given potential,

(3) two equilibrium reactions, between neutral monomers and polarons, and between polarons and bipolarons are said to occur.

Based upon the three assumptions above, the 'monomer unit' model is applied to the absorption data for the polypyrrole films. Similar treatments [40-42] with other electroconducting polymers have been undertaken.

The absorption band at 410nm is assigned to the π-π^* transition of the neutral pyrrole monomers and the band at around 800nm was assigned to the fully oxidised pyrrole monomers. However it is important to note, that the $\pi \rightarrow \pi^*$ transition band and the band due to the fully oxidised pyrrole monomers, did not always appear at these wavelengths. The character of the bands, however, was found to be similar with the latter being broad in nature and the former being sharp in character.

The absorption data are treated according to the Nernst equation, assuming Beer's Law.

At 410nm

$$E = E^{o}_{1} + \frac{0.059}{n_1} \text{Log}\left\{\frac{([Py^{+n1}])}{([Py^{0}])}\right\}$$

$$E = E^{o}_{1} + \frac{0.059}{n_2} \text{Log}\left\{\frac{(\Delta Abs_{max} - \Delta Abs)}{(\Delta Abs)}\right\} \quad \ldots\ldots \quad 4.1$$

At 800nm

$$E = E^{o}_{2} + \frac{0.059}{n_2} \text{Log}\left\{\frac{([Py^{+n2}])}{([Py^{+n1}])}\right\}$$

$$E = E^{o}_{2} + \frac{0.059}{n_2} \text{Log}\left\{\frac{(\Delta Abs)}{(\Delta Abs_{max} - \Delta Abs)}\right\} \quad \ldots\ldots 4.2$$

where E is the potential applied to the electrode, E^{o}_{1} and E^{o}_{2} are the formal electrode potentials, n_1 and n_2 are the number of electrons transferred and Py^{o}, Py^{+n1} and Py^{+n2} are the neutral monomer, the slightly oxidised monomer and the fully oxidised monomer respectively. The ΔAbs's are the absorbance change relative to the fully oxidised spectrum at 410nm and that relative to the fully reduced spectrum at 800nm. The $(\Delta Abs)_{max}$ is the maximum absorbance change between the fully reduced and oxidised states. It is important to note that the contributions of the counterions to the equations is omitted for convenience.

It has been found previously [33] that deviations away from linearity occur. However it is possible from the linear portion of the plot to obtain n values and formal electrode potentials from the slope and intercept respectively.

4.2.3 RESULTS AND DISCUSSION

Figure 4.2(a) shows the optical absorption spectrum of a freshly prepared polypyrrole film, formed in a degassed aqueous solution of pyrrole (0.1M) and sodium dodecylbenzenesulphonate (DBS 0.1M). The potential of the working indium tin oxide electrode was held at 1.0volt until a PPDBS layer was deposited.

From the optical absorption spectrum two distinct bands can be observed. The broad band at 830.0nm has previously [33,34] been assigned to the $\pi \rightarrow \pi^*$ transition of the oxidised pyrrole monomers. The degree of doping of the polymer has an affect on what species will be present within the polymer matrix. At high doping levels for polypyrrole, mid gap energy states known as bipolarons are formed. It has been reported [34] that there are 3 main transitions that can occur within/across the bandgap of this polymer. There is the transition from the valence band to the conduction band, which occurs at 345nm. The value of this absorption is at lower wavelength to the bandgap transition of the neutral polymer due to the wider bandgap associated with the heavily doped polymer. Concerning the transitions within the gap of the heavily doped polymer, there are the bands associated with the transitions from the valence band to the bonding dication level (1450nm) and also from the valence bnd to the antibonding dication level.

When the polymer is lightly doped, the dominant species are polarons. Again several possible transitions have been reported for polypyrrole in the lightly

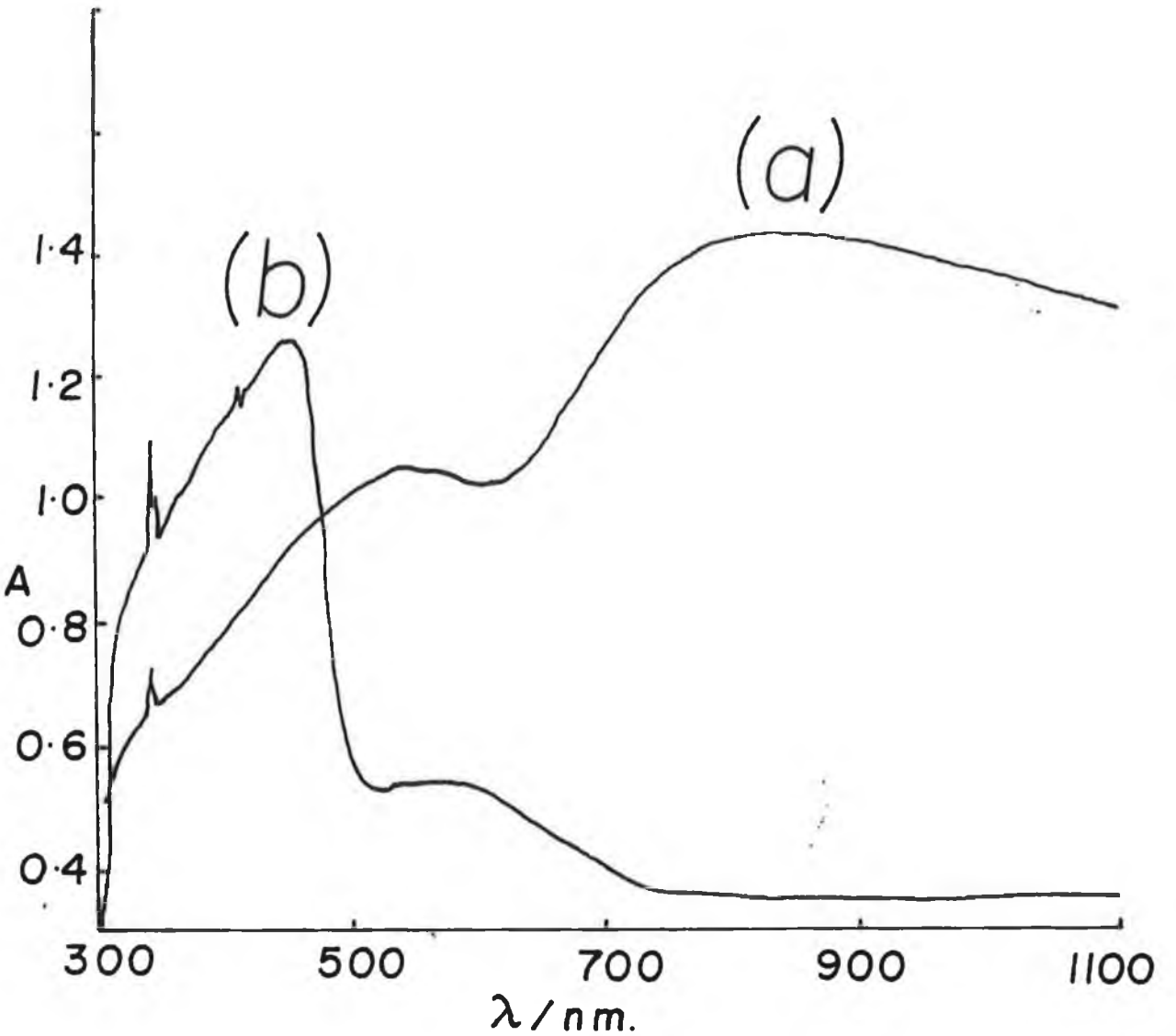

Figure 4.2 The optical absorption spectrum (a) of a freshly prepared polypyrrole film, formed by holding the potential at 1.0V in an aqueous solution of pyrrole (0.1M) and sodium dodecylbenzenesulphonate, DBS, (0.1M), (b) of the reduced PPDBS layer, after being reduced to -1.2V in an aqueous solution of NaCl (0.1M).

doped state [34,43]. The possible transitions that can occur within/across the bandgap for the polaron state are as follows:

(i) transition from the valence band to the antibonding cation level ACL (540nm),
(ii) transition from the bonding cation level (BCL) to the ACL (690nm),
(iii) transition from the BCL to the conduction band (540nm),
(iv) transition from the valence band to the conduction band (390nm),
(v) transition from the valence band to the BCL (2480nm).

It has also been reported [43] that a band at 440nm was observed, possibly being due to the transition from the valence band to the antibonding cation/dication level.

From Figure 4.2 it is possible to assign transitions to the two bands observed. The band at 535.0nm (Figure 4.2(a)) is probably due to the transition from the valence band to the antibonding cation level. The broad band at 830.0nm could represent the high energy tail of the transition from the valence band to the bonding cation level. It is possible from this spectrum to conclude that the polymer is in the conducting state.

Figure 4.2(b) shows the absorption spectrum of the same polymer film, PPDBS, upon reduction in an aqueous solution of NaCl(0.1M). When the potential of the film reaches a value of -1.2V is Ag/AgCl, a strong band centred around 420nm appears, and at the same time absorption above 500nm falls. The band at 420nm most likely represents the bandgap transition in the neutral polymer. It has been

reported [33] that as the potential of the polymer is gradually swept negative, leading to reduction, a band around 400nm appears and it shifts to lower energies as the potential is swept further negative.

Also the electrochromic property of the polypyrrole films is illustrated when the polymer films are deposited onto ITO electrodes. It was seen that when the layers are in the oxidised state they are black in appearance and upon electrochemical switching to the reduced state, the films take on a yellow colour. It is this property of conductive polymers upon electrochemical switching that has led to them to be used as smart windows [8].

When the PPDBS layer in Figure 4.2 was reoxidised, it was observed that there was hysteresis present, therefore indicating not perfect reversibility upon electrochemical switching.

Figure 4.3 shows the change in absorbance at all three wavelengths (420nm, 535nm and 830nm) versus applied potential. These results agree well with previous results obtained for a polypyrrole film [33]. Also not perfect reversibility was observed in the absorbance measurement, upon electrochemical cycling, of polythiophene films [44]. However it was noticed that the introduction of alkyl substituents onto the polymer chain increased the reversibility of the system.

Upon reduction of the PPDBS film, the potential was scanned in a negative direction from +0.4volts at a slow scan rate of 0.2mV/s. This scan speed was choosen so that the polymer layer was always in an equilibrium condition. Previously [33] a polypyrrole layer was stepped in 0.1volt intervals at a scan

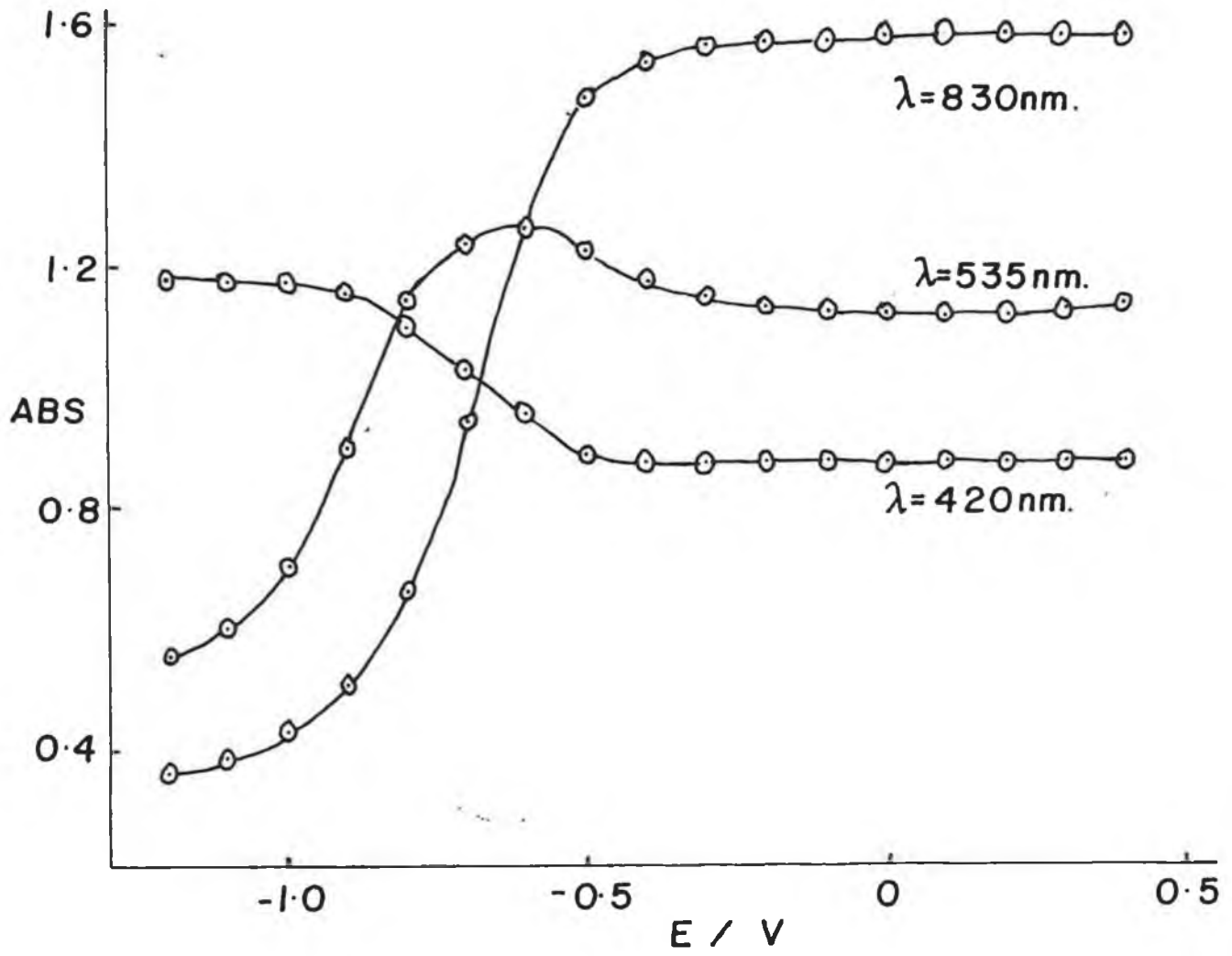

Figure 4.3 Change in absorbance at three wavelengths (420nm, 535nm and 830nm) versus applied potential for the PPDBS layer described in Figure 4.2.

speed of 5mV/s, and after each interval the current was allowed to decay to a steady value. However it was mentioned that this took 30 minutes, therefore a slower scan speed was chosen in our experiments so the current flowing was always small in magnitude. Values of absorbance at selected wavelengths were monitored as a function of potential and the scan was terminated when the polymer layer was fully reduced. It appears from Figure 4.3 that the assumption that the bands do not overlap is not justified since the absorbance at 535nm is not symmetrical.

The Monomer Unit Model, previously described, was applied to the PPDBS absorption data. Figure 4.4 shows the Nernst plots of the absorbance data at 450nm and 830nm. It can be seen that the two plots are not linear, however nearly linear portions occur in certain potential regions.

It is from the slope and intercept of the linear regions that the values for the apparent number of electrons transferred and the formal potential are obtained. These results are summarised in Table 4.1 given below. It is seen that there are deviations away from linearity, and these have been observed previously [33,44]. The non integer values for n_1 and n_2 (see equation 4.1 and 4.2) are similar to these found elsewhere. Ameyama [33] found $n_1 = 0.217$ and $n_2 = 0.217$ for PPCl.

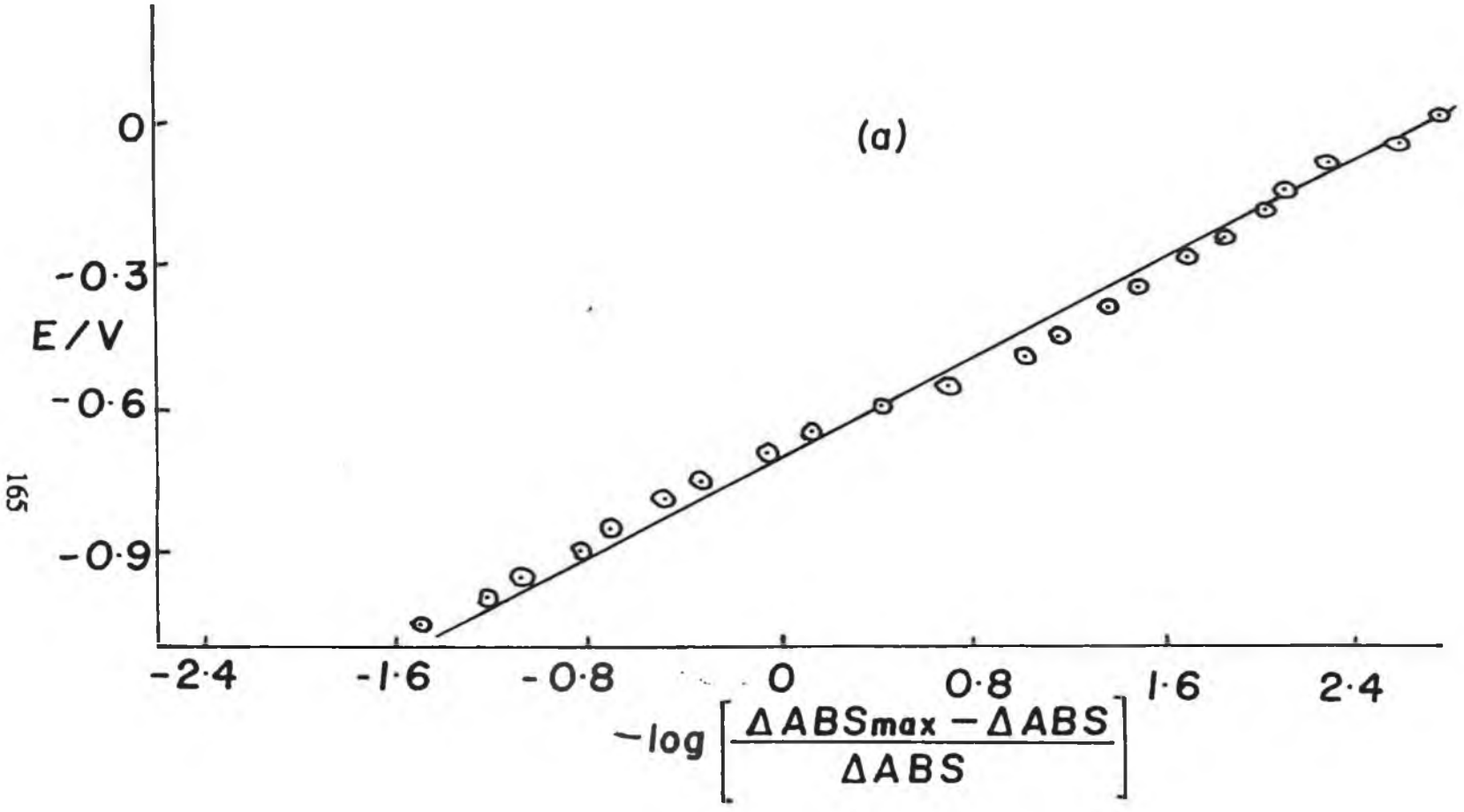

Figure 4.4 Nernst plots for the absorbance data shown in Figure 4.3, (a) 830nm and (b) at 450nm.

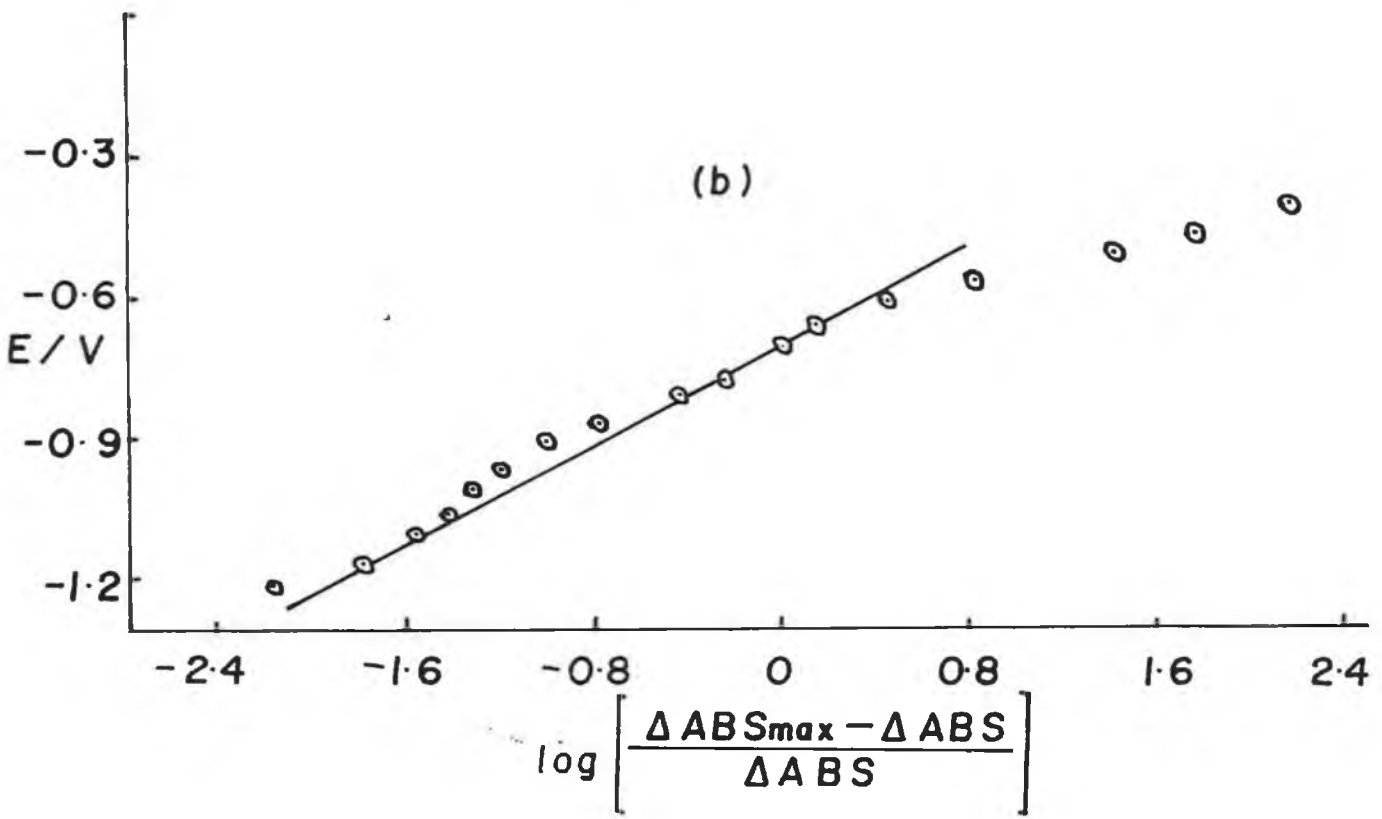
(b)
-0·3
-0·6
E / V
-0·9
-1·2
-2·4
-1·6
-0·8
0
0·8
1·6
2·4
log [ΔABSmax − ΔABS / ΔABS]

TABLE 4.1

ELECTROCHEMICAL PARAMETERS OBTAINED FROM APPLICATION OF THE NERNST EQUATION TO THE SPECTROSCOPIC DATA OF POLYPYRROLE FILMS

Polymer Layer	Apparent Number of Electrons Transferred		Formal Potentials (Volts)	
	n_1	n_2	E_1^0	E_2^0
PPDBS	0.236±0.01	0.206±0.05	-0.670	-0.705
$PPClO_4$	0.118±0.02	0.118±0.01	-0.485	-0.570

Figure 4.5(a) shows the optical absorption spectrum of a freshly prepared polypyrrole film, formed in a degassed aqueous solution of pyrrole (0.1M) and $NaClO_4$ (0.1M) by holding the potential of the ITO working electrode at 1.3 Volts.

It can be seen that a broad band from 700nm to at least 1100nm is present, possibly being the high energy tail of the transition from the valence band to the bonding cation level. Also a band at 443 nm is observed, possibly being due to the transition from the valence band to the antibonding cation/dication level.

When the $PPClO_4$ layer was reduced in a degassed aqueous solution of $NaClO_4$ (0.1M) until the applied potential was -1.8 volts, a band at 392 nm was obtained,

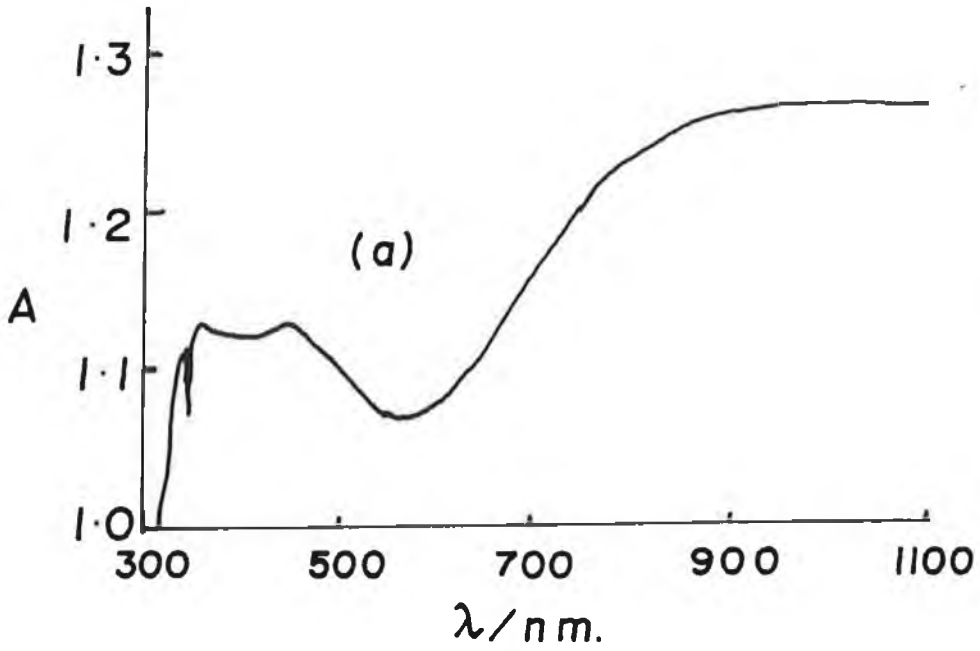

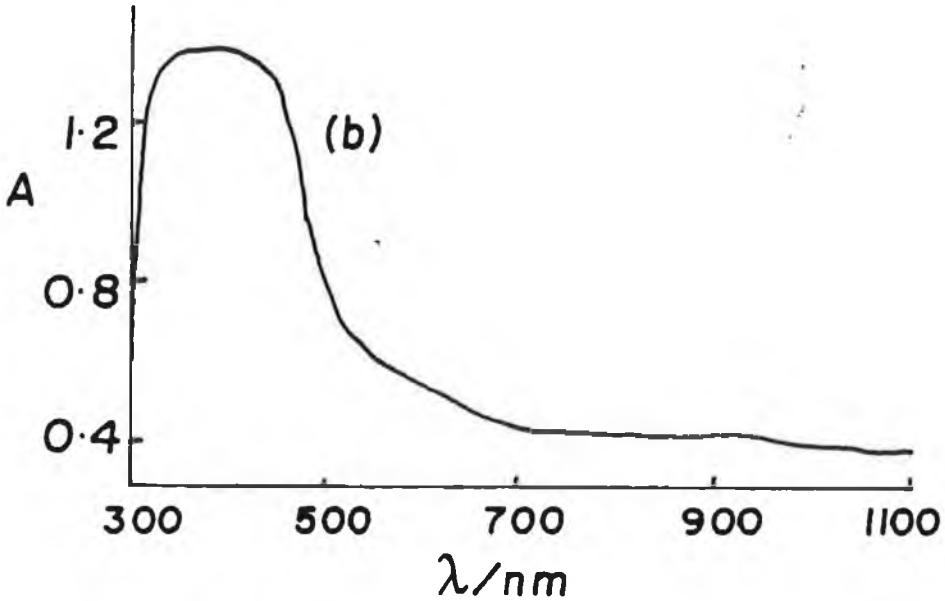

Figure 4.5 The optical absorption spectrum

(a) of a freshly prepared polypyrrole film, formed by holding the potential at 1.3V in an aqueous solution of pyrrole (0.1M) and $NaClO_4$ (0.1M).

(b) of the reduced $PPClO_4$ layer after being reduced to -1.8V in an aqueous solution of $NaClO_4$ (0.1M).

as seen in Figure 4.5(b). This band is characteristic of the bandgap transition of the neutral polymer. Again, the $PPClO_4$ was reduced at a slow scan speed with absorption data being recorded at specific potential values.

Figure 4.6 shows the change in absorbance at the two wavelengths (1100nm and 400nm) versus applied potential. The Monomer Unit Model was applied and the resulting plots for the $PPClO_4$ layer are shown in Figure 4.7. It can be seen that the plots are not linear. However it is possible to estimate the apparent number of electrons transferred and the formal potentials from the linear region in the plots. These results are also summarised in Table 4.1

It is possible to calculate the concentration profiles of the neutral pyrrole species, polarons and the bipolarons by application of equations 4.1 and 4.2 along with the equation

$$[Py^{o}] + [Py^{+n1}] + [Py^{+n2}] = C \qquad \ldots\ldots \quad 4.3$$

where C is a constant. The above equation assumes that the only species present within the polymer matrix are that of neutral monomers, polaron and bipolarons.

Figure 4.8 and 4.9 show the resulting concentration profiles of the three species for both the PPDBS and $PPClO_4$ layers respectively. These profiles are different to those reported [43] previously, where a polypyrrole layer was analysed according to a Polaron/Bipolaron model.

The Polaron/Bipolaron model treats the redox reactions of the polypyrrole film in terms of a unit cell consisting of several monomers. The redox mechanism is

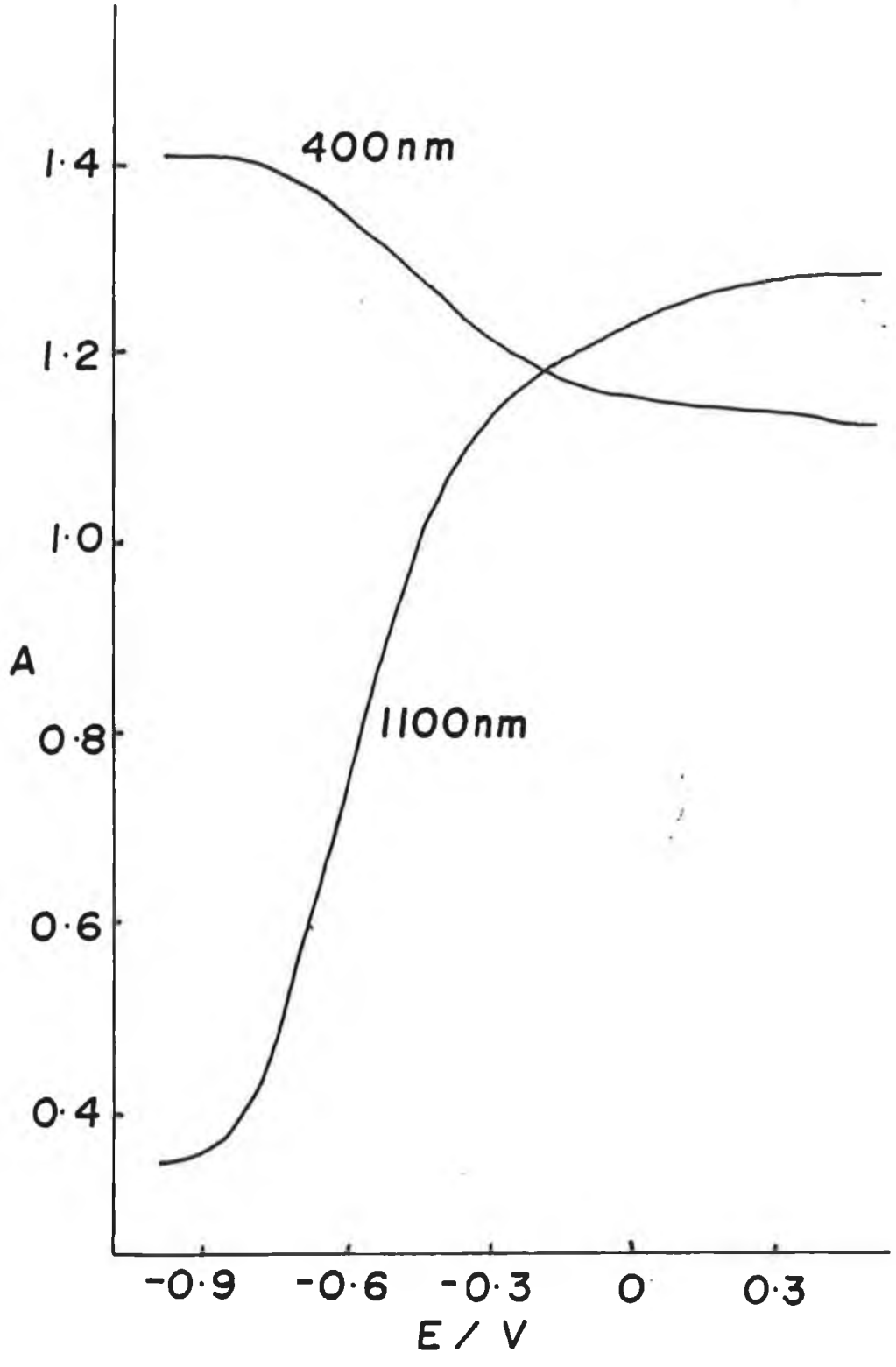

Figure 4.6 Change in absorbance at two wavelengths (1100nm and 400nm) versus applied potential for the $PPClO_4$ layer described in Figure 4.5.

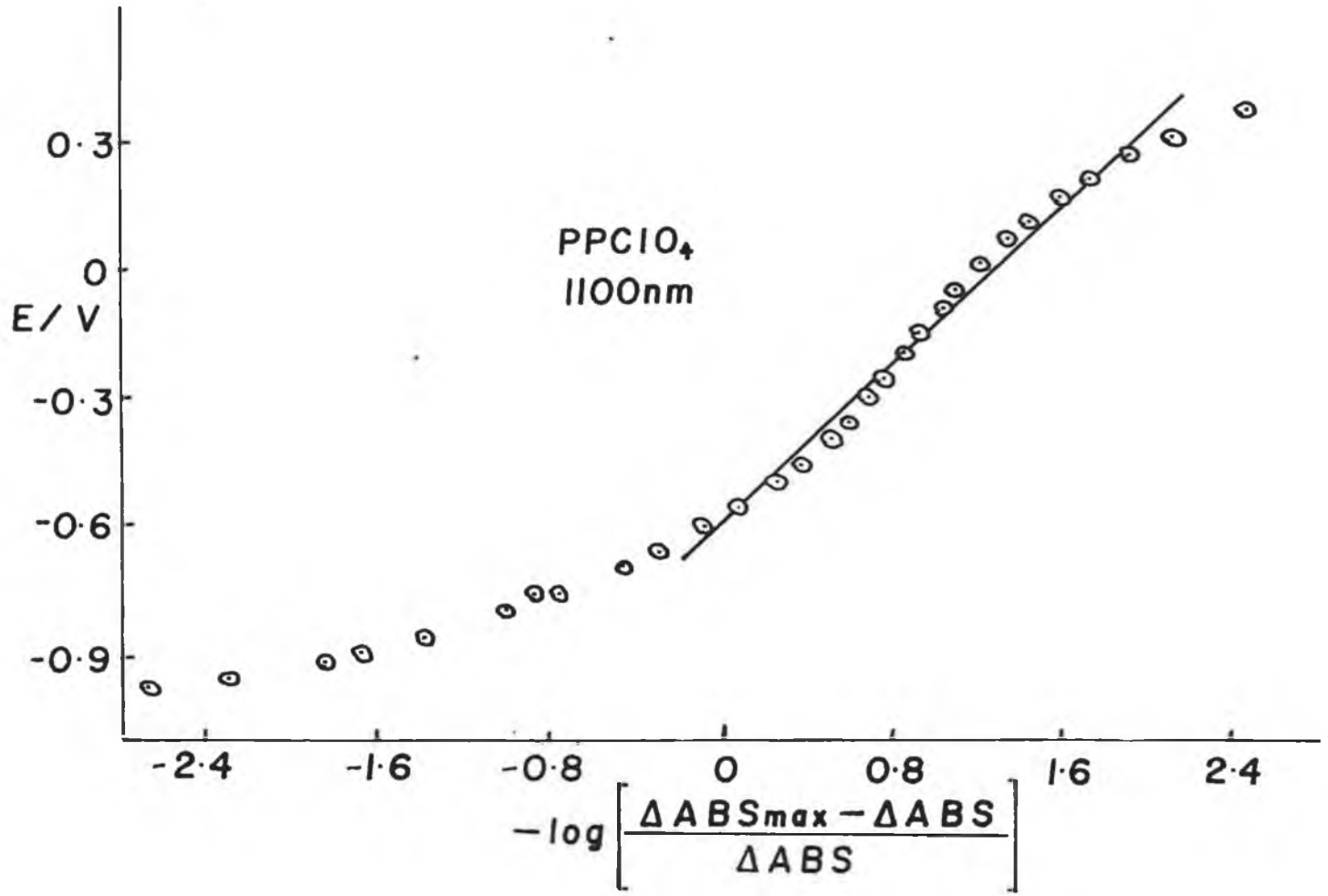

Figure 4.7 Nernst plots for the absorbance data shown in Figure 4.6 for 1100nm and 400nm.

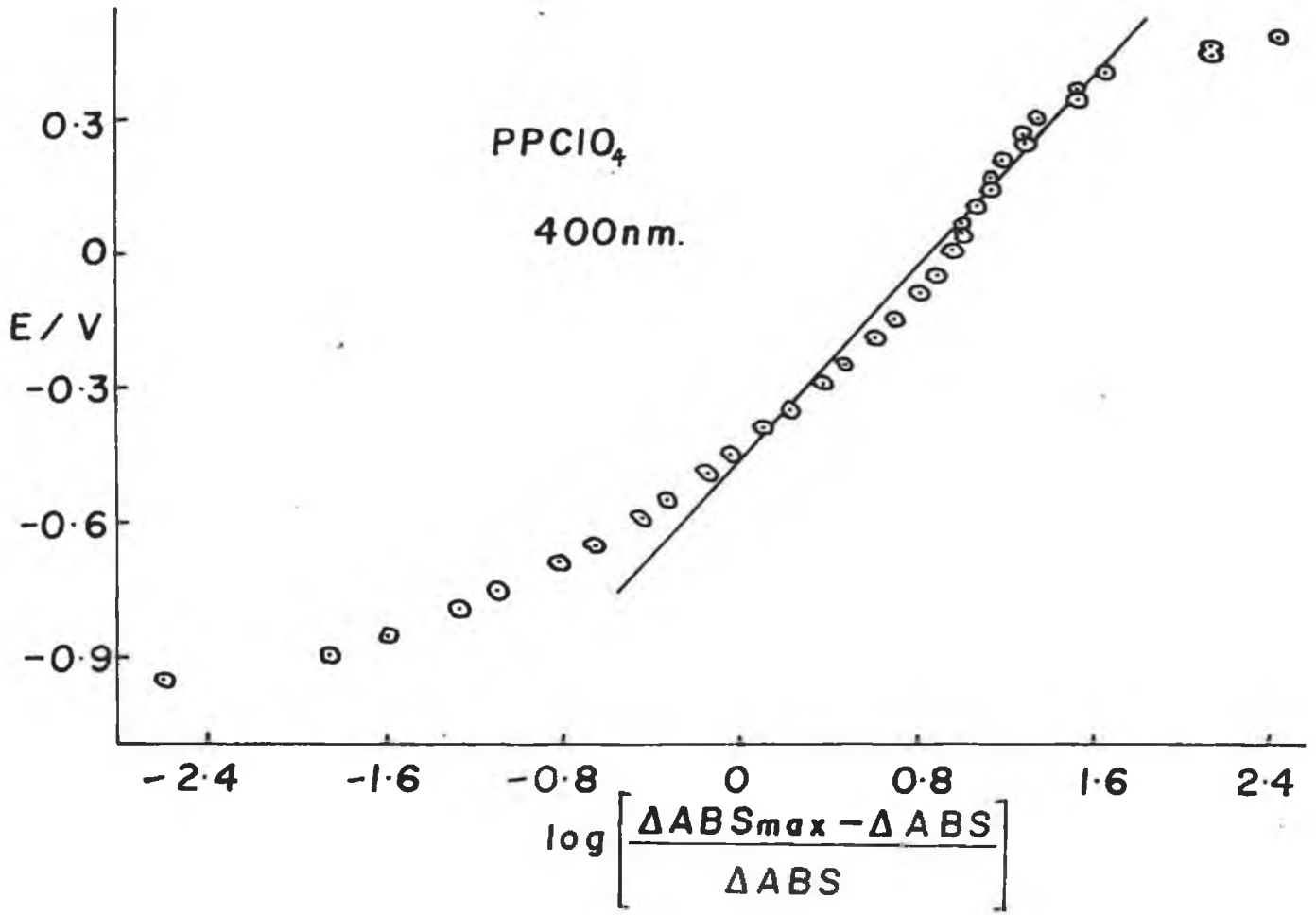
0·3
0
E / V
-0·3
-0·6
-0·9
PPClO4
400nm.
-2·4
-1·6
-0·8
0
0·8
1·6
2·4
log [ΔABSmax − ΔABS / ΔABS]

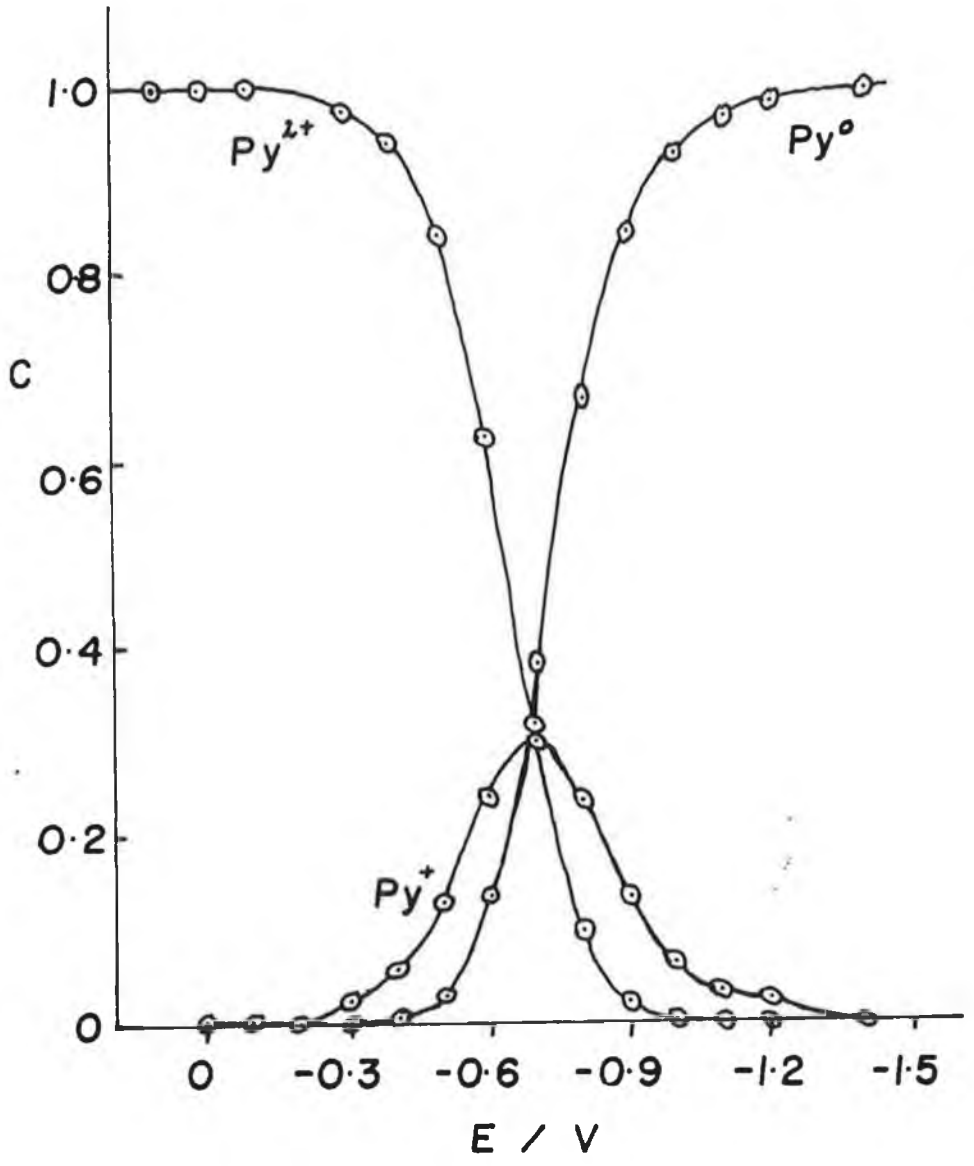

Figure 4.8 Concentration profiles of neutral pyrrole, P_y^o, slightly oxidised pyrrole, P_y^{+n1}, and fully oxidised pyrrole, P_y^{+n2}, predicted from Eq. 4.1 - 4.3. The formal electrode potentials (E_1^o = -0.670V, E_2^o = -0.705V), and the n values (n_1 = 0.236, n_2 = 0.206) were obtained for the PPDBS layer from the plots shown in Figure 4.4.

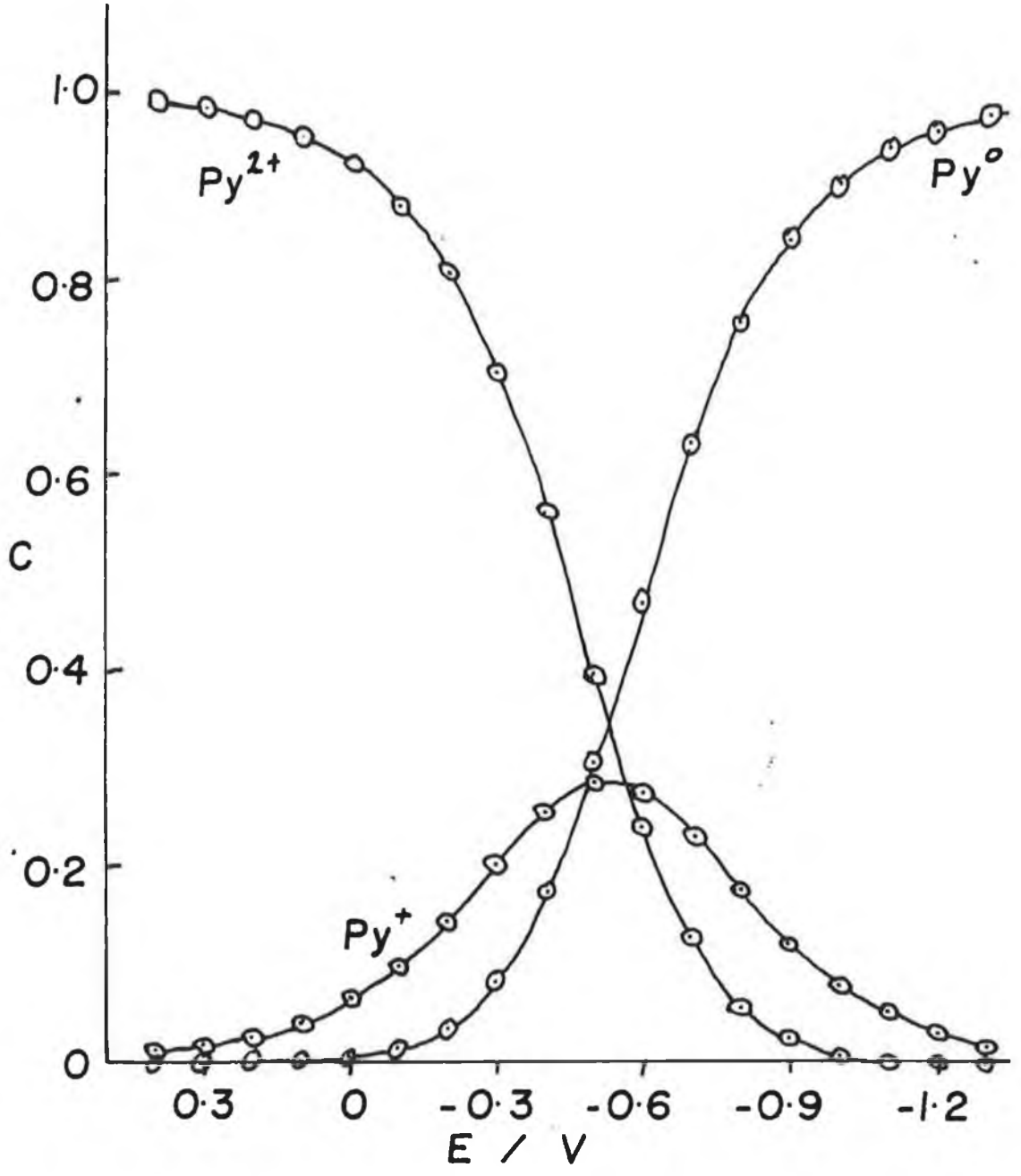

Figure 4.9 Concentration profiles of neutral pyrrole, P_y^o, slightly oxidised pyrrole, P_y^{+n2}, predicted from Eq. 4.1-4.3. The formal electrode potentials (E_1^o = -0.485V, E_2^o = -0.570V) and the n values ($n_1 = n_2 = 0.118$) were obtained for the $PPClO_4$ layer from the plots shown in Figure 4.7.

described by two monoelectronic transfers. The concentration profiles as a function of applied potential obtained for the PPDBS layer agree well with the appearance of current in cyclic voltammograms obtained for these layers. However there is a slight difference in formal potential, for both the $PPClO_4$ and PPDBS layers, obtained by absorption data and a normal cyclic voltammogram. This may be accounted for by the electrochemical system employed, with an ITO electrode being used as the working electrode.

To check the validity of the Monomer Unit Model, it was applied to absorption data obtained for the reduction of ferricyanide in aqueous solution. An aqueous solution of $K_3Fe(CN)_6$ was prepared, with KCl (0.1M) as background electrolyte, the solution was degassed and placed in the electrochemical cell. The ferricyanide solution was reduced from 0.6 volts to a negative potential, -1.4V, by scanning the potential at a slow scan speed, 0.5 mV/s. The absorbance of the ferricyanide at 420nm was monitored as a function of potential. The absorption data was analysed by the Nernst equation used in the Monomer Unit Model for the wavelength characteristic of the oxidised polymer.

Figure 4.10 shows the resulting Nernst absorption plot for the reduction of the ferricyanide. Again, it can be seen that there are deviations away from linearity, however a large linear region is obtained. The value of n and E^o obtained from the slope and intercept are 0.118 and -0.530 volts respectively. It can be seen that the number of electrons involved is only one tenth of the true value, the reduction of $Fe(CN)_6^{3-}$ being monoelectronic. Also the measured electrode potential is over 0.5 volt more negative than expected. The inaccuracy in the values obtained can be accounted for by the fact that when the spectrum of

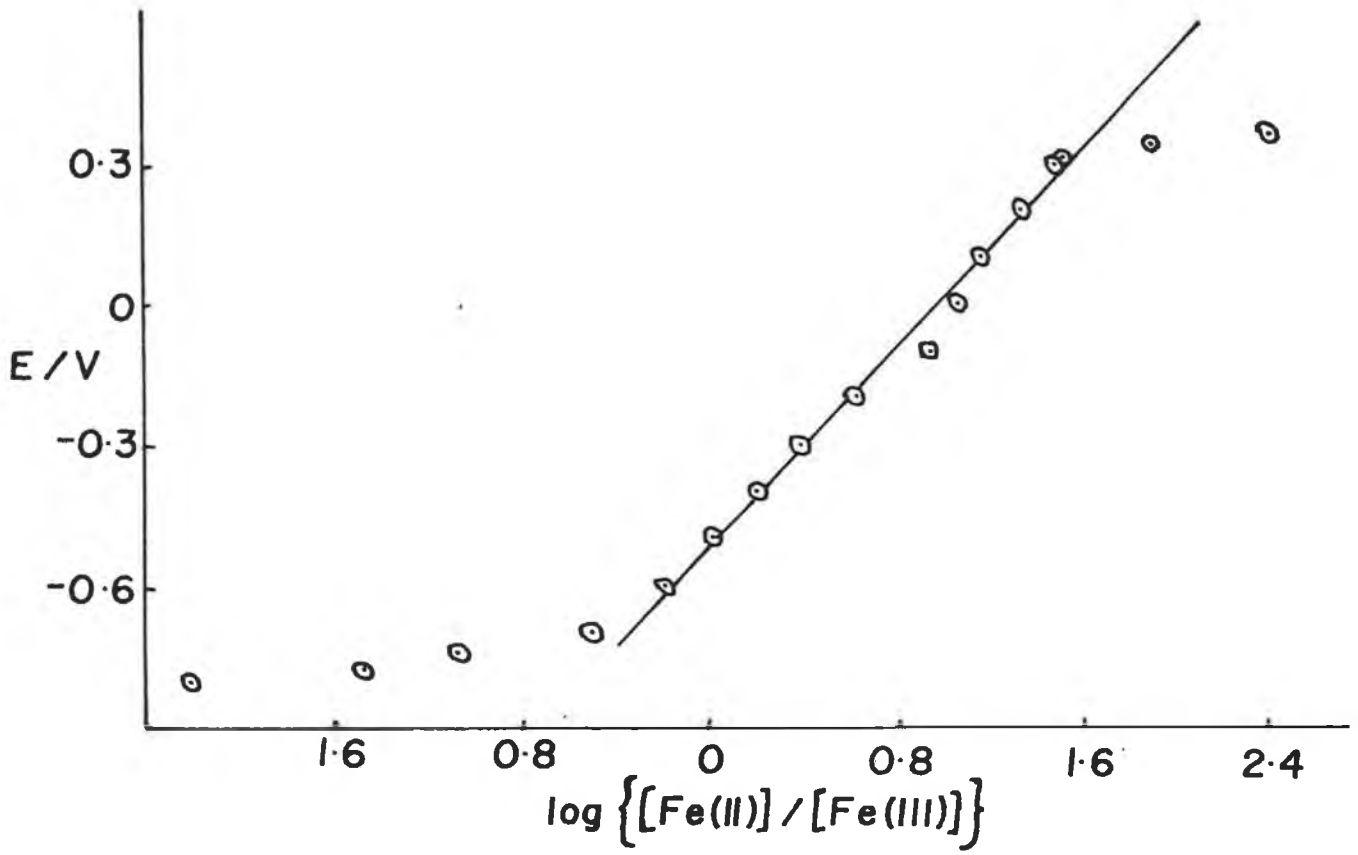

Figure 4.10 Nernst plot for the wavelength 420nm, for the reduction of $K_3Fe(CN)_6$ in 0.1M KCl.

solution at -1.4V was run, it was seen that a peak at 420nm, characteristic of ferricyanide in solution, was still observed. By taking the value of the absorbance initially and at -1.4V, it can be concluded that there is still 40% of the original ferricyanide present. The inaccuracy in the experiment is not therefore necessarily with the model employed for analysis, but more so with the spectroelectrochemical cell employed. The ITO electrode could possibly be not an ideal electrode material for the reduction of ferricyanide. A possible explanation for the inaccuracy in the n value is the thickness of the layer of solution at the electrode surface. It is important that the cell width is narrow and that the concentration of ferricyanide is as small as possible. Therefore by possibly using a cell of smaller dimensions with a fresh unused ITO electrode, of large area, could improve the absorption data for the reduction of the ferricyanide to ensure complete reduction. The reason why the formal potential is so negative may be because of resistance of the ITO.

It has already been mentioned, and seen, that the absorption Nernst plots for both layers, $PPClO_4$ and PPDBS, are not linear over the entire potential range. There are marked deviations away from linearity, as has been reported elsewhere [33]. Also it has been reported [44] that 'super Nernstian' slopes are obtained when the redox thermodynamics of three polythiophene polymers are studied by means of Nernst plots constructed from the in-situ absorbance measurements. To explain the slopes obtained, two reasons are put forward by the authors, that is, the effect of coulombic interactions between charged sites and the effect on the polymer lattice from the insertion of counterions. It was mentioned that doping of the polythiophenes is accompanied by an expansion of the polymer volume, due to insertion of counterions and also polymer swelling

due to solvent. This increase in polymer volume is said to affect the redox thermodynamics in two ways. It will cause distortions in the polymer chain and therefore affect the mean conjugation length. A change in the mean conjugation length can affect the concentration of charged species within the polymer. These charged species differ by the energy needed for their creation and also in the minimum conjugation length required by the charges. The charges in short chain phenylene-vinylene oligomers are stored as polarons due to the limited conjugation length [45].

The expansion of the polymer volume leads to a mechanical strain resulting in an additional contribution to the electrode potential. Marque et Rancali [44] used this as an explanation for the deviations observed in their Nernst plots for polythiophene. This mechanical work is the work required to achieve the expansion of the polymer lattice caused by the insertion of counterions and solvent molecules.

It was mentioned previously the voltages at which the polymer layers were deposited. These values are 0.5 volts higher than what would be required to form an identical polypyrrole layer on a platinum disc electrode. This is due to the poor adherence of the polymer films to the ITO electrode and also due to the difference in resistance along the length of the ITO electrode. The increase in resistance along the electrode accounts for all the polymer films forming first at the air/solution interface, with a large amount of charge having to be passed until the polymer films had grown over the ITO's surface. Therefore due to these reasons, it was found difficult to form homogeneous polymer films upon the ITO electrodes. One solution to these problems would be to use unused ITO electrodes with small surface areas.

In addition, between different absorption spectra experiments, each electrode had to be washed with distilled water and acetone. It was found that continual washing of the surface lead to a loss of conductivity of the ITO electrode.

Another application of the optical absorption measurements, is the calculation of the bandgap energy of the neutral polymer. This was undertaken previously for polypyrrole and p-polyphenylene films [34].

If parabolic energy bands are assumed, the absorption coefficient α is related to the photon energy by the equation below:

$$(\alpha h\nu)^{2/n} = B(h\nu - Eg) \qquad \ldots\ldots \quad (4.4)$$

where h is Plancks constant, ν is the photons frequency, B is a constant, Eg is the bandgap energy and n is a parameter that takes the value of 1 for direct transitions and 4 for indirect transitions.

Therefore if the relative absorption intensity multipied by $h\nu$ all raised to the power of 2 (direct) or ½ (indirect) is plotted versus $h\nu$, for the low energy rise in the absorption band at 400 nm for the reduced polymer, an estimate of the bandgap energy can be obtained.

Figure 4.11 shows the resulting plot for a polypyrrole dodecylbenzenesulphonate layer, taking n to be equal to 1. It can be seen that the plot is linear with a value for the bandgap energy of 2.5eV. This value was lower than that obtained by Blackwood [44] (2.7eV). Possible explanations could be the change in anion

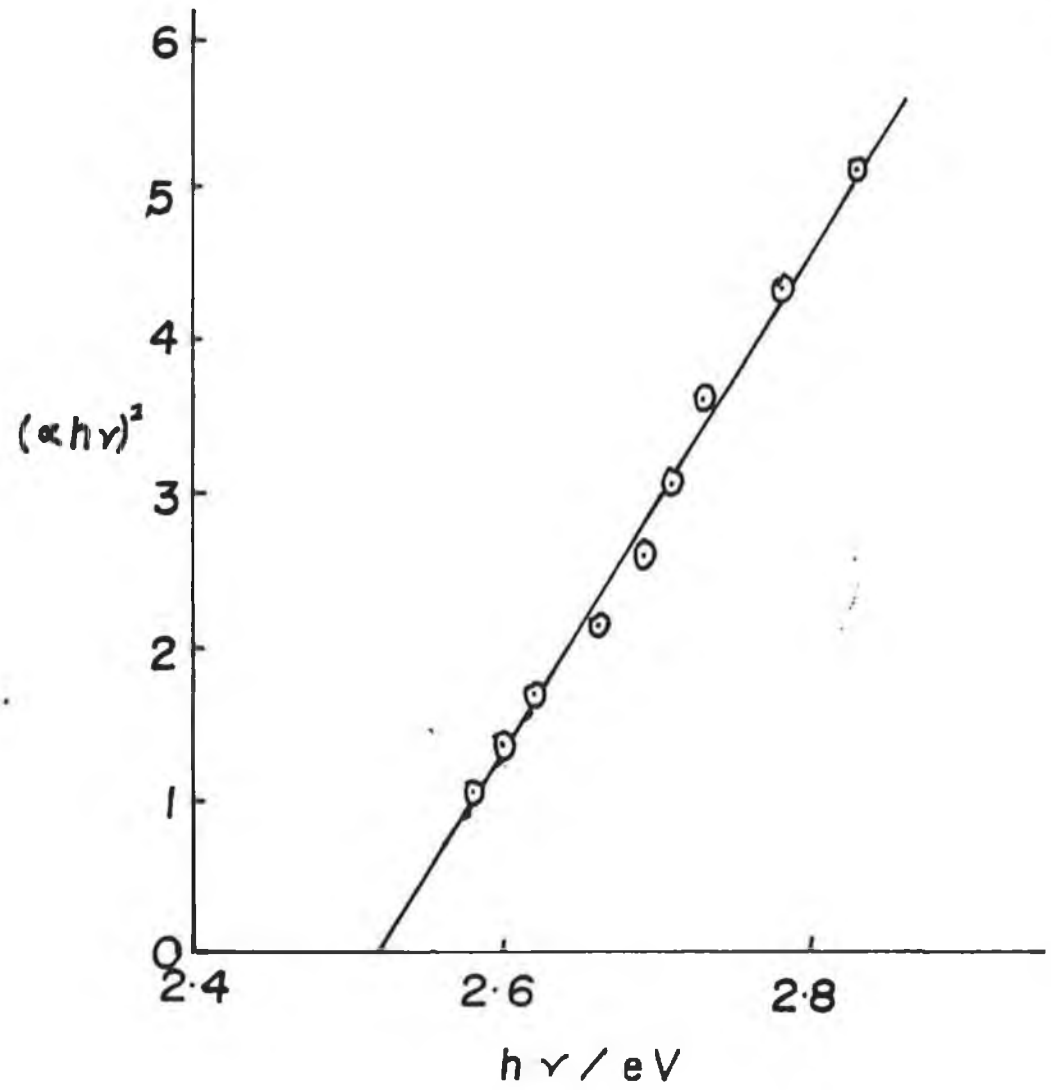

Figure 4.11 Evaluation of E_g for the reduced form of PPDBS, shown in Figure 4.2 (b).

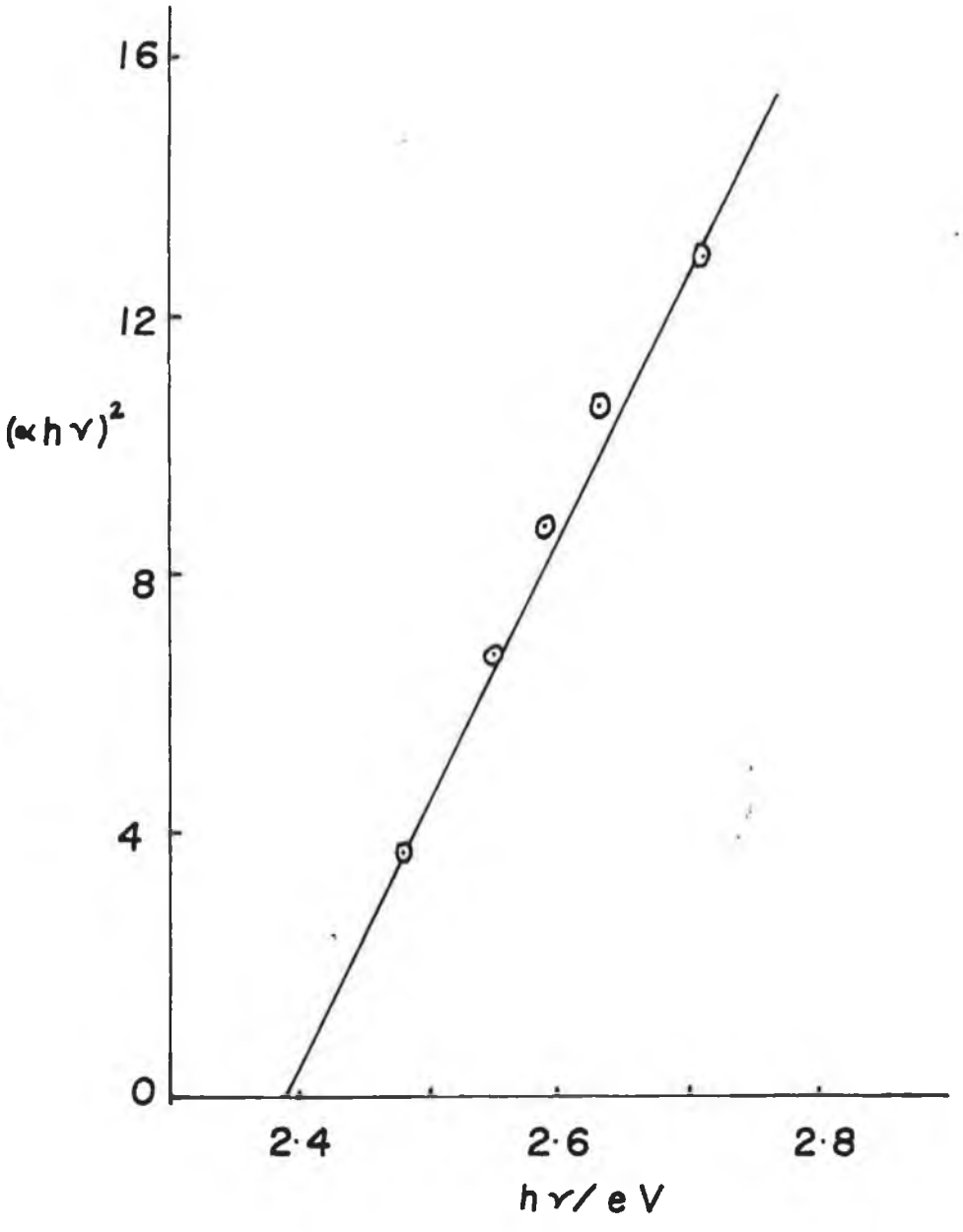

Figure 4.12 Evaluation of E_g for the reduced form of $PPClO_4$, shown in Figure 4.5 (b).

employed as the dopant within the polymer film, also another explanation could be that the band observed at ≅ 540nm could contribute to the low energy end of the band at 400nm.

Figure 4.12 shows the resulting plot for a polypyrrole perchlorate layer, the plot is linear with a bandgap energy value of 2.39eV being calculated from the intercept. It can be seen that the dopant anion will have an effect upon the bandgap energy of the neutral polymer.

4.2.4 CONCLUSION

The redox thermodynamics of several polypyrrole layers have been analysed by using Nernst plots determined from absorption spectra of the polymer films. The Monomer Unit Model is used to analyse the results, and electrochemical parameters, n and E^{o1}, have been established for the layers. From this concentration profiles for the three species, neutral pyrrole monomers, polarons and bipolarons have been calculated and they agree well with previous results. Two reasons are given for the deviations away from linearity of the Nernst absorption plots. The first being the coulombic interactions between charged sites and the second being the mechanical work required to achieve the expansion of the polymer lattice caused by the insertion of counterions and solvent molecules. It also must be realised that three assumptions are made in order that Nernst plots can be calculated. These assumptions being that overlapping in the spectra is ignored, two equilibrium reactions occur, and finally that there are only three species exist in the polymer film at one given potential.

It was also seen that it was possible to calculate the bandgap energy of neutral polypyrrole films by means of a very simple technique.

Finally it should be noted that there are several experimental problems associated with the spectroelectrochemical technique, and that improvement in these factors could yield more accurate information.

4.3 CHARACTERISATION OF THE REACTION BETWEEN PYRROLE AND TETRACYANOETHYLENE

4.3.1 EXPERIMENTAL

All reagents employed were reagent grade. Tetracyanoethylene (TCNE) was used as received and it was stored below 10°C. Pyrrole was distilled and stored, in the dark, under nitrogen, at below 10°C.

For the calculation of the molar extinction coefficient and equilibrium constant for the π complex, a stock solution of tetracyanoethylene (2×10^{-4}M) was prepared in dichloromethane. A high molar mass of pyrrole was added to an aliquot of TCNE solution so that two phases with a purple interface were formed. The time of mixing of the two phases was taken as the zero time. The purple reaction mixture was transferred rapidly to a stoppered quartz absorption cell in the chamber of a double beam spectrometer (Shimadzu UV-160; ±4nm).

For the reference cell a quartz cell with dichloromethane was employed. The decrease in absorbance at 518nm was measured as a function of time. This procedure was repeated for various concentrations of pyrrole.

Electrochemical experiments were performed in a single compartment three electrode cell. A carbon rod was used as the auxiliary, a Pt disk as the working and a S.C.E. as the reference electrode. All solutions employed in the electrochemical experiments were degassed with oxygen free nitrogen for approximately 10 minutes. A ramp generator (H.B. Thompson 16 bit), a potentiostat (Edt ECP 100) and an electronic integrator (Sycopel DP301S) linked to a J.J. Lloyd X-Y Chart Recorder, were used.

The infrared spectra were recorded on a Perkin Elmer 1710 Fourier Transform Infrared Spectrophotometer with the Perkin Elmer PP-1 printer accessory.

4.3.2 RESULTS AND DISCUSSION

One aim of this work with conductive polymers is to examine the formation of a polypyrrole layer in the presence of various anions. A good electron accepting species is tetracyanoethylene (TCNE). Polypyrrole has previously been deposited from a mixture of pyrrole (0.1M), perchlorate (0.1M) and tetracyano-p-quinodimethane, TCNQ, (0.01M) [34]. The states of polymerisation and doped anions within a polypyrrole structure and the interaction between the polymer backbone and the dopants, were recently analysed by FTIR reflection absorption spectroscopy for a PP(TCNQ) (BF_4) polymer [46].

In this work it was found that a polypyrrole layer could be deposited from a solution of pyrrole (0.1M) and TCNE (0.01M) in acetonitrile. This implied that TCNE existed as the anion within the layer, this result was curious, as TCNE exists as a neutral species.

These observations can be explained by the fact that TCNE and pyrrole possibly form a charge transfer complex, PP^{+} $TCNE^{-}$, in solution. Both spectroscopic and electrochemical evidence has been obtained to support the formation of PP^{+} $TCNE^{-}$ complex.

Upon initial mixing of a solution of pyrrole and TCNE in acetonitrile a λ_{max} of 518nm is observed along with the appearance of an immediate purple colour.

It was found that this π complex with a λ_{max} of 518nm, begins to decompose with a shift in λ_{max} from 518nm to 417nm, with an associated colour change (purple to yellow).

There is no doubt that the 'purple complex' which is formed in the first step is a 1:1 π complex derived from pyrrole and TCNE. This assumption is in accord with its rapid formation, characteristic of other π complexes [37] and with the well known ability of TCNE to form π complexes with amines [35].

The stability of the π complex was found to be solvent dependent, with the solvents dichloromethane and chloroform stabilising the π complex, for several weeks even months, where the initial purple colour of the π complex was still present.

Whilst other solvents, such as, acetonitrile and acetone, promote the decomposition of the π complex. This affect of solvent has been found before [35] for the π complexes of aromatic amines and TCNE.

Previously Rappoport [37] evaluated the molar extinction coefficient and equilibrium constant for their π complex between TCNE and dimethylaniline. The same method was employed for the evaluation of the latter 2 parameters of the π complex between TCNE and pyrrole. The following equation was employed for the evaluation of the extinction coefficient and equilibrium constant

$$\frac{[TCNE].L}{Abs} = \frac{1}{K\varepsilon[Pyrrole]} + \frac{1}{\varepsilon} \quad \ldots\ldots \quad 4.5$$

where Abs is the absorbance of π complex at 518nm, L is the path length (1cm), ε is the molar extinction coefficient and K is the equilibrium constant. Pyrrole was kept in excess and a stock solution of TCNE of known concentration ($2x10^{-4}$M) was prepared, as previously described in the experimental section.

Figure 4.13 shows the plot of the dependence of the reciprocal of the pyrrole concentrations on $\frac{[TCNE]}{Abs}$ for the 1:1 π complex. The value of ε is obtained in reciprocal form as an intercept, and therefore the above method doesn't yield results of great accuracy.

However the value of the molar extinction coefficient and the equilibrium constant, obtained from the plot, are 2,500± 1500 $dm^3mol^{-1}cm^{-1}$ and 2.77± 0.2

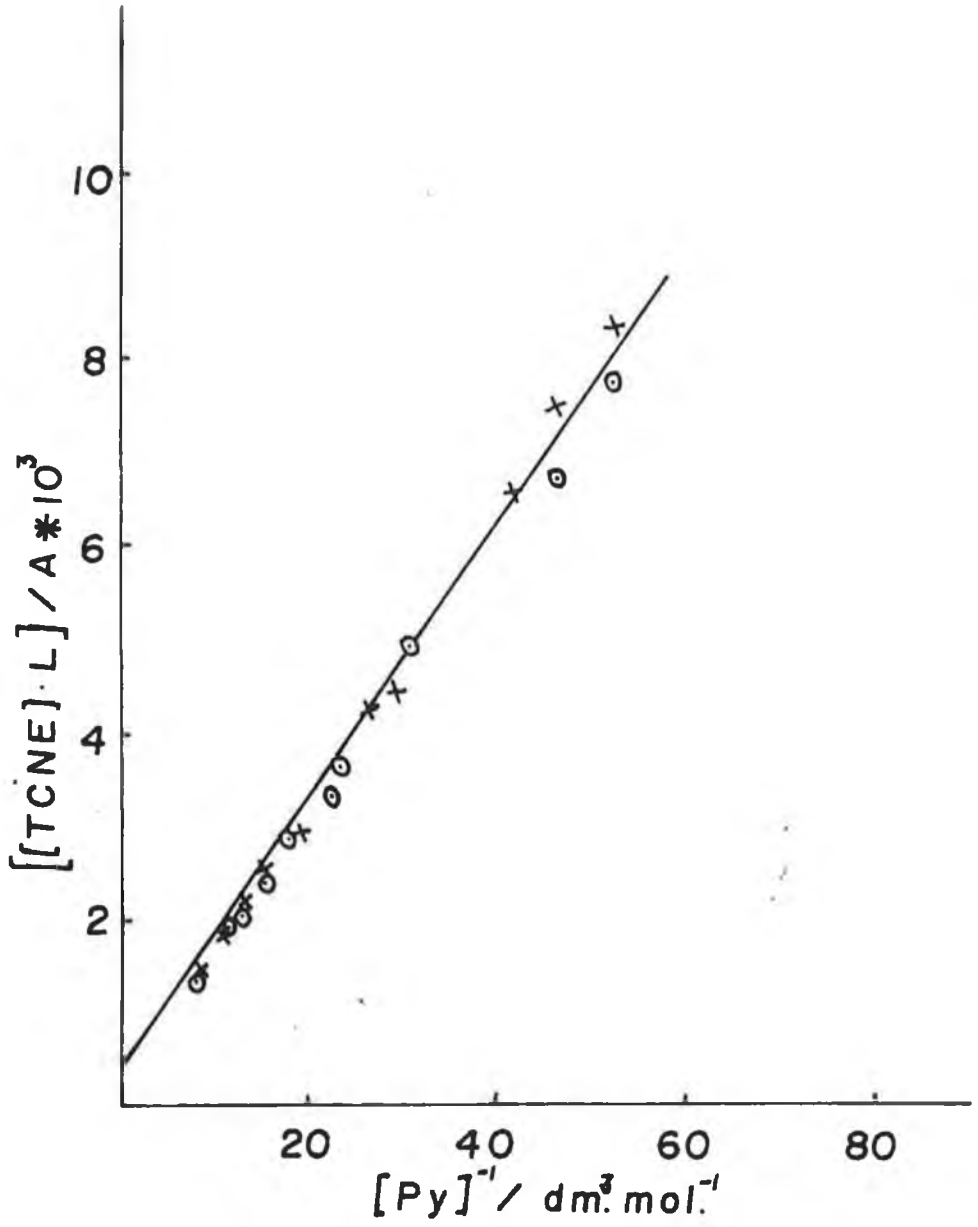

Figure 4.13 Plot of the dependence of the reciprocal of the pyrrole concentrations on [TCNE]/Abs for the 1:1 π complex.

dm^3mol^{-1} respectively. These values agree well with previous results obtained for the π complexes of amines with TCNE [35].

It was also noted that the decomposition of the π complex was dependent upon the pyrrole concentration. When the pyrrole is in excess (>500[TCNE]) then the decomposition occurs rapidly irrespective of solvent.

This decomposition of the π complex to a final product has also been observed for the complex formed between TCNE and dimethylaniline [37]. Also it has been reported [35] that the reaction between aniline and TCNE yields a tricyanovinylaniline product, with a λ_{max} of 350nm. It was also reported by the author that TCNE was present, as suggested by electron spin resonance experiments, the spectrum of TCNE is observed in the spectrum of the final product.

This may apply to the reaction between pyrrole and TCNE, with the $TCNE^-$ being present. The fact that a polypyrrole layer could be formed from a solution of pyrrole and TCNE in acetonitrile after complete reaction indicates strongly that the anion of TCNE is present. This electrochemical evidence will be discussed later.

The UV-vis spectra of the neutral TCNE molecule, $TCNE^-$ and $TCNE^{2-}$ have been reported previously [51]. $TCNE^-$ has a λ_{max} of around 415nm, with various vibrational components evident. Therefore possibly the λ_{max} observed

for the final product, from reaction of pyrrole and TCNE, at ≅415nm could indicate the presence of the mono anion of TCNE.

Figure 4.14 shows the infra-red transmission spectrum of freshly distilled pyrrole. According to the investigation of the IR spectrum of the pyrrole monomer [47], the pyrrole monomer has $C_{2\upsilon}$ symmetry which yields 24 normal vibrational modes, υ_1-υ_{26}. These correspond to NH stretching, out-of-plane, and in-plane deformation vibrations, CH in plane and out of plane modes and also ring stretching modes.

From Figure 4.14 there are several bands of importance, these are listed below:

(i) 3402cm^{-1} NH stretching mode.

(ii) 3130cm^{-1} and 3103cm^{-1} are CH stretching modes.

(iii) The peaks at 1015cm^{-1}, 1048cm^{-1} and 1076cm^{-1} can be assigned to the assymmetric CH in-plane mode, $\upsilon_{11}(B_1)$, the CH out-of-plane mode, $\upsilon_{24}(B_2)$, and the symmetric CH in-plane mode, $\upsilon_2(A_1)$, respectively. However the peak at 1048cm^{-1} is mixed with the CH in-plane deformation mode, $\upsilon_{12}(B_1)$.

(iv) 4 ring stretching modes, namely the assymmetric mode $\upsilon_{14}(B_1)$ 1418cm^{-1}, the symmetric mode $\upsilon_6(A_1)$ 1469cm^{-1}, symmetric $\upsilon_5(A_1)$ 1380cm^{-1}and the assymmetric $\upsilon_{15}(B_1)$ at 1530cm^{-1}.

(v) NH in-plane mode, $\upsilon_{13}(B_1)$ at 1143cm^{-1}.

(vi) The broad band at 736cm^{-1} is characteristic of an unsubstituted pyrrole ring.

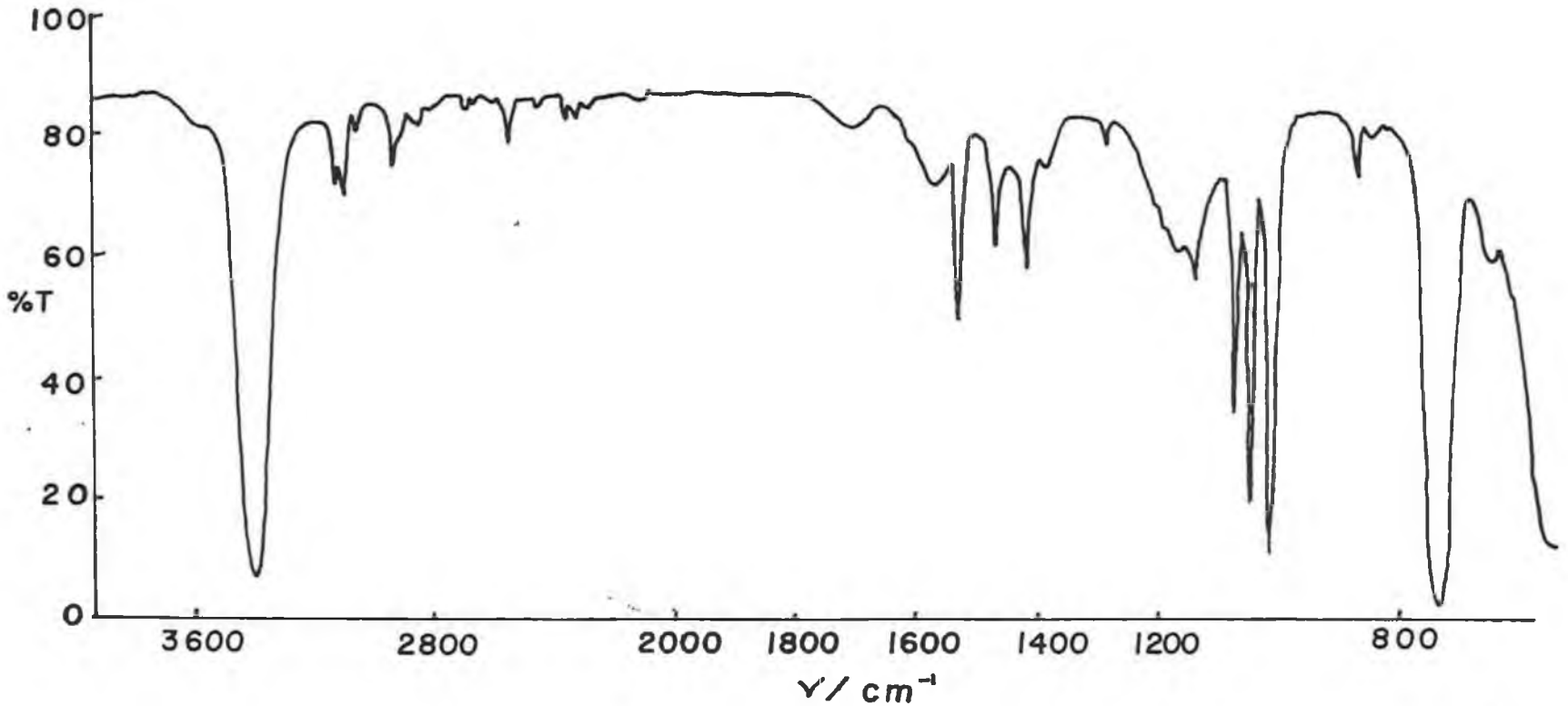

Figure 4.14 Infra-red transmission spectrum of freshly distilled pyrrole monomer.

All these bands, their position and intensity relationships, agree well with other reports for the pyrrole monomer [46,48].

Figure 4.15 shows the KBr transmission spectrum of a polypyrrole perchlorate layer. The $PPClO_4$ layer was formed on a Pt electrode at 0.800V vs. SCE from an aqueous solution of pyrrole (0.1M) and $LiClO_4$(0.1M). The layer was washed thoroughly with deionised water, removed from the electrode and left to dry overnight.

Several features of the spectrum are of importance:

(i) a sharp band at $1111cm^{-1}$ is close to the reported [46] vibrational mode of the ClO_4^- anion ($1100cm^{-1}$),

(ii) the absence of the assymmetric CH in plane mode $\upsilon_{11}(B_1)$ at $1015cm^{-1}$. This occurs due to suppression of this band by the α-α linkage upon polymerisation.

(iii) broad NH stretching band at $3428cm^{-1}$.

(iv) the sharp peak at $794.0cm^{-1}$ can be assigned to the broad band at $736cm^{-1}$in the monomer spectrum, characteristic of the unsubstituted pyrrole ring.

(v) the 4 ring stretching modes are significantly weakened. This has been reported previously for a polypyrrole layer [48] where it was reported that the ring stretching modes are supressed by the α-α conjugated polymer.

(vi) $1090cm^{-1}$ band of the symmetric CH in-plane mode is clearly observed. This situation has also been reported [48] fo the KBr transmission spectrum of a polypyrrole film.

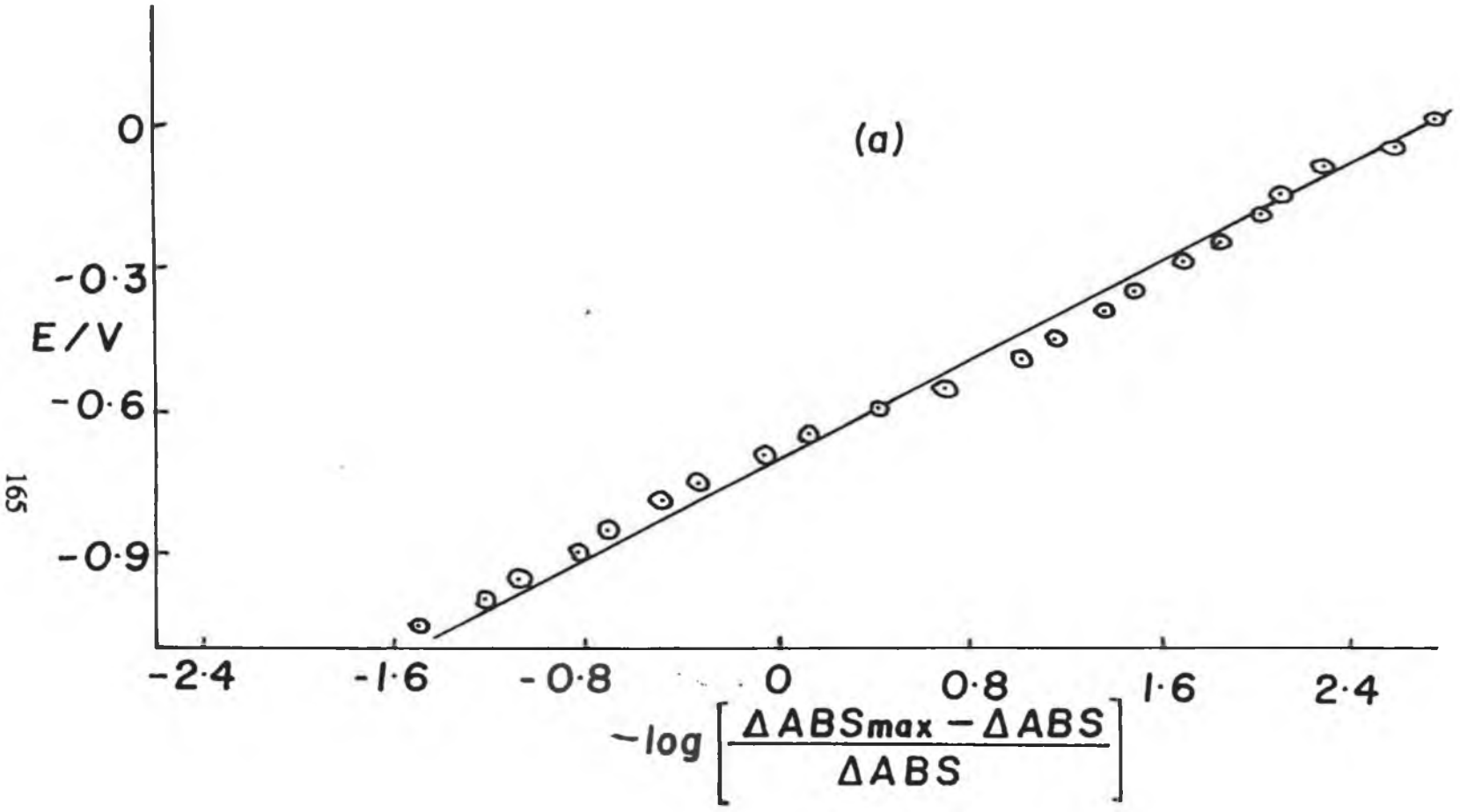

Figure 4.4 Nernst plots for the absorbance data shown in Figure 4.3, (a) 830nm and (b) at 450nm.

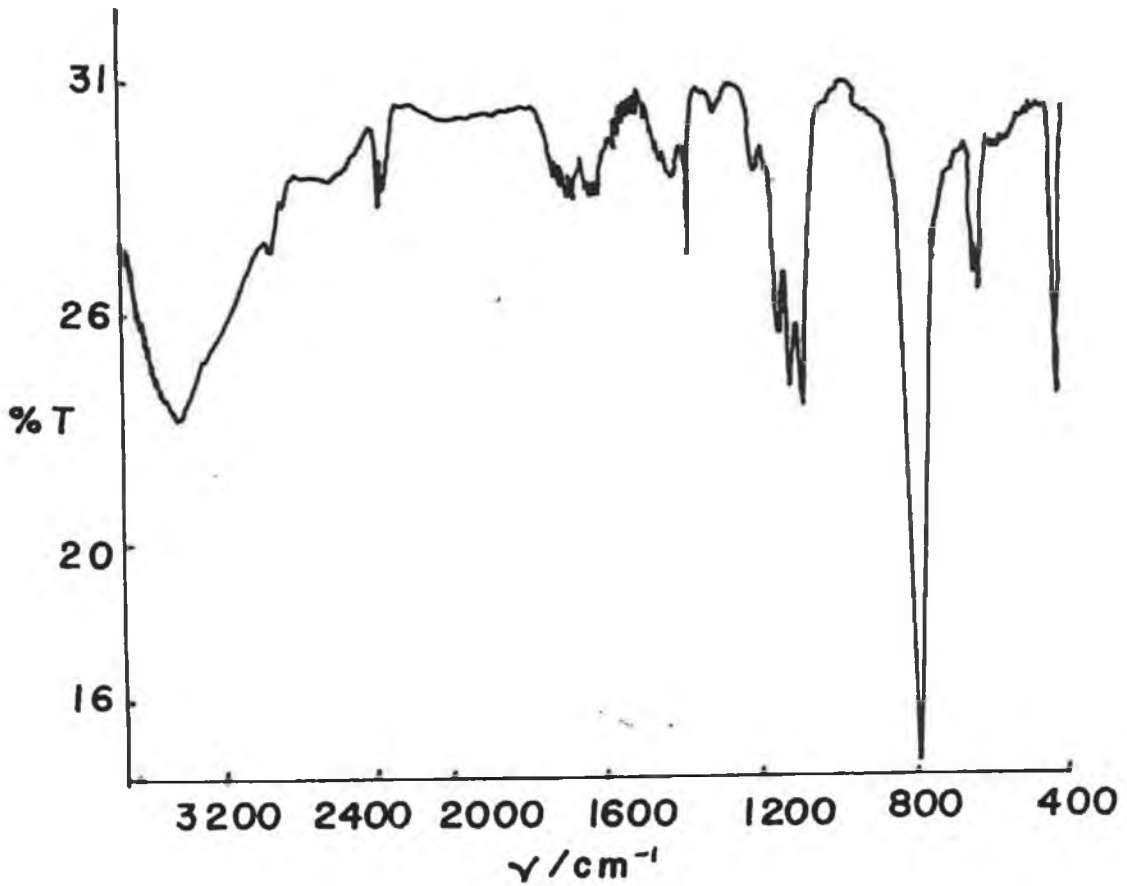

Figure 4.15 KBr IR transmission spectrum of a polypyrrole perchlorate, $PPClO_4$, layer. The layer being previously formed on a Pt electrode at 0.8V from an aqueous solution of pyrrole (0.1M) and $LiClO_4$ (0.1M).

(vii) Two weak bands at 2924cm^{-1} and 2860cm^{-1} are possibly the CH stretching modes at 3130cm^{-1} and 3103cm^{-1}.

(viii) There are 2 bands at 1146cm^{-1} and 1120cm^{-1} which could possibly be the CH in-plane and out-of-planes modes.

It can be concluded that upon polymerisation, only some of the pyrrole monomer modes are conserved in some degree in the polymer spectrum.

TCNE is planar and belongs to the D_{2h} point group. The infra-red transmission spectrum for neutral TCNE, $TCNE^{-}$ and $TCNE^{2-}$ in both the solid state and in solution have received much attention [49,50] with the interaction of the background electrolyte being investigated and also the strong ion pairing of the $TCNE^{2-}$ species with alkali metal cations.

It was hoped that the analysis of the polypyrrole tetracyanoethylene film, by infra-red techniques, could provide some useful information with regard to the state of the TCNE present within the film.

Figure 4.16(a) and 4.16(b) show the KBr and Nujol Mull, respectively, of the neutral TCNE molecule in the nitrile stretching region.

The KBr spectrum shows 3 main bands, all differing in intensity, corresponding to the C≡N stretch of the TCNE molecule.

These are the 2261cm^{-1} (υ_q B_{1v}), 2227cm^{-1} and 2215cm^{-1} bands. These bands have previously been reported for the KBr of neutral TCNE [50]. The nujol

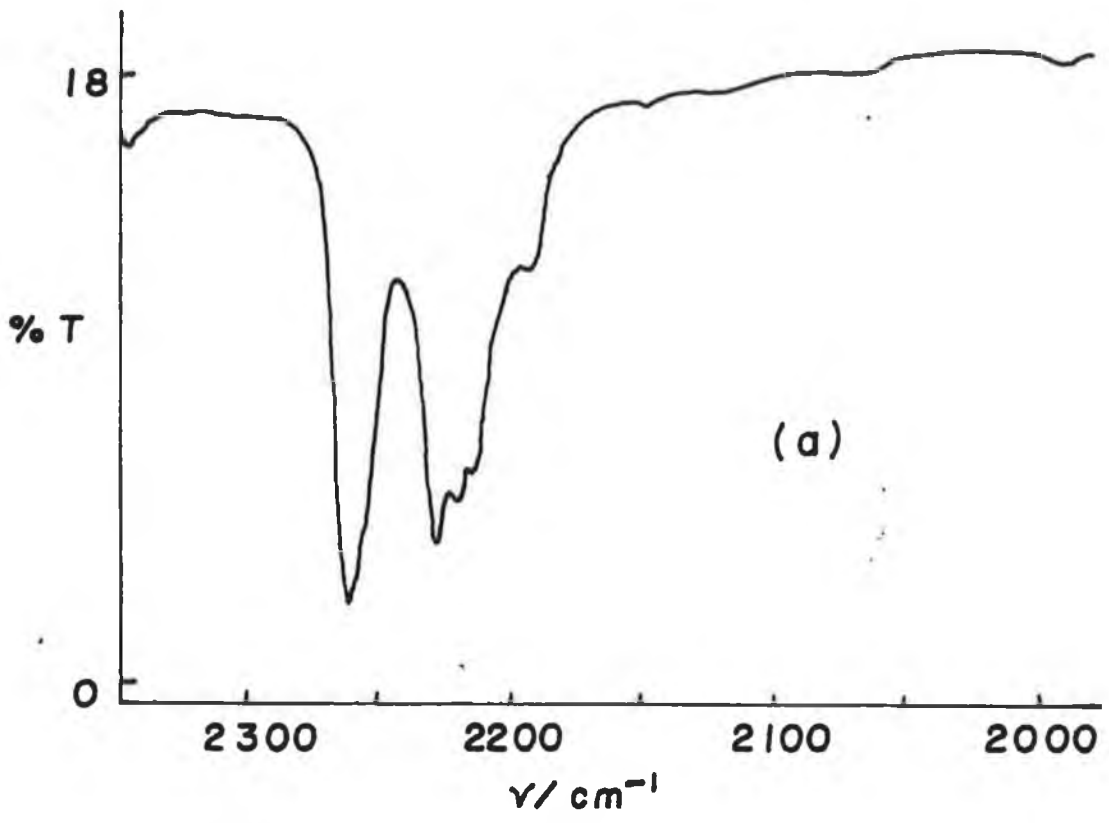

Figure 4.16 Depicts the

(a) KBr IR transmission spectrum of TCNE crystals.

(b) Nujol Mull IR transmission spectrum of TCNE crystals.

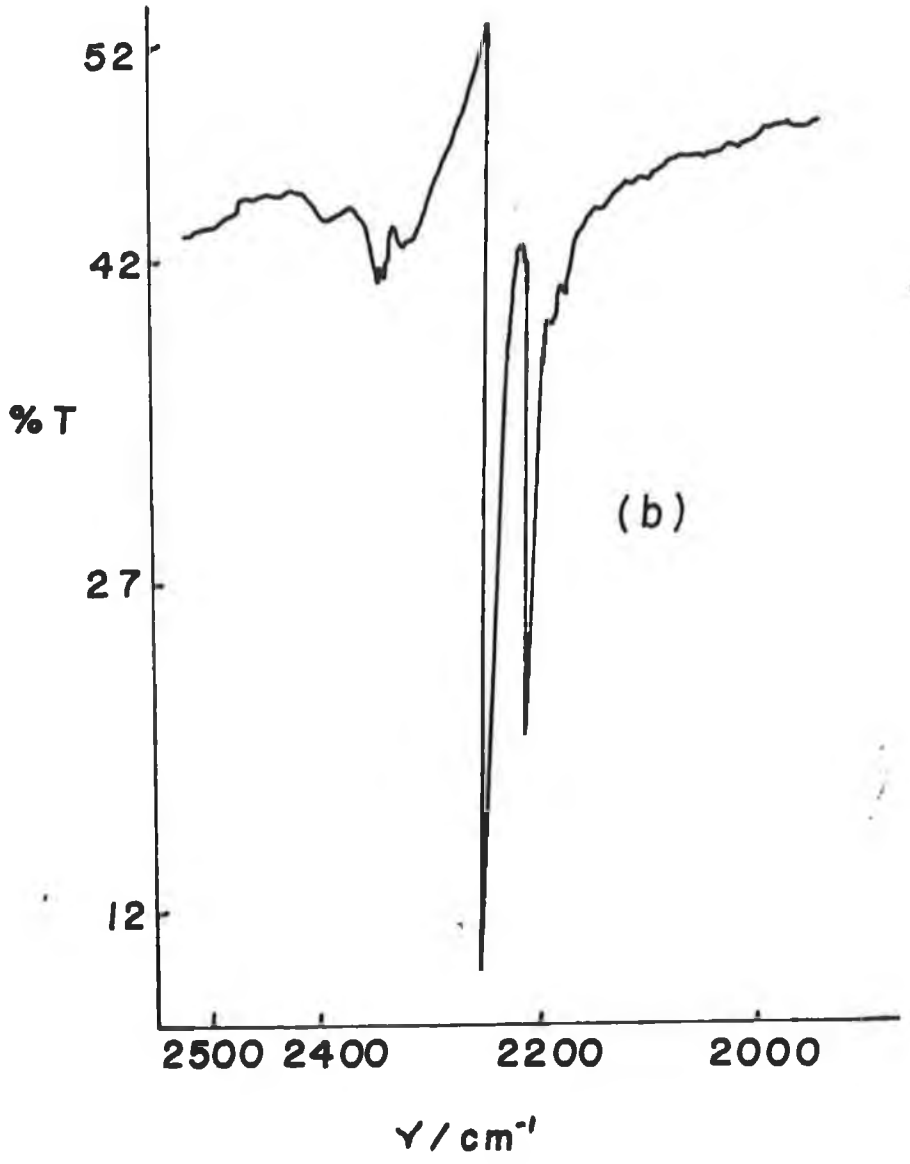
52
42
27
12
%T
(b)
2500 2400
2200
2000
ν / cm⁻¹

mull within this region shows 3 bands, at 2258cm^{-1}, 2220cm^{-1} and 2203cm^{-1}. The broad nature of the 2220cm^{-1} band, possibly indicates that it could contain the 2230 (υ_{15} $B_{2\upsilon}$ C≡N) and the 2215cm^{-1} band, reported previously for neutral TCNE [50].

A polypyrrole tetracyanoethylene layer was formed on a platinum electrode, at 1.0V, from a solution of pyrrole (0.28M) and TCNE (0.06M), when the reaction had gone to completion. The layer was then washed with CH_2Cl_2 and then allowed to dry overnight, this was to ensure that all the solvent had evaporated.

Figure 4.17(a) shows the resulting KBr transmission spectrum of the polymer. It should be noted that a broad band centred around 3446cm^{-1} is observed this corresponding to the N-H stretch. This result can be contrasted to a spectrum of a PP(TCNQ)BF_4 polymer [46] where no definite N-H stretch occured and that due to the appearance of a band at 2140cm^{-1}, it was suggested that TCNQ interacts with the chemically active nitrogen sites of the polypyrrole creating a -N=C=N- bond.

Figure 4.17(b) shows the spectrum of the PP(TCNE) layer in the nitrile stretch region. A broad band at 2226cm^{-1} and a band at 2170cm^{-1} are observed.

Bands at 2185cm^{-1}, 1420cm^{-1}, 1185cm^{-1} and 523cm^{-1} have been seen for the bulk solution anion radical of TCNE. Within the spectrum observed in Figure 4.17(a) none of these bands are observed, however the band at 2225cm^{-1} has been observed for the anion in solution [50]. It is difficult to assign this band at 2226cm^{-1} to the TCNE anion as bands at 2230cm^{-1} and 2215cm^{-1} have been

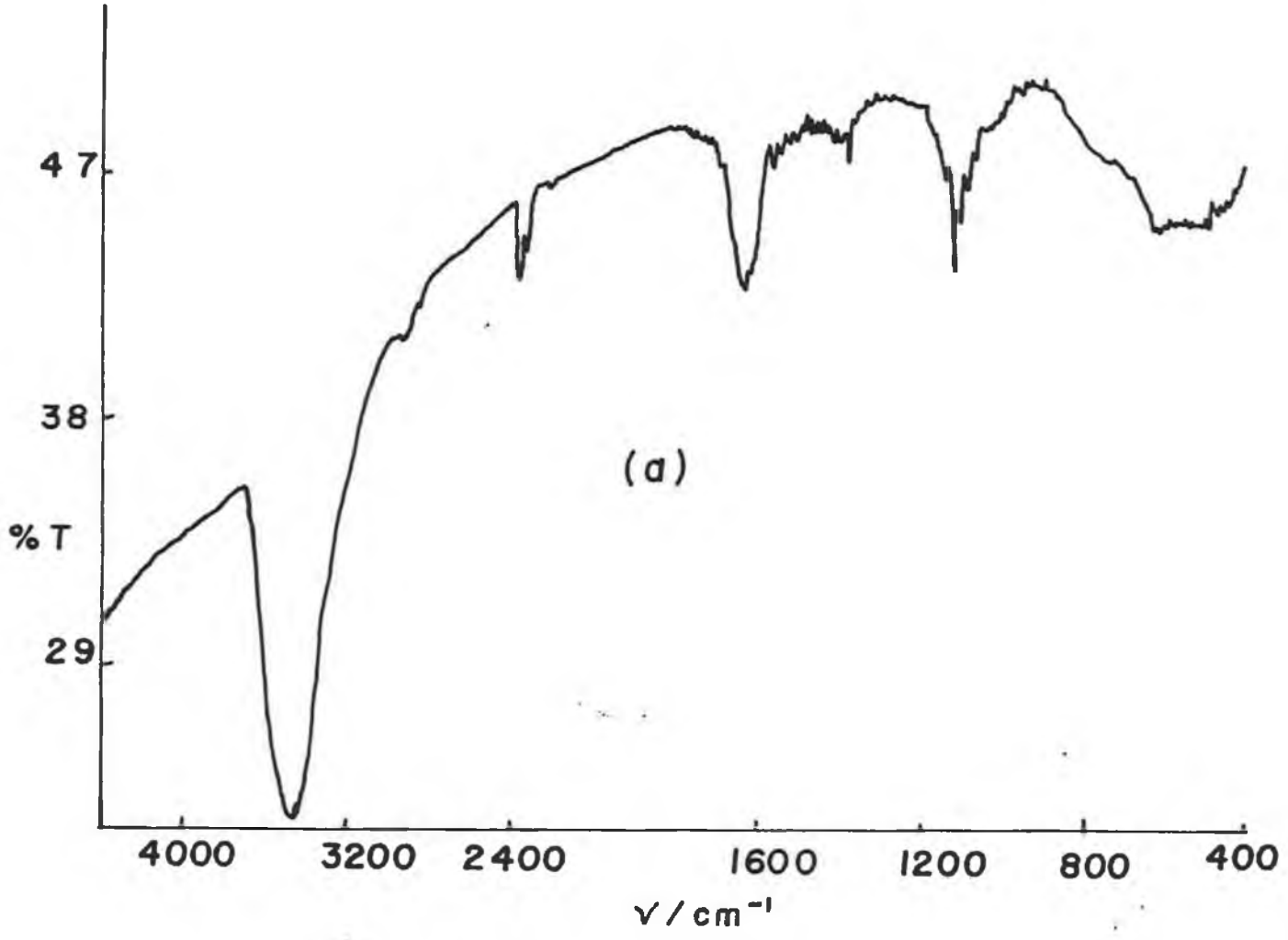

Figure 4.17 (a) KBr IR transmission spectrum of a PPTCNE polymer. The polymer being previously formed on a Pt electrode at 1.0V from a solution of pyrrole (0.28M) and TCNE (0.06M).

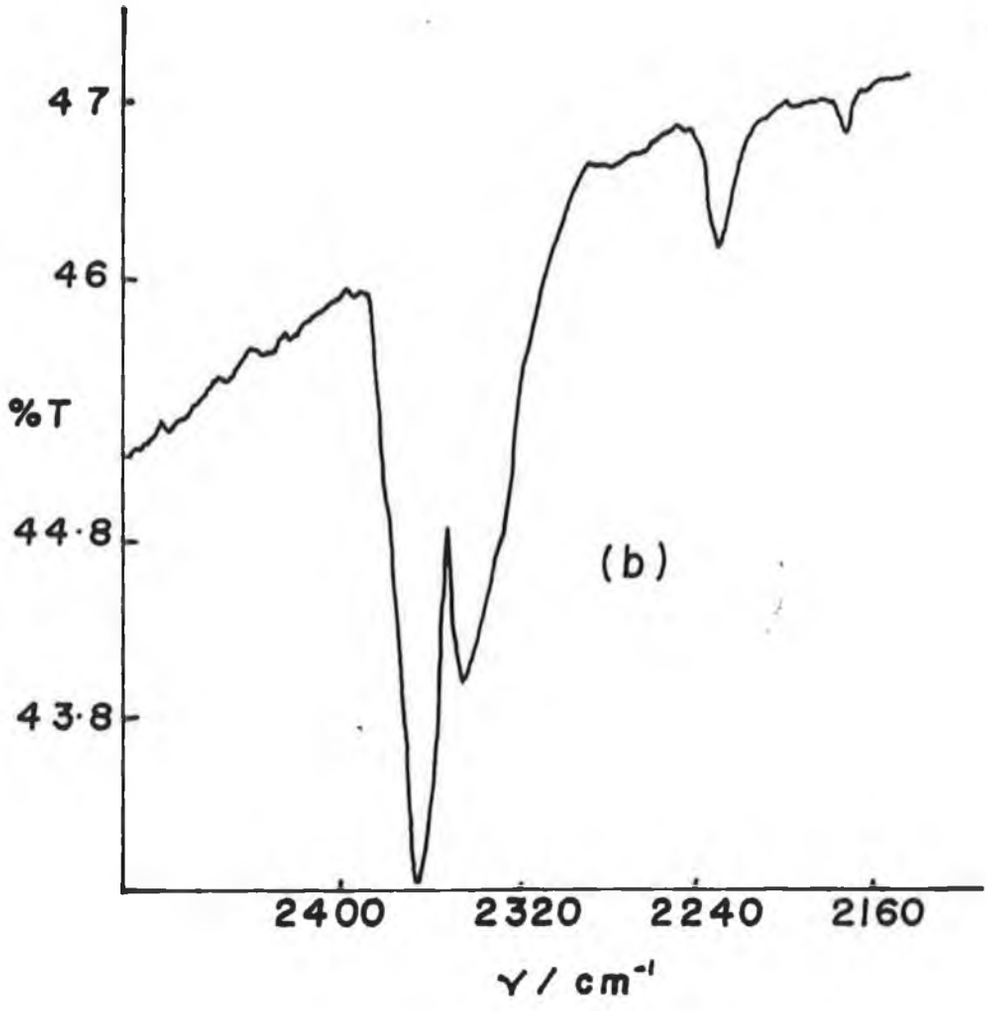

Figure 4.17 (b) Spectrum of PPTCNE layer in nitrile stretch region.

previously [51] reported for neutral TCNE in solution. It is likely that this band is due to neutral TCNE within the layer, as it can be seen in the KBr spectrum of neutral TCNE a band at 2227.7cm^{-1} is observed.

The broad band at 2170cm^{-1} observed is close to the reported band of TCNE in solution (2185cm^{-1}) [50]. However it is seen that none of the other bands are observed associated with the anion. Also redshifting of the C≡N and C=C stretch bands to 2204cm^{-1} and 1512cm^{-1} have previously been reported [50]. Therefore the 2170cm^{-1} could represent a C≡N stretch shifted to lower wavenumber due to electrons being added to the TCNE molecule. The reason for this shift is that the lowest unoccupied molecular orbitals are antibonding with respect to the C≡N bond.

Therefore it can be concluded that no definite evidence exists from the IR transmission spectrum that the TCNE anion is present within the layer. However one conclusion can be drawn, in that, a form of TCNE is present due to the prominent band at 2226.0cm^{-1}. If it were neutral TCNE, it should be washed out of the layer ; perhaps soxhlet extraction could be done.

Analysis of the polymer spectrum again illustrates that most of the bonds associated with the pyrrole monomer have been suppressed, as seen earlier. However the peaks observed for the CH -in-plane and out-of-plane modes in $PPClO_4$, have increased in number. These appear in the PPTCNE layer at 1048cm^{-1}, 1088cm^{-1}, 1109cm^{-1}, 1122cm^{-1} and 1144cm^{-1}. A similar situation has been reported previously for the $PP(TCNQ)(BF_4)$ layer [46].

Suppression of the ring stretching modes is also evidenced, as seen in the $PPClO_4$ layer. An interesting point is that the bond at 794.0cm^{-1} in $PPClO_4$, which was associated with the band at 736cm^{-1}, for the unsubstituted pyrrole ring, is not present in the PPTCNE polymer, perhaps this is an indication of different chain lengths.

A PP^+TCNE^- layer was prepared from an acetonitrile solution of pyrrole (0.28M) and TCNE (0.074M), onto a platinum electrode at 1.0V. The reflectance infra-red of that layer gave rise to a broad band at 2086cm^{-1}. This band has previously been assigned to be due to the υ_1(Ag) C≡N symmetric stretch for flatly adsorbed $TCNE^-$ on Pt electrodes using polarised IR radiation [50].

Figure 4.18(a) shows the cyclic voltammogram of a solution of TCNE (0.01M) and $LiClO_4$ (0.1M) in acetonitrile. Two reduction peaks at -0.64V vs. SCE and -1.10V vs. SCE are seen. These have been reported [49] to be due to the creation of the anion $TCNE^-$ and of the dianion $TCNE^{2-}$, respectively. Only one definite reoxidation wave is observed at -0.550 volts. This corresponds to the reoxidation of the anion to neutral TCNE. There is a slight shoulder at -0.990 volts, this corresponding to the oxidation of the dianion to the anion. The solution was seen to go from colourless, neutral TCNE, to yellow, indicating the creation of both the anion and dianion.

The sign of no definite reoxidation wave of the dianion to the TCNE anion, can be explained by the fact that $TCNE^{2-}$ has been reported [49] to form strongly bond contact ion pairs with alkali metal cations in acetonitrile solution.

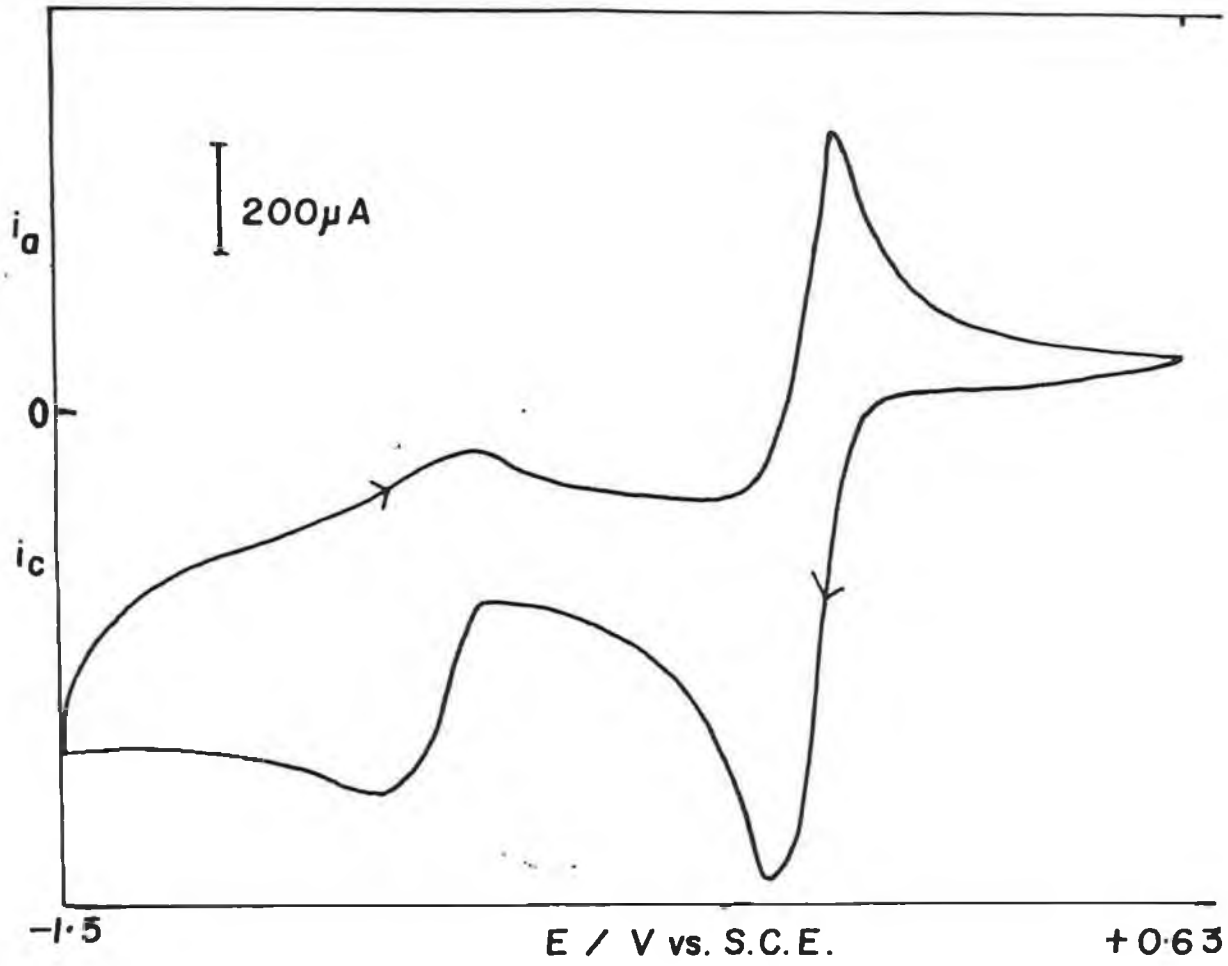

Figure 4.18 (a) Cyclic voltammogram of a degassed solution of TCNE (0.01M), $LiClO_4$ (0.1M) in acetonitrile (ACN).
Scan Rate = 100mV/s.

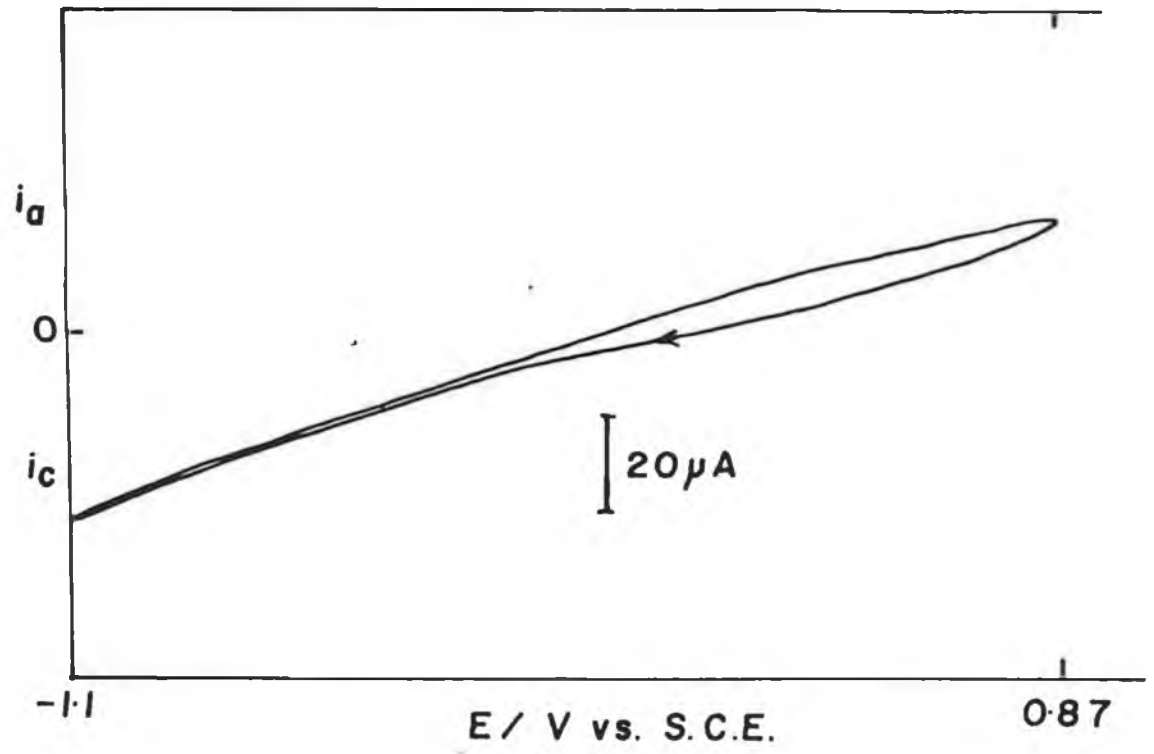

Figure 4.18 (b) Cyclic voltammogram of a solution of pyrrole (0.1M) and TCNE (0.01M) in ACN 48 hours after mixing.
Scan Rate = 100mV/s.

Figure 4.18(b) shows the cyclic voltammogram of a solution of pyrrole (0.1M), and TCNE (0.01M), in acetonitrile 48 hours after mixing. As can be seen the electrochemistry of the TCNE species shown in Figure 4.18(a) is not observed. This supports the theory that TCNE and pyrrole form a stable complex.

Figure 4.19 shows the resulting cyclic voltammogram of a solution of pyrrole (0.06M) and TCNE (0.05M) in acetonitrile solution, 4 minutes after mixing. The potential was scanned between 0.3V and 1.0V, with a resulting anodic current flow, a crossover is also observed on the first scan indicating nucleation. The solution was purple in colour characteristic of the π complex, and after approximately 10 cycles a black ring was seen to form around the outside of the Pt disc electrode. This indicating that a polypyrrole layer doped with TCNE was forming at the electrode surface.

It was also noted that a PP^+ $TCNE^-$ layer could be formed on a Pt electrode after 48 hours of mixing from an acetonitrile solution of pyrrole (0.1M) and TCNE (0.01M).
The layer was formed at 1.0 volts (vs. SCE), and its thickness corresponded to $\cong$ 0.1μm. The layer was then washed with acetonitrile thoroughly and transferred to a degassed $NaClO_4$ (0.01M) acetonitrile solution. The layer was scanned between 0.5V and -1.2V and the resulting cyclic voltammogram is shown in Figure 4.20(a) to see if there is evidence of TCNE electrochemistry. A broad reduction peak at -0.670 volts is observed with a corresponding reoxidation peak at 0.00 volts corresponding to the polymer electrochemistry. The negative region of this reduction peak, at -0.670V, and the fact that the background electrolyte solution remained unchanged in colour indicated that the TCNE

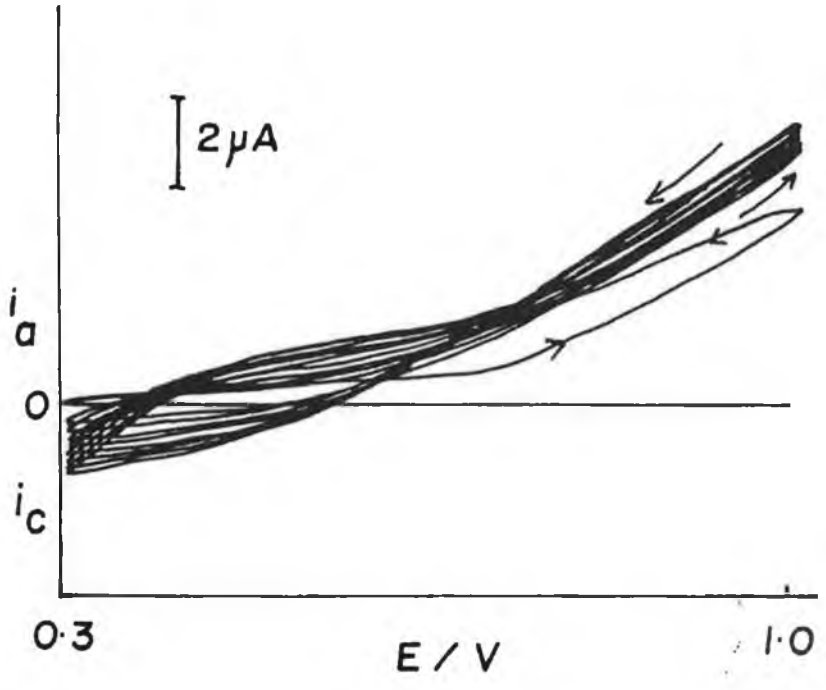

Figure 4.19 Cyclic voltammogram of pyrrole (0.06M) and TCNE (0.05M) in acetonitrile solution, 4 minutes after mixing.
Scan Rate = 50mV/s.

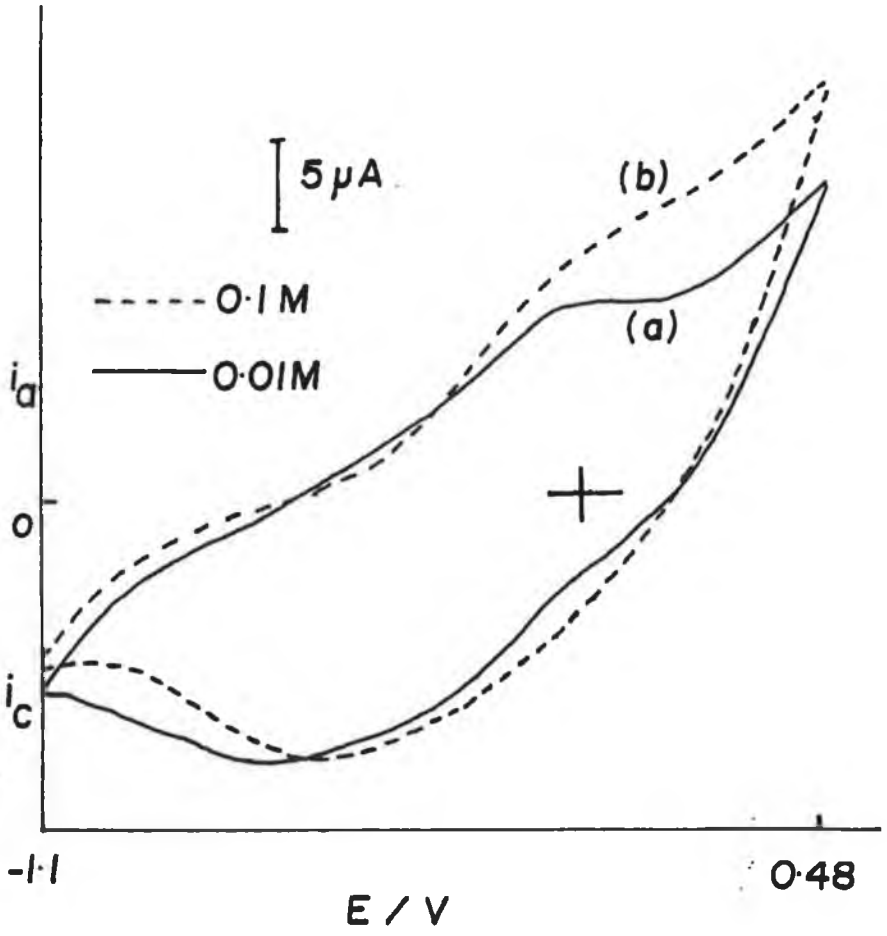

Figure 4.20 Cyclic voltammogram of a PPTCNE layer previously formed in an acetonitrile solution of pyrrole (0.1M) and TCNE (0.01M) 48 hours after mixing by holding the potential at 1.0V, in
(a) $NaClO_4$ (0.01M) (b) $NaClO_4$ (0.1M).

remained within the layer and that it was cation movement in and out of the polymer matrix that occurred upon redox switching.

To prove this, the layer was taken out of the $NaClO_4$ (0.01M) solution washed with acetonitrile and then transferred to higher concentration of $NaClO_4$ (0.1M). The layer was scanned as before and the resulting cyclic voltammogram is shown in Figure 4.20(b). Again a broad reduction wave is observed. However the peak potential of this wave occurs at -0.560V, a shift of 0.110V in a positive direction upon increasing the electrolyte concentration. This positive direction in the shift concludes that it is the Na^+ cation moving in and out of the polypyrrole tetracyanoethylene film upon reduction and reoxidation respectively.

4.3.3 CONCLUSION

It is proposed that the charge transfer complex composed of Py^+TCNE^- can be oxidised to form a conducting polymer with the $TCNE^-$ heavily bound within the layer. The complex is very strong since even at positive applied potentials when the polymer layer is formed, the $TCNE^-$ does not appear to be oxidised.

4.4 A SOLVENT STUDY OF THE ELECTROCHEMICAL BEHAVIOUR OF THE FERRICYANIDE/FERROCYANIDE SYSTEM

4.4.1 EXPERIMENTAL

An aqueous solution of tetrabutylammonium bisulphate (0.1M) was prepared and neutralised by addition of potassium hydroxide (1.0M). This solution was mixed with an equal volume of aqueous solution of potassium ferricyanide (0.3M).

The resulting solution was extracted with dichloromethane several times and the tetrabutylammonium ferricyanide product was isolated by rotary evaporation. Electrochemical experiments were performed upon the $TBA_3Fe(CN)_6$ complex in aprotic solvents and in water.

All chemicals employed for the electrochemical experiments were reagent grade.

Cyclic voltammetric data were recorded in a three electrode, one compartment cell. The working electrode was a polished glassy carbon disc electrode, and auxiliary electrode was a carbon rod and a saturated calomel electrode was employed as the reference electrode. All solutions employed in electrochemical experiments were degassed with oxygen free nitrogen.

A ramp generator (H.B. Thompson 16 bit), a potentiostat (Edt ECP 100) and an electronic integrator (Sycopel DP3015) linked to a J.J. Lloyd PL3 X-Y recorder were used for cyclic voltammetry. All experiments were carried out at room temperature.

4.4.2 RESULTS AND DISCUSSION

The ferricyanide/ferrocyanide redox couple is routinely used as a model electrode reaction by electrochemists. Therefore it is important that its physical

chemistry is well understood. Recently, Noftle and Pletcher [39] investigated the behaviour of the formal potential for the ferricyanide/ferrocyanide couple as a function of solvent composition. Their results indicate that the solvent has an important influence upon the electrochemical behaviour of this couple, with water behaving unlike other solvents.

Figure 4.21 shows the cyclic voltammogram of an aqueous solution of potassium hexacyanoferrate(lll), $K_3Fe(CN)_6$, (10mM) in KCl (0.1M) at a glassy carbon electrode. The formal potential of +0.150V vs. SCE, for the ferricyanide/ferrocyanide couple makes potassium hexacyanoferrate(lll) a strong oxidising agent in aqueous media.

Figure 4.22(a) and (b) shows the cyclic voltammograms of the $TBA_3Fe(CN)_6$ (5mM) complex, with tetrabutylammonium fluoroborate ($TBABF_4$), (0.1M) as background electrolyte, in two dried aprotic solvents, namely acetonitrile and tetrahydrofuran, THF, respectively. The formal potentials for the couple were found to be over 0.7V more negative, compared to the potassium salt in aqueous media. The formal potentials were -0.980V (vs. SCE) and -0.608V (vs. SCE) in acetonitrile and tetrahydrofuran respectively.

Due to these results, it can be concluded that the influence of solvent upon the behaviour of the redox couple, is large with the $TBA_3Fe(CN)_6$ complex not being a strong oxidant in aprotic solvents.

These results are in agreement with previous experimental results [39,52]. It should be emphasised that the ferrocyanide is a strong reducing agent in aprotic media.

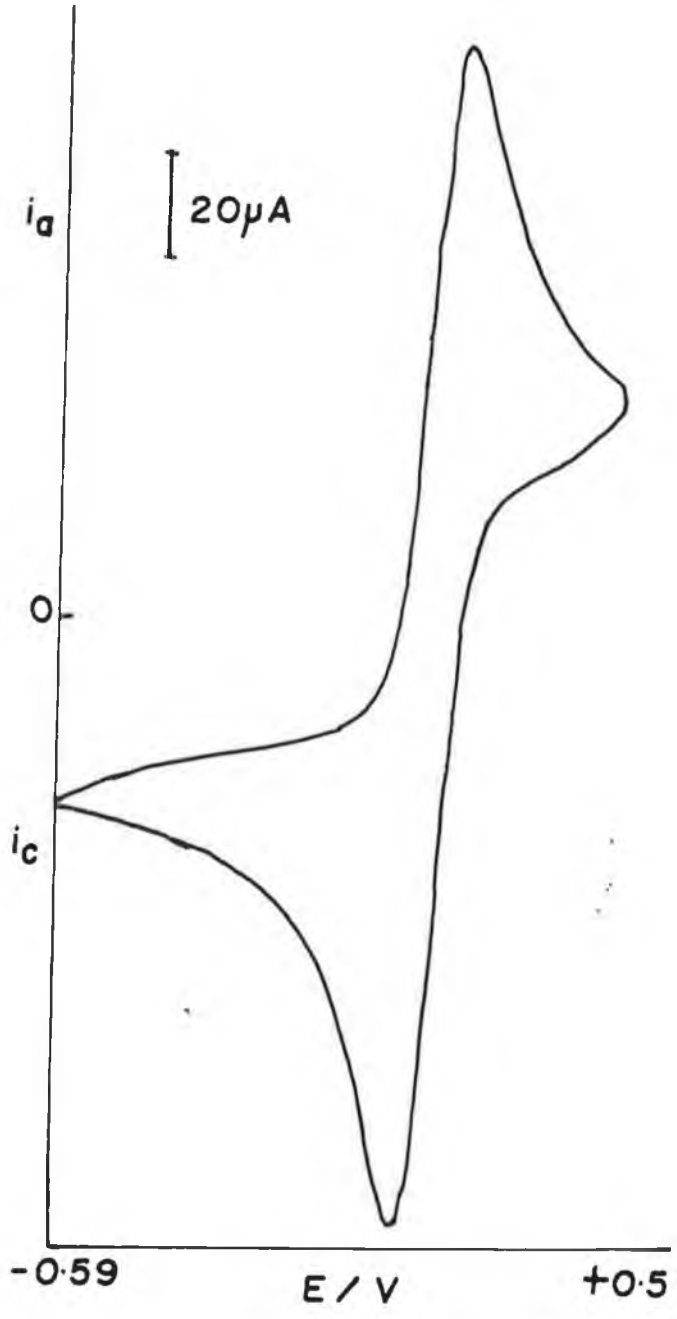

Figure 4.21 Cyclic voltammogram of an aqueous solution of $K_3Fe(CN)_6$ (10mM) and KCl (0.1M) at a platinum electrode.
Scan Rate = 100mV/s.

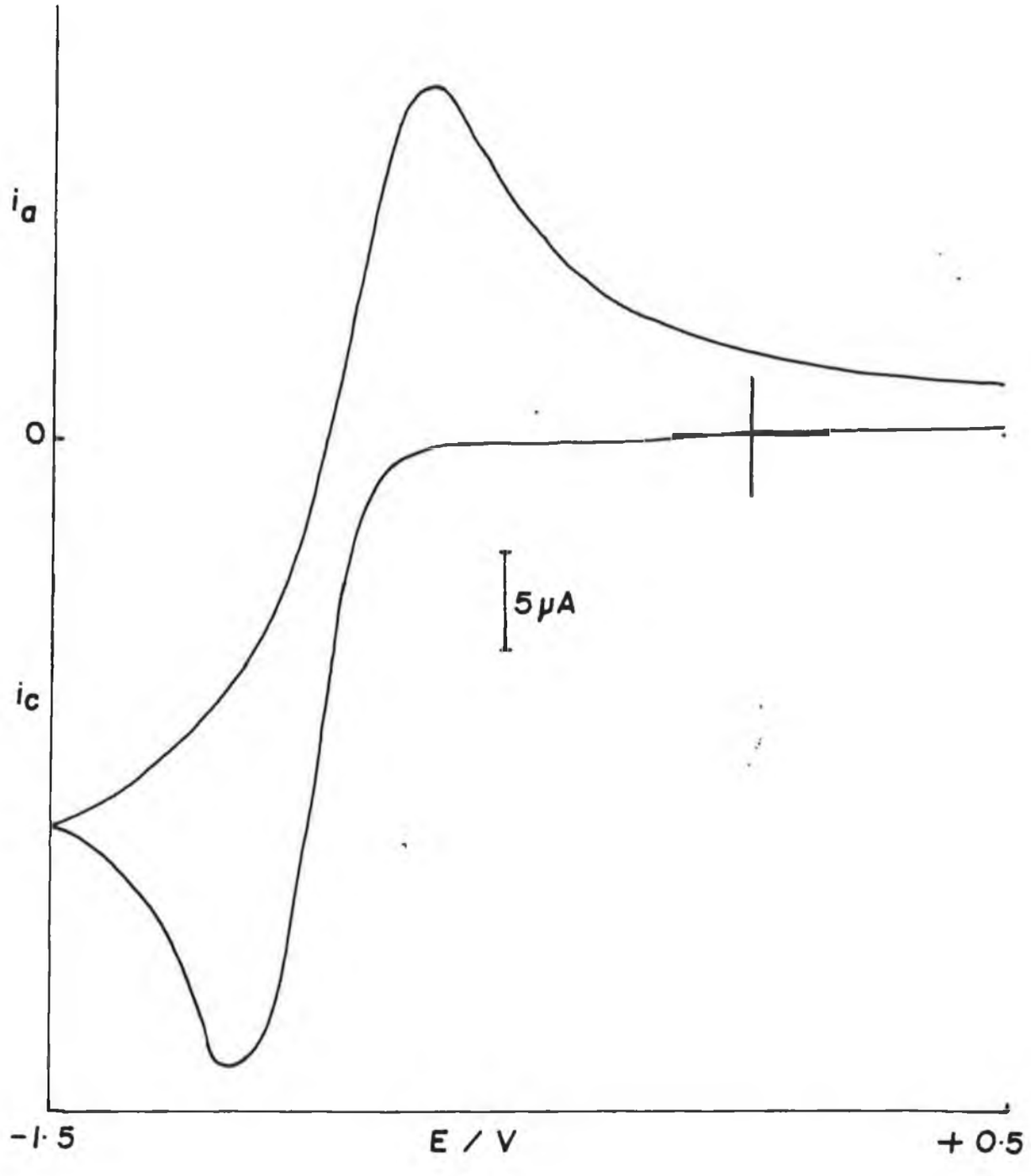

Figure 4.22 (a) Cyclic voltammogram of an acetonitrile solution of $TBA_3Fe(CN)_6$ (5mM) and $TBABF_4$ (0.1M) at glassy carbon. Scan Rate = 100mV/s.

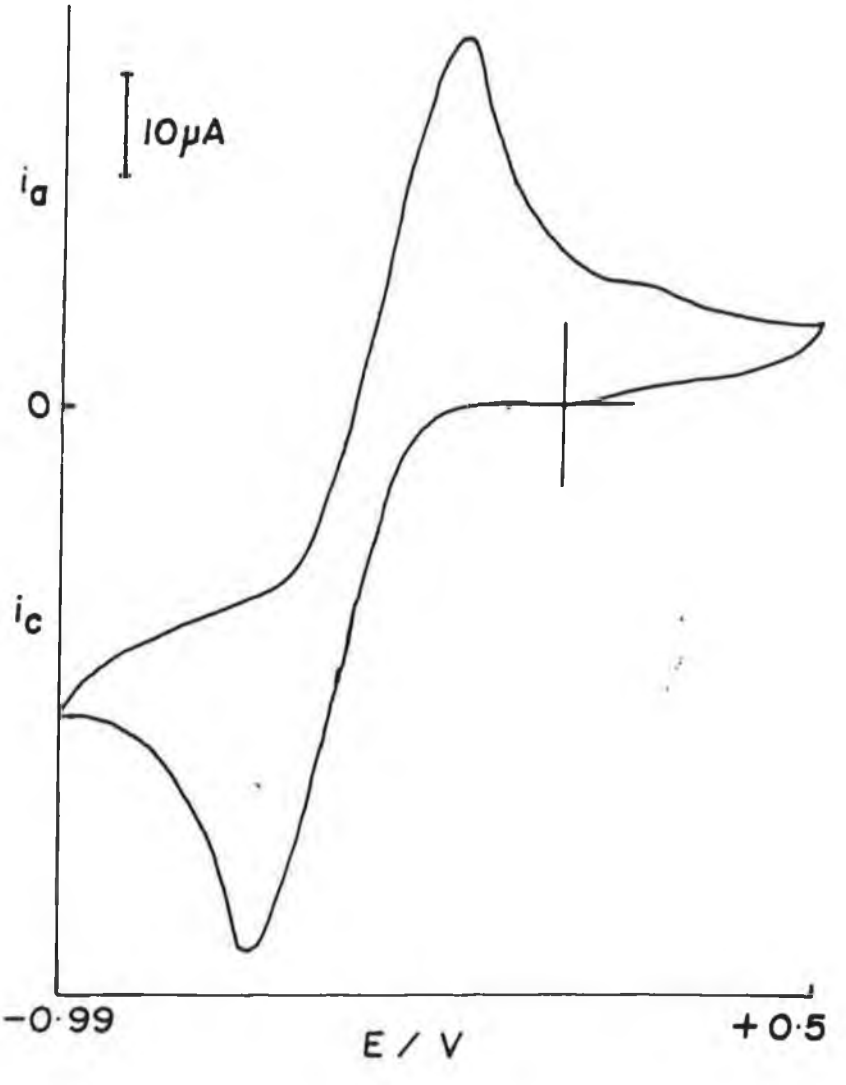

Figure 4.22 (b) Cyclic voltammogram of a tetrahydrofuron solution (THF) of $TBA_3Fe(CN)_6$ (5mM) and $TBABF_4$ (0.1M) at glassy carbon. Scan Rate = 100mV/s.

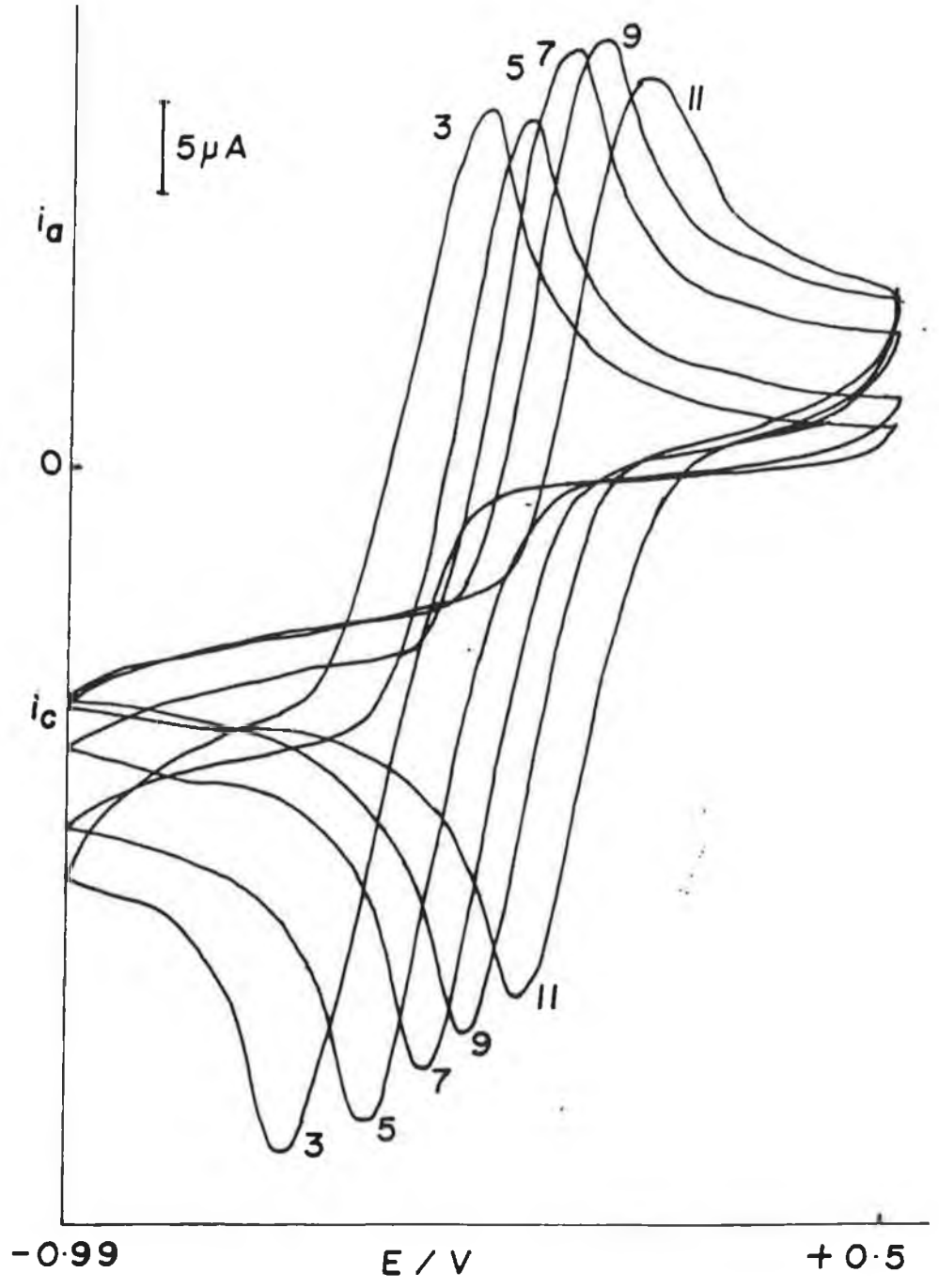

Figure 4.23 Cyclic voltammograms recorded at a glassy carbon electrode for solutions of TBA_3 $Fe(CN)_6$ (5mM) in various THF/H_2O mixtures 3(3% H_2O), 5(5%H_2O), 7(7%H_2O), 9(9%H_2O), 11(11H_2O). Scan Rate = 100mV/s

The influence, upon the formal potential of the ferri/ferrocyanide couple, by the addition of a protic partner to the organic solvent system was investigated.

Figure 4.23 shows the positive shift in the cyclic voltammetric behaviour of the $TBA_3Fe(CN)_6$ complex in THF after the addition of known percentages of water. It can be seen that when the solvent system contains 7% or more of water the formal potential of the couple has shifted in a positive direction by over 0.4V.

These results are summarised in Table 4.2

TABLE 4.2

DATA FOR CYCLIC VOLTAMMOGRAMS RECORDED AT A GLASSY CARBON ELECTRODE FOR SOLUTIONS OF TETRABUTYLAMMONIUM FERRICYANIDE (5MM) IN VARIOUS TETRAHYDROFURAN + WATER SOLUTIONS

% H_2O	Ep^0 VOLTS	Ep^a VOLTS	E_F VOLTS	ΔE_F VOLTS	$\ln[H_2O]$ $MOLL^{-1}$
0	-0.840	-0.370	-0.605	-	-
1.0	-0.680	-0.280	-0.480	0.125	-0.587
2.0	-0.590	-0.240	-0.415	0.190	+0.106
3.0	-0.520	-0.210	-0.365	0.240	+0.511
4.0	-0.440	-0.160	-0.300	0.305	+0.799
5.0	-0.380	-0.120	-0.250	0.355	+1.020
6.0	-0.340	-0.090	-0.215	0.390	+1.204
7.0	-0.280	-0.050	-0.165	0.440	+1.380
8.0	-0.260	-0.020	-0.140	0.465	+1.490
9.0	-0.220	0.000	-0.110	0.495	+1.610
11.0	-0.170	0.050	-0.060	0.545	+1.810

The influence of water upon the formal potential of the ferricyanide/ferrocyanide couple in acetonitrile, AcN, was also investigated. These results are summarised in Table 4.3.

TABLE 4.3

DATA FOR CYCLIC VOLTAMMOGRAMS RECORDED AT A GLASSY CARBON ELECTRODE FOR SOLUTIONS OF TETRABUTYLAMMONIUM FERRICYANIDE (3MM) IN VARIOUS ACETONITRILE + WATER SOLUTIONS BACKGROUND ELECTROLYTE

% H_2O	Ep^c VOLTS	Ep^a VOLTS	E_F VOLTS	ΔE_F VOLTS	$\ln[H_2O]$ MOL l^{-1}
0	-0.970	-0.870	-0.930	-	-
0.5	-0.700	-0.610	-0.655	0.275	-1.280
1.0	-0.540	-0.440	-0.490	0.440	-0.590
2.0	-0.400	-0.310	-0.355	0.575	+0.105
3.0	-0.270	-0.160	-0.215	0.715	+0.510
4.0	-0.160	-0.030	-0.095	0.835	+0.798
5.0	-0.070	+0.070	+0.000	0.930	+0.102
7.0	0.000	+0.140	+0.070	1.000	+1.360
8.0	+0.050	+0.180	+0.115	1.045	+1.490
10.0	+0.090	+0.200	+0.145	1.075	+1.710
15.0	+0.110	+0.210	+0.160	1.090	+2.120
20.0	+0.120	+0.220	+0.170	1.100	+2.410

It can be seen that when the solvent system contains 7%(v/v) of water, that the formal potential of the couple has shifted in a positive direction by over 1.0V. Also after the addition of 20%(v/v) water, the formal potential has reached a steady value of +0.170 vs. SCE, which is in agreement with the formal potential of the potassium salt, in aqueous solution, observed in Figure 4.21.

These results are in agreement with those of Noftle et al [39]. Changes in the dielectric constant of the mixed solvent media do not account for the large shifts in formal potential observed. This was concluded by adding known percentages of methanol to an acetronitrile solution of the $TBA_3Fe(CN)_6$ complex, and performing cyclic voltammetry. Table 4.4 summarises the results obtained.

TABLE 4.4

DATA FOR CYCLIC VOLTAMMOGRAMS RECORDED AT A GLASSY CARBON ELECTRODE FOR SOLUTIONS OF TETRABUTYLAMMONIUM FERRICYANIDE (3mM) IN VARIOUS ACETONITRILE + METHANOL SOLUTIONS

% CH_3OH	Ep^c (VOLTS)	Ep^a (VOLTS)	E_F (VOLTS)	ΔE_F (VOLTS)	$\ln[CH_3OH]$ $MOLL^{-1}$
0	-1.040	-0.920	-0.980	-	-
1.0	-0.920	-0.670	-0.795	+0.185	-1.370
2.0	-0.740	-0.640	-0.690	+0.290	-0.680
3.0	-0.670	-0.580	-0.625	+0.355	-0.270
4.0	-0.640	-0.540	-0.590	+0.390	+0.016
5.0	-0.590	-0.500	-0.545	+0.435	+0.240
7.0	-0.570	-0.470	-0.520	+0.460	+0.576
10.0	-0.550	-0.420	-0.485	+0.495	+0.930
15.0	-0.530	-0.380	-0.455	+0.525	+1.340
20.0	-0.520	-0.360	-0.440	+0.540	+1.630
50.0	-0.460	-0.310	-0.385	+0.595	+2.540
100.0	-0.470	-0.300	-0.385	+0.595	+3.230

It can be seen that there is still a dramatic shift in the formal potential of the ferri/ferrocyanide couple of over 0.4V after the addition of 5%(v/v) methanol.

The change in the dielectric constant of the solvent system only changes from 36.01 to 32.63 for a 0-100%(v/v) of methanol, thereby proving that the observed shift in the formal potential of the couple is not due to a dielectric constant variation.

The difference in the formal potential of the ferricyanide/ferrocyanide couple in aprotic solvents and water, has previously [39] been said to be due to the strong stabilisation of the Fe(ll) complex by water. Gutmann [53] previously stated that the donor-acceptor interactions between the nitrogen of ferrocyanide and the solvents are strong. He stated that the electron pair donor properties at the N-atoms of the coordinated groups are stronger in the reduced form than in the oxidised state for the hexacyanoferrate complex. Therefore it can be concluded that the interaction with a given electron pair acceptor solvent is stronger for the reduced species, in which the induced electron shifts lead to a strong decrease in reducing properties. Therefore it can be said that by increasing the solvent acceptor properties the reducing properties of the Fe(ll) species are more strongly decreased than the oxidising properties of the Fe(lll) species are increased.

It should be noted that water, methanol and acetonitrile have electron acceptor numbers [53] of 54.8, 41.3 and 19.3 respectively. Thereby upon addition of water or methanol to an acetonitrile solution leads to an increase in acceptor number of the solvent mixture, thereby decreasing the reducing properties of the Fe(ll) species. This leads to a positive shift in the formal potential of the ferricyanide/ferrocyanide redox couple.

For the reaction

$$[Fe(CN)_6]^{3-} + e^- = [Fe(CN)_6]^{4-} \quad \ldots\ldots 4.4.1$$

in a pure solvent, the Nernst equation is given below

$$E = E^o_{solvent} + \frac{RT}{nF} \ln\left\{\frac{[Fe(CN)_6]^{3-}}{[Fe(CN)_6]^{4-}}\right\} \quad \ldots\ldots 4.4.2$$

The electrode reaction in solvent/water mixtures may be considered as

$$[Fe(CN)_6(H_2O)_p]^{3-} + (q-p)\ H_2O + e^- = [Fe(CN)_6(H_2O)_q]^{4-} \ldots. 4.4.3$$

The Nernst equation applied to the equation 4.4.3 gives

$$E = E^o_{solvent+water} + \frac{RT}{nF} \ln\left\{\frac{[[Fe(CN)_6(H_2O)_p]^{3-}\ [H_2O]^{q-p}]}{[Fe(CN)_6(H_2O)_q]^{4-}}\right\} \ldots 4.4.4$$

By equating the two potentials, such that equation 4.4.2 and 4.4.4 equal each other gives rise to

$$O = E_{solvent/H2O} - E_{solvent} + \frac{RT}{nF} \ln\left\{\frac{[Fe(CN)_6(H_2O)_p]^{3-}\ [H_2O)^{q-p}[Fe(CN)_6]^{4-}}{[Fe(CN)_6\ (H_2O)_q]^{4-}}\right\}$$

$$\ldots\ldots 4.4.5$$

The equilibrium constants are defined, for the two reactions

$$[Fe(CN)_6]^{4-} + qH_2O = [Fe(CN)_6\ (H_2O)_q]^{4-} \quad \ldots\ldots 4.4.6$$

$$[Fe(CN)_6]^{3-} + pH_2O = [Fe(CN)_6 (H_2O)_p]^{3-} \quad \ldots\ldots \quad 4.4.7$$

The stability constants are given below

$$K_{II} = \frac{[Fe(CN)_6 (H_2O)_q]^{4-}}{[Fe(CN)_6]^{4-} [H_2O]^q} \quad \ldots\ldots \quad 4.4.8$$

$$K_{III} = \frac{[Fe(CN)_6 (H_2O)_p]^{3-}}{[Fe(CN)_6]^{3-} [H_2O]^p} \quad \ldots\ldots \quad 4.4.9$$

By defining $\frac{K_{II}}{K_{III}}$ and then rearranging the equation this gives rise to

$$\frac{[H_2O]^{q-p} K_{II}}{K_{III}} = \frac{[Fe(CN)_6(H_2O)_q]^{4-} [Fe(CN)_6]^{3-}}{[Fe(CN)_6]^{4-} [Fe(CN)_6 (H_2O)_p]^{3-}} \ldots\ldots \quad 4.4.10$$

Equation 4.4.10 is then substituted into equation 4.4.5 and the final expression is obtained.

$$E_{solvent+H2O} - E_{solvent} = \frac{RT}{F} \ln\left\{\frac{K_{II}}{K_{III}}\right\} + \frac{(q-p)\ RT}{F} \ln H_2O$$

$$= \Delta E_f \quad \ldots\ldots \quad 4.4.11$$

It can be seen that equation 4.4.11 predicts a linear plot when the shift in the formal potential of the ferricyanide/ferrocyanide couple, upon addition of water to the solvent system, is plotted versus the $\ln[H_2O]$.

The results given in Table 4.1, Table 4.2 and Table 4.3 are used to obtain linear plots.

Figure 4.24 (a), (b) and (c) show the plots obtained for the THF/H_2O, ACN/H_2O and ACN/CH_3OH mixtures respectively, upon application of equation 4.4.11 to the results given in the previous three tables. It can be seen that from the slope and intercept values for (q-p) and KII/KIII can be obtained for each plot and these results are summarised in Table 4.5 below.

TABLE 4.5

VALUES OF PARAMETERS (q-p) AND K_{II}/K_{III} ESTIMATED FROM FIGURE 4.2.4 (a), (b) and (c).

SOLVENT SYSTEM	q-p	$\frac{K_{II}}{K_{III}}$
THF/H_2O	8.5±0.7	$2.60\pm1.0\times10^{2}$
ACN/H_2O	11.0±2.0	$1.21\pm0.3\times10^{10}$
ACN/CH_3OH	6.0±0.4	$3.53\pm0.7\times10^{6}$

It can be concluded from the results in Table 4.5 that the interaction of the water molecules with the nitrogen atoms of the ferrocyanide species is strong in character due to the large values obtained for the factor KII/KIII.

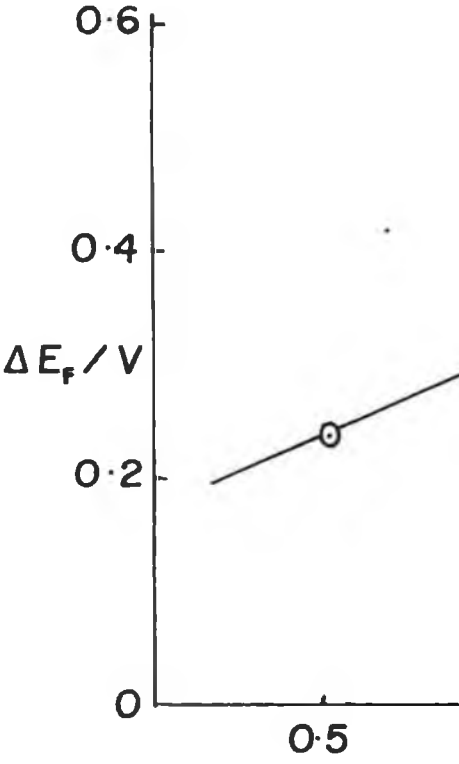

Figure 4.24 (a)

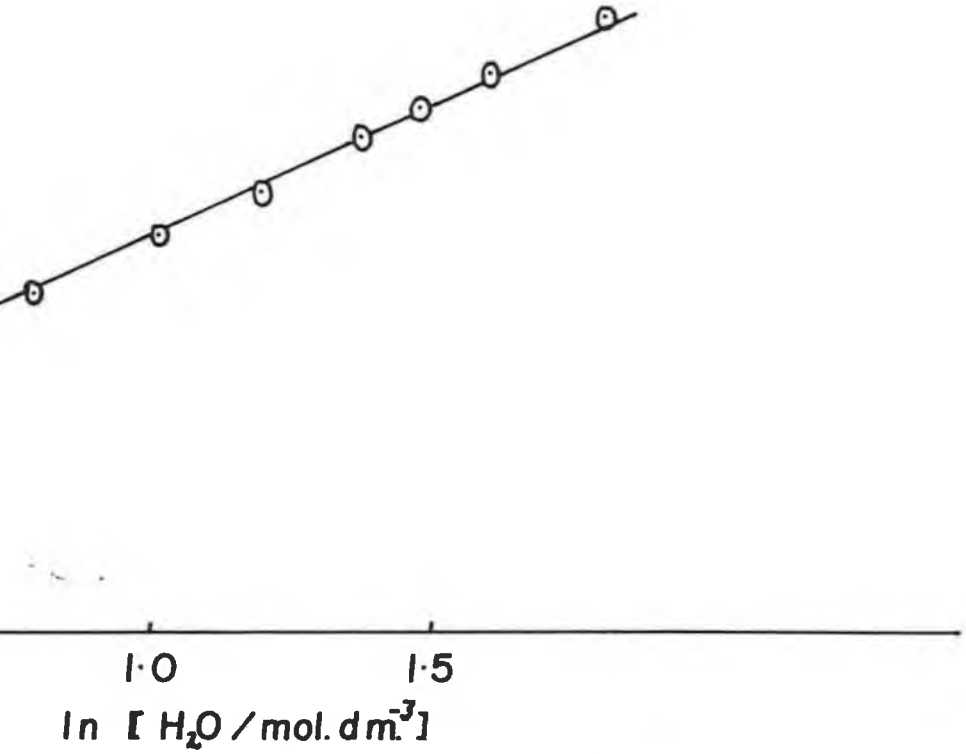

Influence of water on the formal potential for the ferricyanide/ferrocyanide couple in THF.

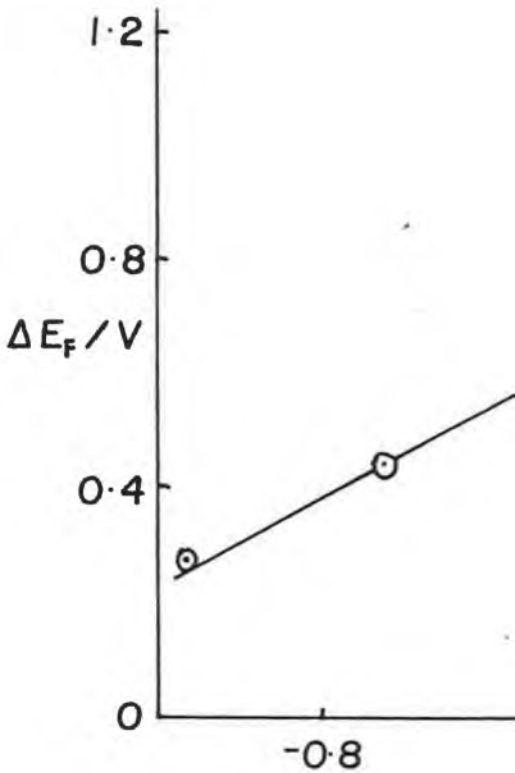

Figure 4.24 (b)

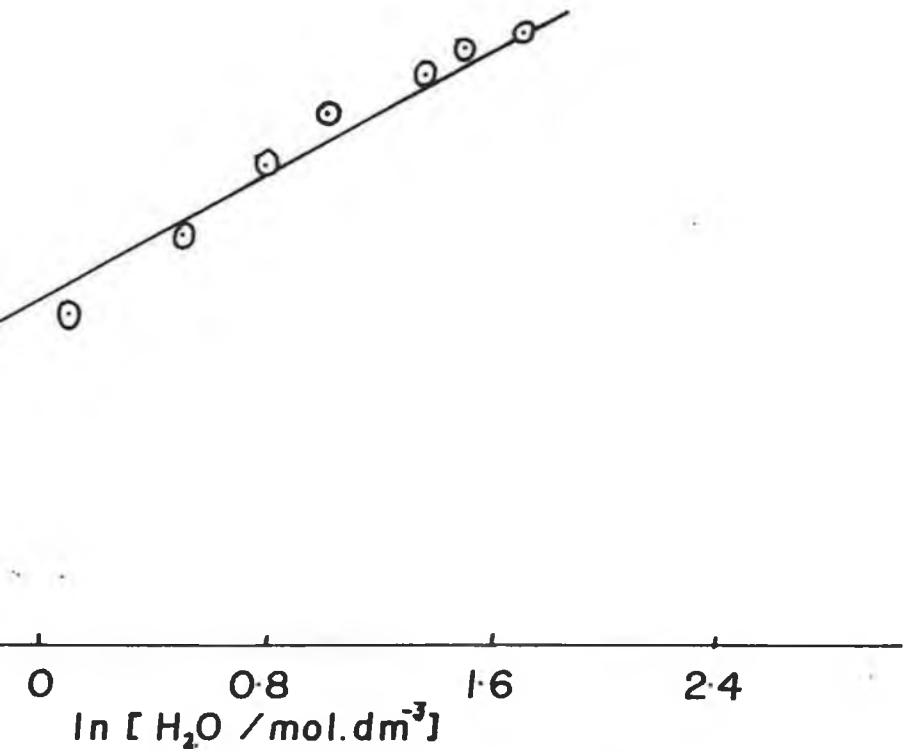

Influence of water on the formal potential for the ferricyanide/ferrocyanide couple in ACN.

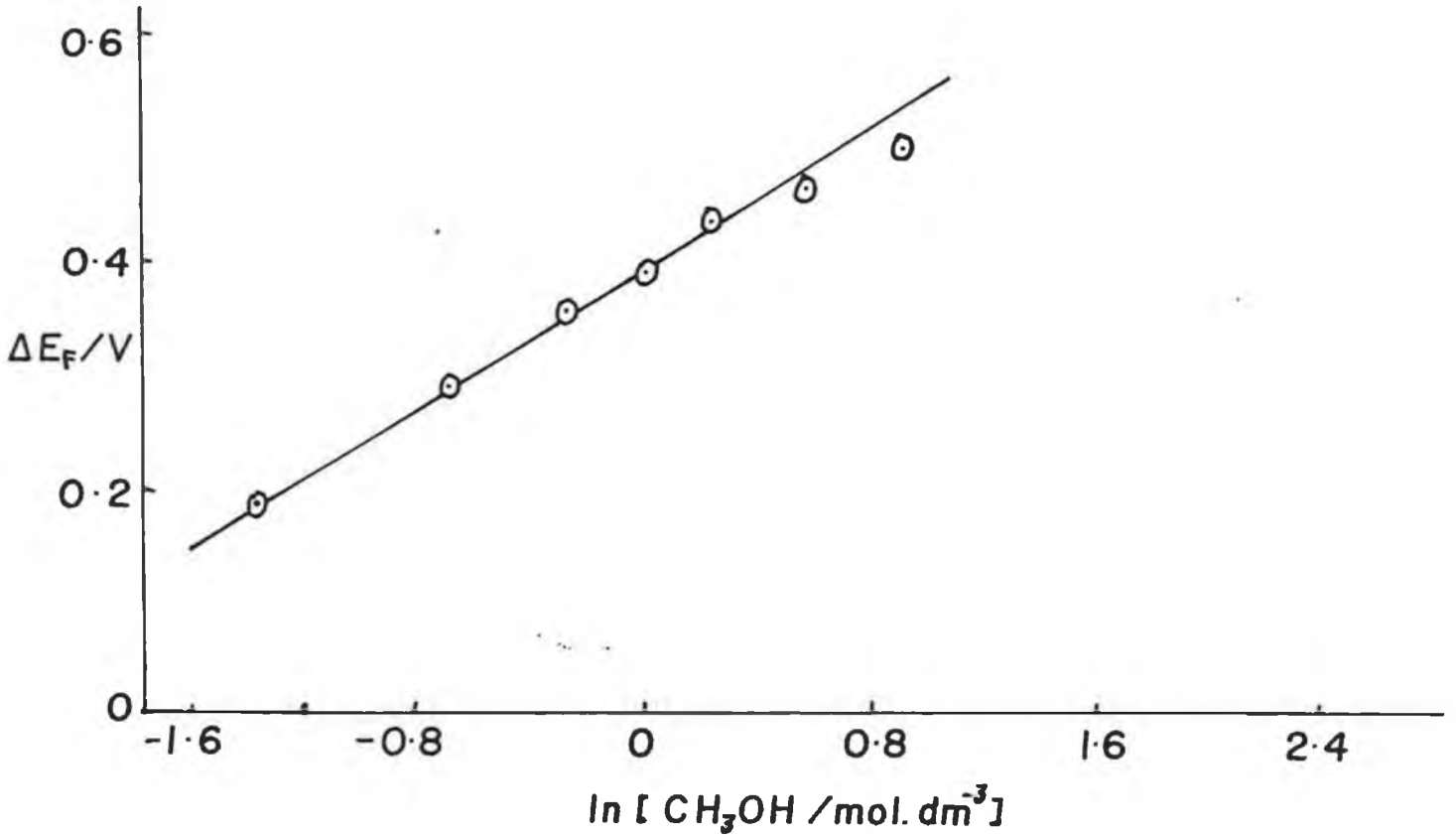

Figure 4.24 (c) Influence of methanol on the formal potential for the ferricyanide/ferrocyanide couple in ACN.

Noftle et al [39] found that q-p was equal to 6.2, therefore they concluded that there was one water molecule associated with each nitrogen atom of ferrocyanide. However this seems sheer coincidence, as their graph contains only 4 points with no mention of errors within the slope and intercept values.

An important point to note is also that the plots in Figure 4.24 are not linear over the entire water concentration range. The major shift in the formal potential of the ferricyanide/ferrocyanide couple occurs below 10% H_2O(v/v). After this value the formal potential shifts to a lesser extent, as it is close to its final steady value.

It was observed that when the amount of water in the mixed solvent system reached about 20% (v/v) then the electrochemistry of the ferryanide/ferrocyanide couple disappeared.

In pure H_20 solution, with tetrabutylammonium hydrogensulphate $TBAHSO_4$, (0.1M), the electrochemistry of the Fe^{3+}/Fe^{2+} is not observed. This is illustrated in Figure 4.25 where it can be seen that during the first scan, a reduction wave is observed with no definite reoxidation wave being observed. Upon further scanning, the reduction wave disappears, and when the positive potential limit is made +0.8V, still no electrochemistry of the couple is observed. The size of the TBA cation in aqueous solution possibly limits the electrochemistry of the ferricyanide/ferrocyanide couple.

The nature of the cation in the background electrolyte was changed to investigate whether any electrochemistry of the ferricyanide/ferrocyanide couple in the

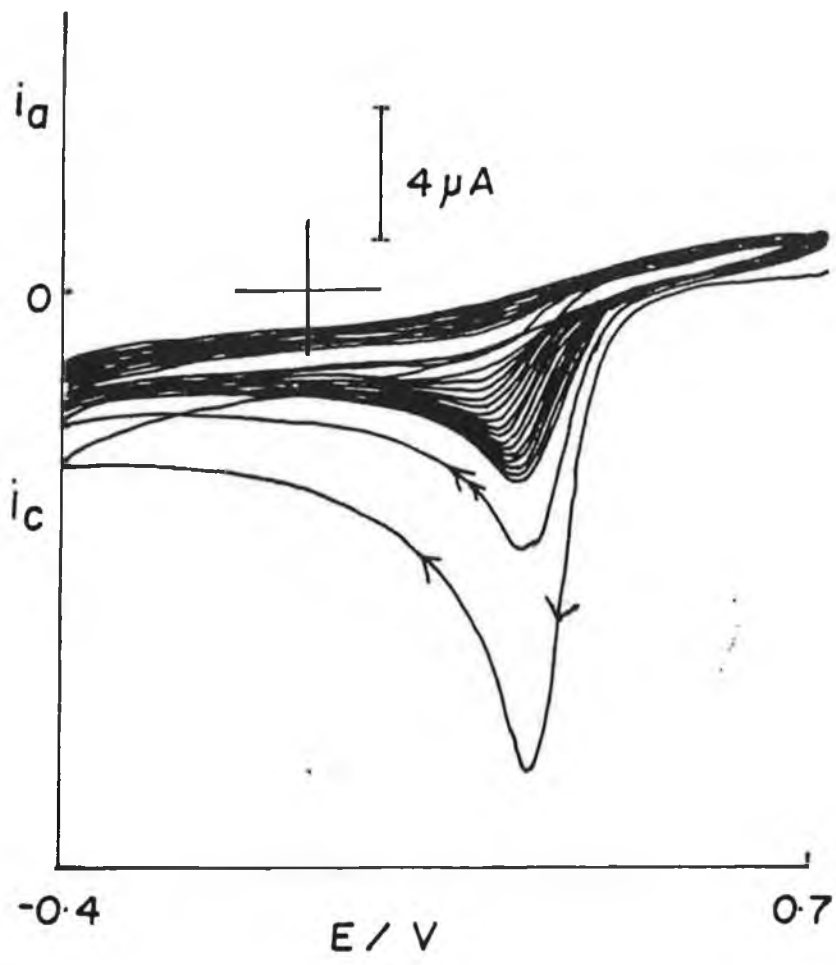

Figure 4.25 Cyclic voltammogram of an aqueous solution of $TBA_3\ Fe(CN)_6$ (10mM) in $TBAHSO_4$ (0.1M) at a glassy carbon electrode. Scan Rate = 100mV/s.

$TBA_3Fe(CN)_6$ could be observed. It has been reported previously [54] that the nature of the cation in the background electrolyte has an effect upon the kinetics of the redox couple $Fe(CN)_6^{4-/3-}$. This led to the theory [55] that the cation in the background electrolyte possibly forms an activated complex with the ferrocyanide upon reoxidation.

Figure 4.26 shows the cyclic voltammogram of an aqueous solution of $TBA_3Fe(CN)_6$ (10mM) in KCl (0.1M). It can be seen that the formal potential of the ferricyanide/ferrocyanide couple was +0.155 volts, this was in close agreement to E_f of the potassium salt of $Fe(CN)_6^{3-}$ in KCl(0.1M) observed in Figure 4.21. This result pointed to the possibility that an exchange process between the tetrabutylammonium cation and the potassium cation occurred. This seemed likely due to the procedure of simple cation exchange used in making the $TBA_3Fe(CN)_6$ complex, described in the experimental section. The same procedure was carried out, using a range of electrolyte cations, alkali metals, alkaline earth metals and group three cations. The background electrolyte anion was kept the same, namely chloride.

Table 4.6 below summarises the results obtained, for the cyclic voltammetric experiments.

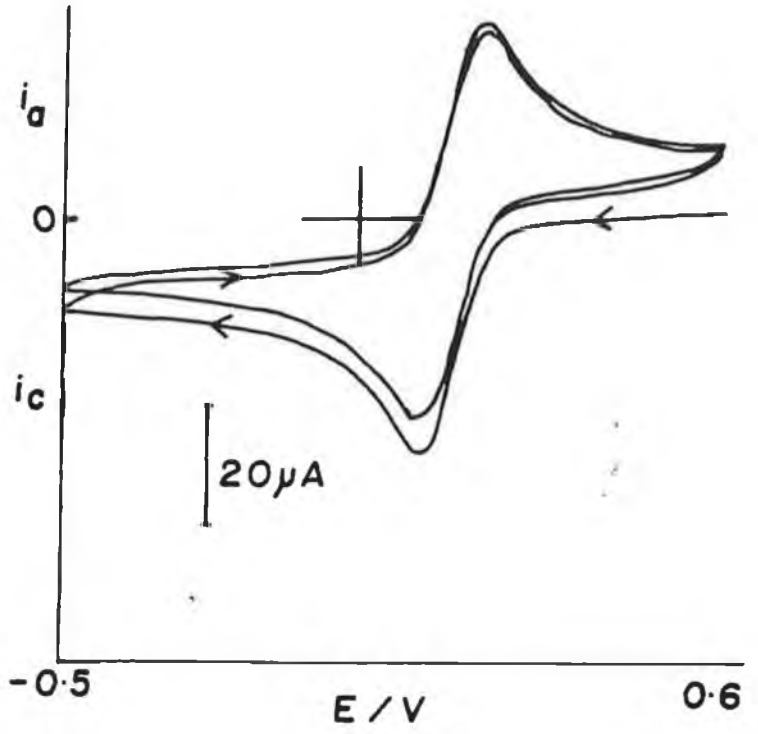

Figure 4.26 Cyclic voltammogram of an aqueous solution of TBA_3 $Fe(CN)_6$ (10mM) in KCl (0.1M) at glassy carbon.
Scan Rate = 100mV/s.

TABLE 4.6

CYCLIC VOLTAMMETRIC DATA FOR THE $TBA_3Fe(CN)_6$ COUPLE AS A FUNCTION OF DIFFERENT ELECTROLYTES

Nature of Cation in Background Electrolyte (0.1M)	(Volts) E_p^a	(Volts) E_p^c	(Volts) E^o
Lithium	+0.190	+0.090	+0.140
Sodium	+0.190	+0.096	+0.143
Potassium	+0.210	+0.100	+0.155
Caesium	+0.230	+0.120	+0.175
Magnesium	+0.240	+0.160	+0.200
Lanthanum	+0.300	+0.220	+0.260
Cerium	+0.300	+0.230	+0.265

It can be seen that all the cations are exchanged into the ferricyanide complex, with a slight shift to more positive potentials for the formal potential, as the charge associated with the cation increases from +1 to +3.

As previously stated no electrochemistry of the $TBA_3Fe(CN)_6$ complex has been observed in an aqueous solution with $TBAHSO_4$ as the background electrolyte. A smaller organic cation was employed in the background electrolyte solution, namely tetramethylammonium nitrate, $(CH_3)_4 N(NO_3)$ (0.1M). A reduction and a reoxidation wave are observed, however the waves are broad in nature with a large peak to peak separation of 0.500V. It can be concluded that the size of the cation, tetramethylammonium, does not inhibit the mechanism of reduction and reoxidation of the ferricyanide/ferrocyanide, perhaps ion pairs are formed.

Also a THF solution of $TBA_3Fe(CN)_6$ and $LiClO_4$ (0.1M) was prepared, it was found that a yellow precipitate was formed with no electrochemistry of the ferricyanide/ferrocyanide couple being observed. The Li^+ cation seemed to be exchanged to some extent with the formation of a complex, which is insoluble in organic solvents.

The electrochemistry of $K_3Fe(CN)_6$ was investigated in solvent mixtures, with KCl (0.1M) being used as the background electrolyte. It has already been mentioned that the formal potential for the $K_3Fe(CN)_6$ species in aqueous solution is +0.150V. It was found that in a 50/50 (v/v)% solution of H_2O/ACN, H_2O/THF and H_2O/CH_3OH that the formal potential of the ferricyanide/ferrocyanide couple was +0.01 volts, +0.07 volts, and 0.035 volts respectively. Though the shifts are not large compared to the shifts obtained for the $TBA_3Fe(CN)_6$, upon addition of a protic solvent, they are worth noting.

4.4.3 CONCLUSION

It was seen that the electrochemistry of the $TBA_3Fe(CN)_6$ complex was strongly dependent upon solvent composition. In acetonitrile and THF solvents, ferrocyanide was a strong reducing agent with ferricyanide being a weak oxidising agent. Large dramatic shifts in the formal potential of the couple were observed, upon addition of a protic partner to the organic solvent system. This shift was due to the increase in acceptor properties of the solvent mixture. The shift was greater upon the addition of water than methanol, due to water being a stronger acceptor.

Values obtained for stability constants and the number of water molecules associated with the $Fe(CN)_6^{3-}$ and $Fe(CN)_6^{4-}$ species, indicated that the water interacted stronger with ferrocyanide than the ferricyanide.

Also electrochemistry of the TBA_3 $Fe(CN)_6$ complex, with $TBAHSO_4$ as the electrolyte, could not be observed in pure aqueous solution. It was found that changing the cation of the background electrolyte led to partial exchange involving the electrolyte cation and the complex.

Finally, it was reported that the electrochemistry of the $Fe(CN)_6^{3-}/Fe(CN)_6^{4-}$ couple, of the potassium salt, also depended upon the solvent composition with negative shifts of over 0.1V being observed when the solvent composition was 50:50 water and aprotic partner.

4.5 INFRARED SPECTROELECTROCHEMISTRY AND ITS APPLICATION TO THE STUDY OF THE REDUCTION AND REOXIDATION OF $TBA_3Fe(CN)_6$

4.5.1. INTRODUCTION

Fourier Transform Infrared Spectroscopy (FTIR) allows rapid acquisition of data, which allows the application of infrared spectroscopy to electrochemistry for the detection of intermediates and products.

The simplest approaches include transmission ir spectroelectrochemistry where the solution and working electrode (a gold minigrid) is wedged between two infrared transparent plates.

Reflection spectroelectrochemistry has also been used with an electrode (Au Pt or even C) polished to a mirror like finish. The thin layer of solution between an infrared transparent plate and the polished electrode can be examined by reflection. The light from the spectrometer is reflected into the cell and off a working electrode surface and into the detector of the spectrometer. Certain electrochemical reactions can be studied by infrared spectroscopy using this method. The first infrared spectrum is taken when the potential of the working electrode is set at a value where no electrochemical reaction occurs.

This spectrum is stored in the memory of the spectrometer as the 'background spectrum'. The potential of the electrode is then scanned to a value where the electrochemical reaction occurs. A spectrum is recorded and this is

automatically referenced to the background spectrum. This spectrum contains information regarding the electrochemical reaction at the electrode surface.

This difference spectroscopy will eliminate all absorbances due to the solvent and electrolyte providing no pertubations of solvent and electrolyte population in the thin layer and at the electrode surface occur.

This technique is used in the following section, to study the electrochemical reduction and reoxidation of the tetrabutylammonium ferricyanide complex.

4.5.2 EXPERIMENTAL

The cell used for the reflectance spectroscopy experiments is shown in Figure 4.27. The working electrode was a platinum wire, wrapped around the working electrode close to the CaF_2 plate. The CaF_2 plate acted as the cell window. The reference electrode was a saturated calomel electrode.

The infrared spectra were recorded on a Perkin Elmer 1710 Fourier Transform Infrared Spectrophotometer with the Perkin Elmer PP-1 Printer as an accessory.

All chemicals employed were of reagent grade. The tetrabutylammonium ferricyanide complex was prepared as previously described in Section 4.4.1. For acetonitrile solutions, tetrabutylammonium fluoroborate ($TBABF_4$) was used as the background electrolyte (0.1M). For aqueous solutions of $K_4 Fe(CN)_6$, 0.1M KCl was used as background electrolyte. All solutions were degassed with pure nitrogen for approximately 10 minutes, prior to use.

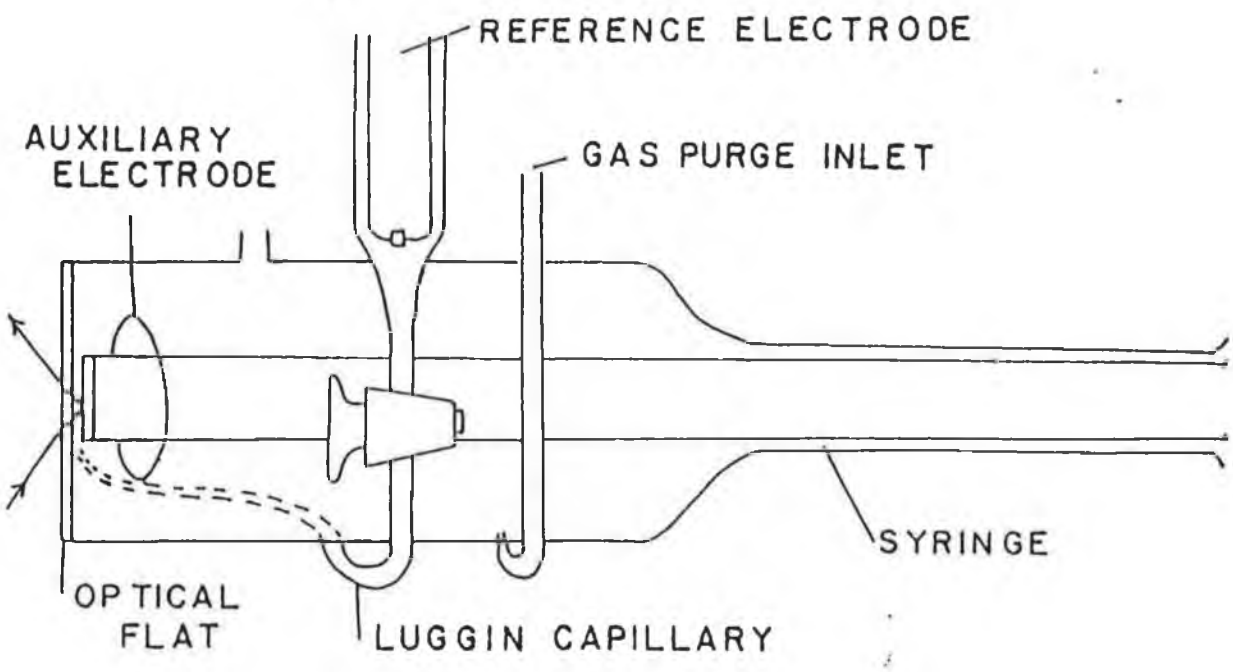

Figure 4.27 Spectroelectrochemical cell employed for reflectance spectroscopy.

The platinum plate working electrode was polished thoroughly with a slurry of 0.3μm alumina on billiard cloth. The electrode was then rinsed with ultrapure water and placed within the reflectance cell shown in Figure 4.27.

It was important to monitor the amount of incident radiation reaching the detector. This was conducted by measuring the energy reflected from the electrode surface and maximising this by moving the mirrors. However reflection from the optical window can occur, therefore the platinum electrode was pushed right up against the window and then pulled back. By monitoring the amount of energy reflected into the detector at the two positions, gave an indication of how much energy was being reflected from the electrode surface.

In order to determine the limitations of the cell and equipment employed, the oxidation of a standard system $K_4Fe(CN)_6$ was performed.

4.5.3 RESULTS AND DISCUSSION

The electrochemical model system, $Fe(CN)_6^{3-}/Fe(CN)_6^{4-}$ has been widely studied [56,57] using in situ infrared (IR) reflectance spectroelectrochemistry. Zhong et al [57] recently studied the electrochemical reactions of $Fe(CN)_6^{3-}$ and $Fe(CN)_6^{4-}$ on a basal plane graphite electrode using FTIR Reflectance Spectroelectrochemistry. They proposed a possible mechanism for both reduction and oxidation of the $Fe(CN)_6^{3-}$ and $Fe(CN)_6^{4-}$, assigning certain bands to intermediate species formed within the process.

The hexacyano-metal anions $[M(CN)_6]^{n-}$, have O_h symmetry. They give rise to three fundamental C≡N stretching vibrations.

These are the υ_1(Alg), the υ_3(Eg) and the υ_6(Flμ) modes, with the υ_6 mode having been reported [56] for the solid salts. These are at 2044cm^{-1} and 2118cm^{-1} for the potassium ferrocyanide and ferricyanide respectively. It has been reported [58] that upon adsorption on electrodes, the symmetry of the hexacyano-metal complex ions is reduced, and the Raman active modes, υ_1(Alg) and υ_3(Eg) may become infra-red active.

For the ferrocyanide species, in the solid potassium salt, the frequencies associated with the υ_1 and υ_3 modes have been reported [56] to be at 2098cm^{-1} and 2062cm^{-1} respectively.

For the ferricyanide species, these frequencies for the υ_1 and υ_3 modes have been reported [61] to be at 2135cm^{-1} and 2130cm^{-1} respectively.

The Nujol Mull of the TBA_3 $Fe(CN)_6$ complex gave a sharp peak at 2096.0cm^{-1} corresponding to the C≡N stretch. This is removed from the reported value of 2118cm^{-1} for the potassium salt of ferricyanide, possibly due to the presence of the TBA cation.

A 0.01M solution of $Fe(CN)_6^{4-}$ in 0.1M KCl degassed with nitrogen, was placed into the cell. The cell was turned on at -0.7V, and the current was allowed to decay to a steady value. The background spectra was recorded at -0.7V, and the potential was then scanned in a positive direction up to +0.9V. A

sample spectrum was recorded at this potential, where oxidation of the ferrocyanide to ferricyanide was complete. For both the background and sample spectra, 5 scans were acquired and averaged with $4cm^{-1}$ resolution.

The sample spectrum, at +0.9V, exhibited an upward going peak at $2037cm^{-1}$, but no definite downward going peak was observed. The upward peak at $2037cm^{-1}$ indicates the decrease in ferrocyanide concentration upon switching the potential to 0.9V. The wavelength that this peak occurs at agrees well with previous results [56,57] and it can be concluded that this is due to the consumption of $Fe(CN)_6^{4-}$. As already mentioned no downward going peak was observed at the wavelength corresponding to ferricyanide.

The solution was then held at 0.9V until the current decayed, a spectrum was recorded and this was used as the background spectrum. The potential of the working electrode was then scanned to -0.9V, the current was allowed to stabilise and then a spectrum was recorded.

Figure 4.28 shows the Fourier Transform Infrared Difference Spectrum obtained from the reduction of ferricyanide.

It can be seen that a bipolar band is observed, comprising of a downward peak at $2037cm^{-1}$ and an upward going peak at $2116cm^{-1}$.

The peak position of 2037 and $2116cm^{-1}$ agree well with the reported values [56,57] for ferrocyanide and ferricyanide, in solution, respectively. They are quite close to the values for those of the solid salts especially for the ferricyanide which indicates little interaction with the solvent. This lack of interaction

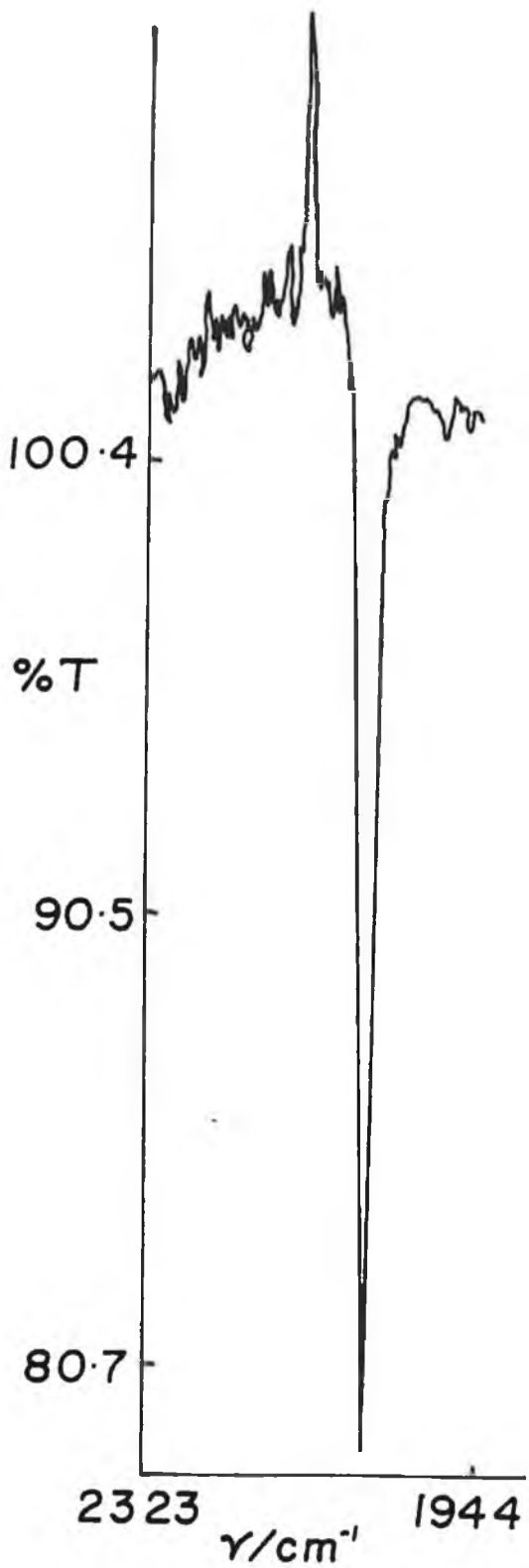

Figure 4.28 Fourier transform infrared difference spectrum for the reduction of ferricyanide, obtained by the oxidation of an aqueous solution of $K_4Fe(CN)_6$ (0.01M) and KCl (0.1M). The background spectrum was obtained at +0.9V. 5 scans were averaged for both the background and sample spectra. Resolution = $4cm^{-1}$.

between ferricyanide and the solvent, is reflected in the value obtained for the factor of (p-q) in Section 4.4. Where p was found to be larger than q, q being the number of water molecules associated with ferricyanide.

An acetonitrile solution of TBA_3 $Fe(CN)_6$ (10mM) and $TBABF_4$ (0.1M) was prepared, degassed and placed into the cell. The cell was switched on at -0.5V and the current was allowed to decay to a steady state value. It was seen earlier that the formal potential of the ferricyanide/ferrocyanide couple was -0.930 Volts (vs. SCE) in pure acetonitrile. Therefore when performing the reflectance infra-red measurements, it was necessary to scan the potential down to -1.2V vs. SCE, to ensure complete reduction of the $[Fe(CN)_6]^{3-}$.

A background spectrum was obtained at 0.5V, with 5 scans being collected and averaged. The potential was then scanned to -1.2V and a spectrum was recorded after the current had decayed.

Figure 4.29 shows the resulting spectrum obtained at -1.2V. As can be seen two upward going bands at $2108cm^{-1}$ and $2094cm^{-1}$ appear, and a downward going band at $2026cm^{-1}$ with a slight shoulder at $2042cm^{-1}$ appear. The two upward going bands correspond to the reduction in concentration of the ferricyanide, and the downward bands correspond to the formation of $Fe(CN)_6^{3-}$. Either the solvent or the replacement of K^+ with TBA^+ is responsible for the difference between Figure 4.28 and 4.29.

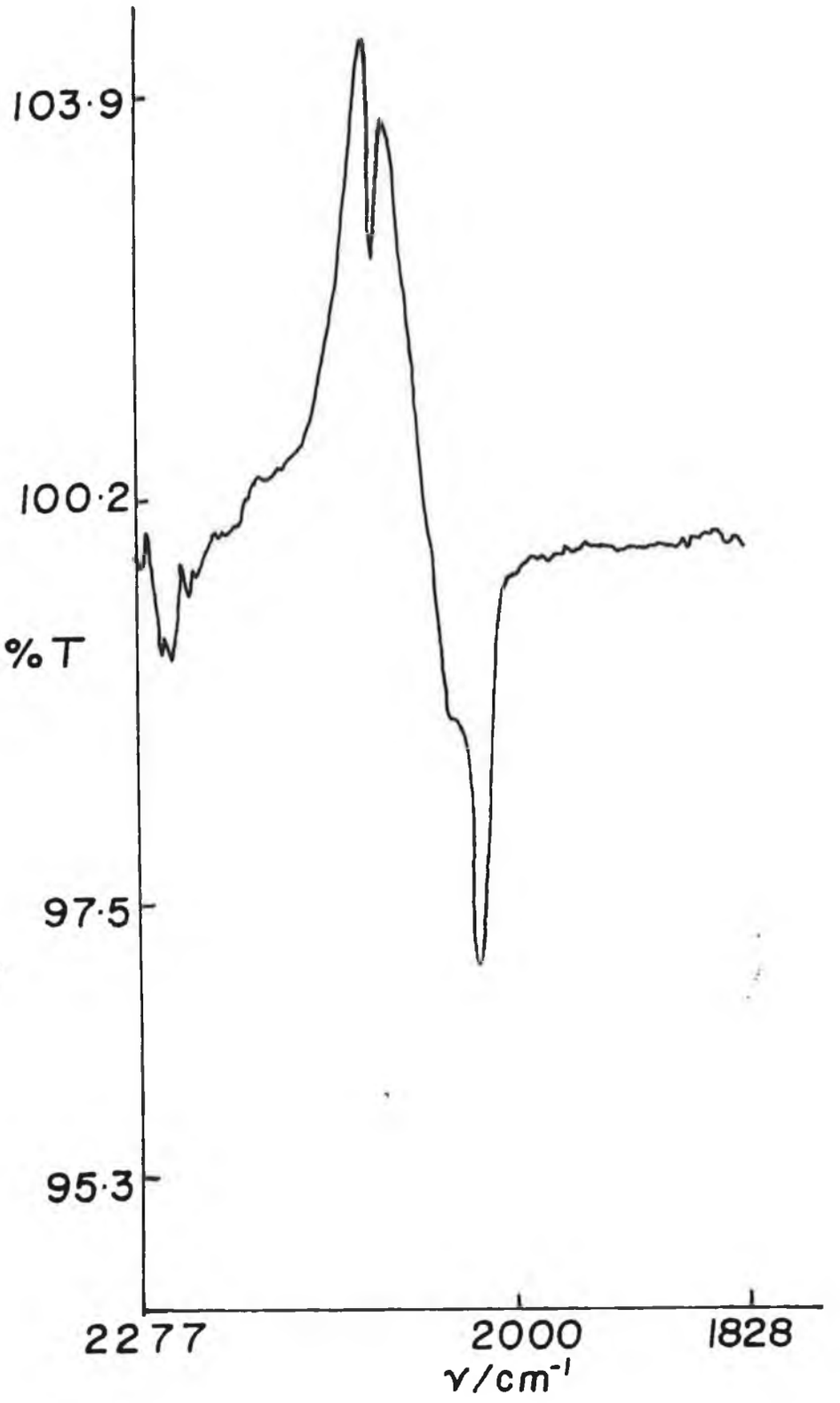

Figure 4.29 Fourier transform infrared difference spectrum for the reduction of a $TBA_3Fe(CN)_6$ (10mM) and $TBABF_4$ (0.1M) in acetonitrile. The background spectrum was obtained at +0.5V, with the sample spectrum recorded at -1.2V. 5 scans were collected and averaged for the background and sample spectra.
Resolution = $4cm^{-1}$.

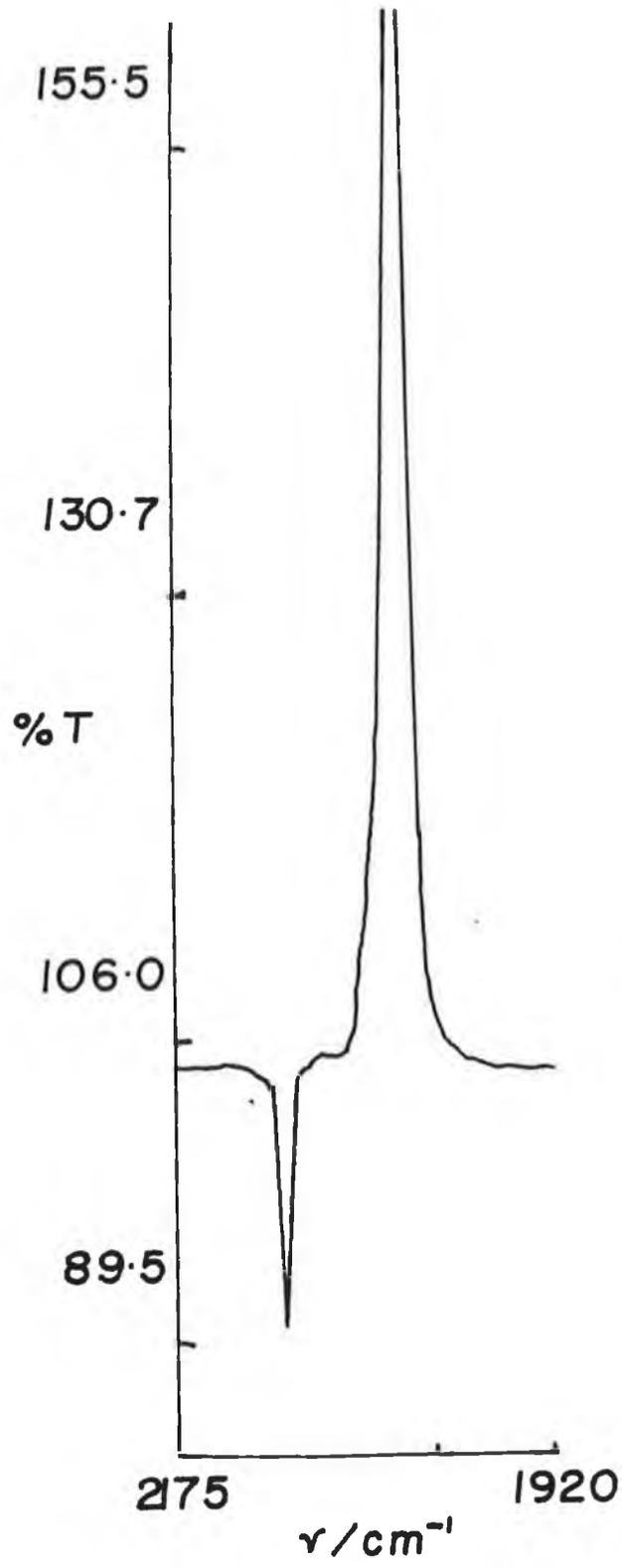

Figure 4.30 Fourier transform infrared difference spectrum for the reoxidation of the ferrocyanide formed as described in Figure 4.29. The background and sample spectra were recorded at -1.2V and 0.5V respectively. 5 scans were averaged for both spectra.

Figure 4.30 represents the spectrum obtained at 0.5V, with the background at -1.2V. This shows reoxidation of the ferrocyanide species, with a downward band at 2103cm^{-1} and an upward band at about 2025cm^{-1} (off scale). This illustrates the creation of ferricyanide (2103cm^{-1}) and the removal of ferrocyanide
(~2025cm^{-1}). By comparing Figure 4.29 and 4.30, the complex upward pointing bands may be due to the superimposition of a downward pointing band (at 2101cm^{-1}) on the broader upper pointing band (due to diffusion of TBA_3 $Fe(CN)_6$ into the thin layer.

4.5.4 CONCLUSION

The reduction and reoxidation of the TBA_3 $Fe(CN)_6$ complex in acetonitrile solution, was monitored spectroscopically. Bipolar bands were observed, with bands in the infra-red occurring corresponding to both ferricyanide and ferrocyanide species. The position of these bands were found to be at lower wavenumbers (~10cm^{-1}) as compared to the potassium salt of ferrocyanide and ferricyanide.

The reason for this possibly being due to the nature of the solvent and/or the background electrolyte cation present.

4.6 REFERENCES

1. 'Topics in Current Chemistry; Electronically Conducting Polymers', Electrochemistry IV, J. Heinze, (1990), pp. 1-47.
2. J.L. Brédas, B. Thémans, J.M. André, J. Chem. Phys., 78 (1982), 6137.
3. W.K. Ford, C.B. Duke, W.R. Salaneck, J. Chem. Phys., 77 (1982), 5030.
4. J.L. Brédas, R. Silbey, D.S. Boudreaux, R.R. Chance, J. Am. Chem. Soc., 105 (1983), 6555.
5. R.R. Chance, J.L. Brédas, R. Silbey, Phys. Rev., B 29 (1984) 4491.
6. J.L. Brédas, J. Mol. Struct., 107 (1984) 169.
7. J.L. Brédas and G.B. Street, Accounts Chem. Res., 18 (1985) 309.
8. M.G. Kanatzidis (1990) December 3, Chemical and Engineering News.
9. M. Mechtachein, F. Devreux, F. Genouol, E. Vieill, J.M. Pernaut and E. Geniés, Synth. Met. 16 (1986) 59.
10. J.F. Oudard, R.D. Allendoerfer and R.A. Osteryoung, J. Electroanal. Chem., 241 (1988) 331.
11. G. Zotti and G. Schiavon, Synthetic Metals. 30 (1989) 151-158.
12. W.P. Su, J.R. Schrieffer and A.J. Heeger, Phys. Rev. Lett. 42, 1698, (1979).
13. M.J. Rice, Phys. Lett. 71A, 152 (1979).
14. A.O. Patil, A.J. Heeger and F. Wuoll, Chem. Rev. (1988), 88, 183-200.
15. Ikehata, S., Kaufer, J., Woemer, T., Pros, A., Druy, M.A., Sivak, A., Heeger, A.J., and MacDiarmid, A.G. (1980) 'Solitons in Polyacetylene Magnetic Susceptibility', Phys. Rev. Lett. 45, 1123-1126.

16. T.C.Chung, F.Moraes, J.D. Flood, and A.J.Heeger, (1984) 'Solitons at High Density in Trans - (CH)x; Collective Transport by Mobile Spinless, Charges Solitons' Phys. Rev. B. 29, 2341-2343.

17. E.J.Mele, and M.J.Rice, (1981) 'Semiconductor Metal Transition in Doped Polyacetylene' Phys. Rev. B. 23, 5397-5412.

18. K.Harigaya, and A.Terai, (1991) 'On a Metal-Insulator Transition of Disordered Conducting Polymers' Solid State Commun (in print).

19. F.Moraes, J.Chen, T.C.Chung, A.J.Heeger, (1985) Synth. Met. 11, 271-292.

20. J.Chen., A.J.Heeger, (1988) Synth. met., 2A, 311-327.

21. S.Kivelson, and A.J.Heeger, (1985) Phys. Rev. Lett. 55, 308-311.

22. E.M.Conwell, and S.Jeyadev, (1988) Phys. Rev. Lett. 61, 361-364.

23. E.M.Conwell, H.A.Mizes, and S.Jeyadev, (1989) Phys. Rev. B40, 1630- 1641.

24. M.Dinter, Phys. Rev. B39, 8423-8433.

25. B.R.Bulka, (1988) Synth. Met. 24, 41.

26. A.Takahashi, and H.Fukutome, (1989) Synth. Met. 28, D469-D475.

27. S.Stafström, (1991) Phys. Rev. B (in press).

28. G.W.Bryant, and A.J.Glick, (1982) Phys. Rev. B26, 5855-5866.

29. S.Stafström, and J.L.Brédas, (1988) Phys. Rev. B38, 4180-4191.

30. H. Mao, J. Ochmanska, C.D. Paulse and P.G. Pickup. Faraday Discuss. Chem. Soc., (1989), 88, 000-0001.

31. Adir Bar-Lev (1984) 'Semiconductors and Electronic Devices' 2nd Edition.

32. C.B. Duke, Mol. Cryst. Liq. Cryst. 50, 63 (1979).

33. T. Amemiya, K. Hashimoto and A. Fujishima, K. Itoh (1991) Electrochem. Soc., Vol. 138, No. 10, 2845-2850.

34. D. Blackwood and M. Josowicz. J. Phys. Chem., (1991), 95, 493-502.

35. N.S. Isaacs (1966) J. Chem. Soc. (B) 1053.

36. J.E. Frey, R.D. Cole, E.C. Kitchen, L.M. Supresant, M.S. Sylwestrak. J.Am. Chem. Soc. (1985) 107, 748-755.

37. Z. Rappoport, J. Chem. Soc., (1963) 4498.

38. D.D, Holder and C.C. Thompson. J.C.S. Chem. Comm. (1972) 277-279.

39. R.E. Noftle and D. Pletcher. J. Electroanal. Chem., 293 (1990) 273-277.

40. S.N. Hoier, D.S. Ginley and S.M. Park. J. Electrochem. Soc., Vol. 135, 91(1988).

41. D.D. Cunningham, A. Galal, C.V. Pham, E.T. Lewis, A. Burkhardt, L.L.Davidson, A. Nkansah, O.Y. Ataman, H. Zimmer and H.B. Mark Jr., J. Electrochem. Soc. 135, 2750 (1988).

42. D.E. Stilwell and S.M. Park. J. Electrochem. Soc. 136, 427 (1989).

43. E.M. Genies and J.M. Pernaut. J. Electroanal. Chem., (1985), 191, 111-126.

44. P. Marque and J. Roncali. J. Phys. Chem. (1990), 94, 8614-8617.

45. J. Heinze, J. Mortensen, K. Müllen, R. Scherk, J. Chem. Soc., Chem. Commun. (1987), 701.

46. H. Kato, O. Nishikawa, T. Matsui, S. Honma, H. Kokado, J. Phys. Chem.(1991), 95, 6011-6014.

47. R.A. Jones, G. Bean, 'The Chemistry of Pyrrole', Academic Press, London, (1977) Pg. 463.

48. H. Kata, O. Nishikawa, T. Matsui, S. Honma, H. Kokado, J. Phys. Chem. (1991), 95, 6014-6016.

49. S.B. Khoo, J.K. Foley and S. Pons, J. Electroanal. Chem., 215 (1986) 273-285.

50. S. Pons, S.B. Khoo, A. Bewick, M. Datta, J.J. Smith, A.S. Hinman and G. Zachmann. J. Phys. Chem. (1984), 88, 3575-3578.

51. M. Itoh., J. Amer. Chem. Soc. (1970) Feb. 25, 886.

52. P.K. Mascharak, J. Inorganic Chem. Vol. 25, No. 3, (1986) 245-247.

53. V. Gutmann, Electrochimica Acta, (1976), Vol. 21, 661-670.

54. L.M. Peter, W. Durr, P. Bindra and H. Geriocher. J. Electroanal. Chem., 71(1976) 31.

55. D.J. Blackwood and S. Pons, J. Electroanal. Chem., 244 (1988) 301-305.

56. K. Kunimatsu, Y. Shigematsu, K. Vosaki and H. Kita, J. Electroanal. Chem., 262 (1989) 195-209.

57. J. Zhong, Q. Yin, S. Cai and A. Fujishima. Electrocanalysis, 5, (1993) 517-520.

58. C. Korzeniewski, M.W. Severson, P.P. Schmidt, S. Pons and M. Fleischmann. J. Phys. Chem. 91 (1987) 5568.

CHAPTER 5

INVESTIGATION OF CONDUCTING POLYMER LAYERS FOR A GAS SENSOR

5.1 INTRODUCTION

Due to increasing environmental concern in the past few years a need for new sensors for measuring both physical and chemical parameters has been created.

Sensor technology is a fast growing field of research with several review articles, describing the principles and applications of chemical and biological sensors, being available [1].

Electrochemical sensors have received much interest in recent years, and they fall into two main categories, potentiometric and amperometric sensors.

Potentiometry involves measuring the potential difference across a membrane with respect to a reference electrode. The membrane employed is specific for a particular species which can be extracted into the membrane from the external phase, thereby setting up a potential difference between the two phases. Several problems can be encountered within potentiometric sensors, the presence of liquid junction potentials between the reference and membrane, presence of interferences, and temperature correction must be undertaken. Also since the

interfacial potential is related to the activity of the species in the two phases, conditions may arise where the activity coefficient is not equal to 1, so that the activity does not equal concentration.

One of the first and most important potentiometric sensors to be discovered was that of the glass electrode [2] which is used to measure pH by monitoring the hydrogen ion activity. The mechanism is believed to involve an ion exchange mechanism between the hydroxyl ions on the glassy hydrated surface [3]. Common interferents encountered were the sodium and potassium ions. This has led to specialised glass electrodes for particular metal ions [4] being developed.

The development of membrane based potentiometric sensors containing ion binding or partitioning agents which selectively extract the species under study from the contact solution has received great attention. The binding of specific catalysts such as enzymes onto electrode surfaces by means of a supporting matrix has been researched [5]. Also field effect transistors where the gate is coated with a specific enzyme have been used to monitor for glucose [6].

Amperometric sensors are based on the principle of controlling an external potential applied to an electrode, and the resulting current being measured. The potential is held in a region where the rate of the reaction of the species under investigation at the electrode surface is mass transport controlled thereby eliminating the effect of slow kinetics. The current that flows can be then related directly or indirectly to the analyte's concentration. The classic example of an amperometric chemical sensor is one of industrial importance, that is, the development of the Clark oxygen sensor.

The oxygen diffuses through a thin Teflon or a fluorinated ethylene-propylene copolymer membrane. Behind the membrane is an electrolyte solution containing chloride ions, in which are immersed a platinum or gold working electrode. The working electrode is held at -0.8V relative to a Ag/AgCl electrode, at which potential oxygen reduction occurs. Diffusion of the oxygen through the membrane is the rate limiting step and it depends on the gradient of the O_2 partial pressure across the membrane.

Several amperometric biosensors have been developed recently. Beh et al [7] have developed a glucose biosensor based upon a modified electrode based on a mixture of carbon paste and ferrocene with glucose oxidase immobilised over the indicator electrode. Wring et al [8] have developed screen printed carbon electrodes chemically modified with selected ferrocene, phthalocyanine and hexacyanoferrate (lll) derivative mediators for the determination of reduced glutathione. Metallophthalocyanines mixed with polystyrene in a suitable solvent have been found to be good mediators for oxygen reduction. When a glucose oxidase overlayer was deposited, glucose could be determined. Ferrocene-polystyrene composites have also been used for the same purpose [9].

Besides electrochemical sensors, there are numerous types of sensors available. Surface acoustic wave devices have been explored with review articles being available [10]. Chuang et al [11] developed a thin membrane surface acoustic wave vapour sensing device. Monitoring of gases such as nitrogen dioxide has been achieved using a surface acoustic wave gas sensor with metallophthalocyanines as chemical interfaces[12]. Recently Zhang and Zelles [13] developed a surface acoustic wave sensor coated with the square-planar Pt(ll)-olefin π - complex $PtCl_2$- $[(1\text{-hexene})(\text{pyridine})]_2$ for the detection of 1,3

butadiene. The sensor response is based upon the displacement of two 1-hexene molecules by each butadiene molecule and the formation of the bridged complex $[PtCl_2$ (pyridine)$]_2$ 1,3 butadiene. This elegant system allows specificity, which is a problem with many sensors. Other mass sensitive systems such as peizoelectric crystals were first employed by King [14] for gas detection. Later a peizoelectric crystal detector was developed for hydrocarbons in the atmosphere [15]. Recently [16] piezoelectric crystals coated with 4-ethyl-3-thiosemicarbazide and 2,6-diacetylpyridine were used for the determination of formic acid vapour, which is present in significant amounts in the atmosphere and in acid rain.

All of the aforementioned methods, for sensor applications, have been extensively studied in relation to gas sensing. Conducting polymers have been investigated as new sensitive matrices to fabricate chemical or electrochemical sensors, with review articles on the subject being available [17]. It has been stated that electroconducting conjugated polymers are valuable within the field of sensor technology in two ways. Firstly the polymer films can be used as sensitive components where the electronic conductivity of the film is modulated by the interaction with various substrates. Secondly the polymer film can act as a matrix for specific immobilisation of molecules that are capable of substrate recognition.

Miasik et al [18] used polypyrrole films electrochemically deposited over electrode arrays, to obtain responses to NH_3, NO_2 and H_2S gases. Blanc et al [19] performed gas sensing experiments on polypyrrole films doped with $[Fe(CN)_6]^{4-}$ and exposed this film to a variety of gases such as O_2, NH_3, NO_2 in N_2 or air, with NO_2 having a poisoning effect upon the polymer films.

Hanawa et al [20] showed that the gas sensitivity of polypyrrole films to NO_2 in an N_2 atmosphere was enhanced by the elimination of the dopant anions, using an electrochemical reduction procedure. They used Fourier Transform Infrared Spectrometry to show that polypyrrole films which had been reduced and then exposed to NO_2, led to the formation of NO_2^- ions. They concluded that the gas sensitivity results mainly from chemical doping by NO_2.

Bartlett et al [21] describe the use of dual microband gold electrodes with polypyrrole deposited across the electrodes, as gas sensitive chemiresistors. Results were obtained [22] for the response of the polymer to methanol vapour. Reversible and rapid responses were obtained. They found that the time course and concentration dependence of the resistance changes are consistent with a model in which the methanol interacts with sites within or on the surface of the film, leading to an increase in the resistance. Four different conducting polymers [23] were employed as sensors for organic vapours. Upon exposure to vapours the polymers showed conductivity changes that were rapid and in general reversible at room temperature.

The response of polypyrrole films to electron acceptor gases such as PCl_3, SO_2 and NO_2 at room temperature were investigated by Hanawa and Yoneyama [24]. They found that the polymers only responded to these gases in the reduced state.

Recently Blackwood and Josowicz [25] studied the interactions between conducting polymers and organic vapours spectroscopically. They concluded that organic vapours were interacting with the polymer layer by either donating electrons into the film or accepting electrons from the film. Little work has been done in trying to characterise the interactions between conducting polymer layers

and vapours. Slater et al [26] found that the responses of polypyrrole layers to certain vapours were all of a Fickian type.

Topart and Josowicz [27] proved that a bulk absorption occurs upon the interaction between polypyrrole and methanol vapour, also their data point to the formation of a weak charge transfer complex

In this chapter, the responses of various polypyrrole layers, deposited across interdigital array electrodes, to organic and inorganic vapours are presented. A spectroscopic investigation of the interaction between organic vapours and polypyrrole layers is presented. Finally preliminary results on the use of Prussian Blue as a gas sensing element within a gas sensor are described.

5.2 EXPERIMENTAL

5.2.1 FABRICATION OF GOLD INTERDIGITAL ARRAYS

The interdigital arrays take the form of comb like electrodes which are designed in such a way that no contact is made between the two sets of gold electrodes. The electrodes are deposited onto an insulator, namely mylar, by a process known as microlithography. This procedure was carried out elsewhere using a mask designed for this purpose [29].

The first step in the procedure involves washing the insulator (cut to the correct dimensions) with methanol to remove any grease and then the insulator sheet is dried.

Gold is then sputtered onto the substrate and a layer of photoresist is then placed on top, by means of spin coating.

The substrate is then placed in the oven at 80-90°C for 20 minutes. After which the mask is placed on top of the substrate and this is then put under U.V. light for approximately 1 minute. The substrate is then placed in a 1:1 mixture of water and a developer (Isofine K820) and submerged. After which it is soaked in water, aqua regia and then finally water.

The remaining photoresist is then dissolved off with acetone, and finally any traces of acetone are removed by methanol. The processed sheets are then kept clean in a sealed container until encapsulation of the electrodes is undertaken.

5% SO_2 in air was purchased from Air Products Ltd. and used directly.

5.2.2 ENCAPSULATION OF GOLD MICROBAND ELECTRODES

The encapsulation of the gold interdigital arrays involves two main steps. In the first step the sheet of processed interdigital arrays, is cut into separate electrodes. Two electrical connections are made on either side of the array, by epoxying (Silver loaded epoxy, Radionics) two wires, one on each side. The conductive ink is then cured in the oven at 50°C for 1 hour.

The second step involves supplying the mechanical strength to the two electrical connections by means of epoxy resin (Araldite). It was ensured that the conductive ink was fully cured before the epoxy resin was used to cover the connections. It was also important to ensure that all the sputtered gold was covered, except the digits, with epoxy to ensure that the polymer was only deposited on top and across the digits. This procedure proved difficult for the microband electrodes, as the epoxy tended to spread out over the digits upon drying. This was not a problem for the screen printed carbon ink electrodes, as the area of the electrode surface was larger and easier to deal with.

However to ensure that the digits were not covered with epoxy resin, a plastic straw was cut into several cylindrical pieces. These pieces were then epoxyed

on top of the digits and all remaining exposed gold was fully encapsulated. This was performed on the screen printed carbon ink electrodes, and it helped to ensure that the exposed area, for polymer growth, was kept constant for each array.

It is important to note that three main types of gold arrays were employed. They differed only in the interdigital spacing, and digit widths. These arrays had digit widths of 10, 30 and 50 microns and similar spacing.

Screen printed carbon electrodes were fabricated using a mask, initially prepared in house using a screen (120T, Serigraf) and drawn designs. Subsequently, a screen made elsewhere (Screentech) with spacings and digit widths of 700 microns was employed. The ink (Electrodag 432SS, Acheson Colloids) was used for screen printing and the substrate was mylar (Agar supplies) or Micanite (a type of thin circuit board).

5.2.3 DEPOSITION OF POLYPYRROLE LAYERS ON TO INTERDIGITAL ARRAYS

Before use, each electrode was thoroughly washed with deionised water. Electrochemical polymerisation was carried out from degassed aqueous solutions of pyrrole (0.1M) and supporting electrolyte (0.1M). The working electrode was the interdigital array, with a carbon rod as the auxillary and a S.C.E. as the reference electrode. All polypyrrole films were grown by holding the potential of the working electrode at a constant value until the polymer grew across the inter -electrode gap. The optimum conditions of electrodeposition for the

polypyrrole layers were determined by varying the monomer and electrolyte concentration.

After deposition, the films were thoroughly washed with deionised water and allowed to dry in the open atmosphere. The resistance of the deposited polypyrrole film was then determined by means of a multimeter (Keithley 169 Multimeter).

A ramp generator (H.B. Thompson 16 bit), a potentiostat (Edt ECP 100) and an electronic integrator (Sycopel DP301S) linked to a J.J. Lloyd PL3 X-Y recorder were used for the electrodeposition and all the electrodes characterisation experiments.
Figure 5.1 shows an SEM of the gold interdigital (10 μm spacing) electrode. The SEM was taken with an ISI Super III A SEM in the DIT.

Figure 5.2 shows the circuit used for the gas sensing experiments, where the interdigital array electrode coated with the polymer film forms one arm of a Wheatstone Bridge arrangement.

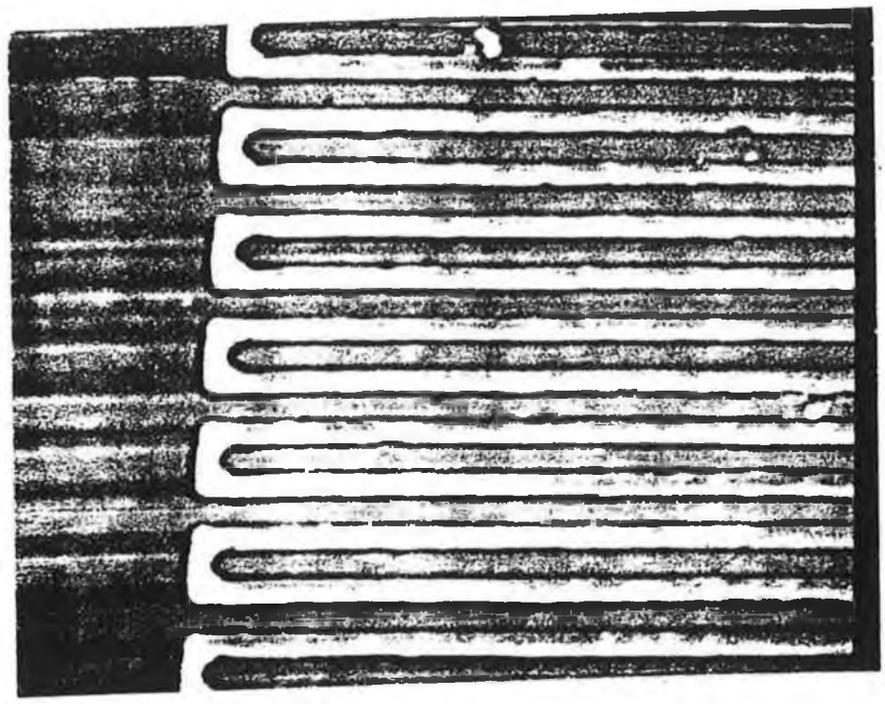

Figure 5.1 SEM of the gold interdigital (10μm spacing) electrode.

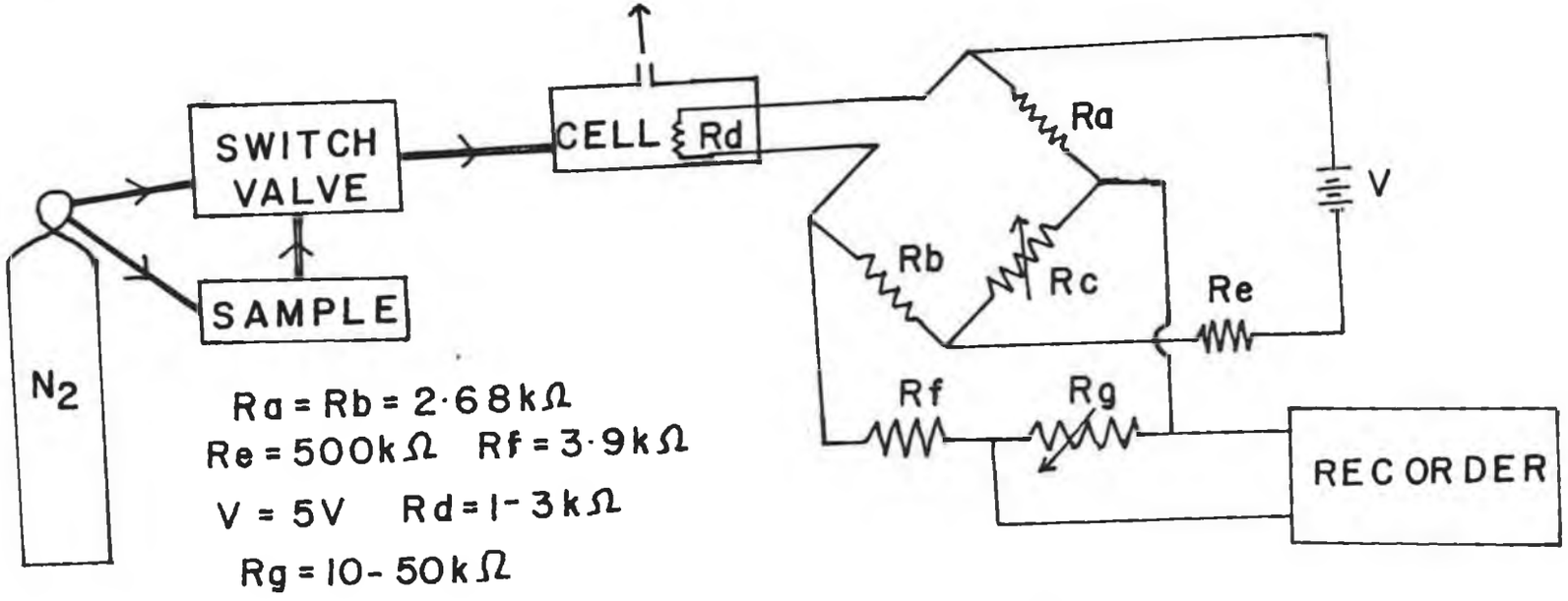

Figure 5.2 Circuit employed for gas-sensing experiments.

5.3 RESULTS AND DISCUSSION

5.3.1 CHARACTERISATION OF GOLD INTERDIGITAL ARRAYS AND SCREEN PRINTED CARBON INK ELECTRODES

Before film growth all electrodes were washed thoroughly with deionised water. Both sets of electrodes were checked, by means of measuring the resistance between the two sets of digits, to ensure that they were not shorted. For all electrodes employed, an infinite resistance was obtained for the interdigital resistance, this ensured that shorting had not occurred.

The gold interdigital arrays were characterised in terms of a steady state current obtained when the arrays were cycled in an aqueous solution of $K_3Fe(CN)_6$ (5mM) with KCl(1.0M) as the supporting electrolyte. One set of digits was used as the working electrode and the other as the auxiliary electrode. A S.C.E. was used as the reference electrode. The solution was degassed for approximately 10 minutes and then cyclic voltammetry was performed.

A sigmoidal plot should occur at slow scan rates. This arises due to the fact that linear concentration profiles develop between the working and auxiliary electrodes.

The cell was switched on at 0.5V, and then the potential was scanned in a negative direction at a variety of scan rates.

Figure 5.3 shows the cyclic voltammogram obtained for a 30μm interdigital gold electrode, at a scan rate of 100mV/s. It can be seen that no definite steady state current is obtained, with hysteresis being present. It was noted that on using the 50μm electrode, a worse situation arose, with no steady state current and a large amount of hysteresis. On reducing the scan rate to 10mV/s, no definite steady state current was obtained and hysteresis, even though on a smaller scale, was still present.

However, Figure 5.4 (a) to (c) shows the cyclic voltammograms obtained for the screen printed carbon ink interdigital arrays in $K_3Fe(CN)_6$ (5mM) and KCl (0.1M) solution. The gap between these digits was typically of the order of 500 microns. It can be seen that these electrodes yielded an apparent steady state current (Figure 5.4 (a), (b) and (c)) with decreasing hysterisis with scan rate. It can be seen that the kinetics of electron transfer of these electrodes are very slow probably due to the nature of the ink employed (Electrodag 432SS, Acheson Colloids, Prince Rock, Plymouth PL4 OSP).

In conclusion, the sputtered interdigital gold arrays are not that well behaved. The poor behaviour of the gold arrays could possibly be due to the problem of encapsulation, mentioned earlier, and possibly the gold's surface not being completely clean. It proved difficult to polish these electrodes, as has been done previously [21] for reusable gold dual microband electrodes. The carbon ink electrodes were found to be very sluggish where electron transfer was concerned.

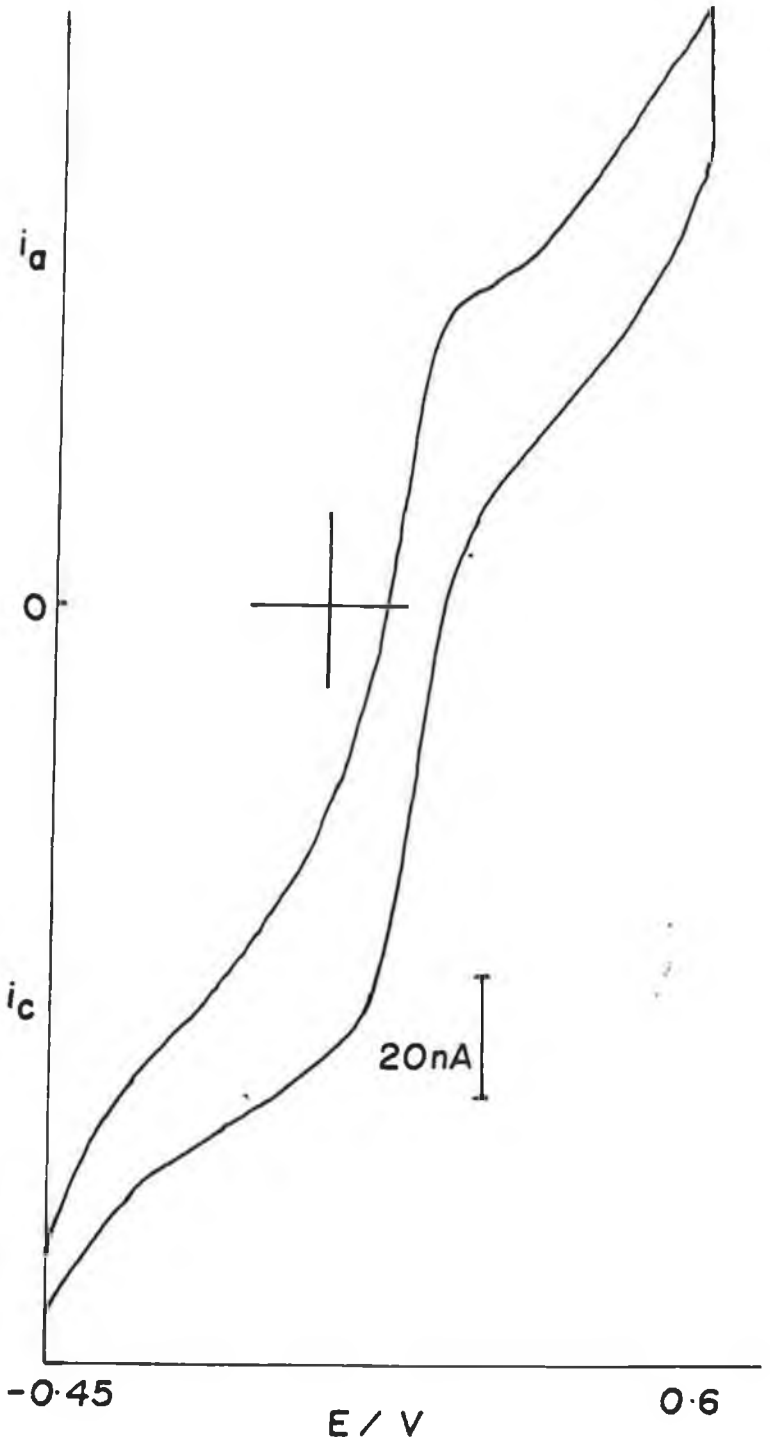

Figure 5.3 Cyclic voltammogram of a 30μm interdigital gold electrode in an aqueous solution of $K_3Fe(CN)_6$ (5mM) with KCl (1.0M). Scan Rate = 100mV/s.

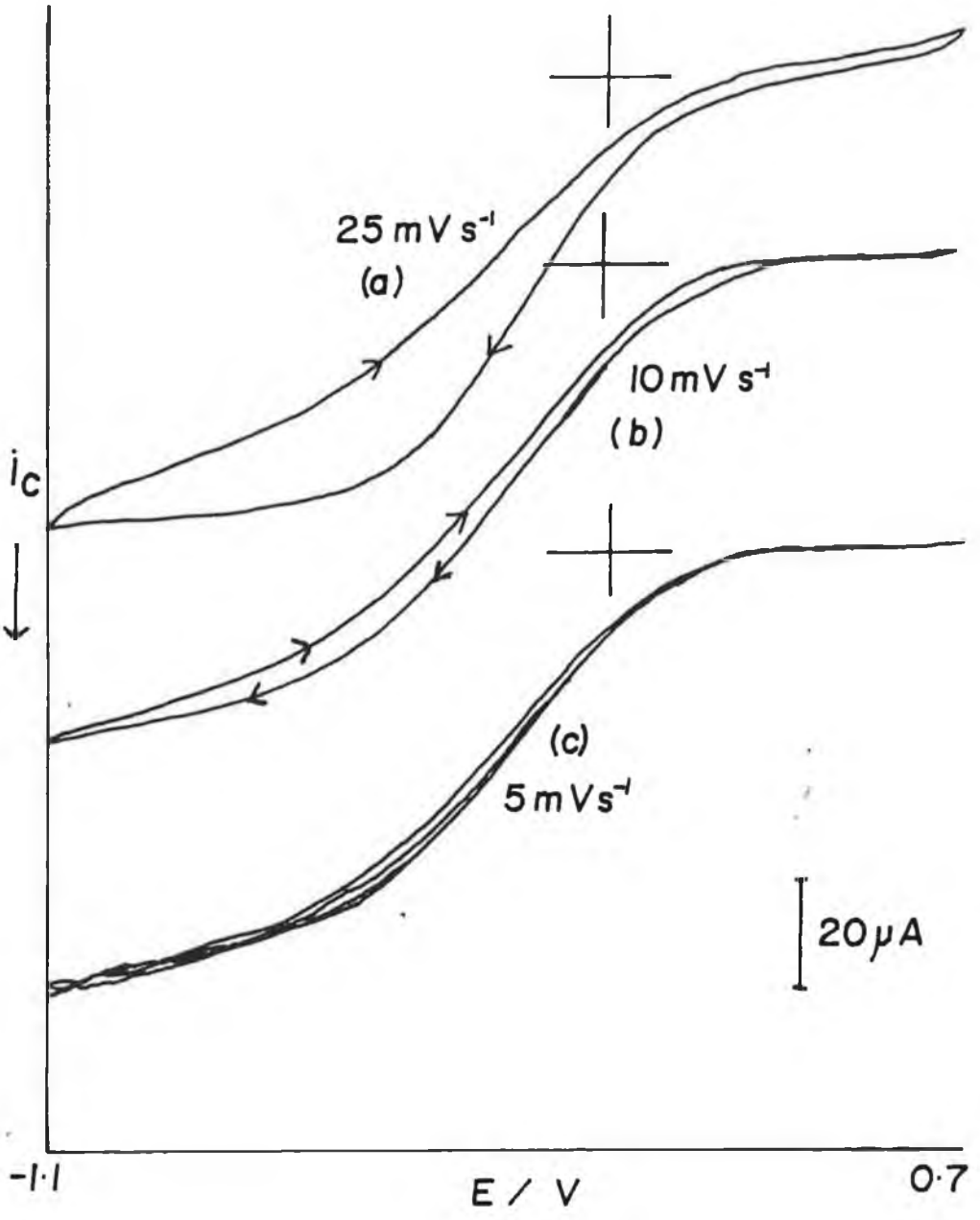

Figure 5.4 Cyclic voltammogram of a 500μm interdigital carbon ink electrode in an aqueous solution of $K_3Fe(CN)_6$ (5mM) with KCl (0.1M).

5.3.2 PRELIMINARY GAS SENSING EXPERIMENTS

Two polypyrrole layers were deposited on screen printed carbon ink electrodes, allowed to dry and their response to methanol vapour was investigated. The screen printed carbon ink electrodes employed were manufactured in house as described above.

The layers were deposited onto the arrays by holding the potential of the working carbon ink electrode at 0.9V vs. SCE, in an aqueous solution of pyrrole (0.1M) and the supporting electrolyte (0.1M). The layers were a polypyrrole perchlorate layer and a polypyrrole dodecylbenzenesulphonate layer. The charge used to deposit these two layers was monitored, being 263mC for the $PPClO_4$ layer and 2,676mC for the PPDBS layer. The difference in charge used can be accounted for by the fact that the $PPClO_4$ layer adhered better to the micanite substrate than the PPDBS layer, thereby allowing less charge to be passed in order that the polymer bridged the gap between the two digits.

The layers were washed with deionised water and allowed to dry. The resistance of the layers, $PPClO_4$ and PPDBS, was then measured and found to be between 1-3 kΩ

The electrode with the deposited polypyrrole layer was placed in the wheatstone bridge arrangement, and the response of the layer to a concentration step of methanol vapour was monitored as previously described in the experimental section.

Figure 5.5 (a) and (b) shows the response of the two polypyrrole layers, $PPClO_4$ and PPDBS, on exposure to the methanol vapour at room temperature respectively. The responses are seen to be stable and reproducible, with the PPDBS layer showing a slower response. This slower response could be due to the fact that the PPDBS layer deposited was thicker, as seen by the charge passed during the electrodeposition process.

These preliminary results for the response of polypyrrole layers were encouraging. Further work was carried out by use of the microband gold arrays and of the industrially made carbon ink interdigital electrodes.

In order to help elucidate the response profiles obtained for the polypyrrole layers exposure to gas, the responses were drawn using a Fickian axis, that is, signal versus the square root of time.

Figure 5.6 shows such a plot obtained for the response of the polypyrrole dodecylbenzenesulphonate layer to a concentration step of methanol vapour, shown in Figure 5.5 (b).

A Fickian response is obtained as the plot is linear, indicating a constant diffusion coefficient, and also that the interaction of the polymer layer with methanol vapour is diffusion controlled.

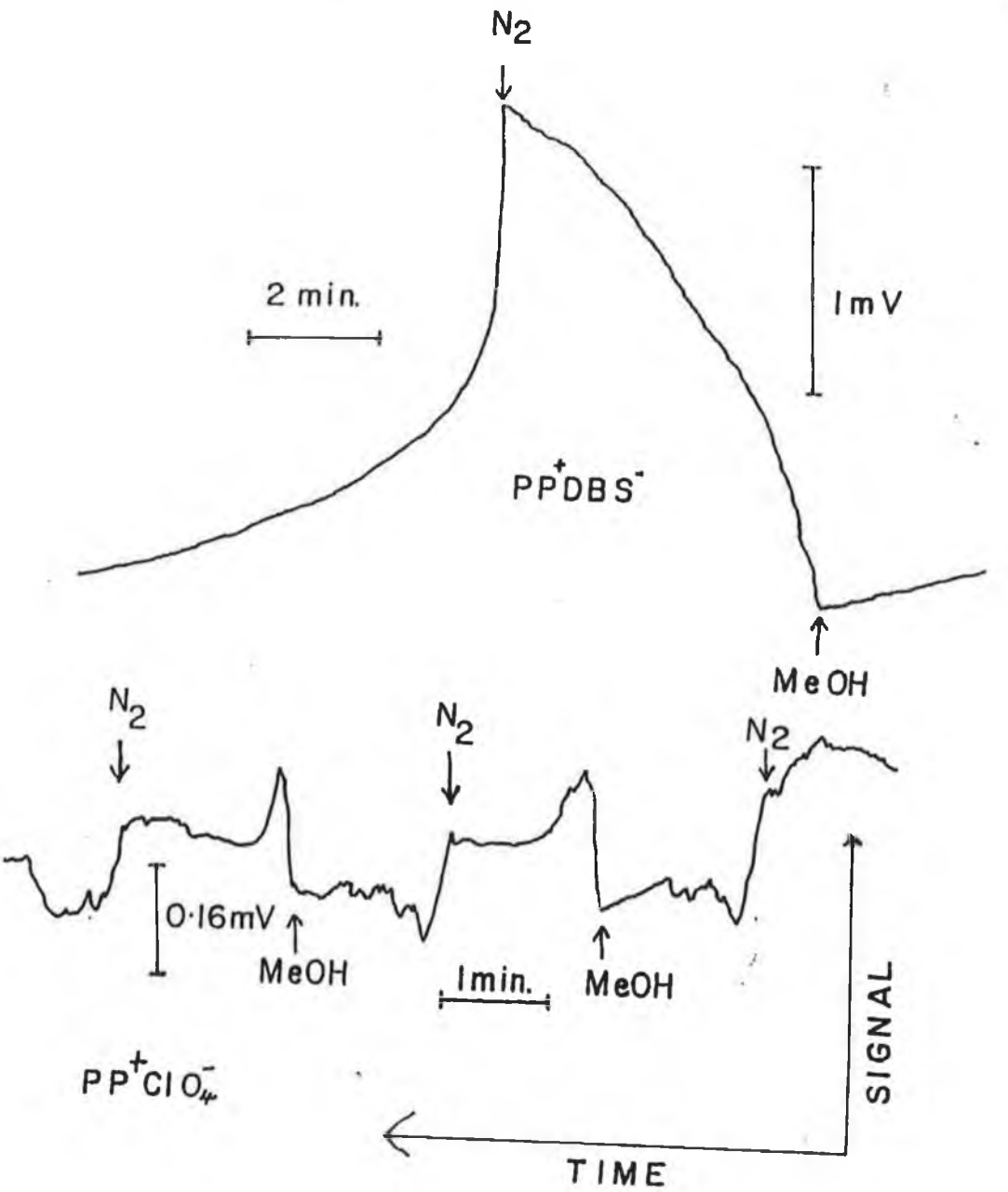

Figure 5.5 Response of two polypyrrole layers (a) $PPClO_4$, (b) PPDBS to methanol vapour at room temperature.

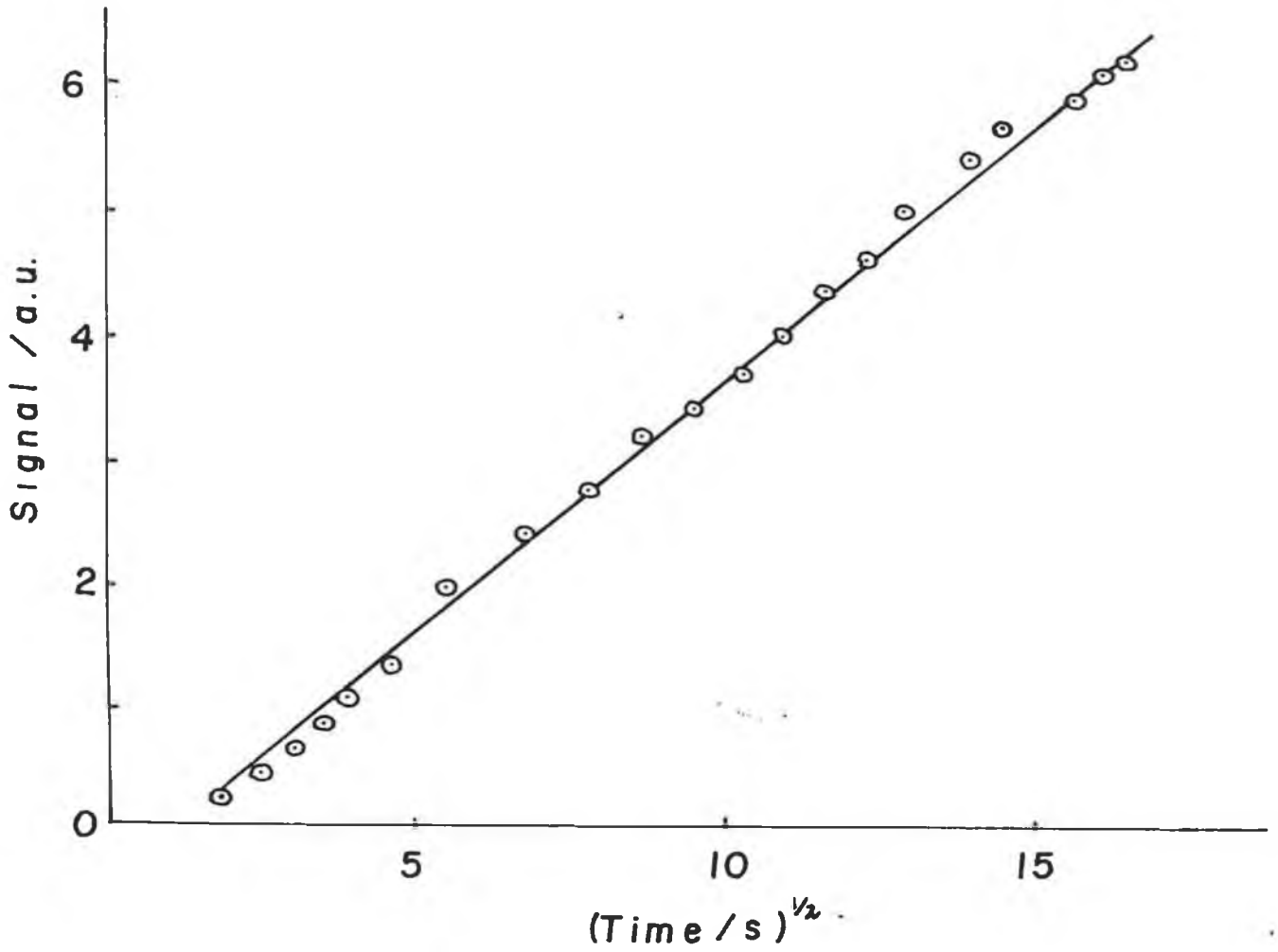

Figure 5.6 Plot of √t versus signal for the response of the PPDBS layer to methanol vapour, as seen in Figure 5.5 (b).

5.3.3 RESPONSE OF POLYPYRROLE FILMS DEPOSITED ACROSS GOLD MICROBAND ELECTRODES TO VARIOUS VAPOURS

A polypyrrole Cu(II) tetrasulphonated phthalocyanine layer (PPTSP) was deposited across a 10μm gold microband electrode, by holding the potential of the gold array at +0.9V in an aqueous solution of pyrrole (0.1M) and Cu(II) tetrasulphonated phthalocyanine (1×10^{-3}M). The electrode was kept at this potential until 50×10^{-3} coulombs of charge had been deposited. The layer was then rinsed with deionised water and allowed to dry. The resistance of the electrode was found to be 2.64Ω

The coated IDA electrode was then placed in the Wheatstone bridge arrangement, shown in Figure 5.2, as its response to 5% SO_2 in Air in a N_2 stream along with other vapours was investigated.

Figure 5.7 (a) shows the response profile obtained, it can be seen that the response is not always simple. It can be seen that all the responses obtained are rapid, with response times in the order of seconds. This can be explained by the thinness of the polymer film, as compared to the thick polypyrrole films deposited across the screen printed carbon ink electrodes.

It can also be seen that the PPTSP layer showed a response upon exposure to n-hexane. This was curious due to the non-polar nature of the n-hexane molecule. It must be emphasised that the polymer layer has already responded to SO_2, methanol and water vapour. Therefore the resistance change observed upon

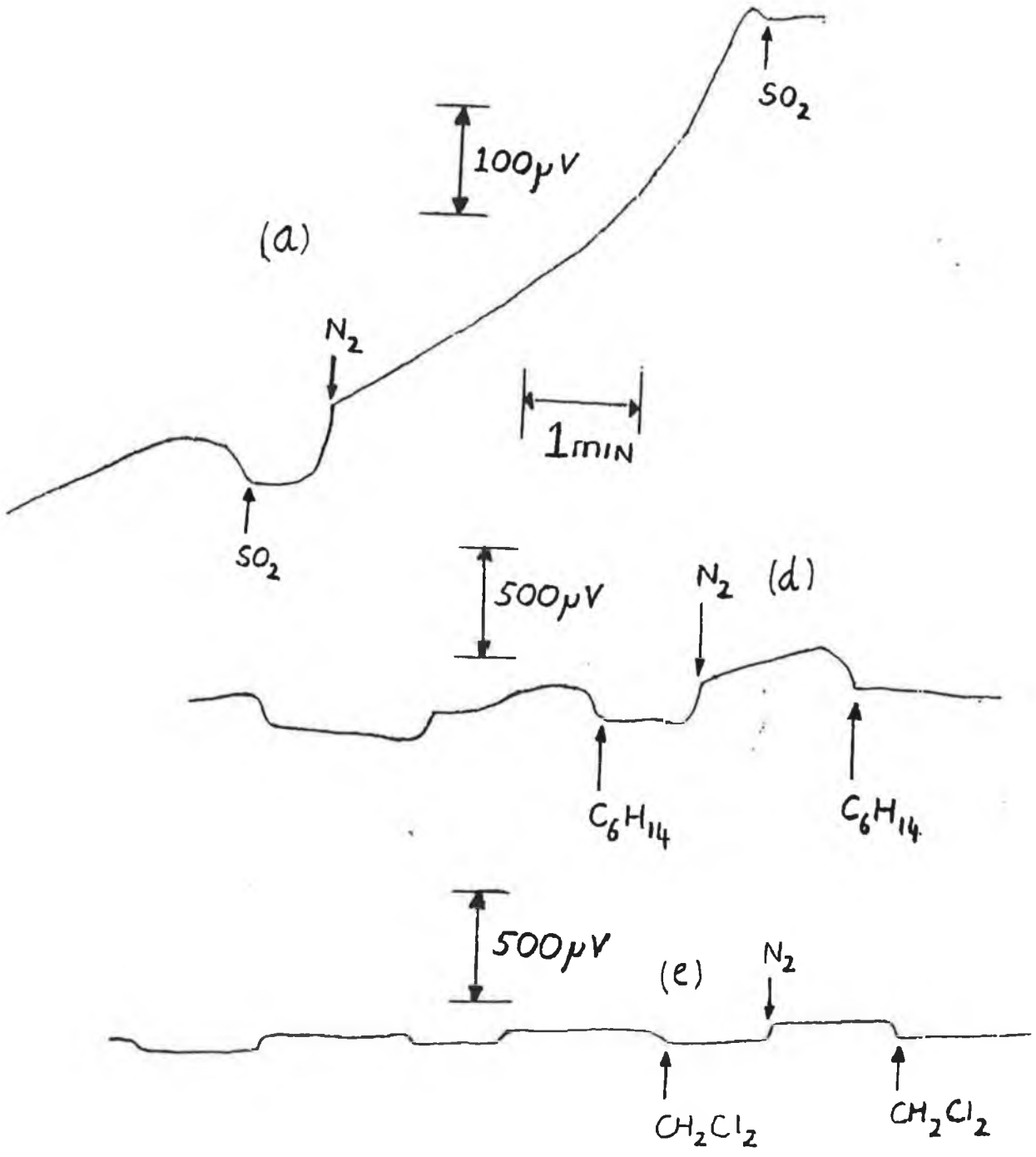

Figure 5.7 Response profiles for a PPTSP layer deposited across a 10μm gold electrode, by holding the potential at 0.9V in an aqueous solution of pyrrole (0.1M) and Cu(II) TSP ($1x10^{-3}$M), to a variety of gases.
(a) 5% SO_2 (d) hexane, C_6H_{14} (e) CH_2Cl_2 (c) H_2O (b) CH_3OH.

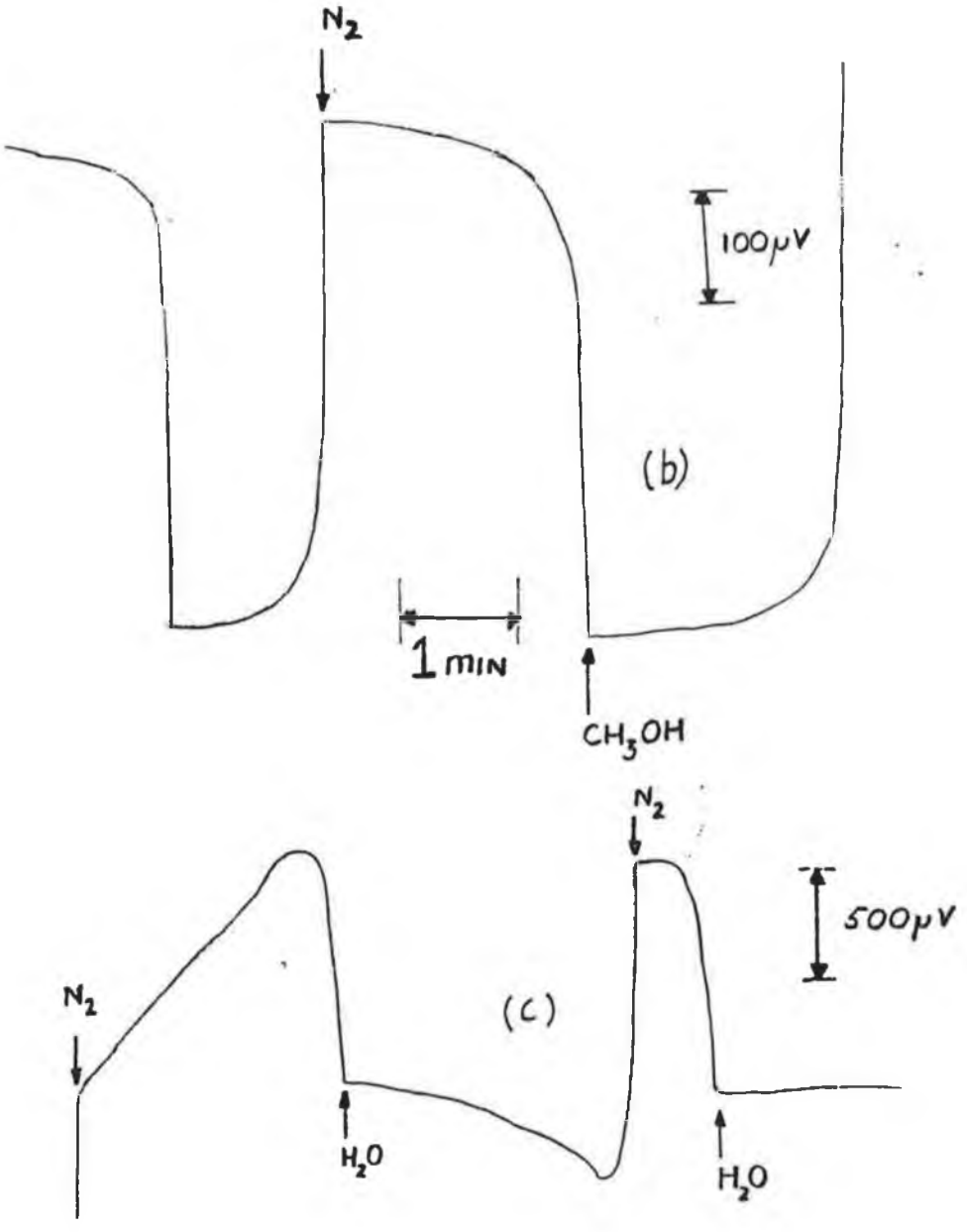
N2
100μV
(b)
1 MIN
CH3OH
N2
500μV
N2
(c)
H2O
H2O

exposure of the PPTSP layer to n-hexane, could possibly be due to the displacement of trapped gaseous dopants within the layer or a 'history effect'.

The PPTSP was not studied further as its response to sulphur dioxide was sluggish and difficult to characterise. The main aim was to find a doped polypyrrole layer which could respond to 5% SO_2 rapidly and reversibly.

However, a qualitative concentration study was performed upon the exposure of the PPTSP layer to methanol vapour. Figure 5.8 shows the resulting response time profiles obtained when various quantities of liquid methanol were directly injected into the nitrogen stream.

Two main points should be noted about the response profile, namely, that, there is an increase in signal with increasing amount of methanol and that the time for the signal to return to baseline increases. A more accurate experiment is required to gauge the sensitivity of the layers.

5%SO_2 seemed to induce no history effect upon the PPTSP layer, as the layer gave the same response to a concentration step of methanol, after SO_2 exposure, as a freshly prepared PPTSP layer would.

As already mentioned the main aim was to develop a conductive polymer layer that would respond to 5% SO_2. Two layers were investigated, these being a polypyrrole chloride layer and a polypyrrole dodecylbenzenesulphonate (PPDBS) layer. Both layers were deposited across the gold microband electrodes as described in the experimental section.

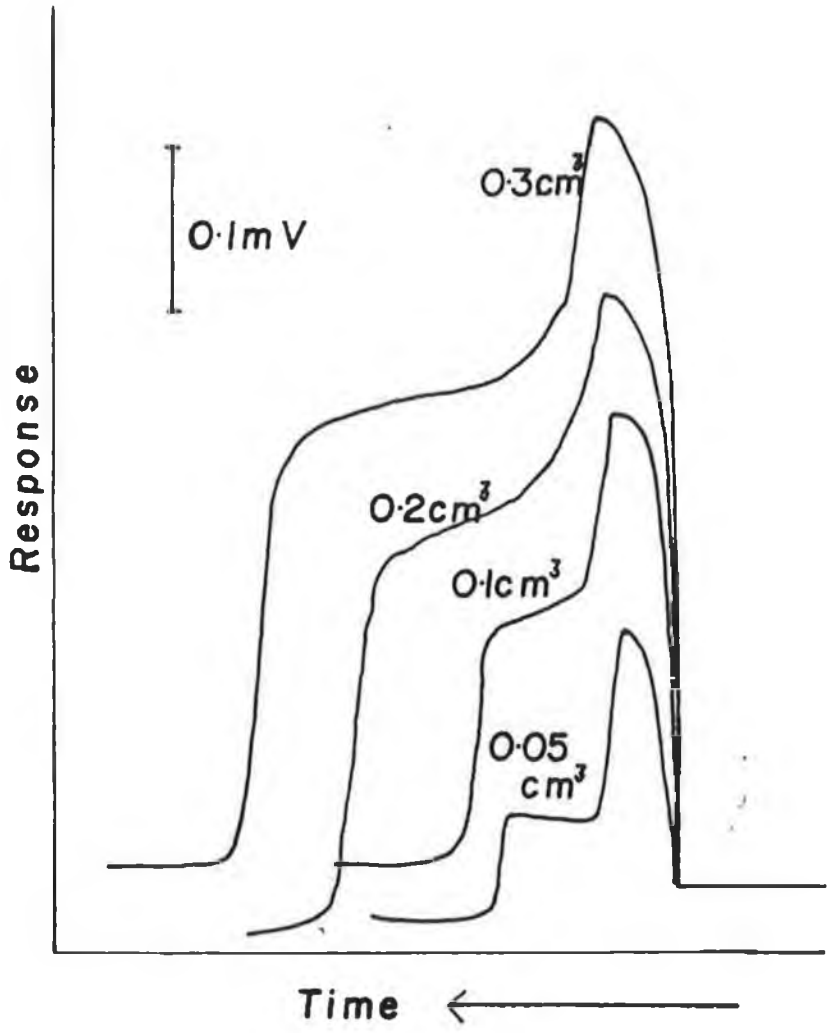

Figure 5.8 Response profiles for a PPTSP layer deposited across a 10μm gold electrode, as described in Figure 5.7, to various amounts of methanol.

Figure 5.9 (a) and (b) show the responses obtained for the PPCl and PPDBS layers, upon exposure to a concentration step of 5% SO_2 pulses, respectively. It can be seen that both responses are rapid, with the response of the PPDBS layer being reversible at room temperature.

The response profile of a PPCl to 5% SO_2 was drawn using a Fickian axis. The resulting plot is illustrated in Figure 5.10. It is seen that the plot is not linear, thereby indicating a change in the diffusion coefficient with time. The curve obtained indicates a decrease in diffusion rate with time. This can be explained by the fact that the initial SO_2 diffusing into the polymer matrix sites inhibits the further diffusion of SO_2 into the layer, by possibly filling all of the active sites within the film. This is illustrated by the curve reaching a plateau at longer times, thereby indicating a diffusion coefficient that depends upon concentration.

5.3.4 RESPONSES OBTAINED WITH SCREEN PRINTED CARBON INK ELECTRODES

The circuit shown in Figure 5.2 was modified, and an operational amplifier was inserted into the circuit. Figure 5.11 shows the resulting circuit, it can be seen that the only resistances within the circuit are those in the arms of the bridge and those associated with the operation of the amplifier.

The output voltage from the bridge is given by the equation below:

$$V_B = V_S \left[\frac{R_A}{R_P + R_A} - \frac{R_B}{R_B + R_C} \right] \quad \ldots\ldots \quad 5.1$$

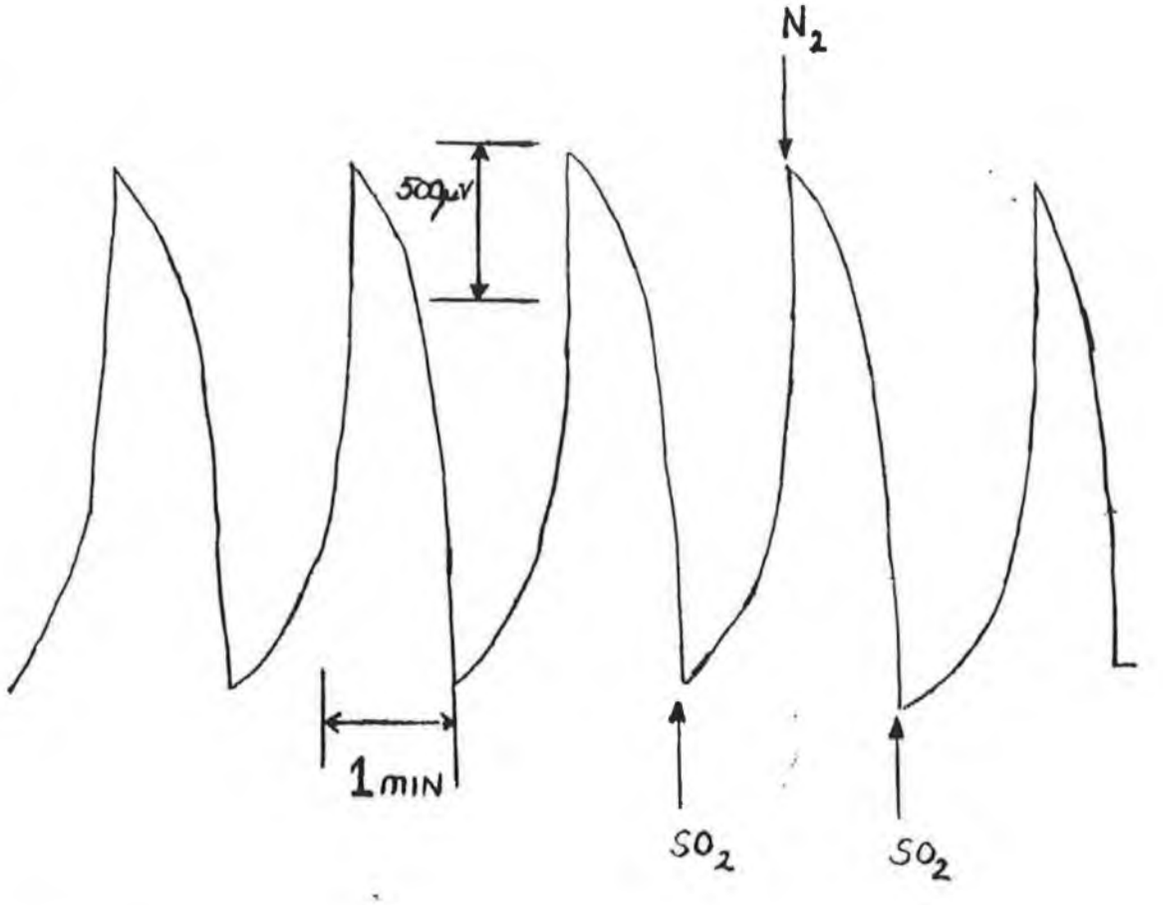

Figure 5.9 (a) Response of a PPCl layer, previously formed by holding the potential at 0.8V in an aqueous solution of pyrrole (0.1M) and NaCl (0.1M), to a concentration step of 5% SO_2 pulses.

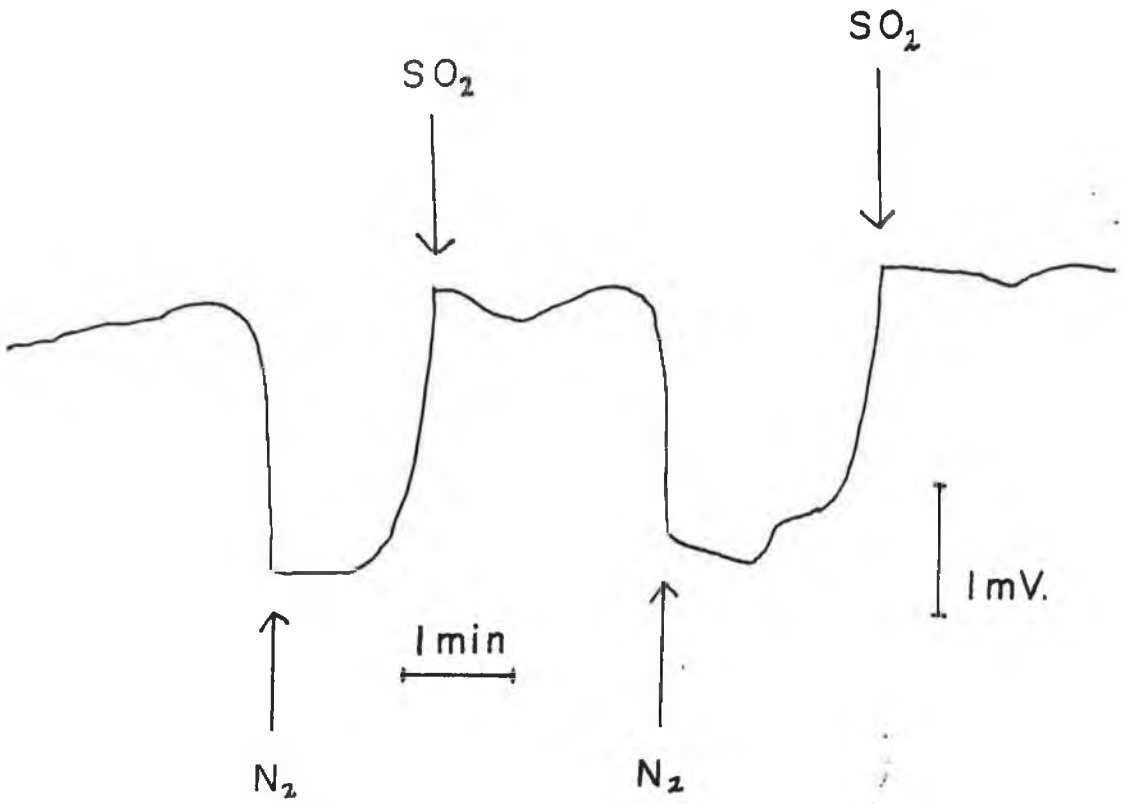

Figure 5.9 (b) Response of a PPDBS layer to a concentration step of 5% SO_2.

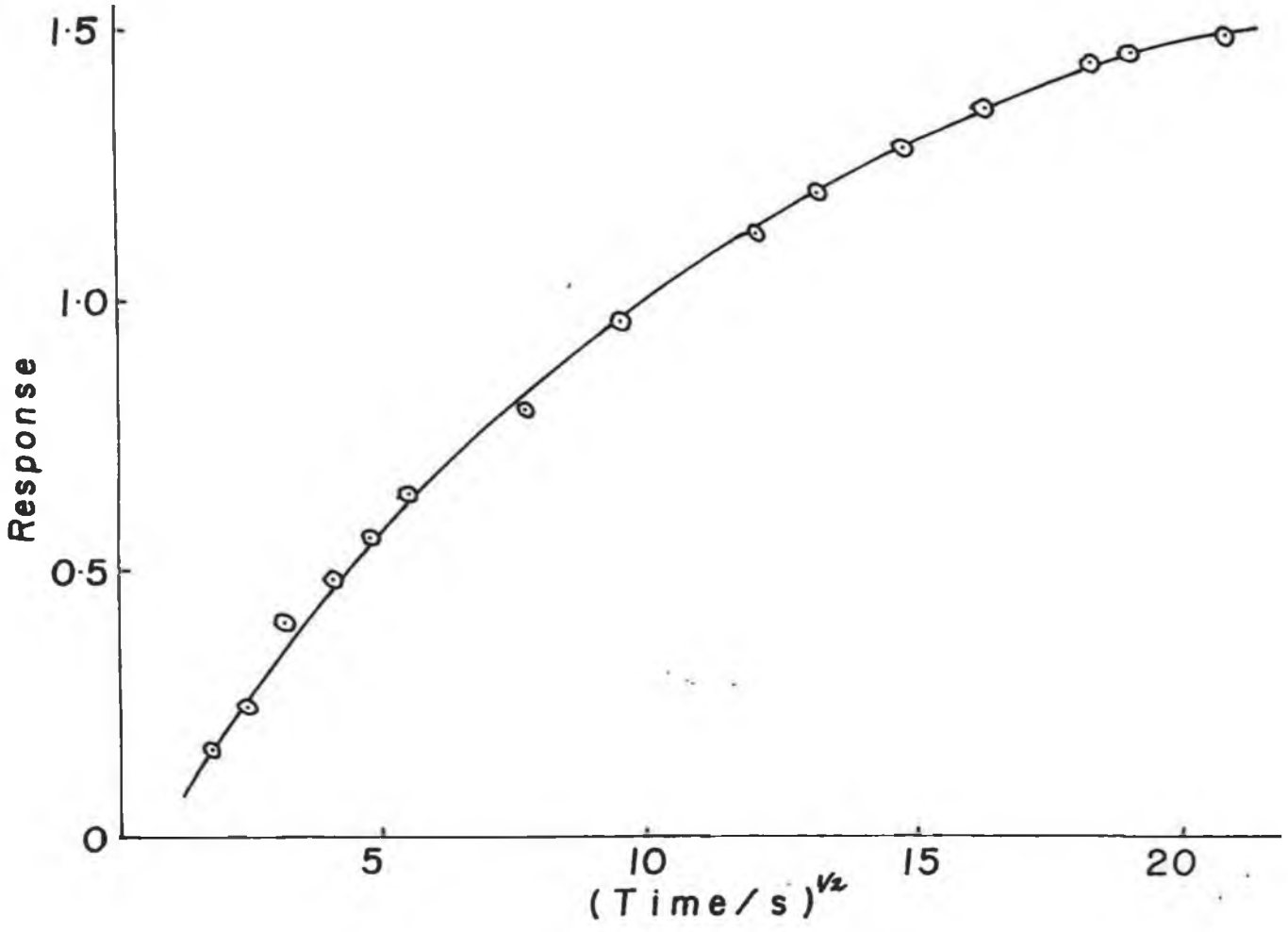

Figure 5.10 Plot of √t versus signal for the response of the PPCl layer to 5%SO_2, as seen in Figure 5.9 (a).

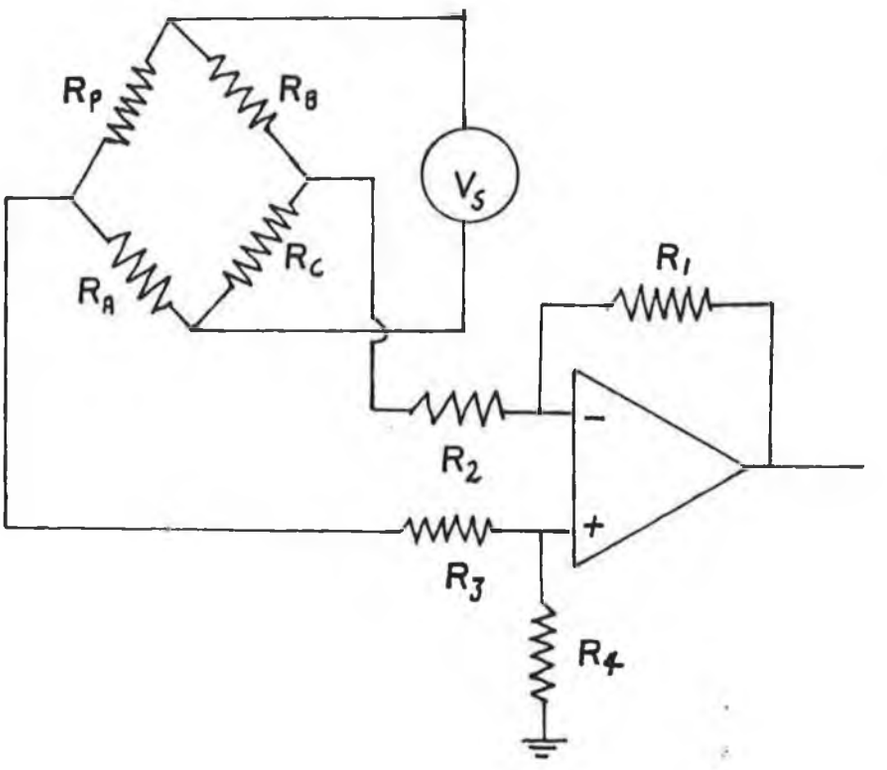

Figure 5.11 Modified circuit employed for gas sensing experiments.

where R_P is the resistance of the interdigital array electrode coated with the polymer film, V_S is the supply voltage (5 volts), V_B is the bridge output, and the other resistances are the remaining resistors within the bridge (See Figure 5.11).

The values of R1 and R4 are chosen to be equal, as R2 and R3 are, shown in Figure 5.11. The gain of the operational amplifer is given by:

$$\text{GAIN} = \frac{R_1}{R_2} = \frac{R_4}{R_3} \qquad \ldots\ldots 5.2$$

It is thus possible from knowing the gain of the amplifer and the values of R_A, R_B, R_C and the initial polymer resistance, to calculate the magnitude of the resistance change of the polymer film upon exposure to a particular vapour.

The electrodes employed were the industrial screen printed carbon ink elecrodes, where the interdigit gap is approximately 700μm. The area of each electrode, upon which the polymer was electrochemically deposited, was kept constant by a plastic tube being epoxyed over the digits. This ensured that the polymer only was deposited inside the tube. Therefore by the deposition charge being monitored it was ensured that a constant polymer film thickness was employed for each array.

One main type of doped polypyrrole film was investigated, and its response to 5% SO_2 was of particular interest. Polypyrrole doped with perchlorate anions ($PPClO_4$) was the layer employed. All layers were deposited at 0.8V vs. SCE

in an aqueous solution of pyrrole (0.1M) and $NaClO_4$ (0.1M). The electrodeposition was stopped when 800 mC of charge had passed. The layers were rinsed thoroughly with deionised water, their resistance measured and then allowed to dry for 24 hours at room temperature.

Three $PPClO_4$ layers were formed and each were exposured to three different gases, namely, 5% SO_2, in air and nitrogen saturated with $C_2H_4Cl_2$ or H_2O.

Figure 5.12 (a) shows the response profile obtained for a $PPClO_4$ layer to a concentration step of dichloromethane. It can be seen that the responses are rapid, but not totally reversible, as the layer upon being switched back to a N_2 stream doesn't return to the original baseline. There seems to be a history effect present.

From the use of equations 5.1 and 5.2, the change in resistance of the $PPClO_4$ layer upon exposure to $C_2H_4Cl_2$ was found to be in the order of +5.2%.

An important point to note was that the layer was found to be quite stable, with its resistance only drifting from 1.136 KΩ to 1.180 KΩ after several exposures and a period of over 24 hours after the layer was first exposed to $C_2H_4Cl_2$.

Figure 5.12 (b) shows the responses obtained for another $PPClO_4$ layer to water vapour. Again it can be seen that the responses are rapid but not completely reversible. There was a 2.6% change in the resistance of the $PPClO_4$ to water vapour. Again over a period of 24 hours and after several exposures to water vapour the resistance of the $PPClO_4$ drifted from 0.687 kΩ to 0.626 kΩ.

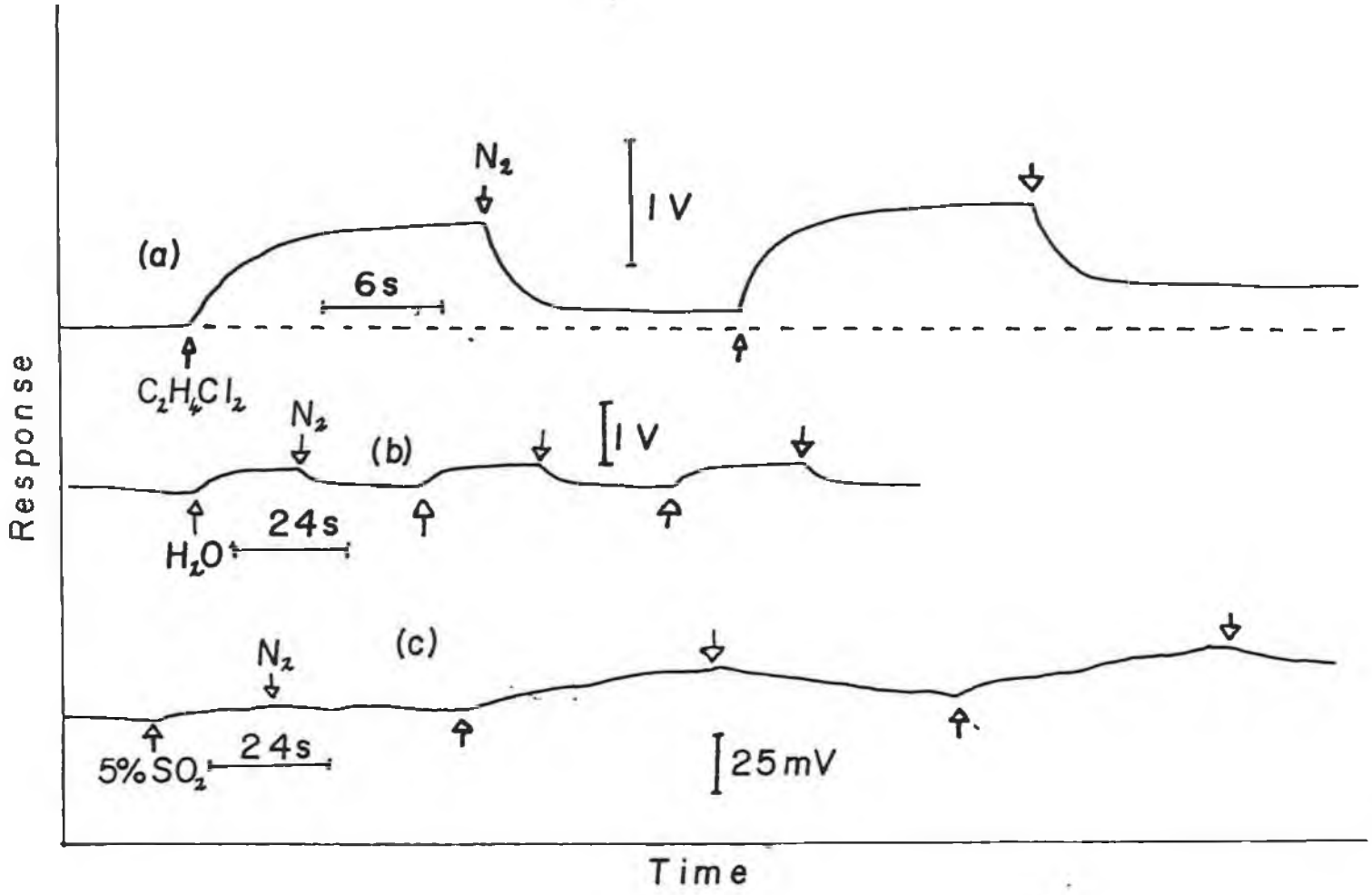

Figure 5.12 Response profiles for a $PPClO_4$ layer, to concentration steps of (a) CH_2Cl_2 (b) H_2O (c) 5%SO_2.

Figure 5.12 (c) shows the response profile obtained for a third $PPClO_4$ layer to 5% SO_2. It can be seen that the responses are sluggish, with little interaction between the $PPClO_4$ layer and the SO_2 vapour. It should also be noted that the change induced in the resistance of the electrode was 0.12%.
It can be seen that the layer responds more to " solvating vapours " rather than to small gaseous molecules capable of layer reduction.

5.3.5 CONCLUSION

It has been shown that conductive polypyrrole layers can be electrochemically deposited across gold microbond electrodes and screen printed conductive carbon ink electrodes. Once the layers were deposited, they were found to have an initial resistance characteristic of the polymer in the conductive state.

All layers investigated showed resistance changes upon exposure to methanol vapour. The layers also showed responses to water vapour and 5% SO_2. PPDBS and PPCl deposited across gold microband electrodes showed rapid responses to 5% SO_2, with a $PPClO_4$ layer exhibiting a little interaction with SO_2.

5.4 SPECTROSCOPIC INVESTIGATION OF THE EFFECT OF ORGANIC VAPOURS ON POLYMER FILMS.

5.4.1 INTRODUCTION

Since spectral changes accompany the changes in oxidation state of the polymer it is possible that the changes in polymer properties could be monitored by UV-vis spectroscopy. This would indicate whether exposure lead to oxidation or reduction of the layer and also lead to their possible use in fiber optic sensors.

5.4.2 EXPERIMENTAL

For the investigation of the effect of organic vapours upon the UV/vis spectra of the conducting polymer, all polymers were deposited potentiostatically onto glass slides that had been coated with a layer of indium tin oxide (a gift from Prof. K. Tokuda, TIT, Nagatsuta). The polypyrrole films (PP) were deposited from solution of acetonitrile containing 0.1 mol dm^{-3} pyrrole monomer with 0.1 mol dm^{-3} doping anion as a supporting electrolyte. The potential of the working electrode was held at 0.9 volts with a carbon rod being used as the auxiliary and a S.C.E. as the reference electrode. A ramp generator (H.B. Thompson 16 bit), a potentiostat (Edt ECP 100) and an electronic integrator (Sycopel DP301S) were used for the electrochemical deposition of the polypyrrole films.

After deposition all films were rinsed in the plain solvent and placed in an oven at $\cong$ 50°C for 20 minutes to allow them to dry.

The organic vapours were obtained by bubbling nitrogen gas directly through the solvent of interest at room temperature. During experimentation, the polypyrrole layers were switched between a stream of pure nitrogen and a vapour flow, by means of a six way crossover valve (Dublin Valve and Fitting Co.). Before the initial switch to organic vapour, all layers were flushed with nitrogen until the absorbance values at the selected wavelengths were constant.

UV/visible absorption spectra of the polymer films were obtained on a Shimadzu UV-160. The machine was placed in the photometric mode and the absorbance of the film at five selected wavelengths was monitored as a function of time upon exposure to organic vapours. For the reference cell within the spectrometer, a clean ITO electrode was employed.

5.4.3 RESULTS AND DISCUSSION

Figure 5.13 shows the absorption spectrum of a freshly prepared oxidised film of polypyrrole perchlorate ($PPClO_4$). The film was prepared from an acetonitrile solution of the monomer and supporting electrolyte, as described previously. It can be seen from the spectrum that there is only one definite absorption peak, at 434 nm. This has previously been reported [29] for polypyrrole films, it is due to the transition from the valence band to the antibonding cation/dication level. The broad band observed above 600 nm is assigned to the high energy tail of the transition from the valence band to the bonding cation level. However there is a slight shoulder observed around 800 nm, this possibly being due to the interband transition from the bonding cation to the antibonding cation level.

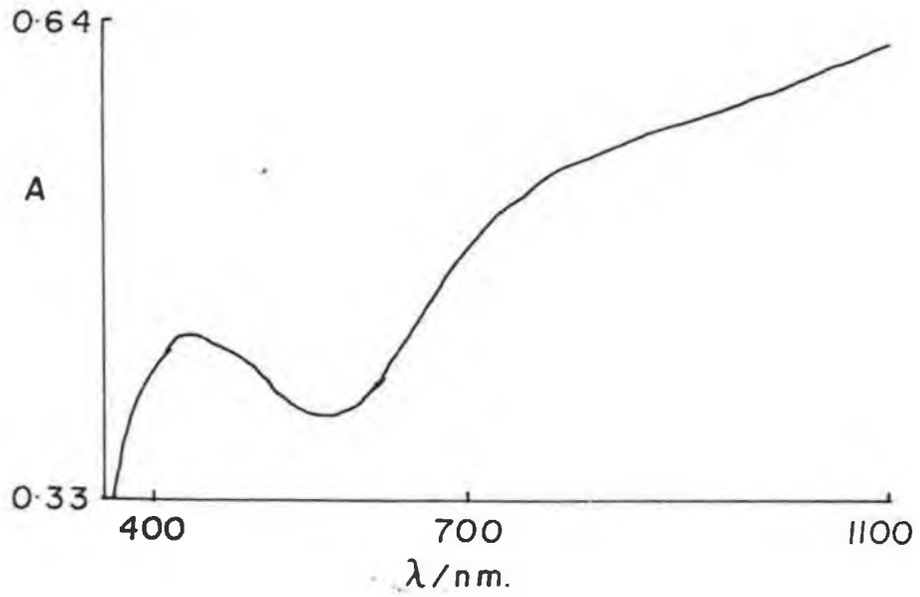

Figure 5.13 Absorption spectrum of a freshly prepared $PPClO_4$ film, previously formed by holding the potential at 0.9V in an acetonitrile solution of pyrrole (0.1M) and $LiClO_4$.

The layer is flushed with a nitrogen stream, and then it is exposed to methanol vapour. It was seen that there was a decrease in absorption above 600 nm but an increase in absorption below this value. This suggests that the methanol gas is electron donating, that is, donating electrons into the polymer matrix thereby affecting the concentration of cations/dications in the film. Two wavelengths (700nm and 450nm) are monitored in terms of absorption upon continual switching between nitrogen and methanol vapour.

Figures 5.14 (a) and 5.14 (b) show the variation in absorbance at 700nm and 450nm respectively. If the wavelength 700nm is considered to be part of the high energy tail associated with the transition from the valence band to the bonding dication level, then the results could be explained by the fact that the methanol is interacting with the bipolarons, donating electrons and therefore leading to a decrease in bipolaron concentration and simultaneously an increase in polaron concentration, as depicted below

$$PP^{2+} + e^{-} \rightarrow PP^{+} \qquad \ldots\ldots \ 5.3$$

Therefore it can be concluded that the methanol is acting as an electron donor, most likely through the lone pairs on the oxygen. These results agree well with previous gas sensing experiments performed on polypyrrole films [26] and also it is in agreement with the resistance changes observed in the polypyrrole film, upon exposure to methanol, presented earlier.

It can be seen that it is the initial exposure to methanol vapour, that produces the greatest change in absorbance. However it can also be seen that the effects

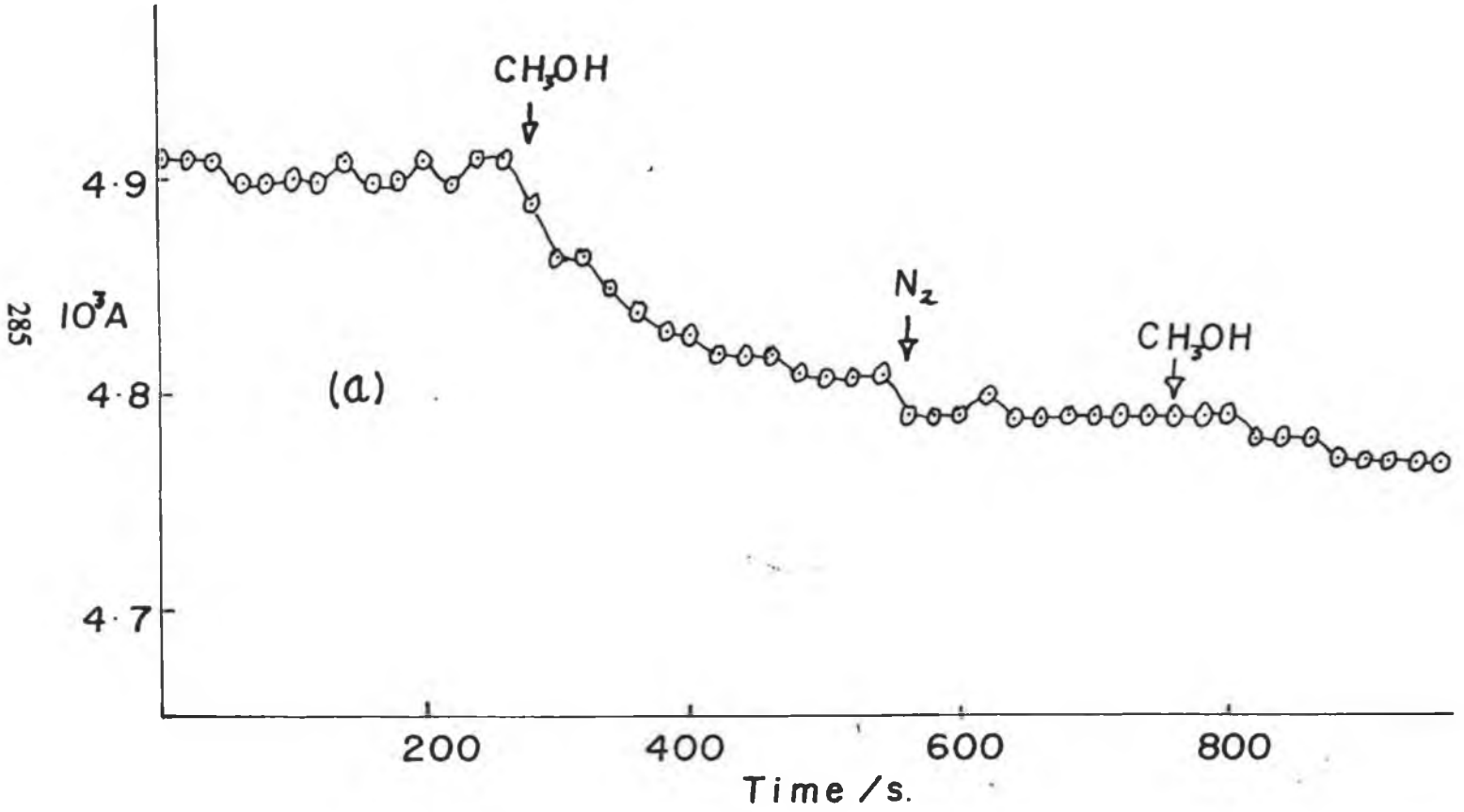

Figure 5.14 (a) Effect of exposure to CH_3OH vapour on the absorbance of the $PPClO_4$ layer at the wavelength 700 nm.

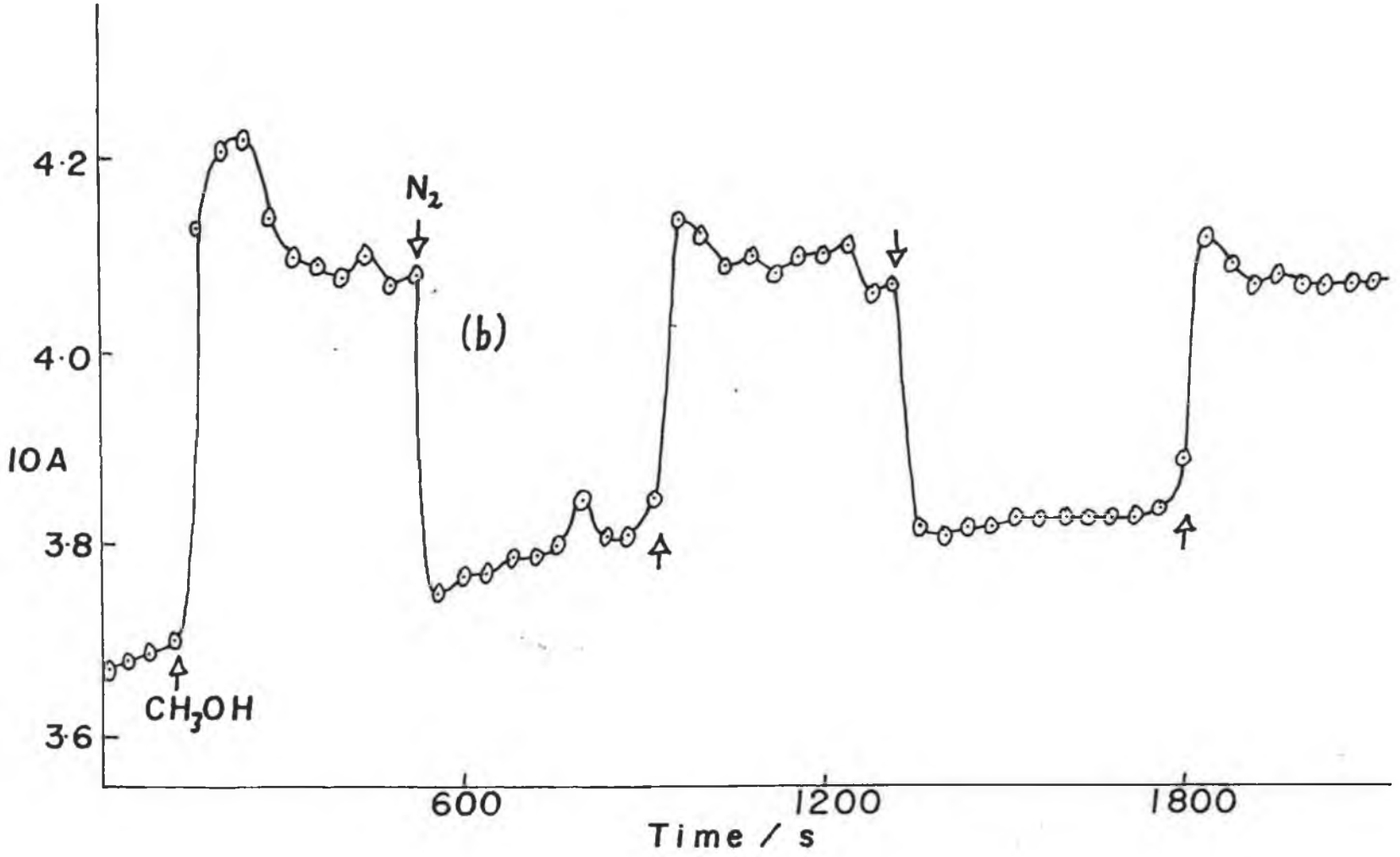

Figure 5.14 (b) Effect of exposure to CH_3OH vapour on the absorbance of the $PPClO_4$ layer at the wavelength 450 nm.

produced by the methanol vapour are not totally reversible for the polypyrrole perchlorate layer.

Referring to Figure 5.14 (b) it can be seen that the change observed in the absorbance at 450nm, upon switching between methanol and pure N_2, is well behaved. The change is both reversible and dramatic. This increase in absorbance, at this wavelength, illustrates that the polaron concentration within the polymer film is increasing. This is in accordance with equation 5.3, where the donation of electrons into the polymer matrix, leads to a decrease in bipolaron concentration, but an increase in polaron concentration.

A fresh $PPClO_4$ was formed in acetonitrile and its response to acetonitrile vapour was recorded. It was seen that upon switching the polymer film to acetonitrile vapour, led to an increase in absorbance, across the entire wavelength range (350nm $\rightarrow$ 1100nm). This change in absorbance is illustrated in Figure 5.15 at 434 nm. It can be concluded from these results that the acetonitrile is acting as an electron acceptor towards the polymer film. This leads to an increase in the concentration of polarons/bipolarons within the film, and this is illustrated by the increase in absorption obtained.
Again it is seen that these effects of the acetonitrile vapour, on the optical absorption properties of the $PPClO_4$ layer are not totally reversible since a drift can be seen.
Various other layers were investigated, their change in absorbance at various wavelengths being monitored upon exposure to various vapours. Polypyrrole

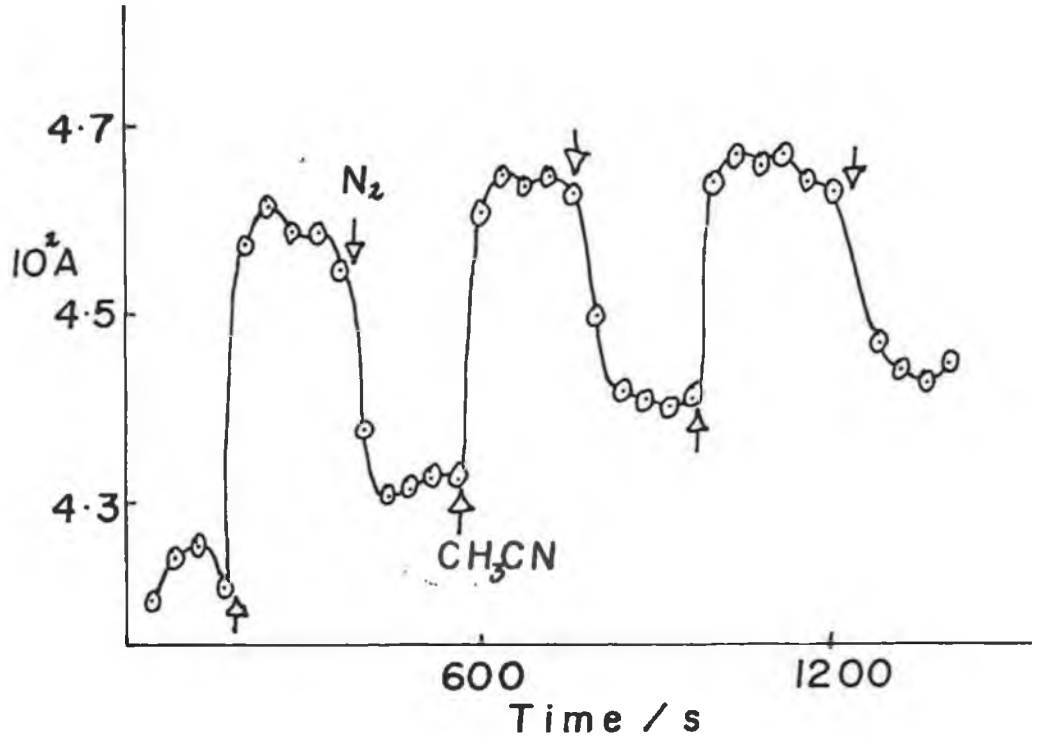

Figure 5.15 Effect of exposure to ACN vapour on the absorbance, of a freshly prepared $PPClO_4$ layer, at the wavelength 434nm.

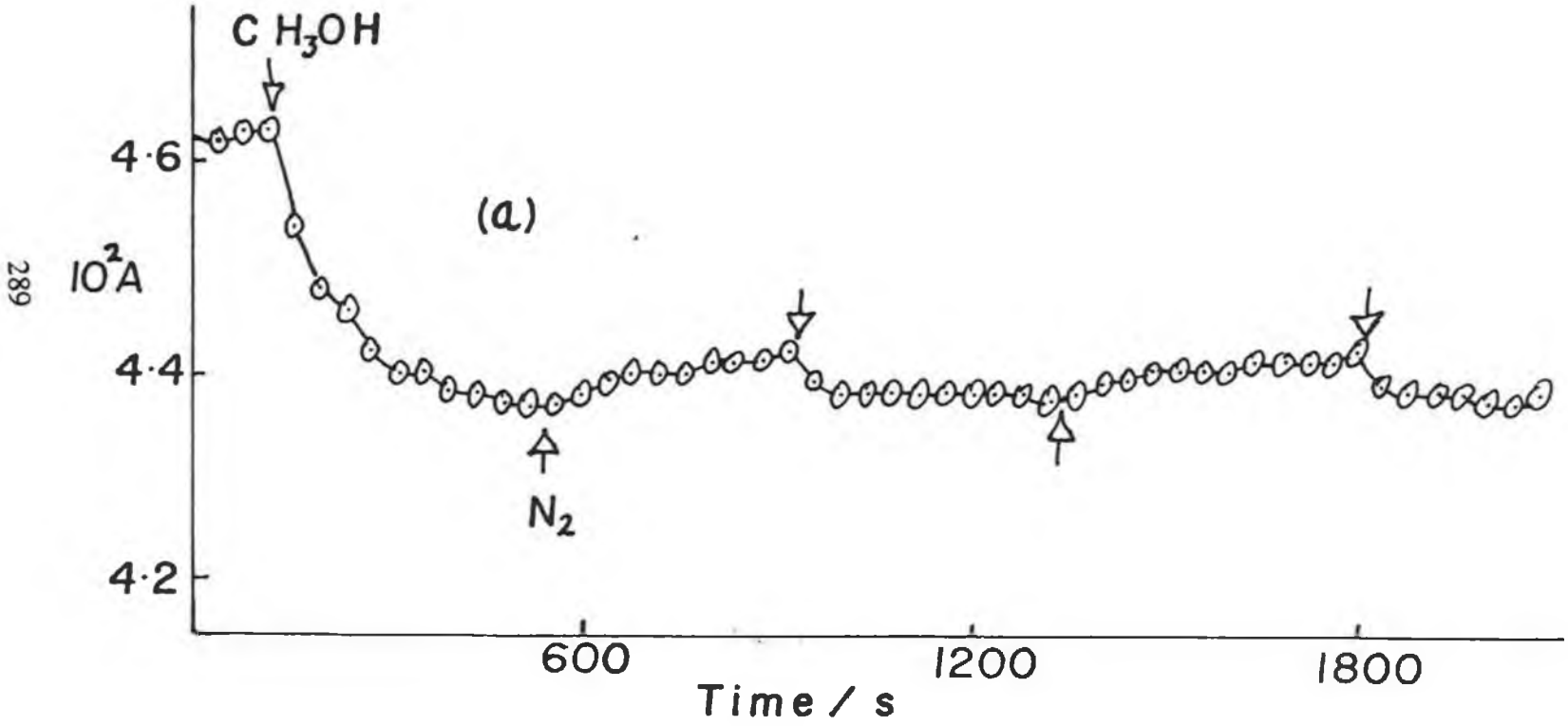

Figure 5.16 (a) Effect of exposure to CH_3OH vapour on the absorbance, of a $PPClO_4$ deposited from aqueous solution, at the wavelength 700nm.

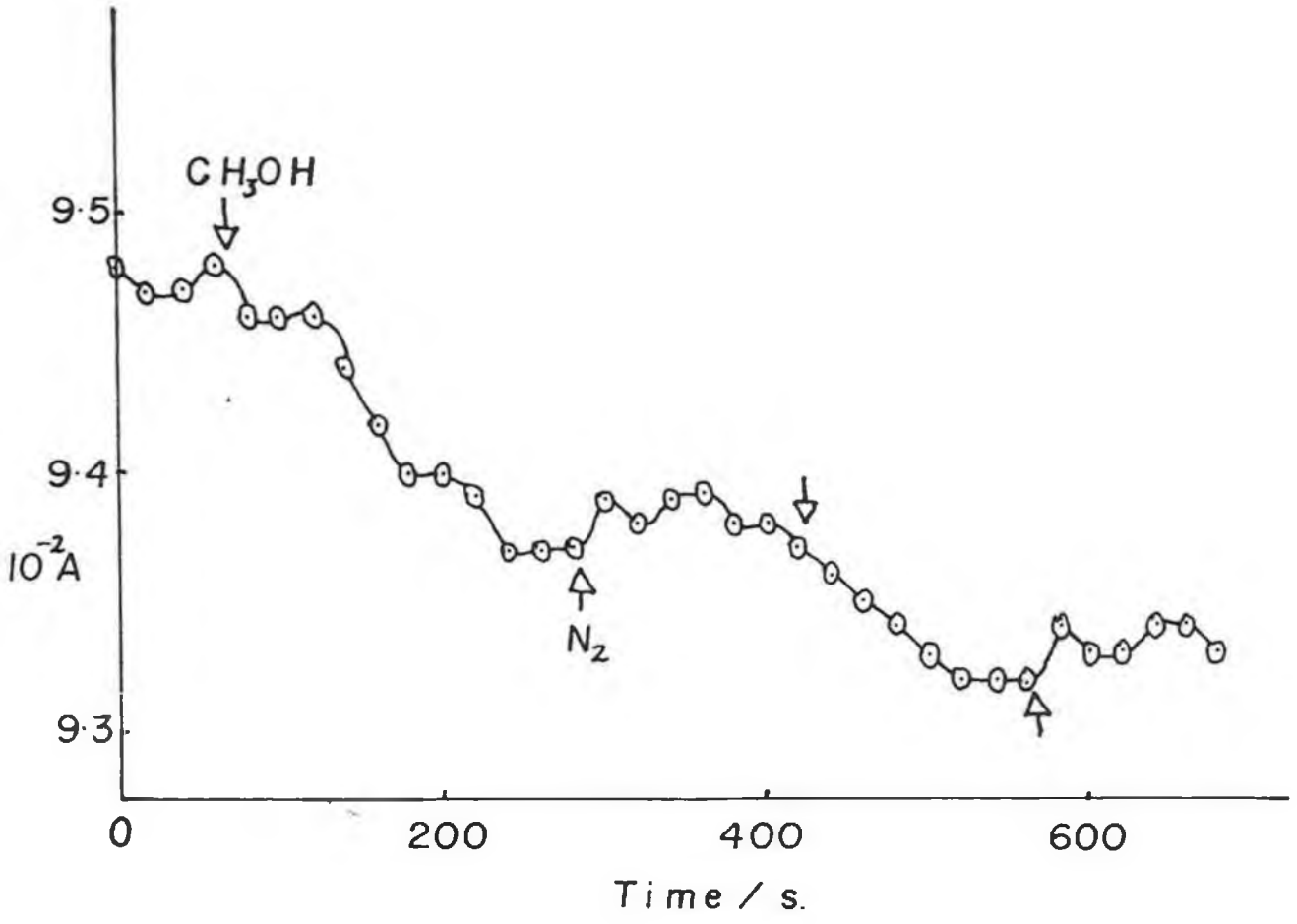

Figure 5.16 (b) Effect of exposure to CH_3OH vapour on the absorbance, of a PPCl layer deposited from an aqueous solution of pyrrole (0.1M), at the wavelength 900nm.

layers deposited from aqueous solutions of pyrrole (0.1M) and dopant electrolyte (0.1M). The two main layers are polypyrrole perchlorate ($PPClO_4$) and a polypyrrole chloride (PPCl). The reason for investigating $PPClO_4$ layer, deposited from an aqueous solution, was to see if the solvent from which a layer was deposited had a particular affect upon the response of that layer.
Figure 5.16 (a) and 5.16 (b) show the changes in absorbance at 700nm and 900nm for the $PPClO_4$ (AQ) and PPCl layer respectively, upon exposure to a concentration step of methanol vapour. It can be seen that there is a net decrease in absorbance at both wavelengths for the two layers upon switching to methanol. Again it can be seen that the maximum change occurs upon the first exposure and that the changes are not reversible.

TABLE 5.1

CHANGES INDUCED IN THE ABSORBANCE OF POLYPYRROLE FILMS BY EXPOSURE TO VAPOURS

VAPOUR	POLYMER LAYER	CHANGE IN ABS 10^3 ΔA/A						DONOR ACCEPTOR
		980nm	800nm	700nm	630nm	450nm	434nm	
CH_3OH	$PPClO_4$/AcN	-20.0	-30.7	-68.30	-	+139.2	-	DONOR
AcN	$PPClO_4$/AcN	+12.13	+12.70	+16.08	-	-	+97.40	ACCEPTOR
CH_3OH	$PPClO_4/H_2O$	-	-12.30	-20.40	-	-	-	DONOR
CH_2Cl_2	$PPClO_4/H_2O$	-	+3.35	-	+6.9	+14.9	-	ACCEPTOR
CH_3OH	$PPCl/H_2O$	-11.60	-	-19.80	-	-	9.80	DONOR
CH_2Cl_2	$PPCl/H_2O$	-	-31.25	-	-25.0	-9.11	-	DONOR
ACN	$PPCl/H_2O$	-	-6.00	-	-	-	+6.80	DONOR
n-C_6H_{14}	$PPCl/H_2O$	-	-0.41	-	-5.1	10.49	-	DONOR

Table 5.1 illustrates the changes in absorbance at the various wavelengths for all the polypyrrole layers investigated, upon exposure to various organic vapours. The changes in absorbance recorded are the maximum changes incurred upon the

initial switch to the organic vapour. All the results are normalised at each wavelength by dividing by the amount of light absorbed by the film in the absence of vapour, hence data is displayed in the form of $\Delta A/A$.

Negative values indicate that the absorbance decreases upon exposure to the vapour.

Looking at Table 5.1, a few conclusions can be made about the results obtained.

(i) Most of the organic vapours have electron donating properties towards the polymer film on account of their polarity.

(ii) The effect of the dopant anion is observed to have an effect upon how a gas interacts with the layer. It is seen the CH_2Cl_2 acts as a donor to the PPCl (aq) layer but as an acceptor towards the $PPClO_4$ (aq) layer.

(iii) There is little interaction between a polypyrrole chloride layer and hexane vapour. This is expected due to the non polar nature of the organic vapour.

(iv) Most of the changes produced by the organic vapours are irreversible, with the polymer exhibiting the most change upon first exposure to the gas.

5.4.4. CONCLUSION

From Figure 5.14 and Figure 5.15, it can be seen that changes in absorbance occur on exposure to polar solvent vapours. This could perhaps be used in a threshold fiber optic sensor for polar gases or perhaps humidity.

5.5 ELECTROCHEMICAL INVESTIGATION OF PRUSSIAN BLUE FILMS AS OVERLAYERS ON POLYPYRROLE LAYERS.

5.5.1 INTRODUCTION

Prussian Blue, ferric ferrocyanide, is an important member of the metal hexacyanometalates. It is well known that there are two forms of the mixed valent compound, namely the water insoluble form ($Fe_4^{III}[Fe^{II}(CN)_6]_3$) and the water soluble form ($KFe^{III}Fe^{II}(CN)_6$) [30,31]. Keggin and Miles [32] proposed a face centred cubic lattice structure for the soluble form. This involved the high spin ferric and low spin ferricyanide sites being surrounded octahedrally by -NC and -CN groups respectively, with the K^+ ion occupying an interstitial site.

Ludi et al [33] suggested a cubic lattice structure to describe the insoluble Prussian Blue form. One fourth of the $Fe^{II}(CN)_6$ units are missing, with their nitrogen sites occupied by water molecules coordinated to Fe(III) sites with eight water molecules located interstitially.

The Prussian Blue films can be grown onto a variety of electrode materials, such as, doped SnO_2[30], Au [34] glassy carbon [35] and Platinum [31].

Prussian Blue films can be electrochemically reduced to Prussian White and oxidised to Prussian Green. The reduction procedure has been reported [31] to lead to incorporation of cations into the film irrespective of whether the soluble

or insoluble Prussian Blue forms are involved. However it has been reported [31] that the ferrocyanide/ferricyanide oxidation reactions involve the incorporation of anions for the insoluble form and the loss of cations for the soluble form.

In this section, the electrochemistry associated with the reduction of Prussian blue films on Pt electrodes is reported. A bilayer configuration is also investigated, where prussian blue films are grown on top of conductive polypyrrole films. In the last section solid state voltammetry is performed on prussian blue films deposited across carbon ink interdigital array electrodes, and also the possible use of PB films as gas sensors is studied.

5.5.2 EXPERIMENTAL

All chemicals employed were of reagent grade, and were used without further purification.

For the cyclic voltammetric experiments, the Prussian Blue films were prepared electrochemically onto platinum disk ($0.0707cm^2$) electrodes. The Pt electrodes were polished thoroughly with 0.3μm alumina and rinsed with deionised water, prior to use.

Prussian blue films were deposited from a freshly degassed aqueous solution of $FeCl_3$ (20mM), $K_3Fe(CN)_6$ (20mM) and HCl (0.01M). The films were formed by cycling the electrode in the solution above, between +0.5V and -0.1V vs. SCE, or by holding the potential of the Pt working electrode at 0.5 volts. For the cyclic voltammetric experiments, the layers were washed with deionised

water and transferred immediately to an aqueous solution of background electrolyte. All solutions employed for degassed with oxygen free N_2 for approximately 10 minutes prior to use.

A ramp generator (H.B. Thompson 16 bit), a potentiostat (Edt ECP 100) and an electronic integrator (Sycopel DP 301S) linked to a J.J. Lloyd PL3 X-Y recorder were used for cyclic voltammetry. All voltammetric experiments were carried out at room temperature in a single compartment three electrode cell. A saturated calomel electrode was used as the reference electrode with a carbon rod as the auxiliary electrode.

5.5.3 RESULTS AND DISCUSSION

Figure 5.17 shows the cyclic voltammogram obtained upon the electrochemical deposition of a Prussian blue (PB) layer onto a Pt disk electrode. The electrode was cycled between +0.5V and -0.1V in an aqueous solution of $FeCl_3$ (20mM), $K_3Fe(CN)_6$ (20mM) and HCl (0.01M). It shows a reduction and oxidation wave at +0.04V and +0.19V respectively. However both waves are seen to shift in potential and the current increases upon further scanning.

The Prussian blue modified electrode was then rinsed with HCl (0.01M) and transferred to a degassed aqueous solution of KCl (1.0M) and HCl (0.01M). Figure 5.18 shows the resulting cyclic voltammogram obtained when the

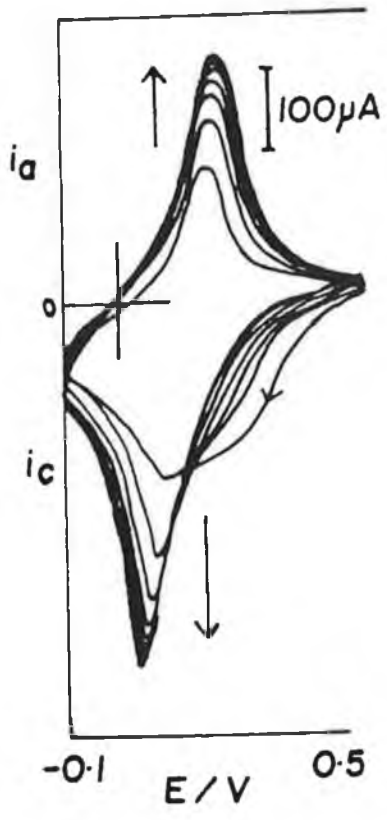

Figure 5.17 Cyclic voltammogram of the deposition of a Prussian blue film onto a Pt disk electrode. The deposition aqueous solution contained $FeCl_3$ (20mM), $K_3Fe(CN)_6$ (20mM) and HCl (0.01M).
Scan Rate = 50mV/s.

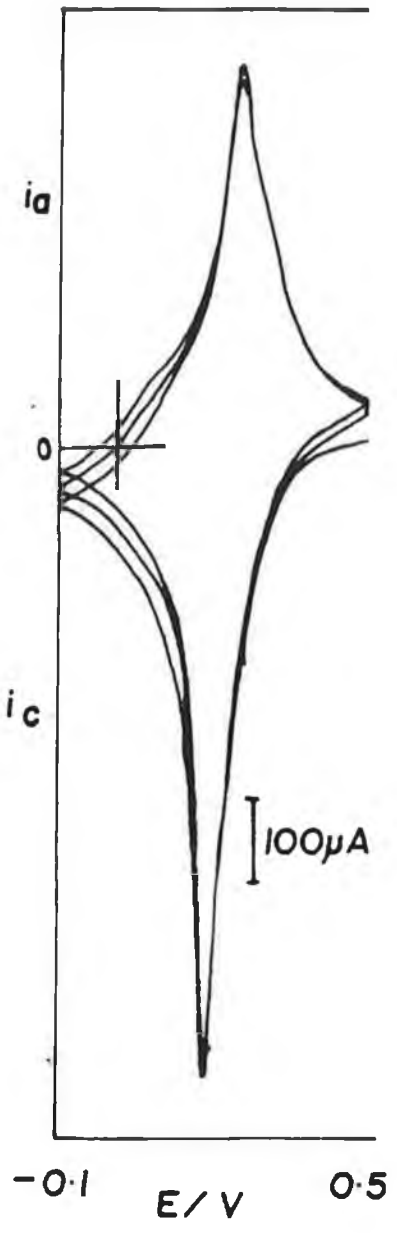

Figure 5.18 Cyclic voltammogram of the PB film, deposited as described in Figure 5.17, in an aqueous solution of KCl (1.0M) and HCl (0.01M). Scan Rate = 50mV/s.

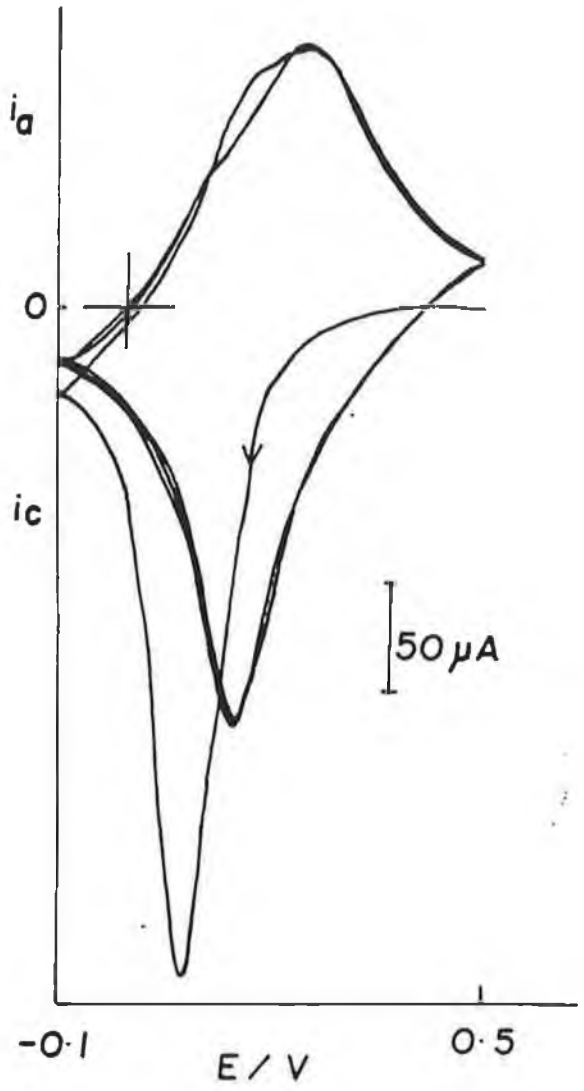

Figure 5.19 Cyclic voltammogram of a PB film, deposited as described in Figure 5.17, in an aqueous solution of NH_4Cl (1.0M) and HCl (0.01M). Scan Rate = 50mV/s.

electrode was scanned between +0.5V and -0.1V. This cyclic voltammogram is typical of that reported previously [31].

A negative potential scan causes the reduction of the mixed valent ferric/ferrocyanide form to Fe(II/II), known as prussian white. The reduction wave and reoxidation wave occur at +0.175V and +0.225V vs. SCE respectively ($E^{o1} = 0.200V$).

To confirm that cation movement in and out of the PB film was occurring upon reduction and reoxidation, variations in both the cation and anion of the background electrolyte were undertaken.

All Prussian blue films were formed under identical conditions and from the same solution.

It was observed that when a PB modified electrode was cycled between +0.5V and -0.1V in a solution of KNO_3 (1M) in 0.01M HCl that the formal potential of the layer upon reduction and reoxidation was 0.195V as compared to 0.200V in 1M KCl. Also electrochemistry of the PB film, was recorded in NH_4Cl (1M) in 0.01M HCl solution. The resulting cyclic voltammogram is shown in Figure 5.19. The peaks are broader in nature, with a positive shift in formal potential to +0.250V occurring, thereby confirming that it is the cation passing in and out of the PB film. This has been reported previously [31], irrespective of whether or not the soluble, $KFe^{III}[Fe^{II}(CN)_6]$, or insoluble $Fe_4^{III}[Fe^{II}(CN)_6]_3\ 6H_2O$ form of prussian blue had been formed.

To try and elucidate the porosity of a PB film formed by cycling, cyclic voltammetric experiments were carried out in a background electrolyte solution of tetrabutylammonium hydrogensulphate $TBAHSO_4$ (0.1M) in 0.01M HCl. The PB film was formed by cycling the Pt electrode, with approximately the same amount of deposition charge being used to deposit the film, as previously used for layers in alkali metal electrolytes.

No electrochemistry was observed in the $TBAHSO_4$ electrolyte, upon reduction of the PB film. A similar situation was reported [31] for prussian blue films run in Et_4N^+ electrolyte.

This result was interesting as the ionic size of TBA^+ (5.12Å) is similar to the hydrated diameter of K^+ (4.64Å), which is seen to enter and exit th PB film readily, as described earlier. This implies that the K^+ cation enters into the layer as a partially dehydrated state. It has previously been proposed [31] that the alkali metal cations do not retain a complete hydration shell upon entrance to the Prussian blue crystal lattice.

The reason for the investigation of Prussian Blue modified electrodes was due to the films size exclusion properties. It has previously been mentioned that specificity of polymer based gas sensors is a major problem, in that, a conductive polymer layer can interact with a variety of gases. It was believed that Prussian blue since it is zeolite in nature, could be used as an overlayer on the polymer layer, thereby introducing specificity into the polymers response to gases, due to it's size exclusion properties.

The first step involved investigation of whether or not a PB film could be deposited electrochemically over a polypyrrole conductive layer on a glassy carbon electrode.

A polypyrrole perchlorate layer $PPClO_4$ was formed on a glassy carbon electrode from an aqueous solution of pyrrole (0.1M) and $NaClO_4$ (0.1M) by holding the potential at 0.8V until 50 mC of charge had been deposited. The layer was then rinsed thoroughly with deionised water and transferred to an aqueous solution of $NaClO_4$ (0.1M) and HCl (0.01M) and cycled between +0.5V and -0.7V. The resulting voltammogram is shown in Figure 5.20, a broad reduction wave and oxidation wave are observed at -0.180 Volts and +0.045V vs. SCE respectively. Also it should be noted that a large background current is observed when the polymer is in the oxidised state, this being characteristic of conducting polymers.

A 50 mC $PPClO_4$ layer was formed as previously described, and placed in a solution of $FeCl_3$ (20 mM), $K_3Fe(CN)_6$ (20 mM) and 0.01 mM HCl. A Prussian blue film was then formed onto the polymer layer by cycling the electrode from +0.5V to -0.1V. The characteristic cyclic voltammogram of the growth of the PB film, as shown in Figure 5.17, was obtained. The electrode modified, with $PPClO_4$ and PB was washed with deionised water and placed in an aqueous solution of KCl (1 M) and 0.01M HCl. The layer was cycled between +0.5V and -0.1V, and the resulting cyclic voltammogram is shown in Figure 5.21. A sharp reduction peak and sharp oxidation peak are observed with the halfway potential of +0.195V. This is attributed to the electrochemistry of the Prussian Blue film.

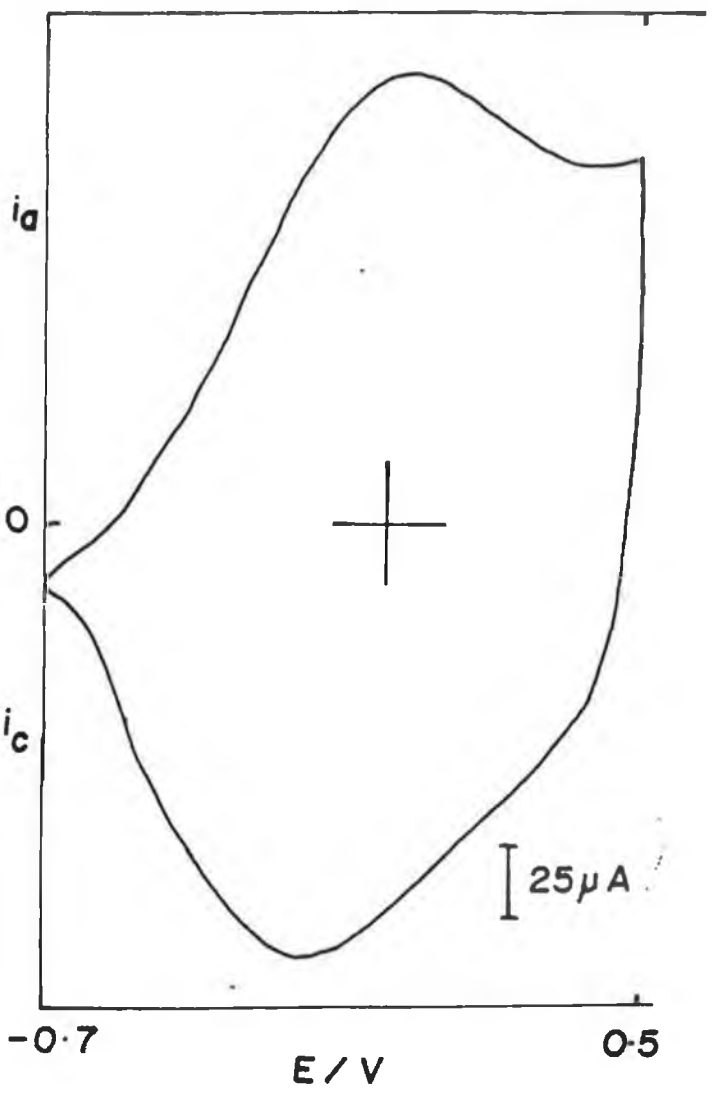

Figure 5.20 Cyclic voltammogram of a $PPClO_4$ in an aqueous solution of $NaClO_4$ (0.1M) and HCl (0.01M). The layer previously being deposited by holding the potential at 0.8V in an aqueous solution of pyrrole (0.1M) and $NaClO_4$ (0.1M). Scan Rate = 50mV/s.

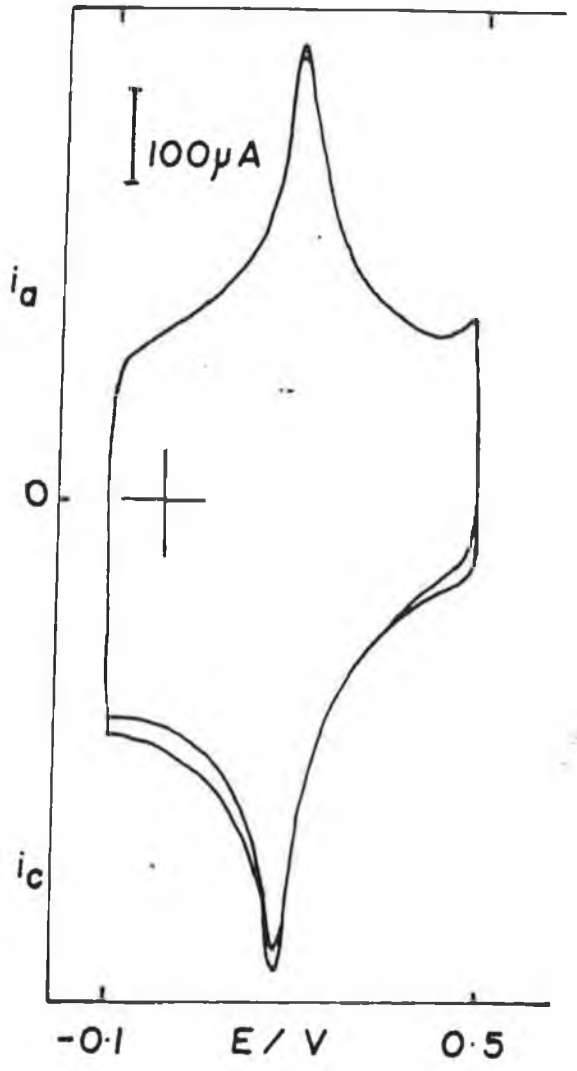

Figure 5.21 Cyclic voltammogram of a $PPClO_4$/PB bilayer modified electrode in an aqueous solution of HCl (0.01M) and KCl (1.0M). The $PPClO_4$ and PB layers being previously formed as described in Figure 5.20 and Figure 5.17, respectively. Scan Rate = 50mV/s.

An important point to note is the presence of a large non-faradaic current being observed at +0.5V and -0.1Volts. Due to its presence at -0.1V, it can be concluded that the underlying $PPClO_4$ layer is still in the oxidised, that is, conducting state. The negative potential limit was set at -0.65V and the modified electrode was cycled between +0.5V and -0.65V, to see if any electrochemistry associated with the polymer could be observed. Figure 5.22 shows the resulting cyclic voltammogram, it can be seen that no definite waves are observed for the polymer. However a broad reduction wave is observed at -0.350V on the first scan with an associated broad oxidation wave at -0.220V. On continuous scanning these are seen to decrease in magnitude, thus indicating that even though it is clear that the polymer layer has been reduced, there is difficulty in observing its electrochemistry.

A fresh $PPClO_4$ layer was formed as described previously, and a Prussian blue film was formed on top of this film by holding the potential of the polymer modified electrode at +0.5V in a solution of $FeCl_3$ (20 mM), $K_3Fe(CN)_6$ (20mM) and 0.01M HCl.

The modified electrode was then removed and placed in KCl (1M) and HCl (0.01M) solution. The resulting cyclic voltammogram is shown in Figure 5.23. Again it can be seen a pair of redox waves appears in the potential range of 0.2 - 0.3V, which are due to the redox reaction of Prussian Blue/Prussian White. This is similar to a cyclic voltammogram obtained for a polypyrrole film doped with Prussian Blue [36]. When this doped polypyrrole film was placed in lM KCl two redox peaks in the range 0.2V →0.3V were obtained. Also the non faradaic component of the current for the polymer in the oxidised state was

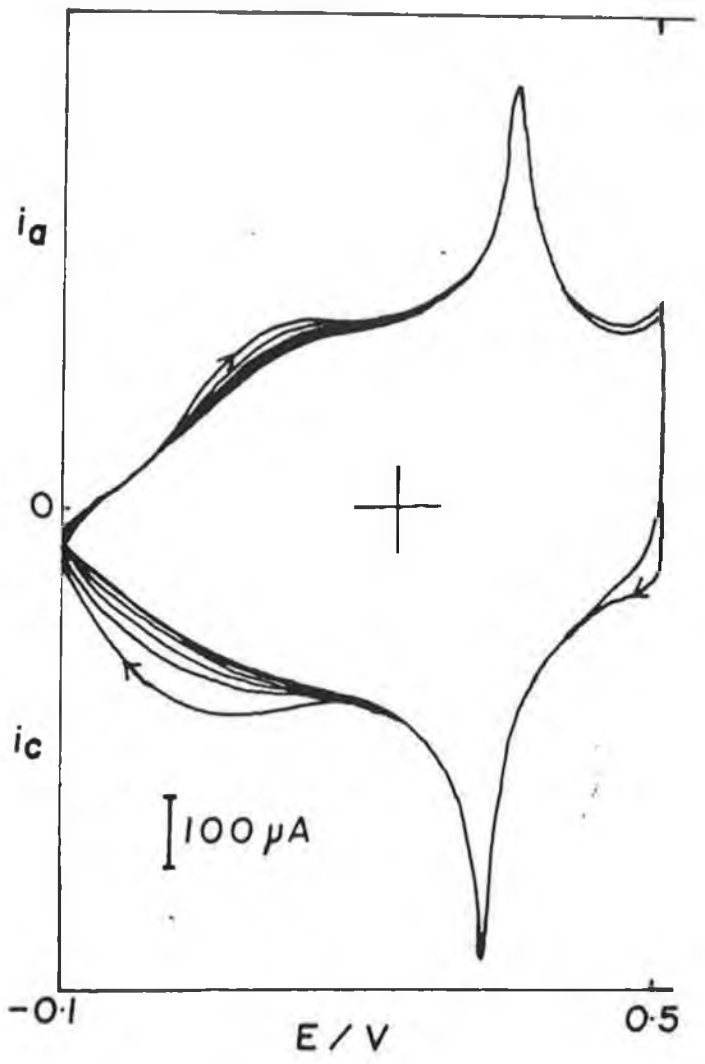

Figure 5.22 Cyclic voltammogram of the $PPClO_4$/PB bilayer electrode, described in Figure 5.21, in an aqueous solution of HCl (0.01M) and KCl (1.0M). Scan Rate = 50mV/s.

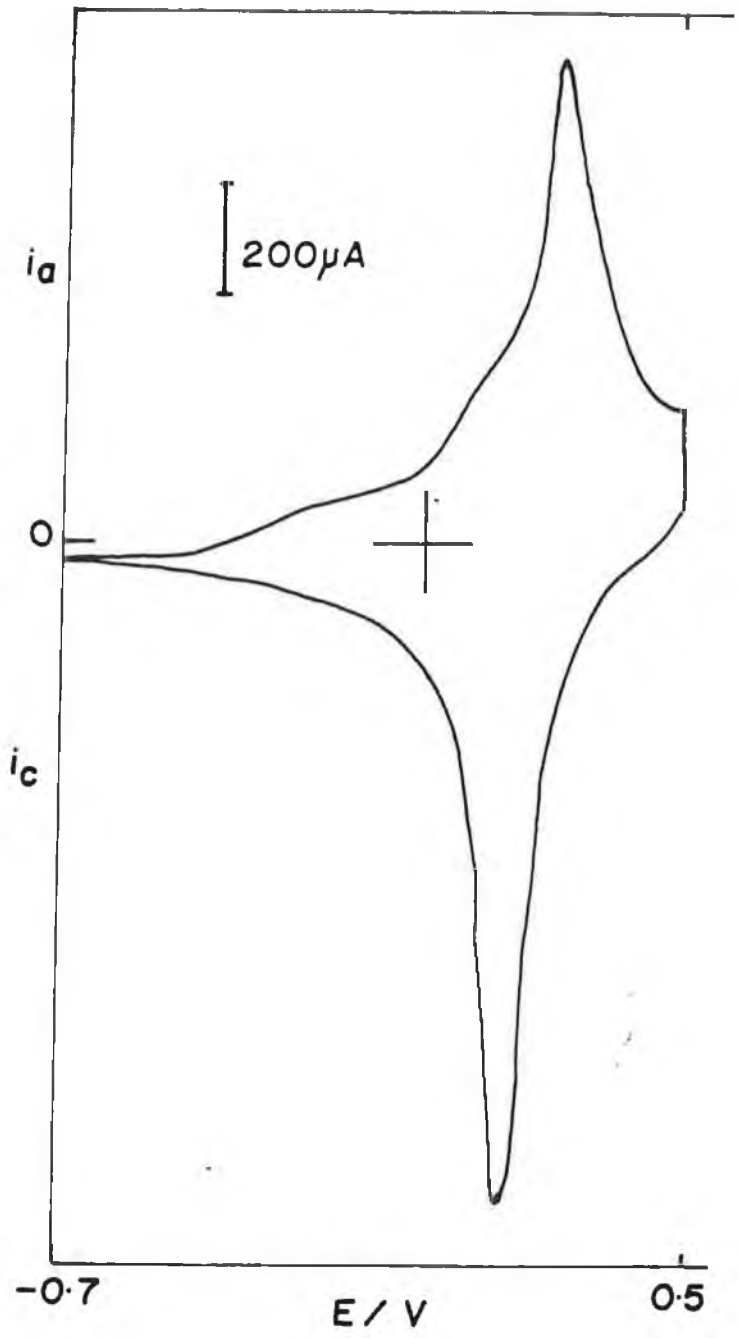

Figure 5.23 Cyclic voltammogram of a $PPClO_4$/PB bilayer electrode in an aqueous solution of KCl (1.0M) and HCl (0.01M). The $PPClO_4$ layer was formed as described in Figure 5.20. The PB film was deposited by holding the potential at 0.5V in an aqueous solution of $K_3Fe(CN)_6$ (20mM), $FeCl_3$ (20mM) and HCl (0.01M). Scan Rate = 50mV/s.

present at potentials as far negative as -0.5V. This is also seen to a much lesser extent in the cyclic voltammogram in Figure 5.23, where the disappearance of this non faradaic current indicates the polymers reduction, again no definite redox waves are observed for the polymer films electrochemistry. Ikeda and Yaneyama [36] formed PP doped with PB but did not see any clear electrochemistry for the PP itself.

It was therefore seen that it was possible for a Prussian Blue film to be formed electrochemically, by either cycling or holding the potential at +0.5V, over a polypyrrole layer. It appears that forming the PB layer by cycling allows it to be more porous.

Feldman and Murray investigated electron diffusion in wet and dry Prussian Blue Films on Interdigital Array Electrodes [37]. They performed solid state voltammetry upon prussian blue films coated on the arrays. The interdigital array (IDA) coated with the PB layer was exposed to a selected gas and a potential (ΔE) applied across the two terminals of the IDA was slowly scanned. One side of the IDA is the working electrode with the other as the auxiliary, no reference or bathing solvent was used. Current was found to flow when ΔE became large enough to disproportionate the prussian blue, that is, simultaneous FeIII/II $\rightarrow$ FeII/II reduction and FeIII/II $\rightarrow$ FeIII/III oxidation occur at opposing film/electrode interfaces. Steady state voltammograms were obtained at slow scan speeds.

In this work Prussian Blue films were deposited across the carbon ink interdigital arrays by holding the potential of the array at +0.5V in a solution of $FeCl_3$

(20mM) $K_3Fe(CN)_6$ (20 mM) and 0.01M HCl, and also by cycling the electrode between +0.52V and -0.34V. Figure 5.24 shows the resulting cyclic voltammogram obtained under these conditions.

The coated IDA was rinsed with HCl (0.01M) and then used immediately. A potential of +0.5V was applied across the digits, with one electrode terminal being used as the working electrode and the other terminal as a pseudo reference/auxiliary. A steady current of 55.5μA upon breathing onto the array, being observed. This corresponded to a decrease in resistance of the PB film from 8.93 kΩ to 8.68 kΩ, It was also found that upon exposure to SO_2 vapour, the steady state current increased by 3μA.

It was found that when the layer was allowed to dry at room temperature, the steady state current decreases from 55.5μA to 0.02μA. However even on drying the steady state current still increased upon application of SO_2 and breath.

These results can be explained by the fact that the presence of water acts to solvate internal counterionic species in the Prussian Blue film and thereby has control over their mobility. Therefore interstitial water is necessary for conduction within the Prussian Blue film. For Prussian Blue films in the absence of an external electrolyte solution, they require resident mobile counterions, which must migrate from one side of the film to another, for reasons of maintaining electroneutrality at all points within the film during solid state voltammetry.

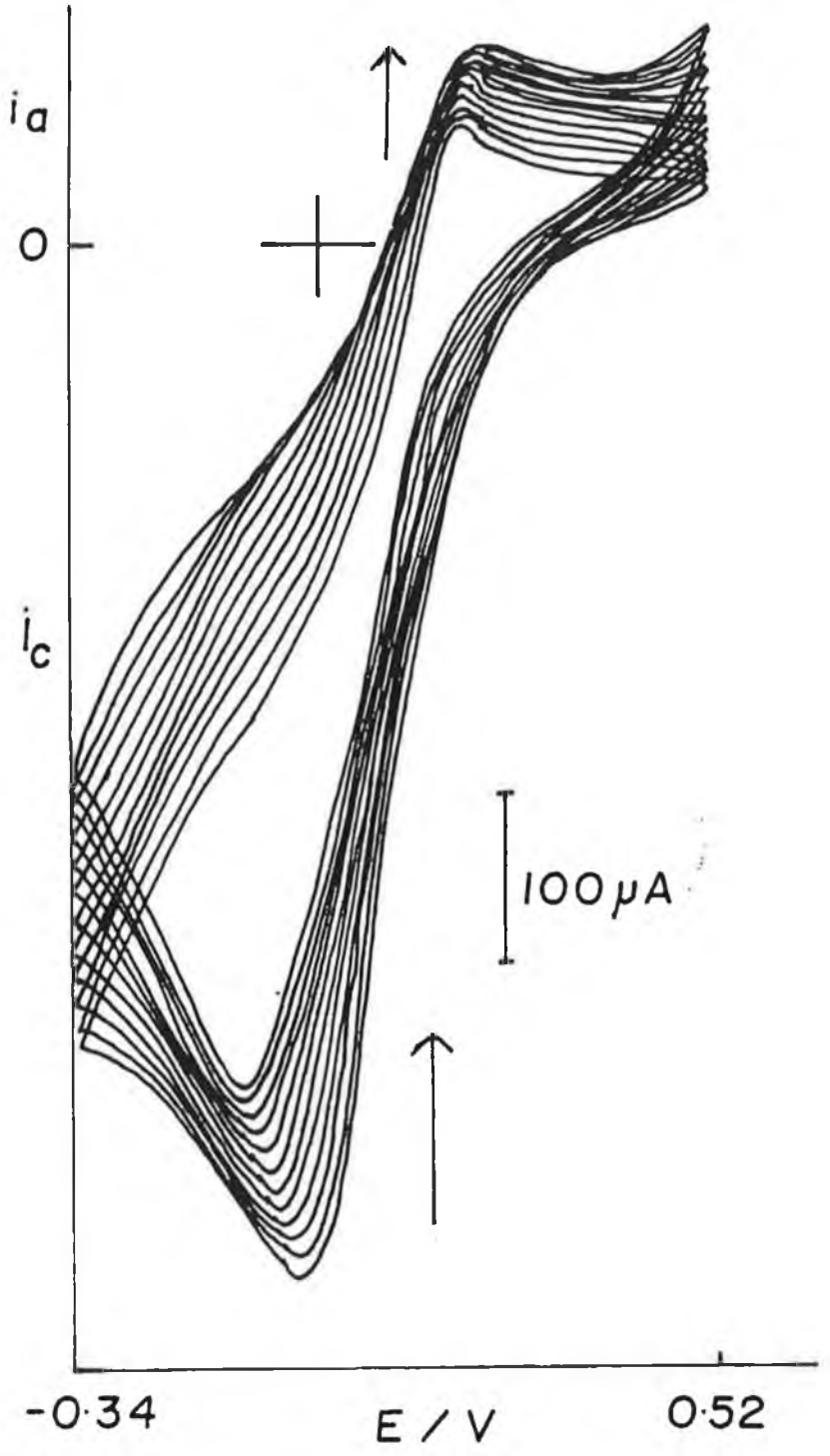

Figure 5.24 Cyclic voltammogram of the deposition of a PB film onto a screen printed carbon ink electrode, as described in Figure 5.17.
Scan Rate = 50mV/s.

These preliminary results for the solid state voltammetry of Prussian Blue films deposited across carbon ink electrodes, led to the idea that these films alone could be used as a sensing element within a gas sensor.

A fresh Prussian Blue film was deposited across a IDA electrode by holding the potential of the array at +0.5V in a solution of $FeCl_3$ (20 mM), K_3 $Fe(CN)_6$ (20 mM) and 0.01M HCl. It should be noted that it took over an hour to deposit the PB film across the digits, as the PB tended to grow onto the epoxy resin of the array, used for electrode encapsulation.

The layer was then washed with 0.01M HCl and allowed to dry at room temperature. Solid state two electrode voltammetry was then performed on the layer, the potential of the electrode was scanned at 10mV/s from 0.0V to 1.5V, where typical resistive behaviour was observed. Previously Feldmann and Murray [37] obtained sigmoidal voltammograms with a steady state current being observed above 1.0V. However in our results, the resistance of the PB film dominates the response, this is due primarily to the dimensions of the macroelectrode, whereas Feldmann and Murray [37] employed microelectrodes, therefore obtaining thinner Prussian Blue films.

Figure 5.25 shows the effect of dry nitrogen upon the steady state current obtained when +0.5V is applied across the two terminals of the PB modified IDA. This illustrates the effect upon the current time transient of water removal at $\Delta E = 0.5V$. This decrease in current by 60% illustrates how the mobility of the internal counterionic species is reduced due to the removal of interstitial

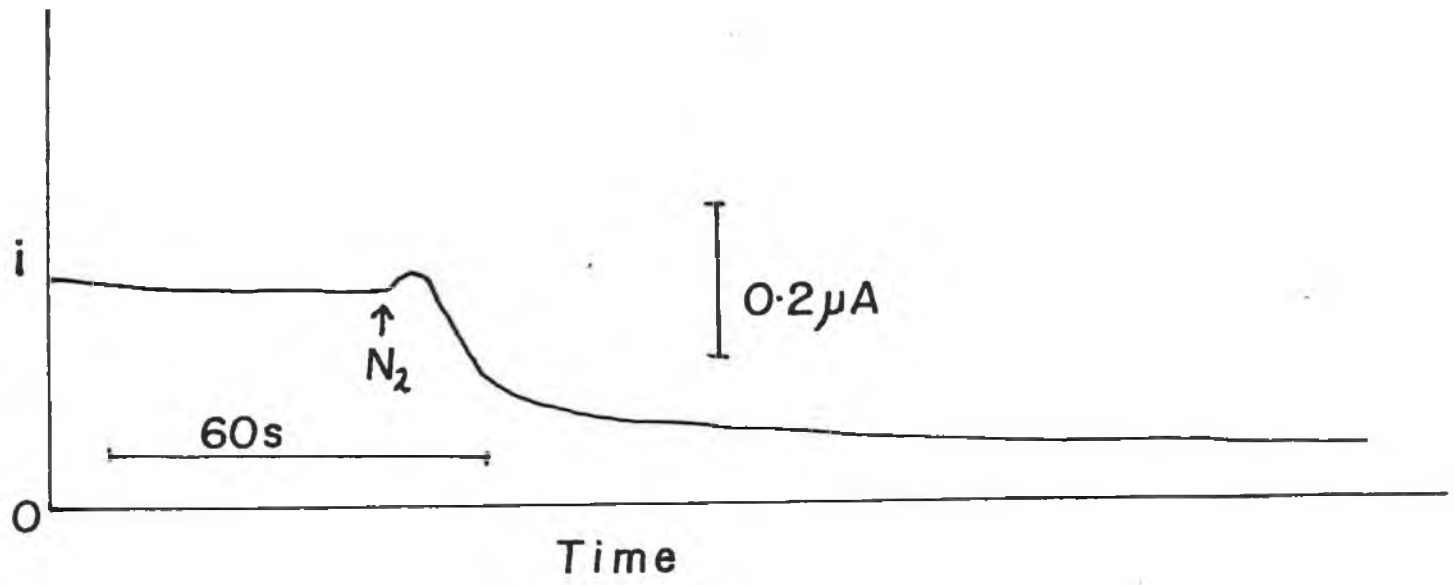

Figure 5.25 Effect of dry nitrogen upon the current obtained when +0.5V is applied across the two terminals of a PB modified interdigital array electrode. The PB film was previously formed as described in Figure 5.23.

water, thus lowering the mobility so severely as to become limiting upon electron mobility. A similar situation has been reported previously [37].

Figure 5.26 shows the effect of methanol vapour upon the current at $\Delta E = +0.5V$. It can be seen that switching to methanol vapour leads to an increase in current. This can be explained by the fact that the methanol vapour is helping to increase the mobility of the internal counterionic species, thus leading to an increase in the observed current. It acts in an opposite manner to dry N_2, which is seen to reduce the current back down, upon switching the film from being exposed to methanol to N_2.

The reversibility of this change in current, upon switching between different bathing gases for the PB film, was investigated for a series of methanol pulses. The current-time profile obtained is shown in Figure 5.27 (a). It can be seen that the process is reversible with a rapid response time in the order of 10-15 seconds.

Figure 5.27 (b) and 5.27 (c) illustrate the response of the Prussian Blue film to water vapour and dichloroethane, respectively. All changes are seen to be reversible with a rapid response time, of approximately 5 seconds.

All three gases, namely, methanol, water vapour and dichloroethane lead to an increase in current at $\Delta E = +0.5V$. Therefore it can be concluded that these gases all help to solvate the internal counterionic species, and lead to an increase in mobility. Another possiblity is that the bathing gas is acting as an oxidant or reducing agent, therefore changing the concentration profiles of the FeIII/III,

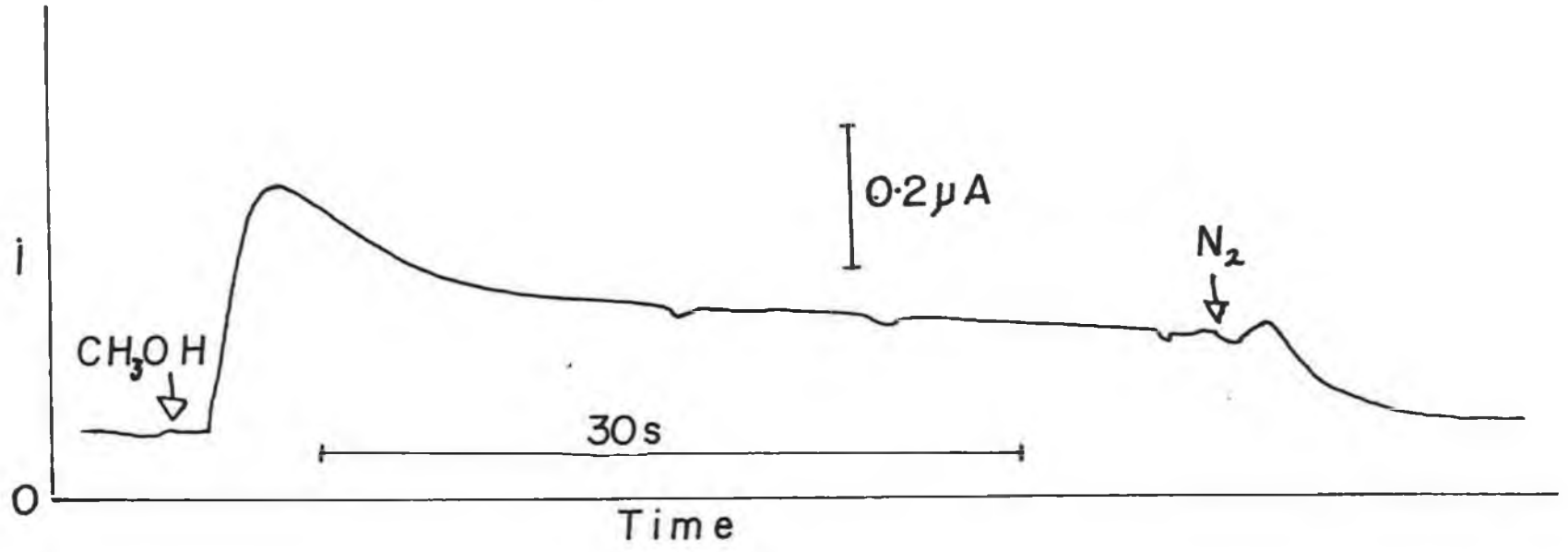

Figure 5.26 Effect of a concentration step of methanol vapour upon the current at $\Delta E = +0.5V$, for a PB modified IDA electrode.

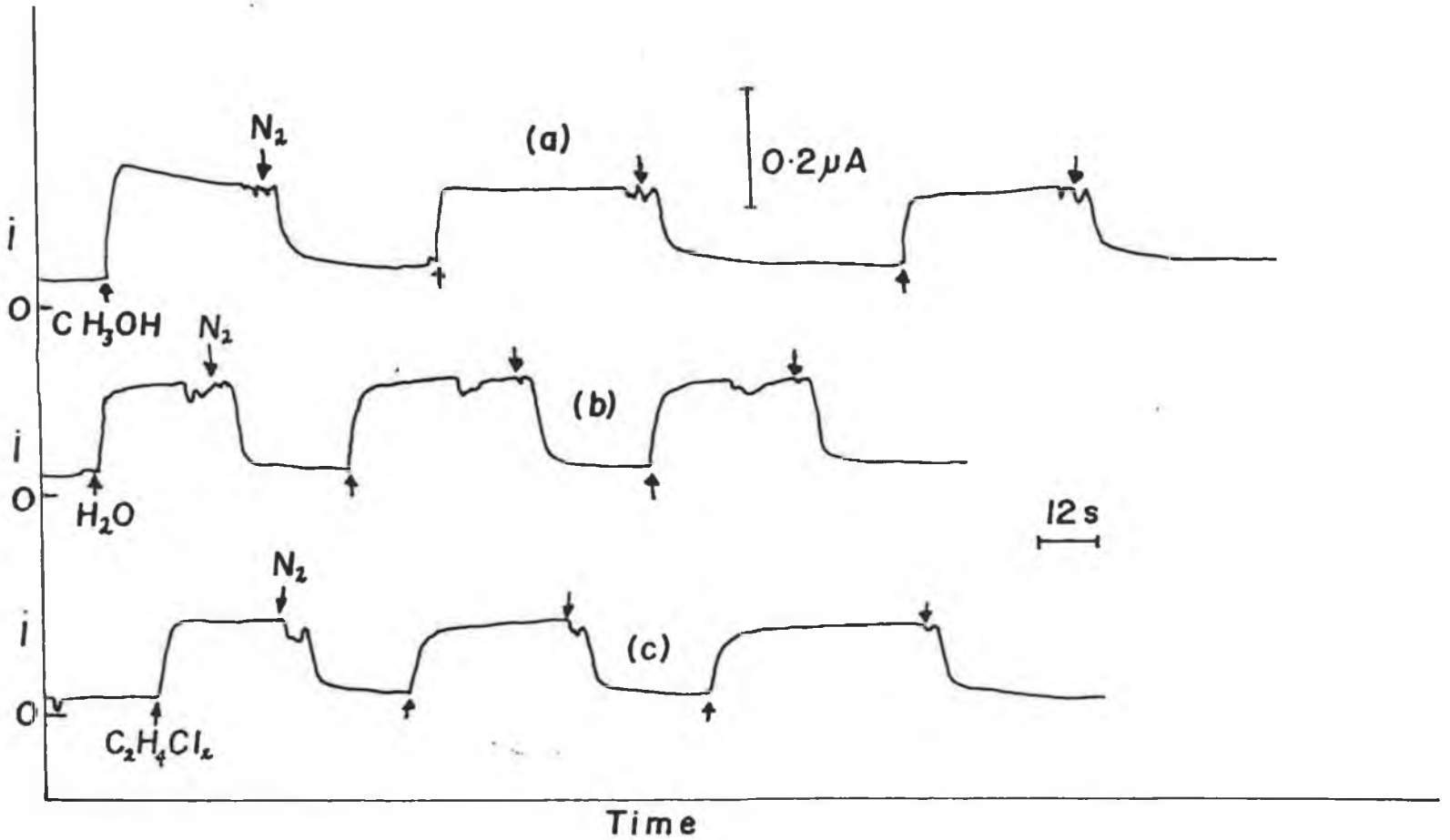

Figure 5.27 Effect upon the current at ΔE = +0.5V, for a PB modified IDA electrode, by concentration steps of different bathing gases
(a) CH_3OH (b) H_2O (c) $C_2H_4Cl_2$.

FeIII/II and FeIII/II species within the film and hence leading to a change in the current.

5.5.4 CONCLUSION

It can be concluded that Prussian Blue films can be electrochemically deposited on top of polypyrrole films, by either cycling or holding the potential of the working electrode at +0.5V. Within the bilayer modified electrode, the Prussian Blue → Prussian White electrochemistry was observed with no definite electrochemistry of the polymer layer being observed.

Prussian Blue films were deposited across carbon ink array electrodes and solid state voltammetry was performed. The current measured from the array, when the potential across the two electrode array was +0.5V, was found to be dependent upon the nature of the bathing gas. This indicates that Prussian Blue films themselves could be a sensing element within a gas sensor.

5.6 REFERENCES

1. K. Camann, U. Lemke, A. Rohen, J. Sander, H. Wilken and B. Winter. Angew. Chem. Int. Ed. Eng. 1.30 (1991) 516-539.
2. F. Haber, Z. Klemeciewicz, Z. Phys. Chem., 67, (1919) 385.
3. D.T. Sawyer, J.L. Roberts Jr., Experimental Electrochemistry for Chemists, Wiley, New York, (1974) pp. 308-310.
4. A.J. Bard, L.R. Faulkner, Electrochemical Methods, Fundamentals and Applications, Wiley, New York, (1980), pp. 78.
5. L. Companella, M. Tomassetti, M.P. Sammartino, Sensors and Actuators 16 (1989) 235.
6. Y. Hanazato, S. Shiano, Proc. Int. Meet. Chem. Sensors, Amsterdam, Elsevier, (1983) pp 513.
7. S.K. Beh, G.J. Moody, J.D.R. Thomas, Analyst, (1991), Vol. 116, 459-462.
8. S.A. Wring, J.P. Hart and B.J. Birch. Analyst, (1991), Vol. 116, 123-129.
9. S. de Smet, J.Cassidy, T.McCormac,N.A.Maes, Electroanalysis (in press).
10. D.P. Morgan,Ultrasonics, (1973), 121-131.
11. C.T. Chuang, R.M. White and J.J. Bernstein. IEEE Electron Device Letters, Vol. EDL -3, No. 6, (1982), 145-148.
12. M.S. Nieuwenhuizen, A.J. Nederlof, Anal. Chem. (1988), 60, 236-240.
13. G.Z. Zhang and E.T. Zellers, Anal. Chem. (1993), 65, 1340-1349.
14. W. H. King, Anal. Chem. (1964), 36, 1735.

15. W.H. King, J. Environ Sci. Technol., (1970), 4, 1136.

16. J.A. Munez Leyra, J.L. Hidalgo de Cisneros, D.G. Gomez de Darreda and A.J.F. Becerra, Analyst, (1993), Vol. 118, 175-178.

17. G. Bidan, Sensors and Actuators, B. 6 (1992), 45-56.

18. J.J. Miasik, A. Hooper, B. Tofield, J. Chem. Soc. Faraday Trans. 1, (1986), 82, 1117-1126.

19. J.P. Blanc, N. Derouiche, A. El. Hadri, J.P. Germain, C. Maleysson, H. Robert. Sensors and Actuators, B1 (1990), 130-133.

20. T. Hanawa, S. Kuwabata, H. Yoneyama. J. Chem. Soc., Faraday Trans. 1, (1988), 84(5), 1587-1592.

21. P.N. Bartlett, P.B.M. Archer and S.K. Ling-Chung. Sensors and Actuators, (1989), 20, 126-139.

22. P.N. Bartlett and S.K. Ling-Chung. Sensors and Actuators, (1989), 20, 287-292.

23. P.N. Bartlett, S.K. Ling-Chung. Sensors and Actuators, (1989), 19, 141-150.

24. T. Hanawa and H. Yoneyama. Bull. Chem. Soc. Jpn., 62, (1989), 1710-1714.

25. D. Blackwood and M. Josowicz. J. Phys. Chem. (1991), 95, 493-502.

26. J.M. Slater, E.J. Watt, N.J. Freeman, I.P. May and D.J. Weir. Analyst, (1992), Vol. 117.

27. P. Topart and M. Josowicz. J. Phys. Chem. (1992), 96, 8662-8666.

28. Mask Purchased from NMRC Cork. Gold interdigital arrays manufactured by Dr. David Cameron, Department of Electronics, Dublin City University.

29. E.M. Genies and J.M. Pernaut. J. Electroanal. Chem., (1985), 191, 111.

30. K. Itaya, T. Ataka and S. Tashima. J. Am. Chem. Soc. (1982), 104, 4767-4772.

31. C.A. Lundgren and R.W. Murray. Inorg. Chem. (1988), 27, 933-939.

32. J.F. Keggin and F.D. Miles. Nature (London), (1936), 137, 577.

33. H.J. Buser, D. Schwarzenbach, W. Petter and A. Ludi. Inorg. Chem. (1977), 16, 2704.

34. D. Ellis, M. Eckhoff, V.D. Neff. J. Phys. Chem. (1981), 85, 1225.

35. K. Itaya, N. Shaji, I. Uchida. J. Am. Chem. Soc. (1984), 106, 3423.

36. O. Ikeda and H. Yoneyama. J. Electroanal. Chem., 265 (1989), 323-327.

37. B.J. Feldman, R.W. Murray. Inorg. Chem. (1987), 26, 1702-1708.

APPENDIX ONE

Fortran Simulation Programme for Differential Pulse Voltammetry of Conducting Polymer Layers.

```
C     A DIFFERENTIAL PULSE PROGRAM FOR  A THIN LAYER OF SOLUTION
C     ORTHOGONAL COLLOCATION. THIS TAKES INTO ACCOUNT A SERIES
C     OF RESISTANCES FOR EXCESS ELECTROLYTE AND CHARGE
C     BALANCING IONS.
      IMPLICIT REAL*8(A-H,O-Z)
      COMMON AZ,BETA,SCAN,TEMP,THETA,SLAMBD,E0,ESWIT,ESTART
      COMMON XLAM,DELTAE,AM1,CONC,CO0,CO1,CR0,CR1,SS,RO
      COMMON DD(100),DIFF,E,DIST,SUM,RRB,RE,RCT,ES,RT,RB
      COMMON TS1,TS2,TS3,TS4,TS5,DELTAT,DP1
      COMMON AA(100),BB(100),POT(10000),CUR(10000),RR(20)
      COMMON N,N2,N3,NSCAN,NACT,NFL,NFLIP,NP,NELECT,NFX,NPT
      DIMENSION ROO(20),VECT(20),DIF1(20),DIF2(20),DIF3(20)
      DIMENSION Y(100),F(100),AUX(16,100),PRMT(5),DERY(100)
      EXTERNAL FUN,OUT
      OPEN(UNIT=5,FILE='DV4.DAT',STATUS='OLD')
      OPEN(UNIT=6,FILE='DV5.DAT',STATUS='NEW')
      OPEN(UNIT=7,FILE='DV6.DAT',STATUS='NEW')
      N=6
      NO=1
      NP=1
C     NMR IS A COUNTER FOR THE OUTPUT OF THE CONC. PROFILES.
      NMR=0
      N1=1
C     EVERY NPTth CURRENT IS OUT /NFX #COUNTER
C     EVERY NPUth PROFILE IS OUT /NFY #COUNTER
      AL=0.D0
      BE=0.D0
      N2=N+2
      NFX=0
      ND=15
      N3=2*N
      CALL JCOBI(ND,N,NO,N1,AL,BE,DIF1,DIF2,DIF3,ROO)
      DO 18 I=1,N2
   18 RR(I)=ROO(I)
      DO 4 I=1,N2
      CALL DFOPR(ND,N,NO,N1,I,1,DIF1,DIF2,DIF3,ROO,VECT)
      DO 4 J=1,N2
    4 AA((J-1)*N2+I)=VECT(J)
      DO 7 I=1,N2
      CALL DFOPR(ND,N,NO,N1,I,2,DIF1,DIF2,DIF3,ROO,VECT)
      DO 7 J=1,N2
    7 BB((J-1)*N2+I)=VECT(J)
      DO 27 I=1,N2
   27 DD(I)=AA(N2*(N2-1)+1)*AA(I*N2)/AA(N2*N2)-AA((I-1)*N2+1)
      READ(5,22)ESTART,ESWIT,DELTAE,E0,DP1
      READ(5,22)CONC,SCAN,TEMP,DIFF,DIST
      READ(5,22)RB,RE,RO,T1,T2
C    DP1 IS THE PULSE AMPLITUDE
      READ(5,21)NSCAN,NELECT,NOPT,NPT
C     NOPT = 0
C     NOPT = 1 OPTIMISATION OF STEP LENGTH OCCURS
   22 FORMAT(5E10.4)
   21 FORMAT(4I5)
      AZ=NELECT*96487.*SCAN/(8.314*TEMP)
      TS1=AZ*T1
      TS2=AZ*T2
      TS3=TS1-TS2
      THETA=DEXP(96487.D0*(E0-ESTART)/(8.314*TEMP))
      BETA=DIFF/(AZ*DIST**2)
      NPU=4*NPT
      PRMT(1)=ESTART
      PRMT(2)=NSCAN*DABS(ESTART-ESWIT)*96487.D0/(8.314D0*TEMP)
      PRMT(4)=1.0D-3
      DO 9 I=1,N
```

```
      Y(I)=0.D0
      Y(I+N)=1.D0
    9 CONTINUE
      DO 10 I=1,N3
   10 F(I)=1.D0/FLOAT(N3)
      DELTAT=DELTAE*96487.D0/(8.314D0*TEMP)
C     BETA OPTIMIZATION
      J=0
      IF(NOPT.EQ.0)GO TO 174
   72 DO 73 I=1,N
      Z=BB(I*N2+I+1)+BB(N2*(N2-1)+I+1)*AA(N2*I)/AA(N2*N2)
      H1=Z*BETA
      H1=0.65/DABS(H1)
      IF(H1.LT.DELTAT) GO TO 79
      H2=Z+DD(I+1)*(-BB(I*N2+1)+BB(N2*(N2-1)+I+1)*AA(N2)/
     1AA(N2*N2))/(2*DD(1))
      H2=BETA*H2
      H2=0.65D0/DABS(H2)
      IF(H2.LT.DELTAT) GO TO 79
      H3=BB(I*N2+I+1)
      Z=-BB(I+1)*DD(I+1)/DD(1)+BB(N2*(N2-1)+I+1)*AA(N2)*DD(I+1)/
     1(AA(N2*N2)*DD(1))
      H3=BETA*(H3+Z)
      H3=0.65/DABS(H3)
      IF(H3.LT.DELTAT) GO TO 79
      H4=BETA*(BB(I*N2+I+1)+Z/2)
      H4=0.65/DABS(H4)
      IF(H4.LT.DELTAT) GO TO 79
   73 CONTINUE
      IF(J.EQ.0)GO TO 198
      GO TO 153
   79 DELTAT=DELTAT*0.5
      J=J+1
      IF(J.EQ.1000)GO TO 64
      GO TO 72
   64 WRITE(6,65)
   65 FORMAT('ERROR!')
      GO TO 199
  198 DELTAT=DELTAT*2.0
      GO TO 72
  199 DELTAT=0.001
  153 NACT=1
  174 BETA=DIFF/(AZ*(DIST)**2)
      DELTAE=(8.314*298.16)*DELTAT/96487.D0
      WRITE(7,80)BETA,DELTAT,DELTAE
   80 FORMAT('      BETA =     ',E12.6,'   DELTAT = ',E12.6,' DELTAE',
     1E12.6)
      NFL=1
      NFLIP=0
C    INITIAL VALUE
      SUM=0.05
      XLAM=96487.D0*DABS(ESTART-ESWIT)/(8.314D0*TEMP)
      PRMT(3)=DELTAT
      TS4=TS3-2.D0*DELTAT
      TS5=TS1-2.D0*DELTAT
      WRITE(6,88)TS1,TS2,TS3,TS4,TS5
   88 FORMAT(' TS1  ',E10.4,'  TS2  ',E10.4,'  TS3  ',E10.4,'  TS4  ',
     1E10.4,'  TS5  ',E10.4)
      CALL DHPCG(PRMT,Y,F,N3,IHLF,FUN,OUT,AUX)
      CLOSE(UNIT=5)
      CLOSE(UNIT=7)
      CLOSE(UNIT=6)
      STOP
      END
```

```
C      SUBROUTINE TO CALCULATE THE VALUES OF F(I)
       SUBROUTINE FUN(X,Y,F)
       IMPLICIT REAL*8(A-H,O-Z)
       COMMON AZ,BETA,SCAN,TEMP,THETA,SLAMBD,E0,ESWIT,ESTART
       COMMON XLAM,DELTAE,AM1,CONC,CO0,CO1,CR0,CR1,SS,RO
       COMMON DD(100),DIFF,E,DIST,SUM,RRB,RE,RCT,ES,RT,RB
       COMMON TS1,TS2,TS3,TS4,TS5,DELTAT,DP1
       COMMON AA(100),BB(100),POT(10000),CUR(10000),RR(20)
       COMMON N,N2,N3,NSCAN,NACT,NFL,NFLIP,NP,NELECT,NFX,NPT
       DIMENSION Y(100),F(100),PRMT(5)
       E=ESTART+X*(ESWIT-ESTART)/XLAM
       TS9=(NP-1)*TS1+TS3
       IF(X.GE.TS9)E=E+DP1
       IF(X.GE.NP*TS1)E=E-DP1
       IF(X.GE.NP*TS1)NP=NP+1
       E1=0.5*E
       EZ=1.0
     3 ES=E-E1
C    CURRENT IS IN AMPS
       IF(SUM.LT.1.E-12)RCT=1.E4
       IF(ES.EQ.0.0)ES=0.001
       IF(SUM.GE.1.E-12)RCT=ES/SUM
       XX=DEXP(-38.94D0*(ES-E0))
       FL=DP1/RB
       CVR=XX/(XX+1)
       CVR=DLOG(CVR)*FL/38.94D0
       RRB=DABS(ES/CVR)
       RRB=RRB+RE
       RT=1.D0/RCT+1.D0/RRB+1.D0/RO
       RT=1.D0/RT
       E1=RE*E/(RE+RT)
       FACT=EZ-E1
       EZ=E1
       IF(FACT.GE.0.0001) GO TO 3
       SS=E1/RE
C     RESCALE E
       E=E-START
C    ES IS THE EFFECTIVE POTENTIAL FELT BY THE COUPLe
       SLAMBD=DEXP(38.94*(ESTART-ES))
    81 CO0=0.D0
       DO 34 J=1,N
    34 CO0=CO0+DD(J+1)*Y(N+J)+DD(J+1)*Y(J)
       CO0=-CO0/((1.D0+SLAMBD*THETA)*DD(1))
       CR0=THETA*SLAMBD*CO0
       CO1=0.D0
       DO 35 J=1,N
    35 CO1=CO1+AA(N2*(J+1))*Y(J)
       CO1=CO1+AA(N2)*CO0
       CO1=-CO1/AA(N2*N2)
       CR1=0.D0
       DO 36 J=1,N
    36 CR1=CR1+AA(N2*(J+1))*Y(J+N)
       CR1=CR1+AA(N2)*CR0
       CR1=-CR1/AA(N2*N2)
C       WRITE(6,4)CO0,CO1,CR0,CR1
C     4 FORMAT(4(3X,E12.4))
       DO 1 I=1,N
       TDDER1=0.D0
       TDDER2=0.D0
       DO 2 J=1,N
       TDDER1=TDDER1+BB(J*N2+I+1)*Y(J)
       TDDER2=TDDER2+BB(J*N2+I+1)*Y(J+N)
     2 CONTINUE
       F(I)=BETA*(BB(I+1)*CO0+BB(N2*(N2-1)+I+1)*CO1+TDDER1)
```

```
      F(I+N)=BETA*(BB(I+1)*CR0+BB(N2*(N2-1)+I+1)*CR1+TDDER2)
    1 CONTINUE
      RETURN
      END
C     OUTPUT SUBROUTINE
      SUBROUTINE OUT(X,Y,F,IHLF,NDIM,PRMT)
      IMPLICIT REAL*8(A-H,O-Z)
      COMMON AZ,BETA,SCAN,TEMP,THETA,SLAMBD,E0,ESWIT,ESTART
      COMMON XLAM,DELTAE,AM1,CONC,CO0,CO1,CR0,CR1,SS,RO
      COMMON DD(100),DIFF,E,DIST,SUM,RRB,RE,RCT,ES,RT,RB
      COMMON TS1,TS2,TS3,TS4,TS5,DELTAT,DP1
      COMMON AA(100),BB(100),POT(10000),CUR(10000),RR(20)
      COMMON N,N2,N3,NSCAN,NACT,NFL,NFLIP,NP,NELECT,NFX,NPT
      DIMENSION Y(100),F(100),PRMT(5)
      SUM=0.0
      RRRB=DLOG(RRB)
      DELTAT1=DELTAT/(IHLF+1)
      TS5=NP*TS1-2.D0*DELTAT1
      TS4=(NP-1)*TS1+TS3-2.D0*DELTAT1
      DO 88 J=1,N
      SUM=SUM+AA(J*N2+1)*Y(J+N)
   88 CONTINUE
      SUM=SUM+AA(1)*CR0+AA(N2*(N2-1)+1)*CR1
      SUM=4.D0*SUM*BETA
      SUM=((NELECT*96487.D0)**2)*SCAN*SUM*CONC*
     1DIST/(4.D0*8.314D0*298.D0)
      IF(X.GT.TS5) GO TO 98
      IF(X.GT.TS4) GO TO 97
      GO TO 99
   97 TS6=(NP-1)*TS1+TS3-DELTAT1
      IF(X.LE.TS6)EDIFF=E
      IF(X.LE.TS6)CURLO=SUM
      IF(X.LE.TS6)SSLO=SS
      GO TO 99
   98 TS7=NP*TS1-DELTAT1
      IF(X.LE.TS7)CURHI=SUM
      IF(X.LE.TS7)SSHI=SS
      IF(X.LE.TS7)SSD=SSHI-SSLO
      IF(X.LE.TS7)DIFF=CURHI-CURLO
      IF(X.LE.TS7)WRITE(6,4)EDIFF,RT,RRRB,SUM,SS,SSD
C      IF(X.LT.TS7)WRITE(6,5)CURLO,CURHI,DELTAT
C    5 FORMAT(' CURLO ',E12.4,'  CURHI  ',E12.4,' DELTAT '
C     1,E12.4)
    4 FORMAT(' EDIF ',F5.3,' RT = ',E9.3,' RRB ',E9.3,'SUM ',E9.3,
     1' SS',E9.3,' SSD',E9.3)
   99 RETURN
      END
```